CHARACTERIZATION OF POLYMERS BY MATRIX ASSISTED LASER DESORPTION/IONIZATION FOURIER TRANSFORM ION CYCLOTRON RESONANCE MASS SPECTROMETRY

by

TODD H. MIZE

(Under the direction of I. Jonathan Amster)

ABSTRACT

Synthetic polymers have physical and chemical properties that are directly related to their molecular weight distributions, their component monomer species, and the identity of their initiating and terminating groups. These properties are all a function of the molecular mass of the individual oligomers in the polymer distribution. Matrix assisted laser desorption/ionization (MALDI) mass spectrometry facilitates the analysis of these properties by providing singly charged, gas phase species for measurement while Fourier transform ion cyclotron resonance (FTICR) as a mass analyzer can yield the mass resolution necessary for assigning the components of complicated mixtures. This dissertation details recent improvements to the techniques for analyzing polymers by MALDI-FTICR-MS; specifically, methods for increasing mass accuracy, sensitivity with low abundance and weakly ionizing samples, and resolution of isobaric species are presented.

INDEX WORDS: FTICR-MS, MALDI, Polymer, Copolymer analysis, Mass accuracy, Collision induced dissociation, Block length distribution, Accumulated trapping

CHARACTERIZATION OF POLYMERS BY MATRIX ASSISTED LASER DESORPTION/IONIZATION FOURIER TRANSFORM ION CYCLOTRON RESONANCE MASS SPECTROMETRY

by

TODD H. MIZE

BSAE, The University of Georgia, 1993

MS, Georgia Institute of Technology, 1998

A Dissertation Submitted to the Graduate Faculty of The University of Georgia in Partial Fulfillment of the Requirements for the Degree

DOCTOR OF PHILOSOPHY

ATHENS, GEORGIA

2002

CHARACTERIZATION OF POLYMERS BY MATRIX ASSISTED LASER DESORPTION/IONIZATION FOURIER TRANSFORM ION CYCLOTRON RESONANCE MASS SPECTROMETRY

by

TODD H. MIZE

Approved:

Major Professor: I. Jonathan Amster

Committee: Lionel Carreira
Ron Orlando
John Stickney
Michael Bartlett

Electronic Version Approved:

Gordhan L. Patel
Dean of the Graduate School
The University of Georgia
May 2002

DEDICATION

This is for every co-worker at every filthy, dangerous, and dismal job I have had who ever said to me, “What the hell are *you* doing here?” And, to the one in particular with whom I’ve spent the last 17 years: we’re officially on the wrong side of the Revolution, now...when they line us up hold your head up, shoulders back, and no blindfold.

ACKNOWLEDGEMENTS

It is almost shameful to take sole credit for a work of this size that has taken so long to produce. Therefore, I would like to thank, more than anyone, Professor Jonathan Amster for giving me this opportunity. His generosity–academic, professional, and social–appears to know no bounds. As much or more can be said of his patience with the slow learning, foul tempered character who offers these lines. And, his ability to extend the classroom beyond the walls of the University have been especially enlightening; our studies of complex chemical mixtures as represented by the Single Malt and continuing to many forms of combinatorial studies at the licensed "laboratories" around the country, his demonstration of erratic trajectories at the UGA golf course, and our hard sphere collision studies at the pool tables often found during the conferences have been memorable.

Mike Easterling deserves nearly as much credit as Jon, and for much the same reason. Any insane research tack that he would come up with became an instant challenge, a race to beat him to the first results; the realization that his proposals were completely plausible usually came after losing the race. Cindy Pitsenberger and Mike taught me the fundamentals of ion manipulation while she was trying to finish her dissertation. The generosity of time, materials, and humor that Cindy and Mike proffered were at least matched in kind by my colleagues on the electrospray side of the lab, Keith Johnston, Kristi Taylor, and Shubadha Kulkarni. People say you can't choose your family but those people haven't met the old group.

Bill Simonsick of E. I. DuPont and Nemours' Marshall Research Laboratories in Philadelphia has been a constant, loud, and very supportive friend. From our first encounter at ASMS in Palm Springs and at every discussion since, he has consistently given me just a little bit more information about polymer research than I could digest at the moment.

I also thank the following sources of funding that helped me pursue these studies. The writing of this dissertation was generously supported by the Graduate School of the University of Georgia through its dissertation fellowship program. Jon has, quarter-to-quarter and semester-to-semester allowed me to take advantage of the graduate student stipends written into the various NSF research grants he has received during my stay here. The National High Magnetic Field Laboratory provided a stipend for an academic year in exchange for my design and construction support on an FTICR-MS similar to the one used for these experiments.

My co-authors on the papers included here and elsewhere are only the tip of the iceberg with regard to the scientists that have shared their insight with me. I would like to thank, specifically, Ron Heeren, Sander Koster, Chris deKoster, Adi Eisenberg, Graznya Wilczek-Vera, Owen Terreau, Laszlo Prokai, and Paul Danis.

Finally, I have to thank Jamie Edgar, my wife of the last 16+ years. Our years in shabby housing and dangerous neighborhoods may not yet be over, but sharing the siege with you (especially these last few, hectic months) has made it all seem easy. Your intuitive sense of the absurdity of it all has been an endless source of amusement that resonates with my sense of humor in an eerie way and helps attenuate the savagery of so many of our neighbors and fellow citizens. We may not really have been destined for

one another, but who else would it have been? Thanks for participating in every boneheaded idea that I've proposed (like this one), for treating the wounds, and for letting me do most of the cooking. Now, let's get the hell out of here!

TABLE OF CONTENTS

Page

LIST OF TABLES

LIST OF FIGURES

CHAPTER 1

INTRODUCTION AND LITERATURE REVIEW

INTRODUCTORY REMARKS

The synthetic polymer industry has experienced exponential growth since the end of World War II. This growth is largely due to the shift from what would, these days, be considered a combinatorial or "shotgun" approach–mixing substances together in hope of some fortuitous combination of resulting physical and chemical properties–to a much more systematic form of molecular design. Integral to the implementation of this approach has been the chemical analysis that provides the feedback data. Analysis of an industrial polymer's molecular weight distribution and structural aspects yields invaluable information to the process chemist with regard to kinetics and reaction mechanisms, to guide the synthesis, and to correlate molecular structure with physical properties which determine the suitability of the product for a given purpose.

Parallel to the growth of the polymer industry, the development of Fourier transform ion cyclotron resonance mass spectrometry (FTICR-MS) has developed rapidly in the few years since its birth. And, FTICR-MS has a lineage as impressive as the polymer industry while, at the same time, has experienced a similar tentativeness in the historic events that led to the instrument we see today. Starting with the Omegatron,[1-3] a pre-Fourier transform scanning mass spectrometer which could easily have become an esoteric side application of the nuclear industry's accelerator technology (and, interestingly, is still used in nuclear reactor process control), the instrumentation has blossomed into a variety of vibrant and vital mass spectrometric research tools with unprecedented high mass resolution and the potential for unrivaled mass accuracy that will allow assignment of elemental compositions of target substances. This will be

shown to be the result of circumstance (in that the technology that led to each new step was consistently borrowed from prior applications) and genius in near equal proportions.

Synthetic polymer mass analysis–in spite of the fine tools the FTICR mass spectrometrist has to offer–is still largely a solution phase phenomenon. Though beyond the scope of this work, a cursory subjective analysis exposes perplexing resistance in both the polymer and FTICR communities for what are, essentially, opposite reasons: the ICR offers more information (and of greater variety) than polymer chemists usually require for their routine uses; and, polymers are often considered too simple in structure for the ICR community in light of the myriad biological applications available today. To be more fair, the industrial polymer community, served well by robust methods that provide satisfactory results for their immediate purposes, is often reluctant to invest in large, expensive, and reasonably complex research systems that require, at this point in history, fairly specialized training and personnel dedicated to its use and maintenance; this is especially true while the instrumentation is still under development and rapidly changing in configuration. The FTICR community, it can be argued, sees this and recognizes the immediate opportunity presented by emerging sciences like proteomics and genomics.

The focus of this chapter, then, will be to explain how we–that minority of FTICR mass spectrometrists that find technical polymers both interesting as analytical subjects and useful as support tools for other analyses– have found ourselves in this tenuous position, twixt industry's Scylla and mass spectrometry's Charibdis, as it were. After a brief history of polymer chemistry and a description of the polymer properties that are a function of molecular mass, the history and relevant fundamentals of FTICR will be

Figure 1.1: Number of FTICR mass spectrometers in operation worldwide (left and bottom axes) and similar increase in polymer production in US. Notes: *Polymer production refers to all plastics and resins, data from Furukawa[4] and the US Census Bureau.[5-7] **Marshall consistently reports current data for this statistic; these were a mere sampling through recent years.[8-13]

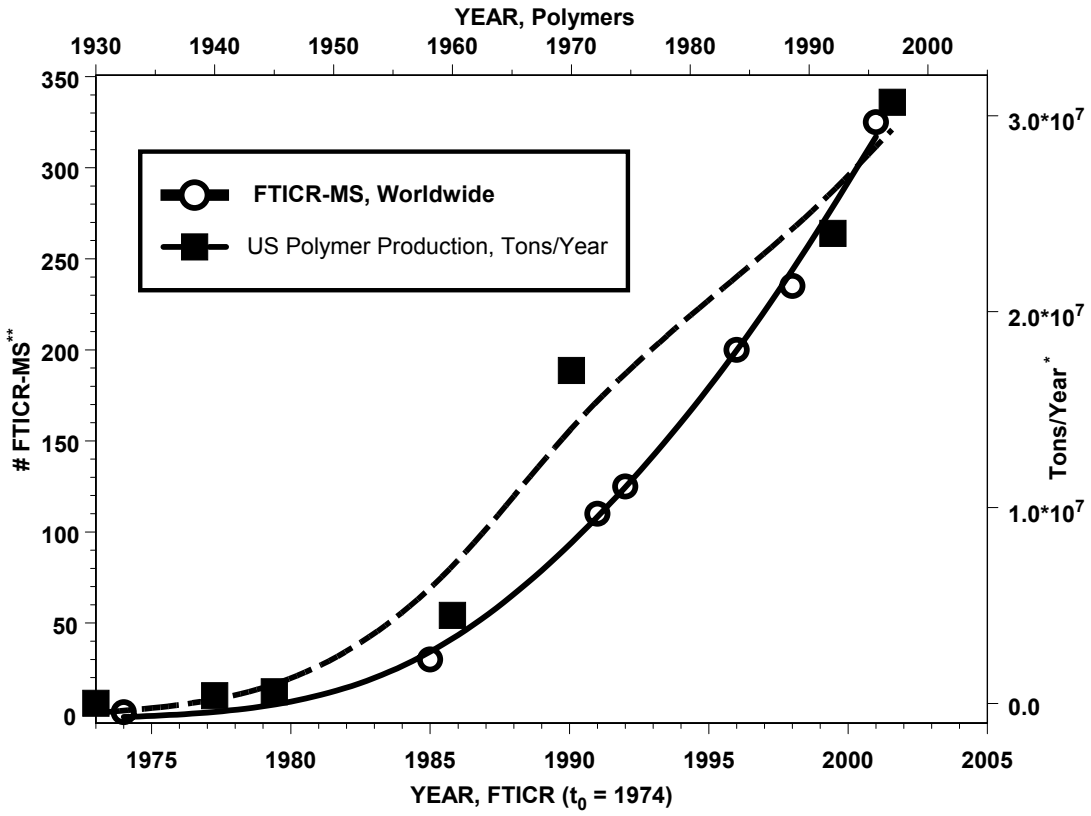
YEAR, Polymers
1930
1940
1950
1960
1970
1980
1990
2000
350
300
250
200
150
100
50
0
FTICR-MS**
FTICR-MS, Worldwide
US Polymer Production, Tons/Year
3.0*10^7
2.0*10^7
1.0*10^7
0.0
Tons/Year*
1975
1980
1985
1990
1995
2000
2005
YEAR, FTICR (t0 = 1974)

explored in an effort to declaw both arguments against the mating of the two. The application of FTICR to polymer analysis as it is performed in this lab will be detailed in Chapter Two and the specific advantages of FTICR to the present research will become more apparent in the research chapters, but this introduction should prove that it is a valuable tool for synthetic polymer analysis and that polymers have an endless variety of interesting analytical aspects.

HISTORICAL PERSPECTIVES IN POLYMER MANUFACTURE & ANALYSIS

Thomas Graham (1805-1869) noted that solutions of some organic compounds such as starches and cellulose would neither pass through filters nor purify in crystalline form. Graham posited that these substances were a previously unrecognized form of matter which he called colloids (after the Greek kolla, or glue). The popular theory of the day held that these substances were not, in fact, molecules composed of huge numbers of atoms but small molecules held together by "association," forces that, while substantial enough to change the physical behavior of the material, was still somewhat less forceful than chemical bonding. After Graham, two generations of chemists would disregard the possibility that the sticky impurities fouling their distillations were actually large molecules.[14, 15]

The properties of colloids made them interesting to the manufacturing industry of the nineteenth century, as well, and a number of new materials were developed, most notably celluloid. Invented by John Wesley Hyatt (1837-1920) in 1870 as a substitute for ivory in billiard balls, celluloid consisted of the nitration product of cellulose combined with camphor and molded into such useful items as combs, photographic film stock,

dishes, piano keys, and countless other things.[14, 16] Cellulose nitrate was also used to develop synthetic fibers when Count Hilaire de Chardonnet (1839-1924) found a method of spinning the material into an artificial silk in 1890.[17] Chardonnet silk became known popularly as "mother-in-law silk" for it's highly combustible nature.

In 1909, Leo Baekeland (1863-1944) developed the first completely synthetic commercial plastic by combining phenol with formaldehyde to form a resin that, upon application of heat and pressure, solidified to a chemically inert and electrically insulating substance. Bakelite, as it was dubbed, served as a more robust substitute for many of the molded products applications that, until this point, were relegated to the natural product, shellac.[18-20]

Still, at that point in history most polymer characterization relied on the physical properties of the finished product (hardness, imperviousness to heat or moisture or electric current, etc.), and much of the "research" generated was purely a matter of trial and error. Synthetic rubber, however, had developed on a more systematic track. Greville Williams (1829-1910), in 1860, distilled natural rubber and isolated isoprene which Gustave Bouchardat (1842-1918) reacted to form a substance similar to rubber. From this result, Bouchardat posited that rubber was a "polymer"(from the Greek for "many parts") of isoprene.[21] By1904, Carl Harries (1866-1923) had published several studies concluding that within the polyisoprene building blocks only one carbon-carbon double bond existed, leaving the possibility of another bond at each of its terminal carbon atoms. Harries reasoned that rubber might be a long, end-to-end chain of isoprene units, but realized that there must be some form of termination step lest the polymer just continue to combine with monomer. Further, he suggested that there may be no end

groups at all and that these materials combined to form a ring structure. This discovery would be all the more amazing if Harries had not stipulated that the bulk of the material was made up of these rings, the rings were only two subunits long, and were held together by those same, old “associative forces.”

It wasn’t until 1920 that Hermann Staudinger (1881-1965) began research designed to prove the presence of long-chain molecules once and for all. Staudinger focused on polyketenes, which the consensus opinion held to be small, ring shaped molecules á la Harries’ rubber theory. Staudinger felt that polyketene end groups were the same as the monomer subunits, but that the polymerization reaction was chain length limited. He proposed long-chain formulas for polyketenes and several other compounds, calling this group of materials "high polymers" (because of the large number of units making up each chain) or, as he preferred, macromolecules. Staudinger also derived a mathematical formula to explain the relationship between macromolecular viscosity--the resistance of polymer solutions to flow--and a dissolved polymer's molecular weight, a measure of the size of the molecule. By the end of the 1920s, instrument development caught up to Staudinger’s macromolecular theory with crystallographic spectroscopy of a number of high polymers, including biological enzymes, something that by definition could not be done to a true colloid.[4]

Instrumental analyses of all sorts developed rapidly at this time. The Norwegian scientest, The Svedberg (1884-1971), developed the ultracentrifuge which separated solutes by size via application of forces in excess of 100,000 times earth's gravity. Svedberg found that hemoglobin, the oxygen-carrying biopolymer in blood, has a molecular weight of over 66,000--four times the highest weight ever assigned to it

before.[22-25] At about the same time Kurt Meyer (1883-1952) and Herman Mark (b. 1895) examined the structure of cellulose and other polymers with x-ray crystallography and proving the multi-unit hypothesis for their structures.[26, 27] Armed with these new data, the DuPont chemical engineer, Wallace Hume Carothers (1896-1937), synthesized and analyzed an extensive series of new polymeric substances, including polyesters, neoprenes, and nylons.[4, 28] Carothers' Du Pont colleague (and later, a Professor at Cornell University), Paul Flory (1910-1985) developed elegant statistical and kinetic models to explain the role of end groups in polymer formation, and was rewarded for this industry building fundamental research with the 1974 Nobel Prize in Chemistry.[29, 30]

Analytical chemistry instrumentation continued it's symbiotic relationship with the growth of the polymer industry throughout the 1930s, with the successful development of online infrared absorption spectroscopy by Shell Development Company which desired process control on the refinement of butadiene for synthetic rubber production. The prototype analyzer built for the Allied war effort led quickly to the introduction of the IR-1, Beckman Instruments first infrared spectrometer for commercial use.[31]

By 1960, continued instrumental development led to applications like the electron microscope, new forms of spectroscopy, and detailed investigations of the behavior of polymeric reactions that helped make polymer design a reality.[32, 33] Understanding and control of properties at the molecular level led to a wealth of polymer applications in all aspects of society. Production of synthetic plastics and resins had grown from 15,000 tons to over 400,000 tons between 1930 and and the end of World War II; in 1960 production had reached three million tons. In 1976, more polymeric material was used

worldwide than steel on a per volume basis; today, that statistic is more than steel, aluminum, and copper combined.[34, 35]

A full exposition of the history of polymers is neither practical nor proper in this venue. The contributions of the synthetic polymer chemists and analysts to society are varied and immense, with the least of these contributions being the impact on the world economy. The development of new materials are constantly being met by new methods of learning about them. The applications from both sides of the chemistry fence, synthesis and analysis, serve the greater industrial community which encompasses, after all, all that we are when we decouple ourselves from ego and politics.

FUNDAMENTALS OF POLYMER MASS ANALYSIS

The entire chemical establishment (not just the polymer industry) has always depended upon quality data to monitor and control the processes of production and to confirm the identity of the final product. It is understandable that there exists a symbiotic relationship between the development of synthetic and analytical methods and means: new instrumentation always seeks a new application and the data derived from the application is either applied to improvements in process control or leads to more questions that need solution, in which case the analytical field seeks to meet the new challenge.

The early days of macromolecular sciences are a prime example of how this relationship expresses itself. The same experiments that led Graham to predict the existence of macromolecules–the imperviousness of colloids to membrane filters–would much later be applied as a separation method (size cutoff filtration) and for average

molecular weight determination due to the colligative properties of dilute polymer solutions (membrane osmometry).

Many of the physical properties of a polymer are directly related to the molecular mass distribution of the substance, a bulk property related directly to the average chain lengths of the individual oligomers. Copolymers, polymers consisting of multiple monomeric species, have structural properties that can be determined, among other methods, by the accurate determination of molecular mass; specifically, the distribution of the constituent monomers can be derived. Determination of the end groups of a polymer will tell the synthetic chemist the tale of initiation and termination and, since the end groups are often different species from the monomer, mass determination is one way to approach the analysis.

Three parameters are most often cited for the determination of the molecular weight distribution, the number average molecular weight, M_n, defined as

$$M_n = \frac{\sum_i n_i M_i}{\sum_i n_i} \tag{1}$$

the weight average molecular weight, M_w,

$$M_w = \frac{\sum_i n_i M_i^2}{\sum_i n_i M_i} \tag{2}$$

and the polydispersity, D,

$$D = \frac{M_w}{M_n} \tag{3}$$

where n_i is the degree of polymerization of the i^{th} oligomer and M_i its molecular mass. M_n, M_w, and D are functions of the monomer feed rate and the rate of the polymerization

reaction.[36] The average distribution parameters are made necessary by the nature of the polymer, which is a mixture of chemically species differing by the number of monomer units.

The molecular mass of an individual oligomer molecule is much more straightforward. For a homopolymer oligomer molecule with degree of polymerization, n, monomer mass, $m_{monomer}$, and end group mass, $m_{end\ group}$, we have

$$m_{oligomer} = n \times m_{monomer} + m_{end\ group} \tag{4}$$

where $m_{oligomer}$ is the oligomer mass. Accurate measurement of the individual oligomer masses in the distribution makes determination of both $m_{monomer}$ and $m_{end\ group}$ a matter of simple regression analysis with the slope of the regression line for $m_{oligomer}$ vs n yielding $m_{monomer}$ and the intercept $m_{end\ group}$.[37]

For the purposes of this discussion, two basic forms of polymerization reaction exist: condensation and addition. In polycondensation, two oligomers with reactive end group species combine to form a longer oligomer and lose a small molecule:

$$\begin{aligned}
&A + B \underset{\leftarrow}{\overset{\rightarrow}{}} C_1 + Z \\
&A + C_x \underset{\leftarrow}{\overset{\rightarrow}{}} AC_x + Z \\
&B + C_x \underset{\leftarrow}{\overset{\rightarrow}{}} BC_x + Z \\
&AC_x + B \underset{\leftarrow}{\overset{\rightarrow}{}} C_{x+1} + Z \\
&BC_x + A \underset{\leftarrow}{\overset{\rightarrow}{}} C_{x+1} + Z \\
&C_x + C_y \leftrightarrow C_{x+y} + Z \qquad \{x, y \geq 1\}
\end{aligned} \tag{5}$$

where A and B represent condensible monomers, and C_i is the i^{th} condensation product of A and B, and Z is the condensation by-product. As shown, these are reversible reactions requiring the removal of the Z species to continue and, occasionally, the reactive end species on a single oligomer can result in a cyclic form of the oligomer product (that is, $m_{end\ group} = 0$). In any case, the reaction will continue until either the reactive groups are exhausted, the reaction reaches equilibrium with the by-product concentration, or some termination reagent is added to quench the reaction (resulting in a change in end group). Polycondensation is typical for polyesters (loss of H_2O for each reaction step) and polyamides (like Nylon, with loss of NH_3 at each step).

Polyaddition reactions have a wider variety of reaction types. At the most basic there is an initiation step in which an ionic or radical species attacks a double bond on a monomer and forms a reactive oligomer of increasing degree of polymerization by addition of monomers until a termination step either neutralizes the reactive oligomer ion or quenches (or transfers) the radical. Again, the possibility exists for cyclic oligomers with no residual end group mass. Additionally, the end group can be a combination of the initiator and terminator, the initiator and a quenching species, or the initiator and a site of unsaturation.

Thus far, the examples have focused on homopolymers, the simplest polymer composition; a few notes on more complex architectures are relevant. As noted above, cyclic polymers have the same structure as their linear counterparts with the exception of the end group which is missing, and linear homopolymers can have a variety of end functionalities. Let “I” represent the initiator or the end functional group at the “head” of the polymer. Also, let “A,” “B,” and “C” be monomer units and “T” and “Z” the end

functionality. For an nonamer (a polymer of n = 9), we could have different functionality:

I-A-A-A-A-A-A-A-A-T

I-A-A-A-A-A-A-A-A-Z

or alternating copolymers (with two monomer units appearing one after the other):

I-A-B-A-B-A-B-A-B-A-T

versus random copolymers (where, obviously, the sequence does not alternate in a regular fashion):

I-A-B-B-A-B-A-A-B-A-T

and block copolymers (where one monomer chain is followed by a chain of the second monomer):

I-A-A-A-A-A-B-B-B-B-T

the immediately previous three of which are indistinguishable by molecular mass, alone. A terpolymer becomes more complicated, still; suppose we have eight condensation units with monomer A able to condense with either monomer, B or C, in which case there would be a distribution at each chain length yielding oligomers

$$I\text{-}(A\text{-}B)_n\text{-}(A\text{-}C)_{8-n}\text{-}T$$

with n = 0 through 8 and the A-B and A-C units randomly distributed. Proteins can be thought of, conceptually, as conserved, random copolymer oligomers with 20 monomer units; however, these and the more complex synthetic copolymers (branched, hyperbranched, graft, and random copolymers) are not considered in detail in this work.

While the present research will use high resolution FTICR-MS to examine these properties, it would be remiss to suggest complete characterization of a polymer can fall

from a single method and to ignore the vast array of other analytical techniques, past and present, that have been used for these analyses. The following subsections will follow the utility of some of the other fields of analytical chemistry for determination of mass and composition related properties of polymers. Some of the techniques are only of historical interest, while others determine essentially identical information from the polymer sample by examination of wildly different properties. The intent is not to present an exhaustive study of all polymer analyses but, rather, to present the pros and cons of the various alternatives to mass spectrometry and to place each in a historical perspective.

MOLECULAR WEIGHT WITHOUT MASS SPECTROMETRY

In 1822, Faraday noted that when a non-volatile solute is dissolved, the boiling point of the solvent is elevated relative to the pure solvent. Beckman later applied this phenomenon to what has come to be known as the ebullioscopic method of mass analysis.[38] The proponents of this mostly obsolete method claim accurate molecular weight determinations to 100,000 Da although agreement with other techniques rarely is seen above 12,000 Da.[39-43] Problems arise from a number of sources; for instance, the boiling point is atmospheric pressure dependant requiring exact duplicate instrumentation to run simultaneously with pure solvent in one ebulliometer and the solute additions in the other. The temperature sensors can be a simple thermistor for large changes in temperature, but with polymeric size (and therefore, molecular mass) the amount of solute added to the solvent becomes smaller as does the boiling point differential; a wheatstone bridge across which matched, high sensitivity thermistors are mounted can

measure these) T (often on the order of 10^{-4} EC), but this exacerbates the question of matching two instruments at once. The typical ebulliometer consists of a two necked flask with a Cottrell pump in the solvent loading area which delivers the boiling vapor to the thermistor(s) mounted in one of the flasks necks; this arrangement is an attempt to minimize the problem of superheating by allowing the vapor a chance to cool to the equilibrium boiling temperature before measurement. The other neck is fitted with a reflux condenser which will always contain some of the pure solvent so that the solvent:solute ratio is always less than at the start of the experiment. Relatively large volumes of solvent are required, which is the real problem for modern analyses. Solubility of the polymer may be too low to use the method. Finally, large polymers tend to foam in boiling solution; the Cottrell pump tends to aggravate this situation. All in all, this remarkably simple concept becomes a very difficult instrumental procedure to apply to polymer systems.[44]

A clever variation on this idea is incorporated in measurement of number average molecular weights by vapor phase osmometry (VPO).[45-48] VPO exploits Raoult's law, which states that the vapor pressure changes in proportion to the mole fraction of the solute, in a slightly different manner than ebullioscopy. VPO uses a thermostated chamber with two hypodermic needles through which droplets of pure solvent and the polymer solution are impelled over thermistors. The chamber is also filled with solvent vapor so that the polymer solution absorbs solvent as the pure solvent evaporates (or, at the very least, the solution evaporates slower). The relative change in temperature of the droplets due to evaporative cooling is measured and related back to the relative change in vapor pressure. There is a specific surface effect wherein the absolute rate of loss of

solvent slows as the droplet shrinks, but this can be corrected by manually maintaining the droplet size.[48] The overall reproducibility (± 9%) is better than ebullioscopy when equilibration time is minimized and calibrants are matched well to the analytes for molar mass.[49]

Another of the older mass measurement techniques, viscometry, was used by Staudinger in the 1930s to characterize cellulose derivatives and was important in proving that polymers were, in fact, large molecules and not aggreagated small molecules. It is based on the fact that a polymer solution has a higher viscosity, 0, than that of the pure solvent (0_0) and that

$$\eta = f(M_v, T, C, \frac{ds}{dt}) \tag{6}$$

where T is the temperature, C the solution concentration, and ds/dt is the shear rate all of which can be held constant making M_v, the viscosity molecular weight, easy to calculate. The viscosity molecular weight can be useful in prediction of viscoelastic properties.[50-52] It has also been shown that determination of the intrinsic viscosity by this method allows accurate prediction of the weight average molecular weight, M_w, up to 10^5 Da.[51, 53, 54] Viscometry is a relative measurement, i.e., it requires calibration against a well characterized standard.

Ultracentrifugation, introduced by Svedberg in the 1920s, yielded the first reliable molecular weights of macromolecules. Sedimentation measurements are time consuming (some measurements can last up to several days) and the instruments are prone to malfunction. Still, highly accurate measurements of weight average (M_w) and centrifuge average (M_z) molecular weights are possible in the range of 200 Da to 10 MDa with as

little as 20 μg sample consumed. Modern ultracentrifuges allow simultaneous equilibrium sedimentation measures of up to eight solution concentrations thus minimizing the problems with polydisperse samples.[55-58]

Nuclear magnetic resonance can be used to give an average molecular weight if the shifts of all the possible end groups are accounted and the monomer unit is known. For example, proton NMR has been used to identify six end groups in a poly(methyl methacrylate) sample and to relate their integrated abundances to each other. These integrated peaks can then be related to the much larger peaks of proton or ^{13}C shifts for one of the monomer moieties thereby yielding an average chain length (and by extension, the molecular weights M_w).[59, 60] The method is impractical for long chains and for polymers with end group species similar to the repeat units, and in highly polydisperse random copolymers the data is highly unreliable (although, as a screening tool the method can extract relative monomer distributions as well as a fairly inaccurate molecular weight distribution).[61]

Rayleigh scattering occurs when light passing through transparent media meets a change in density, or more precisely when the incident light interacts with the electrons in the chemical which induce an oscillating dipole in the molecule that acts as a resonant scattering center for the light. For molecules much smaller than the wavelength of light (< 8 / 20), the scattering is symmetric about a sphere surrounding the solution; with large molecules, however, additional scattering occurs which is inversely related to the concentration and directly to the molecular weight of the solute. In a bulk system, low angle light scattering experiments can yield M_w, mean radius of gyration (from which a measure of polydispersity can be extracted), and the translational diffusion coefficient (if

the solvent is chosen with different refractive index from the sample), the solute is pure (i.e., free of other scattering centers such as dust), and there are no aggregated species (although this can be useful in temperature gradient light scattering experiments). In modern use, low angle light scattering is most often applied as a detection scheme for gel permeation chromatography eluents since most of the above caveats are addressed in the separation.[62-65]

Chromatographic methods are truly the gold standard these days for absolute mass analysis of polymers. Gel permeation chromatography (GPC), also known as size exclusion chromatography (SEC), fractionates the introduced sample by size in solution. An inert, microporous stationary phase is used such that there are channels and eddies along a packed column for solute and solvent to enter and eventually to exit.[66] Smaller molecules (i.e., those with a smaller hydrodynamic radius, as shown in Figure 1.2) are statistically able to enter more of the pores (and, to penetrate them deeper) and, therefore, are retained longer than those with larger radii.[67-71] Coupled with an absolute quantitative analyzer (such as a refractive index detector, a sort of simplified light scattering device), GPC yields quantitative measures of M_n, M_w, and D (with respect to the external calibrant, which can have remarkably different compositional qualities to the analyte).[70, 72-80] Calibration problems have recently been eliminated by coupling the effluent of the non-destructive, quantitative detector to online mass spectrometers to give an absolute calibration on the analyte specie, itself. This is especially important for polymers which have cyclic oligomeric forms that are the same molecular weight (within the limits of the method, at any rate) as their linear counterparts but which elute from the GPC column later due to their constitutionally smaller radii.[67, 70, 73, 75]

Figure 1.2: Cyclic (top) and linear oligomers of poly(neopentyl glycol-alt-isophthalic acid) minimum energy configurations in THF solvent (solvation shells not shown). The longest dimension for each of the molecules is 11 Å for the cyclic oligomer and 18 Å for the linear oligomer. Calculations performed using Spartan molecular modeling software (Wavefunction, Inc., Irvine, CA).

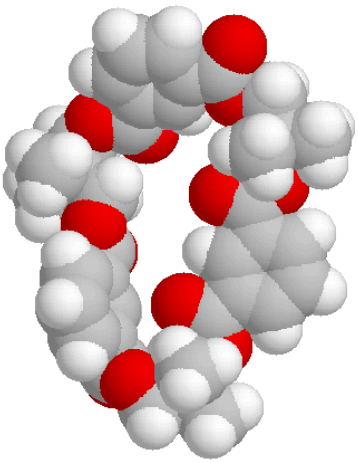

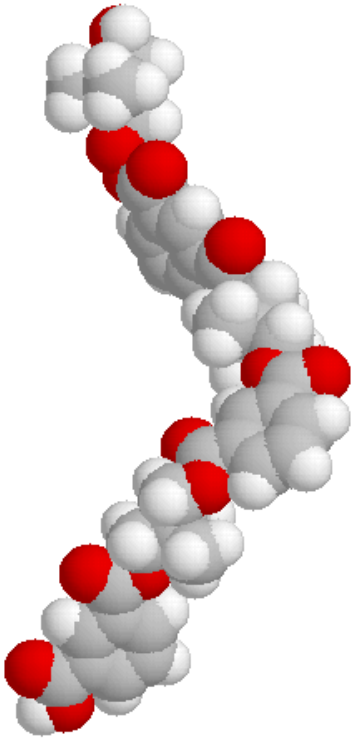

MASS SPECTROMETRIC ANALYSIS OF POLYMERS

While, as stated in the previous section, GPC is the gold standard in polymer molecular weight analysis, mass spectrometrists offer an expansion of the information available from GPC and, like the multitude of other techniques list above (and those grievously omitted), offers unique information and structural detail unavailable in chromatographic methods. Most of the world sees mass spectrometry as a structural analysis tool for low molecular weight materials (MW < 1000 Da); but, macromolecular mass spectrometry, a relatively recent development, has shown astonishing growth. This is in no way simply a case of good public relations as over 2000 research papers on mass spectrometry of industrial polymers have been published in the last 10 years (and a similar number on protein mass spectrometry in the last 6 months, alone).[81] This is a remarkable change compared to just two decades ago when most macromolecular mass spectrometric studies were limited to low mass pyrolysis products of coal oil and other fossil fuels.[82-87]

The next section, then, will start with pyrolysis mass spectrometry used as a way of drawing attention to the ion sources that lead to matrix assisted laser desorption/ionization (MALDI); most of these sources are still important weapons in the polymer analysts arsenal, but the advantages of MALDI will be made clear as we progress. In the logical progression from making gas phase ions to doing something useful with them, the mass analyzers most often employed will be briefly discussed in the following section and, finally, compared to FTICR-MS.

IONIZATION: PREVIOUS EFFORTS

Mass spectrometry requires gas phase ionic species for measurement; neutrals cannot be measured because there is no way to extract information on the movement of the molecules without an electrical charge on the molecule or, indeed, to induce any measureable form of mass dependent movement.[88] The major problem in this equation with respect to industrial polymers and, for that matter, proteins and other macromolecules is not so much the production of charged species since simple adjustment of pH allows many polymers to assume ionic form in solution which is the basis of electrophoretic separations of proteins and, more recently, synthetic polymers,[89-91] but rather to introduce the ions formed into the gas phase. As late as the mid-1980's, pyrolysis of high mass synthetic polymers was the only viable method to determine their structural characteristics by mass spectrometry.[92]

Pyrolysis was the state of the art in volatilization of polymers for two decades starting in the mid 1960's and, as an external source of prefragmented ions for mass spectrometry, for another decade prior.[93] The typical experiment involves heating a sample rapidly (flash or laser pyrolysis) or in gradient manner (gradual pyrolysis) to produce volatile fragments that could be ionized by electron impact (EI) or chemical ionization (CI) and directed into an analyzer such as a sector mass spectrometer.[94, 95] The main problem with pyrolysis mass spectrometric methods is the lack of control over intermediate degradation of the material in the pyrolysis chamber, a matter only partially addressed by the introduction of field ionization which allowed the production of molecular ions in the gas phase polymer fragments.[96-102]

Secondary ion mass spectrometry (SIMS)[103, 104] like its younger sibling, fast atom bombardment (FAB, below),[105-107] applies particle bombardment to the sample in order to produce analyte ions. Primary ions are produced from argon or xenon within a discharge cell and accelerated toward the sample with several KeV kinetic energy; the resulting sputtering effect yields a polychromatic plume of ions, neutral molecules, and larger particles. Careful focusing of the primary ion beam allows depth profiling with approximately 100 D spatial resolution.[108] The energy added in this relatively soft ionization technique is still substantial; for instance, Hercules and coworkers demonstrated that for polyamides, cleavage of bonds in the chain was unavoidable.[109]

The use of ^{252}Cf plasma desorption ionization for mass spectrometry (PDMS) first appeared in 1975.[110, 111] Ions are formed when the ~6 MeV "-particles from the decay of a ^{252}Cf source strike a sample. Intact molecular ions as high as 45 kDa have been observed in a time-of-flight PDMS instrument,[112] but ^{252}Cf is a relatively low producer of ion current (~5000 decays per second in all directions) requiring a mass spectrometer that can simultaneously collect spectra of all species produced. For this reason, ^{252}Cf has most often been coupled to TOF-MS and FTICR-MS,[111, 113-115] to be discussed below. With polymers, ^{252}Cf PDMS has mostly been used as a surface sputtering ion source and, occasionally, as an ionization initiator for mass spectrometric kinetic studies.[116-119]

Fast atom bombardment (FAB), a variation of SIMS utilizing neutral species, was the next contender to provide high mass molecular ions to mass analyzers.[105-107] It is capable of producing ions up to ~20 kDa for samples that can be suspended or dissolved in low volatility liquids (typically glycerin) and accept or release a proton or, for many polymers, accept alkali metal cation attachment upon impact with a steady beam of Cs^0

or Xe^0 atoms.[120-122] It was often used in combination with collisional activation for MS^n experiments.[123, 124]

The development of new techniques to lift molecules and, more importantly, ions into the gas phase for mass spectrometric analysis has since entered a renaissance period in which increasingly higher mass molecules have been more readily mass analyzed. For instance, ions in the 3-5 kDa range were first ionized by field desorption (FD) in 1975.[125] For FD, the sample is deposited on a conductive filament emitter which is charged to several kilovolts, resulting in ion formation and desorption.[125-127] FD was the first of the so called "soft ionization" techniques, i. e. an ionization method that resulted in the production of a preponderance of intact molecular ions.

Laser desorption ionization (LDI or LDMS) has been used since the late 1970's to provide high mass ions for mass spectral analysis.[128, 129] A pulsed laser that is focused on a thin film or other condensed phase sample can result in the rapid vaporization of the sample and production of molecular ions of several possible types: radical molecular ions (as in EI), and/or ions due to adduction or losses of several varieties–$[M + H]^+$, $[M - H]^-$, $[M + \text{alkalai cation}]^+$, etc.[130] Although LDMS has been used succesfully to examine molecular ions to 200 kDa,[131] it requires direct deposition of energy into the analyte. It was studied extensively as a method for macromolecular desorption and ionization, and such studies led to the development of matrix assisted laser desorption/ionization (MALDI),[132] described below.

Electrospray ionization (ESI) was first used by Malcolm Dole as a polymer ion source for mass measurement with a Faraday cage detector, with the reported result of m/z 411,000 for a polystyrene sample.[133] This result has been the topic of much debate

due to the inability to discern the charge state of the sample.[134, 135] Fenn and co-workers coupled an ESI source to a mass spectrometer in 1984, [136, 137] and subsequently used this configuration to measure the molecular weights of polyethylene glycols (PEGs) up to 5 MDa with estimated charge states in excess of 4200.[138]

ESI is achieved by passing a dilute solution of the analyte through a narrow, hollow tip such as a conductive capillary to which is applied a high, static voltage (usually 1-3 kV); typically, a salt or an acid is added to the solution as a source of charge. The charging of the droplet that emerges from the tip causes the formation of a Taylor cone from which a stream of charged droplets flies outward.[139, 140] The electrospray process occurs at atmospheric pressure and then the spray is directed into the vacuum system of the mass spectrometer through a small orifice or capillary where evaporation of the droplets occurs; when the force of repulsion due to the surface charge exceeds the surface tension of the droplet, the droplet explodes. This continues several times until the molecule is delivered into the gas phase with the remaining charge intact. There are two popular models for this mechanism: the charged residue model in which the ion is the remainder after all the solvent has evaporated[133] and the ion evaporation model in which the ion desorbs from the droplet surface as the electric field increases due to droplet shrinkage.[141-143]

One obvious advantage of ESI over other polymer desorption and ionization methods is the ability to couple directly to the atmospheric pressure outlet of an HPLC column.[144-151] Coupled with gel permeation chromatography (GPC), ESI-FTICR-MS has been integral in examining polymers that do not separate comparably to any calibrant due to mixtures of structures within the polymer distribution.[67-71, 120] Pre-fractionation of this

type is also integral in minimizing the mass discrimination that plagues ESI and MALDI (below); smaller molecules of similar structure will take more charges (e.g., protons or cations for positively charged species) that their larger counterparts on a charge site basis.[152]

IONIZATION: MALDI

Matrix assisted laser desorption ionization (MALDI)[132, 153] is a favorite among polymer mass spectrometrists for its ease of sample preparation. Producing mostly singly charge ions, it is unmatched for simplicity of data interpretation. It is reasonably reproducible from experiment to experiment and sample to sample (although the shot-to-shot variation in ion abundance can present problems in certain cases where signal averaging is a must). And, MALDI's mass range is unmatched with respect to mass-to-charge range. MALDI has demonstrated utility for the analysis of a wide variety of synthetic polymers with distinctly different chemical properties. By choosing the appropriate matrix, MALDI can be applied to polar or non-polar, water soluble or organic soluble polymers.[154-156] New matrices and charge transfer approaches are continually being developed.

Most MALDI polymer analysis to date has been carried out using time-of-flight mass spectrometry (TOF-MS), which offers rapid analysis and a high mass capability that can be used to analyze polymers up to several hundred thousand Daltons in molecular weight.[157] Resolution in conventional MALDI-TOF is sufficient to provide separation of individual oligomer units. Methods have been developed to use the masses of the repeat units measured by MALDI-TOF to determine the end-group and repeat unit

masses.[37, 157-160] The error in the TOF-MS mass measurements reduces the certainty in making a chemical assignment for complex samples such as copolymers.[161]

The application of FTMS to MALDI polymer analysis offers improvements in resolution and mass accuracy over TOF-MS. Early reports for MALDI-FTICR-MS of polymers illustrated the ability to trap oligomers up to 14,000 Da.[162] Characterization of molecular weight distributions was carried out by Dey and coworkers by calculating weight and number averages for poly(etheylene) glycol (PEG) distributions.[163] De Koster and coworkers utilized the high resolution of FTMS to determine end-group masses to within 5 ppm for masses under 1000 Da and to within 40 ppm for masses under 4000 Da by using linear regression of the isotopically resolved repeat masses.[164] FTMS is particularly useful for analyzing polymers less than 10 kDa in molecular weight. Such low molecular weight polymers have great commercial significance, particularly as pre-polymers and as subunits for graft copolymers. Improved methods are needed in this mass range for making accurate determination of polymer structures, in particular their molecular weight and end group composition.

In general, MALDI is implemented in FTMS mass spectrometry using one of two approaches. The first is to form ions within or adjacent to the ICR cell, and is commonly referred to as internal MALDI. Internal laser desorption ionization was utilized in the first commercial instrument, the Nicolet FTMS-1000, in which a laser beam was directed through the analyzer cell onto a sample probe for laser desorption (LD). Since MALDI can be performed under the high vacuum required of FTICR-MS, this arrangement is readily implemented, and has been quite successful for a number of applications.[165-173] An advantage of this arrangement is that high trapping efficiency can be obtained for ions

generated near the analyzer cell, since they do not have to be focused across magnetic field gradients or through conductance limits. High trapping efficiency results in increased sensitivity as has been demonstrated by the detection of attomole amounts of peptides using a microdeposition technique with internal MALDI by Marshall and coworkers.[174]

A second configuration used for MALDI-FTICR-MS experiments utilizes external ion generation, in which ions are formed outside of the magnetic field and transported to the analyzer cell. Such MALDI instruments derive from the tandem quadrupole FTICR-MS developed by McIver and coworkers[175] or from the differentially pumped source of Kofel and coworkers.[176] External source MALDI uses either electrostatic ion optics or RF ion guides to achieve spatial focusing of the ions as they travel to the cell. The ion source is differentially pumped, and is isolated from the analyzer by a series of conductance limits. Using an external ion source for MALDI-FTICR-MS experiments, McIver recently reported mass resolution of 830,000 (FWHM) for human insulin and 81,000 (FWHM) for cytochrome C in a 4.7 T instrument.[177] While the external source design has demonstrated excellent performance for proteins, it has been shown, and much of the focus of this dissertation shall be to confirm, that the internal source has some key advantages for polymer analysis, namely that a wide range of masses may be trapped and analyzed with high mass accuracy.

MASS ANALYZERS

Mere development of methods for producing gas phase ions of high molecular weight only partially explains the early, slow development of mass spectrometry as a

polymer analysis tool. The development of accurate detectors with sufficient resolution to elicit structural information was key to the growth of polymer mass spectrometry. Although sensitivity can become an issue due to sample preparation, volatilization, and ionization issues, sample availability is rarely a problem.

SECTOR, QUADRUPOLE, TOF, QIT

The double focusing sector mass spectrometer consists of a magnet that functions as a mass-to-charge analyzer and an electrostatic sector that separates these ions by their kinetic energy. A continuous ion beam is required making it irrelevant to the special cases involving pulsed ion sources like MALDI. However, sector instruments have an upper mass limit of approximately 10,000 Da which is comparable to FTICR-MS in spite of the relatively low resolution provided by the sector instruments (at least, with respect to FTICR mass spectrometers). In a typical (although not exclusive) arrangement of the double focusing sector mass analyzer, an electrostatic analyzer (ESA) is placed at the ion beam entrance to the mass spectrometer. The ion beam enters with a distribution of energies, but generally within a narrow kinetic energy range of a few kV. Although the ESA is more useful as a selector for fragment ions from a given precursor, with intact molecular ions of high mass-to-charge it can serve as a beam monochrometer for the magnetic sector which follows thereby improving mass resolution. In the magnetic sector, ions of a given mass-to-charge are selected by adjusting the magnetic field strength. The selected mass-to-charge will follow the radius of curvature of the flight tube and reach a detector along the resultant path, governed by the equation

$$\frac{m}{z} = \frac{B^2 r^2}{2V} \tag{7}$$

where B is the magnetic field strength, V is the ion beam energy, and r is the radius of the path of the ion.

Quadrupole mass analyzers, consisting of four, parallel, round rods arranged equidistance from a central point use a combination of rF and DC electric fields to contain (and release) ions of a variety of mass-to-charge ratios. The rF and DC fields are scanned to sequentially deliver ions of different m/z to a detector. The quadrupole mass analyzer is by far the simplest to manufacture and to interface to a computer, but it has a limited mass range (typically below 4000 m/z units) and low resolution for ions greater than m/z 1000.

Time-of-flight analyzers represent a vast improvement over the sector and quadrupole mass analyzers in that they simultaneously analyze the entire range of mass-to-charge produced, opening up the possibility of using the pulsed soft ion sources such as SIMS, FAB, LDI, and MALDI. The mass-to-charge range is essentially only limited by the detection clock or the length of the flight tube, since detection involves acceleration of the ions to high kinetic energy with a pulsed electric potential resulting in all ions having

$$E_{kinetic} = \frac{m V^2}{2 z} = \frac{m l^2}{2 z t^2} \tag{8}$$

where V, the velocity, is related to the length of the flight tube, l, and the time of flight. $E_{kinetic}$ is equal to the applied potential plus any energy spread due to the ionization event;

methods have been developed that can reduce the spread in initial kinetic energies, thereby improving resolution. This leaves the resolution essentially a function of the m/z and the length of the flight tube. In practice, the resolution is isotopic up to about 5 kDa and for polymers baseline resolution of individual oligomers can be seen to about 100 kDa. The absolute mass range is continually growing, with a recent high mass example being 1.5 MDa for a sample of polystyrene.[178]

FTICR-MS

FTICR-MS is the most recent development in the long history of mass analysis using the principle of the cyclotron accelerator, dating back to 1949 with the Omegatron (Figure 1.3).[1, 179-181] This instrument employed wires to provide a low amplitude DC field to contain ions formed by electron impact ionization within a magnetic field. A pair of flat electrodes was used to resonantly excite the ions' cyclotron radius until they struck a collector attached to an ion multiplier. At the time, poor quality magnets (low field and inconsistent field homogeneity) and vacuum technology severely limited the resolution and mass range of the technique, relegating it to the workmanlike jobs of leak detection and low mass isotope analyzer, tasks it still performs today as nuclear reactor plasma and residual gas analyzer.[2, 182-186]

The development of methods for achieving high (and then ultrahigh) vacuum,[187-189] and the developments in ionization, excitation, and detection greatly improved the analytical utility of the Omegatron.[190] These techniques were liberally borrowed from another new cyclotron analysis method, dubbed ion cyclotron resonance (ICR).[191-194] In addition to the application of an experimental sequence in preference to continuous

ionization, ion generation and detection in ICR occurred in different regions of a drift cell.[195] After EI ionization, ions were induced to drift perpendicular to the magnetic field by a DC voltage, resulting in a Lorentz force that delivered the ions into the analyzer for excitation and detection. A single frequency rF field was applied and the magnetic field swept, resulting in ion radial excitation as the mass-to-charge came into resonance with the swept magnetic field and the applied electronic rF field. Detection involved first sensing the resonant ions' mass-to-charge ratio via the power loss in a marginal oscillator circuit followed by abundance measurement utilizing total ion current from direct collection at a grounded plate.

Although a DC offset was applied in the detector region of the drift cell, ions were not so much stored as prevented from striking the analyzer. The first true ICR trap, introduced by McIver in 1970,[196] was a single, six plate box in which ions were generated, stored for upwards of 1 second, subjected to excitation, and detected. For the first time, the electron beam was turned off after ion generation thereby eliminating electronic noise and one source of space charge that had plagued the Omegatron and ICR experiments.

The full potential of the ICR experiment moved a giant step closer to realization in 1974 with the introduction of the Fourier Transform ICR (FTICR)[10, 197-200] In FTICR, the ion cyclotron radius is expanded to a level short of the detector cell radius for all species in the ICR cell at once by application of a swept rF field, instead of by sweeping through the magnetic fields. These ions induce a current on an opposing pair of the trap electrodes which is digitized so that a fast Fourier transform (FFT)[201] can extract the magnitude and frequency of each species present.

Salient points in this method are that all ions are detected simultaneously without regard to their mass-to-charge ratio and that the resolution is greatly improved over swept magnetic field versions of the ICR, with initial reports setting resolution at 500,000 (exceeding even the limits imposed by field homogeneity).[201, 202204, 205] This was largely attributed to the symmetric canceling of magnetic field inhomogeneities in the resulting, coherent, circular orbit of the ions.[12, 206, 207]

FTICR-MS FUNDAMENTALS

The fundamental principle of the cyclotron experiment, in all its incarnations, is that a charged particle travelling in a magnetic field experiences the Lorentz force, F_L, an impetus in the direction perpendicular to both the particle velocity vector, V, and the magnetic field vector, B:

$$\vec{F}_L = q\vec{V} \otimes \vec{B} \tag{9}$$

where q is the fundamental charge. If the field is homogeneous as in the FTICR experiment, the Lorentz force is inward and results in containment of motion within the plane perpendicular to the magnetic field. Moreover, since the ion has mass, this inward force is countered by the centripetal force of the resultant new velocity vector effected due to the acceleration of the Lorentz force causing the ion to settle into a circular trajectory with a characteristic frequency (ω_c, the cyclotron angular velocity shown in Figure 1.4) dependent on the ion's mass (m), charge, and the magnetic field strength:

$$\omega_c = \frac{qB}{m} \tag{10}$$

Figure 1.3: A modern Omegatron mass analyzer. The RF field is swept, here, but the ions are still quantified by the collector, as in the classic, swept magnetic field form of the instrument.

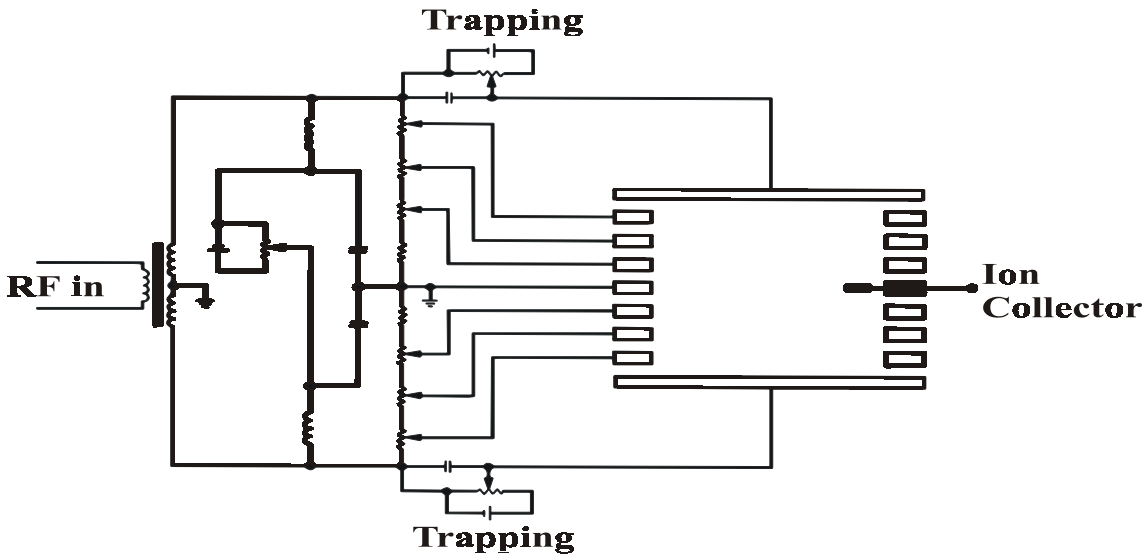
Trapping
RF in
Ion
Collector
Trapping

This equation is especially useful for mass spectrometry because it relates frequency (which is easily measured with high precision and accuracy) to the mass-to-charge ratio, m/q. The frequency is independent of radius which, in turn, means that it is also independent of ion kinetic energy; this is an important point since the ions are measured at an expanded radius that can only be estimated based on signal strength and applied excitation.[208-212] And, the FTICR avoids the complications involved with energy compensation as seen in other mass spectrometric systems dependent on acceleration schemes (such as magnetic sector and time-of-flight instrumentation).[213-217]

Ions contained in the FTICR homogenous region require some additional trapping scheme to prevent longitudinal loss, i.e., along the magnetic field vector, since the cross product of parallel vectors is zero. Most often, this trapping architecture takes the form of an applied DC electric field which creates a three dimensional potential "well" between the two ends of the trapping region. Ions moving along the magnetic field axis can penetrate the potential field to a point equal to their maximum axial kinetic energy, at which point they are reaccelerated in the opposite direction. In most cells, the DC potential assumes a quadratic geometric form, as seen in Figure 1.5, resulting in oscillatory movement of the ions with the characteristic frequency :

$$\omega_T = \frac{2}{a}\sqrt{\frac{qV_T}{m}} \tag{11}$$

where ω_T is the trapping oscillation frequency, a is the trap separation, and V_T the trapping voltage maximum. Typically, ω_T is considered neglible with respect to ω_c in spite of the m/z dependence of ω_T ; however, resonant excitation of this frequency can result in axial expansion causing ion loss and/or line broadening.[218-228]

Figure 1.4: The origin of the cyclotron frequency. A charged particle with a linear velocity (V_0 at time = 0, $V = r\Omega$ at time > 0) experiences a force equal to the cross product of the magnetic field vector, B, with the ion's charge, q, and it's velocity vector, V. This is countered by the centripetal force, $F = mr\Omega^2$, exerted on the orbiting ion.

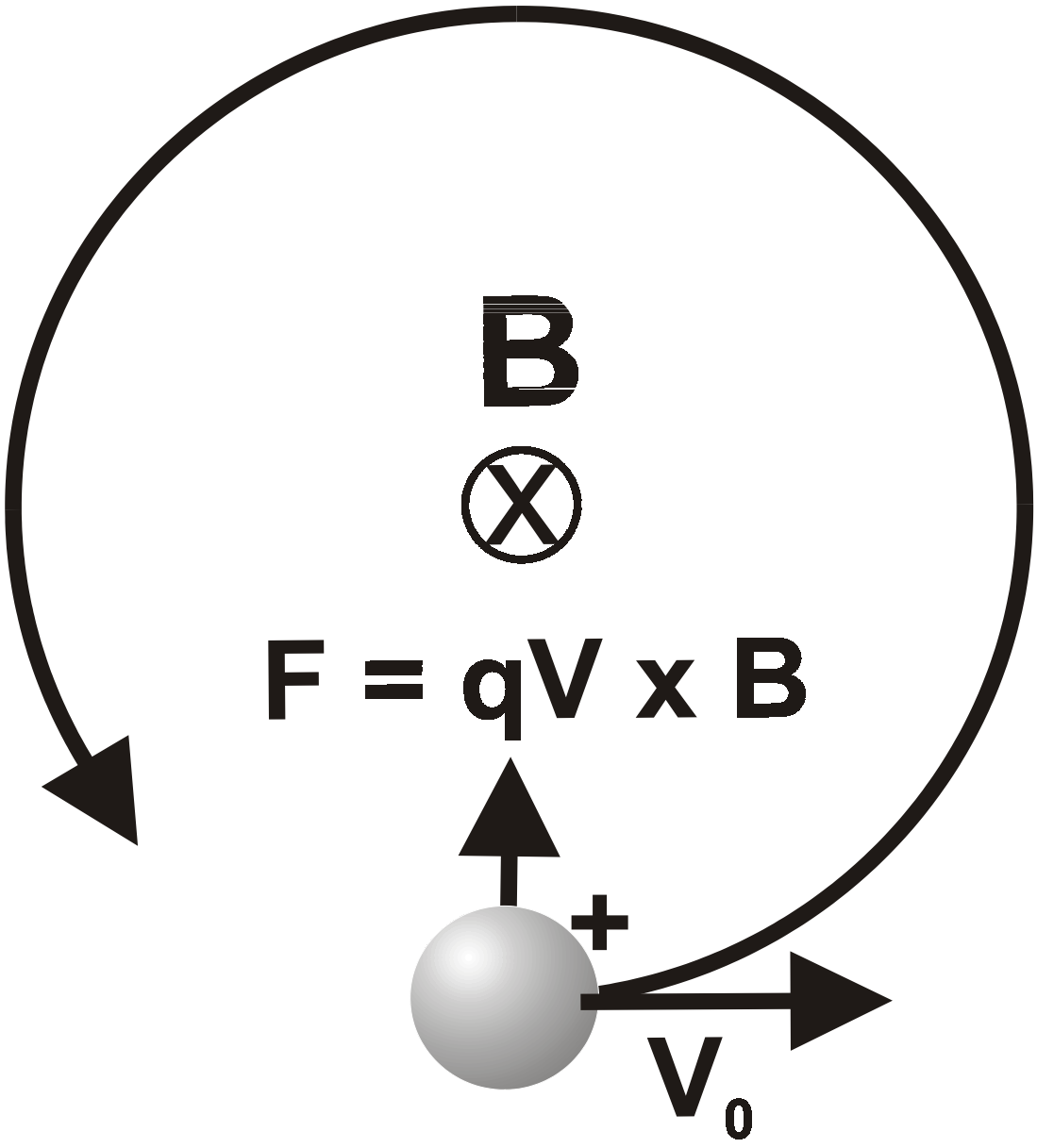
B
⊗
F = qV x B
+
V0

However, another frequency component, the magnetron frequency (T_M), which exists due to the combination of trapping potential and the magnetic field, cannot be ignored in detection.[229-233] The quadratic variation, shown in Figure 1.6, that comprises the electric trapping field gradient has a maximum at the cell's centerline, but decreases to ground potential at the cell electrodes, resulting in an accelerating potential perpendicular to the magnetic field gradient. As ions move down this potential they, once again, experience the Lorentz force, this time opposed by the trapping potential. This is the source of T_M, which causes the ions to slowly course around the cell at a characterizable rate:

$$\omega_M = \frac{2\,\alpha\,V_T}{d^2\,B} \tag{12}$$

where " is a geometry factor for the cell configuration, V is the centerline DC trapping potential, and d is the distance separating opposing excite or detect electrodes. This frequency is usually left unreported in the FTICR experiment because it is independent of mass and charge and because it is compensated easily in calibration of the spectrum (see the introduction to Chapter 3). However, resonant excitation of this mode of ion motion is possible and must be considered, if not for its effect on calibration, then because of the additional radial component that can cause ion ejection.[228230-233] Artifact peaks due to magnetron motion,[234-236] known as sidebands, can also interfere with analysis of isobaric species (i.e., peaks of nominally the same mass but of differing elemental composition).[237]

The FTICR experiment is achieved by addition of translational energy to the trapped ions via an electric field, most often as a linearly applied sinusoidal field

Figure 1.5: The origin of the trapping oscillation. Cutaway of the cylindrical FTICR analyzer. The cell plates at the two ends are held at a DC potential to trap ions in the central analyzer region. The calculated potential field along the central plane of the cell is shown below to demonstrate the trapping well in which ions oscillate between the opposing trapping potentials that equal the ions' maximum translational energies.

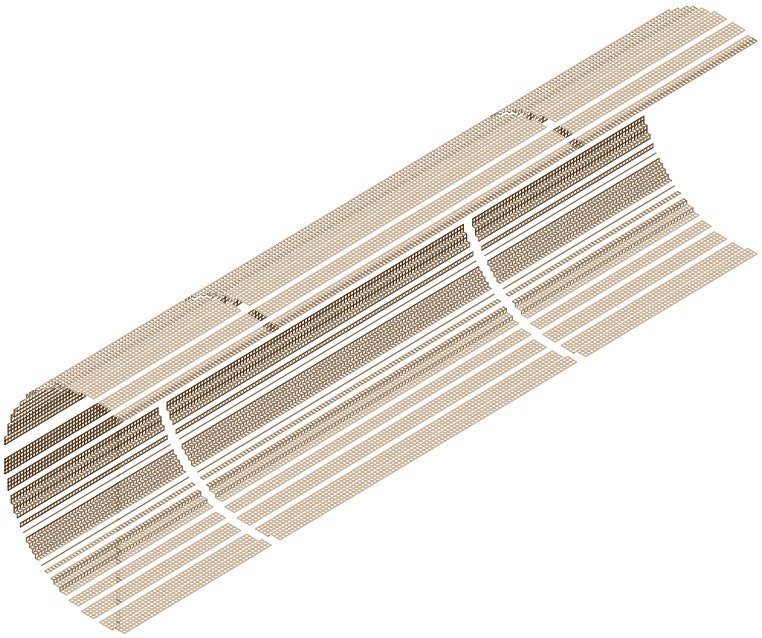

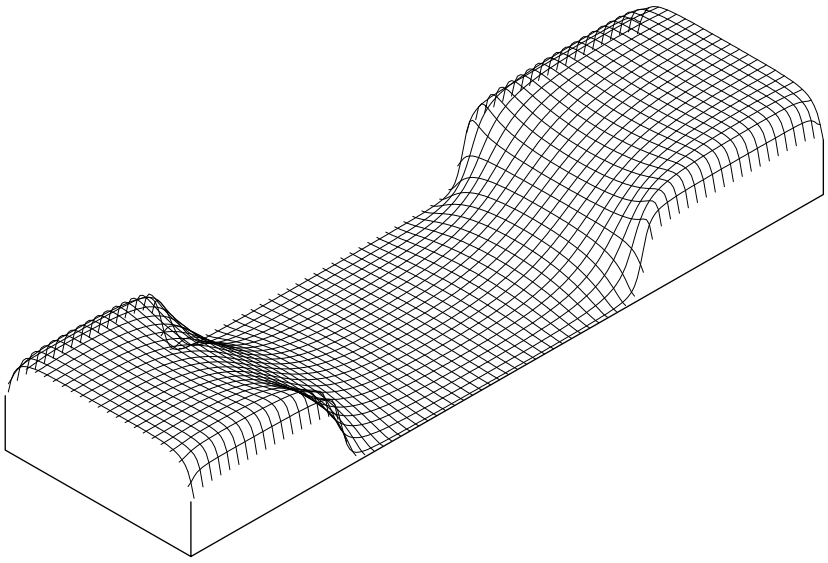

resonant with the cyclotron frequencies of the ions to be excited.[212, 218, 225, 234, 238, 239] Lawrence showed that such a resonant rF field would cause expansion of the ion cyclotron radius linearly with time and proportionally to the magnitude of the applied potential.[240, 241] Once the radius expands enough that the ions contact the cell plates, they are neutralized and pumped away; this is frequently used to discharge unwanted species from the experiment.[228, 242-245] If, on the other hand, rF excitation is ended before radial ejection occurs, then the ions thus excited will retain their new orbit until some transfer of energy returns them toward the center of the cell (or another mode of ejection occurs). At the higher radius, the ions are nearer the detection electrodes so that the measured signal intensity is greater primarily by proximity. The signal is also greater due to the coherent motion of the ions of similar frequency, which occurs because the excitation signal forces the ions into the same phase comparable to a spinning monopole,[246] for which the magnitude is reduced as components lose phase coherence; this is the origin of the exponential damping effect noted in the transient signal of the FTICR. A schematic of the excitation and detection schemes for a cylindrical cell is shown in Figure 1.7.

The net result of the cyclotron equation is that ions, excited to a typical radius (say, 2 cm), travel large distances during an experiment. For example, in a 4.7 T FTICR, an ion of m/z = 1800 Da ($f_c = T_c/2B$ = 40055 Hz) will travel over 5 km/s in its circular orbit. Collisions with background gas phase species will, at the very least, knock this ion out of coherence with the other ions of similar m/z. This transfer of momentum could also activate unimolecular dissociation; or, expansion of the

Figure 1.6: The origin of magnetron motion. The trapping potential, shown here for the cross section of the cell at its longitudinal center, actually reaches a relative maximum at the radial center of the cell and falls of to ground as the coordinate extends radially toward the analyzer and excitation plates. Ions that "roll down" this potential hill experience the Lorentz force, $F = qV \times B$, again but this time it is opposed by the accelerating potential of the trapping field and the mass of the ion.

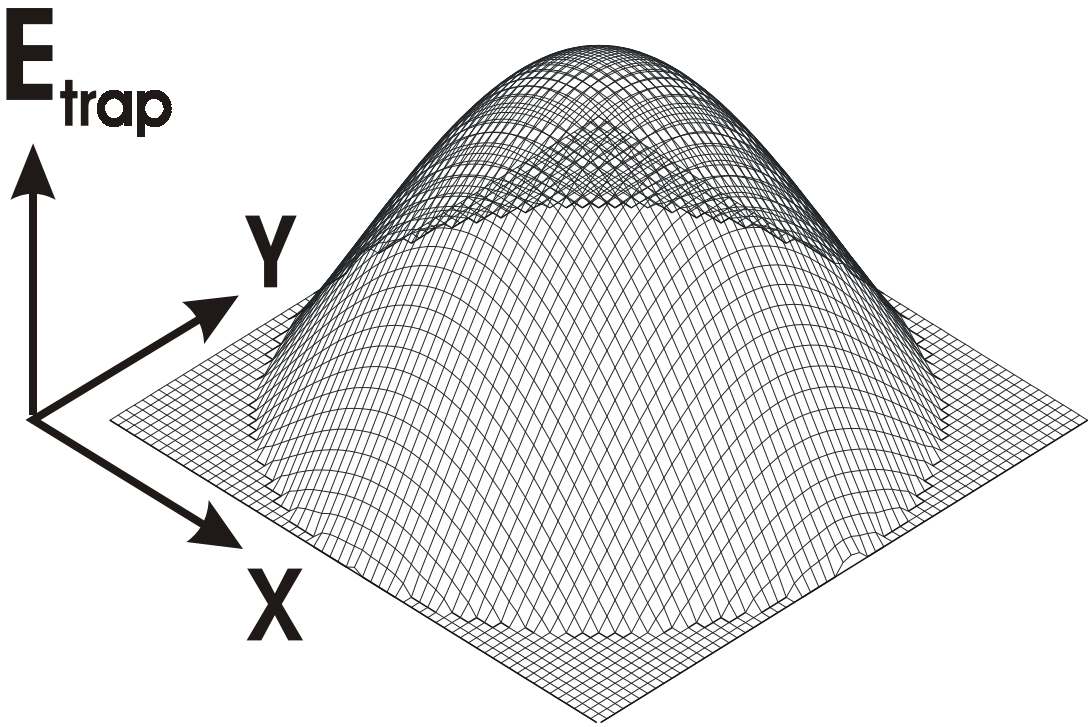
E trap
Y
X

magnetron radius (another consequence of high pressure collisions in the presence of the radially repulsive electric field) could cause radial ejection of the ion as the collision counteracts the retaining forces of, axially, the DC trapping field and, radially, the magnetic field.[229] This magnetron expansion occurs at a slow rate relative to the damping of cyclotron motion or trapping oscillations;[247] this is especially convenient since many applications of FTICR-MS require leaking reagent and/or buffer gases into the vacuum chamber temporarily. The rate of magnetron drift increases with V_T since the lowest quadrupolar trapping energy is at the maximum radius of the cell; therefore, lowering V_T prior to raising the pressure in the system can also attenuate the rate of magnetron expansion.

In order to excite the cyclotron motion of the ions within a broad m/z distribution, one of several schemes must be employed. The most often used form of broadband excitation is a linear sweep (or "chirp") across the frequency range of interest; this is adquate for most purposes in spite of the uneven power distribution delivered to the range of frequencies in the conversion from time- to frequency-domain.[238] Stored waveform inverse Fourier transform (SWIFT) excitation circumvents this problem by defining the desired power spectrum in the frequency domain first and then designing a time domain function to achieve it.[228, 248-252] The excitation waveform corresponds to the inverse Fourier transform of the power spectrum to be applied; the SWIFT function is written to a programmable frequency generator and delivered to the excitation plates of the cell. SWIFT, additionally, can be used to isolate ions while simultaneously ejecting others with front end resolution

Figure 1.7: Ions are accelerated by application of an rF electrical field, resonant with the ions' cyclotron frequency (ω_C), to opposing electrodes in the analyzer cell. Since ω_C is independent of radius, the only way for the velocity, $V = r\omega_C$, to increase is for the radius to expand. This brings the ions nearer to the detector plates, essentially antennae attached to fast amplifier circuits.

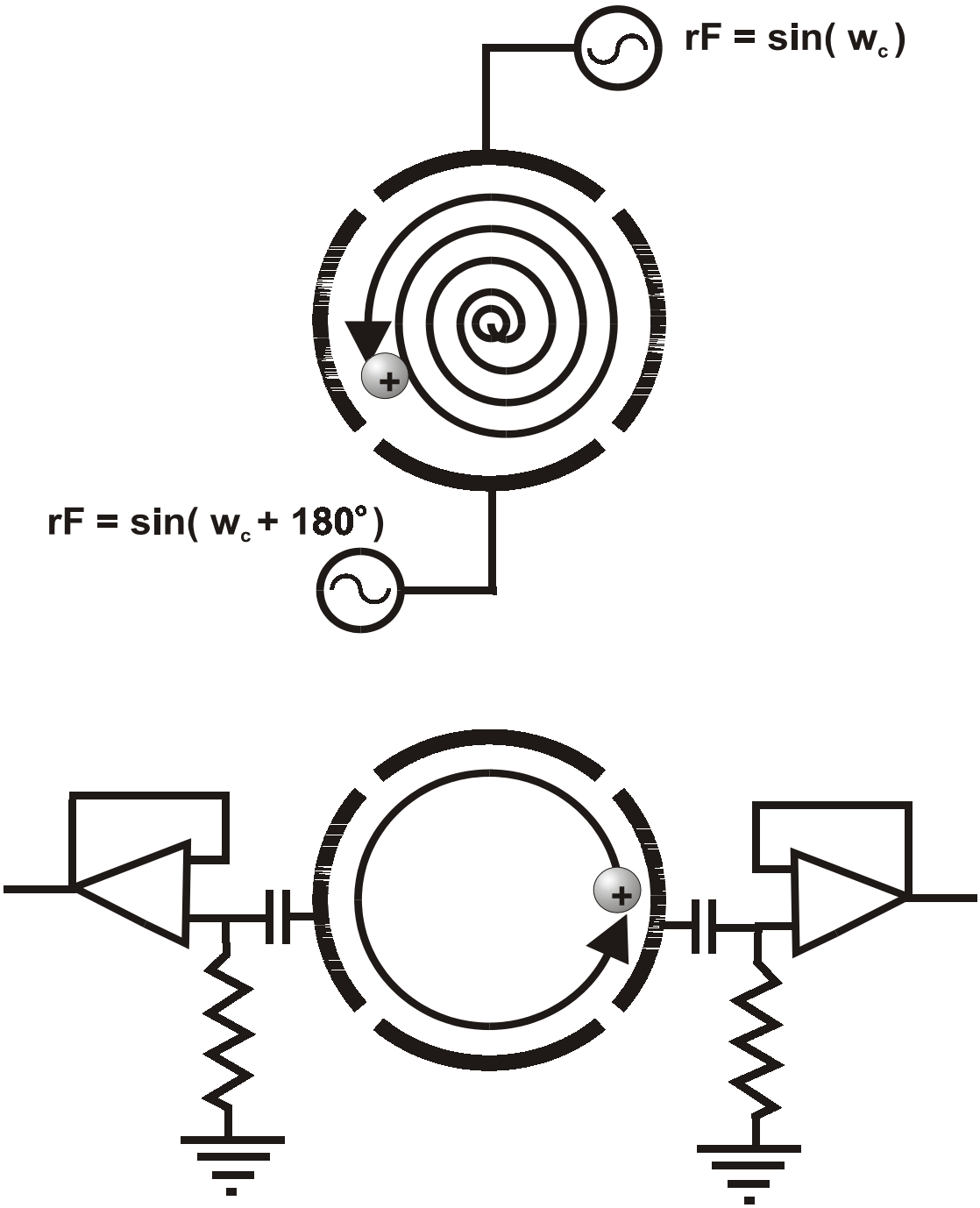
rF = sin(w_c)
rF = sin(w_c + 180°)

in excess of 29,000.[228] Alternative excitation modes such as use of filtered white noise[253, 254] in the frequency range of interest and impulse excitation[255] in which a single, high amplitude, square pulse of nearly negligible duration is applied to the excite plates have each been used with modest results.

As previously mentioned, expansion to high radius greatly increases the kinetic energy of the ions such that the energy transfer involved in their collisions with neutral molecules has the possibility of inducing fragmentation through unimolecular decomposition.[256-259] Manipulation of the equation for ion radius (for on resonance excitation) to calculate angular velocity and to include the mass of the ion yields us the kinetic energy of an ion:

$$E_{kinetic} = \frac{q^2\ B^2\ r^2}{2\ m} \tag{13}$$

The collision induced dissociation (CID) experiment, involves isolation of a narrowly defined species–the precursor ion–followed by introduction of neutral gas and rapid excitation to higher $E_{kinetic}$ so that collisions with the neutrals result in momentum transfer causing excitation of the vibrational modes of the precursor ion to a center of mass energy level, E_{com}, proportional to $E_{kinetic}$ and the mass, m_{gas}, of the collision gas:

$$E_{com} = E_{kinetic} \frac{m_{gas}}{m_{gas} + m_{ion}} \tag{14}$$

A delay allows removal of the collision gas and complete reaction of the excited ion (less distribution of the energy to the various degrees of freedom, therein), and the resulting distribution of ions excited and detected in the normal manner.[258-260] Due to

the nondestructive detection of ions in the FTICR-MS experiment, this experiment can be repeated by selecting a product ion for further examination (MS^n) thereby gaining greater insight into the structure of a substance.[261-268]

V. SCOPE OF THIS DISSERTATION

Following a description of the advantages to mass accuracy achieved by accounting for space charge frequency shifts due to variations in ion population in FTICR-MS, a description of one method of avoiding this problem, altogether, by accumulation of a calibrant in a spectrum after acquiring the analyte will be described. This technique has the added advantage of building up the signal of the analyte species for low abundance samples and for weakly ionizing analytes prior to injection of the internal calibrant.

Direct polymer applications of internal source MALDI-FTICR-MS follow, namely application of the technique to copolyester analysis and to block copolymer analysis. The polyester chapter also explores the use of low resolution GPC separation to improve mass distribution analysis by minimizing the polydispersity of the sample in any one experiment, thereby avoiding the problems of mass discrimination in highly polydisperse samples. End group identity, molecular weight distribution, and (for the copolyester samples) component distributions are identified as well. The component distribution analysis is revisited in Chapter VI with regard to block copolymer distributions for poly(styrene-block-methylstyrene). Ultrahigh resolution techniques are employed in both chapters to identify and quantify overlapping isotopic species known as isobars that would otherwise be mistaken for

another specie as well as resulting in peak broadening that would call the mass accuracy of the experiment into question.

The examination of polymers with MALDI source is rounded out with the direct comparison of the internal energy imparted to Nylon-6 molecules in an internal MALDI source to that of an external ESI source. These oligomer ions are isolated from the full distribution by ejection of the unwanted species and then excited to progressively higher kinetic energies in the presence of a collision gas and their breakdown behavior recorded. For completeness, the method of isolation prior to the dissociation step is interrogated following a method of completely thermalizing the trapped ions, as well.

REFERENCES

(1) Hipple, J. A.; Sommer, H.; Thomas, H. A. *Physical Review* **1950,** *78*, 332-332.

(2) Edwards, A. G. *British Journal of Applied Physics* **1955,** *6*, 44-48.

(3) Caldwell-Nichols, C. J.; Penzhorn, R. D.; Grunhagen, S.; Sirch, M.; George, J. *Fusion Eng. Des.* **2001,** *58-9*, 395-399.

(4) Furukawa, Y. *Inventing polymer science: Staudinger, Carothers, and the emergence of macromolecular chemistry*; University of Pennsylvania Press: Philadelphia, 1998.

(5) Bureau, U. C.;; Economics and Statistics Administration, US Department of Commerce: Washington, DC, 1962.

(6) Bureau, U. C.;; Economics and Statistics Administration, US Department of Commerce: Washington, DC, 1977.

(7) Bureau, U. C.;; Economics and Statistics Administration, US Department of Commerce: Washington, DC, 1997.

(8) Marshall, A. G. *Int. J. Mass Spectrom.* **2000,** *200*, 331-356.

(9) Marshall, A. G.; Hendrickson, C. L.; Jackson, G. S. *Mass Spectrom. Rev.* **1998,** *17*, 1-35.

(10) Comisarow, M. B.; Marshall, A. G. *J. Mass Spectrom.* **1996,** *31*, 581-585.

(11) Marshall, A. G.; Schweikhard, L. *International Journal Of Mass Spectrometry And Ion Processes, Sep* **1992,** *118*, 37-70.

(12) Marshall, A. G. *Accounts Chem. Res.* **1985,** *18*, 316-322.

(13) Marshall, A. G.; Grosshans, P. B. *Anal. Chem.* **1991,** *63*, A215-A229.

(14) Kauffman, G. In *Dictionary of Scientific Biography*; Gillispie, C. C., Ed.; Charles Scribner's Sons: New York, 1972, pp 492-494.

(15) Graham, T. *Journal of the Chemical Society of London* **1864,** *17*, 318-323.

(16) Hyatt, J. W., Jr.;: USA, 1870.

(17) White, J. L. *Int. Polym. Process.* **2000,** *15*, 2-2.

(18) Potter, H. V. *Chem. Ind.* **1945**, 251-253.

(19) Potter, H. V. *Chem. Ind.* **1945**, 242-&.

(20) White, J. L. *Int. Polym. Process.* **2001,** *16*, 222-222.

(21) Stern, H. J. *Chem. Br.* **1979,** *15*, 455-&.

(22) Svedberg, T. *Magyar Kemikusok Lapja* **1972,** *27*, 101-&.

(23) Svedberg, T. *Journal of Physical and Colloid Chemistry* **1947,** *51*, 1-18.

(24) Sihtola, H.; Svedberg, T. *Acta Chem. Scand.* **1948,** *2*, 474-485.

(25) Cecil, R.; Ogston, A. G. *Biochem. J.* **1948,** *43*, 592-598.

(26) Go, Y.; Noguchi, J.; Asai, M.; Hayakawa, T. *Journal of Polymer Science* **1956,** *21*, 147-150.

(27) Marsh, R. E.; Corey, R. B.; Pauling, L. *Biochimica Et Biophysica Acta* **1955,** *16*, 1-34.

(28) Carothers, W. H.;; E. I. du Pont de Nemours & Company: United States, 1938.

(29) Flory, P. J. *Chem. Rev.* **1946,** *39*, 137-197.

(30) Zhou, C. R. *J. Appl. Polym. Sci.* **1992,** *44*, 383-385.

(31) Steele, D. *Theory of Vibrational Spectroscopy*; Saunders: Philadelphia, 1971.

(32) Coleman, B. D.; Markovitz, H. *J. Appl. Phys.* **1964,** *35*, 1-&.

(33) Prebus, A. F.; Zlotowski, I. *Physical Review* **1945,** *67*, 202-202.

(34) Ibell, T.; Burgoyne, C. *ACI Struct. J.* **1999,** *96*, 997-1002.

(35) Flossdorf, F. J. *Stahl Eisen* **1985,** *105*, 77-83.

(36) Flory, P. J. *Principles of polymer chemistry*, 1 ed.; Cornell University Press: Ithaca, New York, 1953.

(37) Vanrooij, G. J.; Duursma, M. C.; Heeren, R. M. A.; Boon, J. J.; Dekoster, C. G. *J. Am. Soc. Mass Spectrom.* **1996,** *7*, 449-457.

(38) Beckman, E. *Physical Chemistry* **1889,** *4*, 532-538.

(39) Hill, F. N.; Brown, A. *Anal. Chem.* **1950,** *22*, 562-564.

(40) Ray, N. H. *Transactions of the Faraday Society* **1952,** *48*, 809-812.

(41) Anderson, J. R. *Anal. Chem.* **1955,** *27*, 864-864.

(42) Smith, H. *Transactions of the Faraday Society* **1956,** *52*, 402-409.

(43) Glover, C. A. *Advances in Chemistry Series* **1973**, 1-8.

(44) Davison, G. In *Analysis of polymer systems*; Bark, L. S., Allen, N. S., Eds.; Applied Science Publishers, LTD: Barking, Essex, England, 1982.

(45) Dohner, R. E.; Wachter, A. H.; Simon, W. *Helv. Chim. Acta* **1967,** *50*, 2193-&.

(46) Hansen, E. H.; Schnitze.M *Anal. Chim. Acta* **1969,** *46*, 247-&.

(47) Wachter, A. H.; Simon, W. *Anal. Chem.* **1969,** *41*, 90-&.

(48) Bersted, B. H. *J. Appl. Polym. Sci.* **1973,** *17*, 1415-1430.

(49) Hunt, B. In *Modern Techniques for Polymer Characterisation*; Pethrick, R. A., Dawkins, J. V., Eds.; John Wiley and Sons: New York, 1999.

(50) Eirich, F.; Riseman, J. *Journal of Polymer Science* **1949,** *4*, 417-434.

(51) Cleverdon, D.; Smith, P. G. *Chem. Ind.* **1951**, 937-937.

(52) Streeter, D. J.; Boyer, R. F. *Industrial and Engineering Chemistry* **1951,** *43*, 1790-1797.

(53) Bywater, S. *Chem. Ind.* **1952**, 67-67.

(54) Gundiah, S.; Kapur, S. L. *Journal of Polymer Science* **1962,** *57*, 373-&.

(55) Suzuki, H.; Leonis, C. G.; Gordon, M. *Makromolekulare Chemie-Macromolecular Chemistry and Physics* **1973,** *172*, 227-231.

(56) Gordon, M.; Leonis, C. G.; Suzuki, H. *Proc. R. Soc. London Ser. A-Math. Phys. Eng. Sci.* **1975,** *345*, 207-&.

(57) Leonis, C. G.; Suzuki, H.; Gordon, M. *Makromolekulare Chemie-Macromolecular Chemistry and Physics* **1977,** *178*, 2867-2886.

(58) Mattern, D. E.; Hercules, D. M. *Anal. Chem.* **1985,** *57*, 2041-2046.

(59) Hatada, K.; Ute, K.; Kashiyama, M. *Polym. J.* **1990,** *22*, 853-857.

(60) Kitayama, T.; Kishiro, S.; Masuda, E.; Hatada, K. *Polym. Bull.* **1991,** *25*, 205-209.

(61) Koenig, J. L. *Spectroscopy of polymers*; Elsevier: Amsterdam, 1999.

(62) Ouano, A. C.; Mercier, P. L. *Journal of Polymer Science Part C-Polymer Symposium* **1968**, 309-&.

(63) Ouano, A. C.; Kaye, W. *J. Polym. Sci. Pol. Chem.* **1974,** *12*, 1151-1162.

(64) Ouano, A. C.; Tu, Y. O.; Carothers, J. A. *IEEE Trans. Electron Devices* **1976,** *23*, 1253-1254.

(65) Ouano, A. C.; Dawson, B. L.; Johnson, D. E. *Abstr. Pap. Am. Chem. Soc.* **1976,** *172*, 177-177.

(66) Yun, H.; Olesik, S. V.; Marti, E. H. *J. Microcolumn Sep.* **1999,** *11*, 53-61.

(67) Prokai, L.; Simonsick, W. J. *Rapid Commun. Mass Spectrom.* **1993,** *7*, 853-856.

(68) Simonsick, W. J.; Ross, C. W.; Prokai, L. *Abstr. Pap. Am. Chem. Soc.* **1996,** *211*, 259-POLY.

(69) Prokai, L.; Kim, H. S.; Zharikova, A.; Roboz, J.; Ma, L.; Deng, L.; Simonsick, W. J. *J. Chromatogr. A* **1998,** *800*, 59-68.

(70) Aaserud, D. J.; Prokai, L.; Simonsick, W. J. *Anal. Chem.* **1999,** *71*, 4793-4799.

(71) Prokai, L.; Aaserud, D. J.; Simonsick, W. J. *J. Chromatogr. A* **1999,** *835*, 121-126.

(72) Jones, D. W.; Hall, G. C.; Sutow, E. J.; Langman, M. F.; Robertson, K. N. *J. Dent. Res.* **1991,** *70*, 874-879.

(73) Kunitani, M.; Dollinger, G.; Johnson, D.; Kresin, L. *Journal of Chromatography* **1991,** *588*, 125-137.

(74) Meyer, G. A.; Lostritto, R. T.; Johnson, J. F. *J. Appl. Polym. Sci.* **1991,** *42*, 2247-2253.

(75) Cheung, P.; Balke, S. T.; Mourey, T. H. *J. Liq. Chromatogr.* **1992,** *15*, 39-69.

(76) Cortes, H. J.; Bormett, G. E.; Graham, J. D. *J. Microcolumn Sep.* **1992,** *4*, 51-57.

(77) Cheng, R. S.; Zhao, S. I. *Acs Symposium Series* **1993,** *521*, 113-121.

(78) Konas, M.; Moy, T. M.; Rogers, M. E.; Shultz, A. R.; Ward, T. C.; McGrath, J. E. *J. Polym. Sci. Pt. B-Polym. Phys.* **1995,** *33*, 1429-1439.

(79) Florea, M. *J. Chromatogr. A* **2000,** *878*, 1-15.

(80) Tang, H. X.; Foran, B.; Martin, D. C. *Polym. Eng. Sci.* **2001,** *41*, 440-448.

(81);, 2002.

(82) Eliseev, V. S. *Journal of Applied Chemistry of the Ussr* **1980,** *53*, 430-432.

(83) Marzec, A. *Fresenius Zeitschrift Fur Analytische Chemie* **1984,** *318*, 445-445.

(84) Genuit, W.; Boon, J. J. *J. Anal. Appl. Pyrolysis* **1985,** *8*, 25-40.

(85) Marzec, A. *J. Anal. Appl. Pyrolysis* **1985,** *8*, 241-254.

(86) Lucht, L. M.; Hill, M. E.; Peppas, N. A. *Angew. Makromol. Chem.* **1987,** *150*, 123-136.

(87) Schulze, T.; Michaelis, W. *Org. Geochem.* **1990,** *16*, 1051-1058.

(88) Biemann, K. *Annu. Rev. Biochem.* **1963,** *32*, 755-&.

(89) Bullock, J. *Journal of Chromatography* **1993,** *645*, 169-177.

(90) Wallingford, R. A. *Anal. Chem.* **1996,** *68*, 2541-2548.

(91) Kok, W. T.; Stol, R.; Tijssen, R. *Anal. Chem.* **2000,** *72*, 468A-476A.

(92) Schulten, H. R.; Lattimer, R. P. *Mass Spectrom. Rev.* **1984,** *3*, 231-315.

(93) Wiley, R. H. *Macromolecular Reviews Part D-Journal of Polymer Science* **1979,** *14*, 379-417.

(94) Schulten, H. R.; Gortz, W. *Anal. Chem.* **1978,** *50*, 428-433.

(95) Lum, R. M. *Abstr. Pap. Am. Chem. Soc.* **1977,** *173*, 141-141.

(96) Schulten, H. R.; Beckey, H. D.; Meuzelaa.Hl; Boerboom, A. J. *Anal. Chem.* **1973,** *45*, 191-195.

(97) Schulten, H. R.; Dussel, H. J. *J. Anal. Appl. Pyrolysis* **1981,** *2*, 293-308.

(98) Dussel, H. J.; Recca, A.; Kolb, J.; Hummel, D. O.; Stille, J. K. *J. Anal. Appl. Pyrolysis* **1982,** *3*, 307-325.

(99) Plage, B.; Schulten, H. R. *Angew. Makromol. Chem.* **1991,** *184*, 133-146.

(100) Lattimer, R. P. *J. Anal. Appl. Pyrolysis* **1995,** *31*, 203-225.

(101) Wilcken, H.; Schulten, H. R. *Anal. Chim. Acta* **1996,** *336*, 201-208.

(102) Lattimer, R. P. *J. Anal. Appl. Pyrolysis* **1997,** *39*, 115-127.

(103) Benninghoven, A. *Surf. Sci.* **1971,** *28*, 541-&.

(104) Huber, W. K.; Selhofer, H.; Benningh.A *Journal of Vacuum Science & Technology* **1972,** *9*, 482-&.

(105) Barber, M.; Bordoli, R. S.; Sedgwick, R. D.; Tyler, A. N. *Nature* **1981,** *293*, 270-275.

(106) Morris, H. R.; Panico, M.; Barber, M.; Bordoli, R. S.; Sedgwick, R. D.; Tyler, A. *Biochem. Biophys. Res. Commun.* **1981,** *101*, 623-631.

(107) Barber, M.; Bordoli, R. S.; Sedgwick, R. D.; Tyler, A. N. *J. Chem. Soc.-Chem. Commun.* **1981**, 325-327.

(108) Evans, C. A. *Anal. Chem.* **1972,** *44*, 67A.

(109) Bletsos, I. M.; Hercules, D. M.; Greifendorf, D.; Benninghoven, A. *Anal. Chem.* **1985,** *57*, 2384.

(110) Torgerson, D. F.; Macfarlane, R. D. *Bulletin of the American Physical Society* **1975,** *20*, 1182-1182.

(111) Macfarlane, R. D.; Torgerson, D. F. *Int. J. Mass Spectrom. Ion Process.* **1976,** *21*, 81-92.

(112) Ens, W.; Sundqvist, B. U. R.; Hakansson, P.; Hedin, A.; Jonsson, G. *Phys. Rev. B* **1989,** *39*, 763-766.

(113) Loo, J. A.; Williams, E. R.; Amster, I. J.; Furlong, J. J. P.; Wang, B. H.; McLafferty, F. W.; Chait, B. T.; Field, F. H. *Anal. Chem.* **1987,** *59*, 1880-1882.

(114) Williams, E. R.; McLafferty, F. W. *J. Am. Soc. Mass Spectrom.* **1990,** *1*, 427-430.

(115) Amster, I. J.; Loo, J. A.; Furlong, J. P.; McLafferty, F. W. *Anal. Chem.* **1987,** *59*, 313-317.

(116) Macfarlane, R. D. *Trac-Trends Anal. Chem.* **1988,** *7*, 179-183.

(117) Quinones, L.; Schweikert, E. A. *J. Vac. Sci. Technol. A-Vac. Surf. Films* **1988,** *6*, 946-949.

(118) Cox, B. D.; Park, M. A.; Kaercher, R. G.; Schweikert, E. A. *Anal. Chem.* **1992,** *64*, 843-847.

(119) Kissel, J.; Krueger, F. R. *Rapid Commun. Mass Spectrom.* **2001,** *15*, 1713-1718.

(120) Prokai, L.; Simonsick, W. J. *Macromolecules* **1992,** *25*, 6532-6539.

(121) Williams, D. H.; Naylor, S. *J. Chem. Soc.-Chem. Commun.* **1987**, 1408-1409.

(122) Williams, D. H.; Findeis, A. F.; Naylor, S.; Gibson, B. W. *J. Am. Chem. Soc.* **1987,** *109*, 1980-1986.

(123) Griffin, P. R.; Kumar, S.; Shabanowitz, J.; Charbonneau, H.; Namkung, P. C.; Walsh, K. A.; Hunt, D. F.; Petra, P. H. *J. Biol. Chem.* **1989,** *264*, 19066-19075.

(124) Namkung, P. C.; Kumar, S.; Walsh, K. A.; Petra, P. H. *J. Biol. Chem.* **1990,** *265*, 18345-18350.

(125) Beckey, H. D.; Schulten, H. R. *Angew. Chem.-Int. Edit. Engl.* **1975,** *14*, 403-415.

(126) Linden, H. B.; Winkler, H. U.; Beckey, H. D. *Journal of Physics E-Scientific Instruments* **1977,** *10*, 657-660.

(127) Henis, N. B. H.; Youngless, T. L.; Bursey, M. M. *J. Chem. Soc.-Dalton Trans.* **1980**, 1416-1418.

(128) Posthumus, M. A.; Kistemaker, P. G.; Meuzelaar, H. L. C.; Ten Noever de Brauw, M. C. *Anal. Chem.* **1978,** *50*, 985.

(129) Vanderpeyl, G. J. O.; Isa, K.; Haverkamp, J.; Kistemaker, P. G. *Int. J. Mass Spectrom. Ion Process.* **1983,** *47*, 11-14.

(130) Hercules, D. M.; Day, R. J.; Baulesanmugan, K.; Deng, T. A.; Li, C. P. *Anal. Chem.* **1982,** *54*, 280A.

(131) Karas, M.; Hillenkamp, F., Bordeaux, France, August 29-September 2, 1988 1988.

(132) Karas, M.; Hillenkamp, F. *Anal. Chem.* **1988,** *60*, 2299.

(133) Dole, M.; Mack, L. L.; Hines, R. L. *J. Chem. Phys.* **1968,** *49*, 2240-&.

(134) Craig, A. G.; Derrick, P. J. *Aust. J. Chem.* **1986,** *39*, 1421-1434.

(135) Fenn, J. B.; Mann, M.; Meng, C. K.; Wong, S. F.; Whitehouse, C. M. *Mass Spectrom. Rev.* **1990,** *9*, 37-70.

(136) Yamashita, M.; Fenn, J. B. *J. Phys. Chem.* **1984,** *88*, 4451-4459.

(137) Yamashita, M.; Fenn, J. B. *J. Phys. Chem.* **1984,** *88*, 4671-4675.

(138) Nohmi, T.; Fenn, J. B. *J. Am. Chem. Soc.* **1992,** *114*, 3241-3246.

(139) Taylor, G. *Proceedings of the Royal Society of London Series a-Mathematical and Physical Sciences* **1964,** *280*, 383-&.

(140) Taylor, G. *Proceedings of the Royal Society of London Series a-Mathematical and Physical Sciences* **1969,** *313*, 453-&.

(141) Thomson, B. A.; Iribarne, J. V. *Rev. Geophys.* **1978,** *16*, 431-434.

(142) Thomson, B. A.; Iribarne, J. V. *J. Chem. Phys.* **1979,** *71*, 4451-4463.

(143) Iribarne, J. V.; Dziedzic, P. J.; Thomson, B. A. *Int. J. Mass Spectrom. Ion Process.* **1983,** *50*, 331-347.

(144) Campana, J. E.; Sheng, L. S.; Shew, S. L.; Winger, B. E. *Trac-Trends Anal. Chem.* **1994,** *13*, 239-247.

(145) McEwen, C. N.; Simonsick, W. J.; Larsen, B. S.; Ute, K.; Hatada, K. *J. Am. Soc. Mass Spectrom.* **1995,** *6*, 906-911.

(146) Oconnor, P. B.; McLafferty, F. W. *J. Am. Chem. Soc.* **1995,** *117*, 12826-12831.

(147) Schwartz, B. L.; Rockwood, A. L.; Smith, R. D.; Tomalia, D. A.; Spindler, R. *Rapid Commun. Mass Spectrom.* **1995,** *9*, 1552-1555.

(148) Maziarz, E. P.; Baker, G. A.; Wood, T. D. *Macromolecules* **1999,** *32*, 4411-4418.

(149) Dolan, A. R.; Maziarz, E. P.; Wood, T. D. *Eur. J. Mass Spectrom.* **2000,** *6*, 241-249.

(150) Nielen, M. W. F.; Buijtenhuijs, F. A. *Anal. Chem.* **1999,** *71*, 1809-1814.

(151) Yalcin, T.; Gabryelski, W.; Li, L. *Anal. Chem.* **2000,** *72*, 3847-3852.

(152) Maziarz, E. P.; Baker, G. A.; Lorenz, S. A.; Wood, T. D. *J. Am. Soc. Mass Spectrom.* **1999,** *10*, 1298-1304.

(153) Tanaka, K.; Waki, H.; Ido, Y.; Akita, S.; Yoshida, S.; Yoshida, T. *Rapid Comm. Mass. Spectrom.* **1988,** *2*, 151.

(154) Danis, P. O.; Karr, D. E.; Mayer, F.; Holle, A.; Watson, C. H. *Org. Mass Spectrom.* **1992,** *27*, 843-846.

(155) Danis, P. O.; Karr, D. E. *Org. Mass Spectrom.* **1993,** *28*, 923-925.

(156) Danis, P. O.; Karr, D. E.; Xiong, Y. S.; Owens, K. G. *Rapid Commun. Mass Spectrom.* **1996,** *10*, 862-868.

(157) Montaudo, G.; Scamporrino, E.; Vitalini, D.; Mineo, P. *Rapid Commun. Mass Spectrom.* **1996,** *10*, 1551-1559.

(158) Montaudo, G.; Montaudo, M. S.; Puglisi, C.; Samperi, F. *J. Polym. Sci. Pol. Chem.* **1996,** *34*, 439-447.

(159) Montaudo, G.; Montaudo, M. S.; Puglisi, C.; Samperi, F.; Sepulchre, M. *Macromol. Chem. Phys.* **1996,** *197*, 2615-2625.

(160) Montaudo, G.; Montaudo, M. S.; Puglisi, C.; Samperi, F. *Rapid Commun. Mass Spectrom.* **1994,** *8*, 981-984.

(161) Wilczekvera, G.; Danis, P. O.; Eisenberg, A. *Macromolecules* **1996,** *29*, 4036-4044.

(162) Castoro, J. A.; Koster, C.; Wilkins, C. *Rapid Commun. Mass Spectrom.* **1992,** *6*, 239-241.

(163) Dey, M.; Castoro, J. A.; Wilkins, C. L. *Anal. Chem.* **1995,** *67*, 1575-1579.

(164) Dekoster, C. G.; Duursma, M. C.; Vanrooij, G. J.; Heeren, R. M. A.; Boon, J. J. *Rapid Commun. Mass Spectrom.* **1995,** *9*, 957-962.

(165) Easterling, M. L.; Pitsenberger, C. C.; Kulkarni, S. S.; Taylor, P. K.; Amster, I. J. *Int. J. Mass Spectrom. Ion Process.* **1996,** *158*, 97-113.

(166) Easterling, M. L.; Mize, T. H.; Amster, I. J. *Int. J. Mass Spectrom.* **1997,** *169*, 387-400.

(167) Easterling, M. L.; Pitsenberger, C. C.; Amster, I. J. *J. Am. Soc. Mass Spectrom.* **1997,** *8*, 195-198.

(168) Easterling, M. L.; Mize, T. H.; Amster, I. J. *Anal. Chem.* **1999,** *71*, 624-632.

(169) Knobeler, M.; Wanczek, K. P. *J. Am. Soc. Mass Spectrom.* **1996,** *7*, 1026-1033.

(170) Hendrickson, C. L.; Drader, J. J.; Laude, D. A.; Guan, S. H.; Marshall, A. G. *Rapid Commun. Mass Spectrom.* **1996,** *10*, 1829-1832.

(171) Pasatolic, L.; Huang, Y. L.; Guan, S. H.; Kim, H. S.; Marshall, A. G. *J. Mass Spectrom.* **1995,** *30*, 825-833.

(172) Solouki, T.; Gillig, K. J.; Russell, D. H. *Anal. Chem.* **1994,** *66*, 1583-1587.

(173) Mize, T. H.; Amster, I. J. *Anal. Chem.* **2000,** *72*, 5886-5891.

(174) Solouki, T.; Marto, J. A.; White, F. M.; Guan, S. H.; Marshall, A. G. *Anal. Chem.* **1995,** *67*, 4139-4144.

(175) Hunt, D. F.; Shabanowitz, J.; McIver, R. T.; Hunter, R. L.; Syka, J. E. P. *Anal. Chem.* **1985,** *57*, 765-768.

(176) Kofel, P.; Allemann, M.; Kellerhals, H.; Wanczek, K. P. *Int. J. Mass Spectrom. Ion Process.* **1985,** *65*, 97.

(177) Li, Y. Z.; Little, D. P.; Koster, H.; Hunter, R. L.; McIver, R. T. *Anal. Chem.* **1996,** *68*, 2090-2096.

(178) Schriemer, D. C.; Li, L. *Anal. Chem.* **1996,** *68*, 2721-2725.

(179) Hipple, J. A.; Sommer, H.; Thomas, H. A. *Physical Review* **1949,** *76*, 1877-1878.

(180) Sommer, H.; Hipple, J. A. *Physical Review* **1951,** *83*, 229-229.

(181) Sommer, H.; Thomas, H. A.; Hipple, J. A. *Physical Review* **1951,** *82*, 697-702.

(182) Bell, R. L. *Journal of Scientific Instruments* **1956,** *33*, 269-272.

(183) Wagener, J. S.; Marth, P. T. *J. Appl. Phys.* **1957,** *28*, 1027-1030.

(184) Cambey, L. A.; Milner, C. J. *Rev. Sci. Instrum.* **1960,** *31*, 776-776.

(185) Krummena.D *Vacuum* **1964,** *14*, 461-&.

(186) Thorne, P.; Wingate, H. C.; Buckingh.Jd *Vacuum* **1965,** *15*, 23-&.

(187) Fitch, R. K.; Moseley, K. *Nuovo Cimento* **1967,** *5*, 216-&.

(188) Kubala, H.; Muller, K. *Vakuum-Technik* **1968,** *17*, 87-&.

(189) Suurmeye.Ep; Francken, J. C. *Vakuum-Technik* **1968,** *17*, 1-&.

(190) Comsa, G.; Mircea, A. *Journal of Physics E-Scientific Instruments* **1969,** *2*, 336-&.

(191) Wobschall, D.; Graham, J. R.; Malone, D. P. *Physical Review* **1963,** *131*, 1565-&.

(192) Wobschal.D; Graham, J. R.; Malone, D. P. *J. Chem. Phys.* **1965,** *42*, 3955-&.

(193) Wobschal.D *Rev. Sci. Instrum.* **1965,** *36*, 466-&.

(194) Wobschal.Dc; Fluegge, R. A.; Graham, J. R. *J. Appl. Phys.* **1967,** *38*, 3761-&.

(195) Beaucham.Jl *Annu. Rev. Phys. Chem.* **1971,** *22*, 527-&.

(196) McIver, R. T. *Rev. Sci. Instrum.* **1970,** *41*, 555-&.

(197) Comisarow, M. B.; Marshall, A. G. *Chem. Phys. Lett.* **1974,** *26*, 489-490.

(198) Comisarow, M. B.; Marshall, A. G. *Can. J. Chem.-Rev. Can. Chim.* **1974,** *52*, 1997-1999.

(199) Comisarow, M. B.; Marshall, A. G. *Chem. Phys. Lett.* **1974,** *25*, 282-283.

(200) Comisarow, M. B.; Marshall, A. G. *J. Chem. Phys.* **1975,** *62*, 293-295.

(201) Cooley, J. W.; Tukey, J. W. *Math. Comput.* **1965,** *19*, 297-&.

(202) Comisarow, M. B. *J. Chem. Phys.* **1978,** *69*, 4097-4104.

(203) Marshall, A. G. *Anal. Chem.* **1979,** *51*, 1710-1714.

(204) Comisarow, M. B. In *Transform Techniques in Chemistry*; Griffiths, P. R., Ed.; Plenum Press: New York, 1978.

(205) Comisarow, M. B. In *Ion cyclotron resonance spectrometry*; Hartmann, H., Wanczek, K. P., Eds.; Springer-Verlag: New York, 1982.

(206) Gross, M. L.; Rempel, D. L. *Science* **1984,** *226*, 261-268.

(207) Craig, E. C.; Marshall, A. G. *J. Magn. Reson.* **1986,** *68*, 283-295.

(208) Chen, R. D.; Wu, A. Y.; Mitchell, D. W.; Hofstadler, S. A.; Rockwood, A. L.; Smith, R. D. *Anal. Chem.* **1994,** *66*, 3964-3969.

(209) Xiang, X. Z.; Grosshans, P. B.; Marshall, A. G. *Int. J. Mass Spectrom. Ion Process.* **1993,** *125*, 33-43.

(210) Limbach, P. A.; Grosshans, P. B.; Marshall, A. G. *Int. J. Mass Spectrom. Ion Process.* **1993,** *123*, 41-47.

(211) Grosshans, P. B.; Marshall, A. G. *Int. J. Mass Spectrom. Ion Process.* **1992,** *115*, 1-19.

(212) Grosshans, P. B.; Marshall, A. G. *Anal. Chem.* **1991,** *63*, 2057-2061.

(213) McLuckey, S. A.; Glish, G. L.; Cooks, R. G. *Int. J. Mass Spectrom. Ion Process.* **1981,** *39*, 219-230.

(214) Brown, R. S.; Lennon, J. J. *Anal. Chem.* **1995,** *67*, 1998-2003.

(215) Vestal, M. L.; Juhasz, P.; Martin, S. A. *Rapid Commun. Mass Spectrom.* **1995,** *9*, 1044-1050.

(216) Franzen, J. *Int. J. Mass Spectrom. Ion Process.* **1997,** *164*, 19-34.

(217) Takach, E. J.; Hines, W. M.; Patterson, D. H.; Juhasz, P.; Falick, A. M.; Vestal, M. L.; Martin, S. A. *J. Protein Chem.* **1997,** *16*, 363-369.

(218) Grosshans, P. B.; Chen, R.; Limbach, P. A.; Marshall, A. G. *Int. J. Mass Spectrom. Ion Process.* **1994,** *139*, 169-189.

(219) Huang, S. K.; Rempel, D. L.; Gross, M. L. *Int. J. Mass Spectrom. Ion Process.* **1986,** *72*, 15-31.

(220) Rempel, D. L.; Huang, S. K.; Gross, M. L. *Int. J. Mass Spectrom. Ion Process.* **1986,** *70*, 163-184.

(221) Beu, S. C.; Laude, D. A. *Int. J. Mass Spectrom. Ion Process.* **1991,** *108*, 255-268.

(222) Beu, S. C.; Laude, D. A. *Int. J. Mass Spectrom. Ion Process.* **1992,** *112*, 215-230.

(223) Beu, S. C.; Laude, D. A. *Anal. Chem.* **1992,** *64*, 177-180.

(224) Mordehai, A. V.; Henion, J. D. *Rapid Commun. Mass Spectrom.* **1992,** *6*, 345-348.

(225) Schweikhard, L.; Marshall, A. G. *J. Am. Soc. Mass Spectrom.* **1993,** *4*, 433-452.

(226) Xiang, X. Z.; Marshall, A. G. *J. Am. Soc. Mass Spectrom.* **1994,** *5*, 807-813.

(227) Xiang, X. Z.; Guan, S. H.; Marshall, A. G. *J. Am. Soc. Mass Spectrom.* **1994,** *5*, 238-249.

(228) Oconnor, P. B.; McLafferty, F. W. *J. Am. Soc. Mass Spectrom.* **1995,** *6*, 533-535.

(229) Dunbar, R. C.; Chen, J. H.; Hays, J. D. *Int. J. Mass Spectrom. Ion Process.* **1984,** *57*, 39-56.

(230) Hendrickson, C. L.; Hofstadler, S. A.; Beu, S. C.; Laude, D. A. *Int. J. Mass Spectrom. Ion Process.* **1993,** *123*, 49-58.

(231) Chen, R. D.; Guan, S. H.; Marshall, A. G. *J. Chem. Phys.* **1994,** *100*, 2258-2266.

(232) Marshall, A. G.; Guan, S. H. *Phys. Scr.* **1995,** *T59*, 155-164.

(233) Guan, S. H.; Huang, Y. L.; Xin, T. P.; Marshall, A. G. *Rapid Commun. Mass Spectrom.* **1996,** *10*, 1855-1859.

(234) Grosshans, P. B.; Shields, P. J.; Marshall, A. G. *J. Chem. Phys.* **1991,** *94*, 5341-5352.

(235) Gorshkov, M. V.; Guan, S. H.; Marshall, A. G. *Rapid Commun. Mass Spectrom.* **1992,** *6*, 166-172.

(236) Spell, T. L.; Delong, S. E.; Creasy, W. R. *Int. J. Mass Spectrom. Ion Process.* **1993,** *124*, 223-239.

(237) Shi, S. D. H.; Hendrickson, C. L.; Marshall, A. G.; Simonsick, W. J.; Aaserud, D. J. *Anal. Chem.* **1998,** *70*, 3220-3226.

(238) Marshall, A. G.; Roe, D. C. *J. Chem. Phys.* **1980,** *73*, 1581-1590.

(239) Guan, S. H. *J. Am. Soc. Mass Spectrom.* **1991,** *2*, 483-486.

(240) Brobeck, W. M.; Lawrence, E. O.; Mackenzie, K. R.; McMillan, E. M.; Serber, R.; Sewell, D. C.; Simpson, K. M.; Thornton, R. L. *Physical Review* **1947,** *71*, 449-450.

(241) Lawrence, E. O. *Science* **1948,** *108*, 677-677.

(242) Grosshans, P. B.; Marshall, A. G. *Int. J. Mass Spectrom. Ion Process.* **1990,** *100*, 347-379.

(243) Farrell, J. T.; Lin, P. P.; Kenttamaa, H. I. *Anal. Chim. Acta* **1991,** *246*, 227-232.

(244) Herman, J. A.; Xu, G. Y.; Herman, K.; McMahon, T. B. *Int. J. Mass Spectrom. Ion Process.* **1992,** *113*, 143-155.

(245) de Koning, L. J.; Nibbering, N. M. M.; van Orden, S. L.; Laukien, F. H. *Int. J. Mass Spectrom.* **1997,** *165*, 209-219.

(246) Jackson, J. D. *Applied Scientific Research Section a-Mechanics Heat Chemical Engineering Mathematical Methods* **1963,** *12*, 315-&.

(247) Guan, S. H.; Kim, H. S.; Marshall, A. G.; Wahl, M. C.; Wood, T. D.; Xiang, X. Z. *Chem. Rev.* **1994,** *94*, 2161-2182.

(248) Marshall, A. G.; Wang, T. C. L.; Ricca, T. L. *J. Am. Chem. Soc.* **1985,** *107*, 7893-7897.

(249) Wang, T. C. L.; Ricca, T. L.; Marshall, A. G. *Anal. Chem.* **1986,** *58*, 2935-2938.

(250) Guan, S. H. *J. Chem. Phys.* **1989,** *91*, 775-777.

(251) Guan, S. H. *J. Chem. Phys.* **1990,** *93*, 8442-8445.

(252) Guan, S. H.; Marshall, A. G. *Int. J. Mass Spectrom. Ion Process.* **1996,** *158*, 5-37.

(253) Marshall, A. G.; Wang, T. C. L.; Ricca, T. L. *Chem. Phys. Lett.* **1984,** *108*, 63-66.

(254) Pitsenberger, C. C.; Amster, I. J. *Eur. Mass Spectrom.* **1997,** *3*, 1-9.

(255) Vartanian, V. H.; Anderson, J. S.; Laude, D. A. *Mass Spectrom. Rev.* **1995,** *14*, 1-19.

(256) Cody, R. B.; Burnier, R. C.; Cassady, C. J.; Freiser, B. S. *Anal. Chem.* **1982,** *54*, 2225-2228.

(257) Cody, R. B.; Freiser, B. S. *Anal. Chem.* **1982,** *54*, 1431-1433.

(258) Cody, R. B.; Freiser, B. S. *Int. J. Mass Spectrom. Ion Process.* **1982,** *41*, 199-204.

(259) Cody, R. B.; Burnier, R. C.; Freiser, B. S. *Anal. Chem.* **1982,** *54*, 96-101.

(260) Fedor, D. M.; Cody, R. B.; Burinsky, D. J.; Freiser, B. S.; Cooks, R. G. *Int. J. Mass Spectrom. Ion Process.* **1981,** *39*, 55-64.

(261) Guan, S. H.; Marshall, A. G.; Wahl, M. C. *Anal. Chem.* **1994,** *66*, 1363-1367.

(262) Huang, Y. L.; Pasatolic, L.; Guan, S. H.; Marshall, A. G. *Anal. Chem.* **1994,** *66*, 4385-4389.

(263) Wood, T. D.; Ross, C. W.; Marshall, A. G. *J. Am. Soc. Mass Spectrom.* **1994,** *5*, 900-907.

(264) Solouki, T.; PasaTolic, L.; Jackson, G. S.; Guan, S. G.; Marshall, A. G. *Anal. Chem.* **1996,** *68*, 3718-3725.

(265) Guan, S. H.; Marshall, A. G. *Anal. Chem.* **1997,** *69*, 1-4.

(266) Tonner, D. S.; McMahon, T. B. *Anal. Chem.* **1997,** *69*, 4735-4740.

(267) Tutko, D. C.; Henry, K. D.; Winger, B. E.; Stout, H.; Hemling, M. *Rapid Commun. Mass Spectrom.* **1998,** *12*, 335-338.

(268) Wu, Q. Y. *Anal. Chem.* **1998,** *70*, 865-872.

CHAPTER 2

EXPERIMENTAL AND INSTRUMENTAL DETAILS

The purpose of this chapter is to expand on the experimental procedures used in throughout this dissertation and detailed in the following chapters with the FTICR mass spectrometrist in mind; here, however, some of the rationale that has led to the use of one or another technique and some detail on the practical aspects of implementing these tools will be described. It may well contain the most useful information for the novice in this volume; the expert, on the other hand, could easily move on to the specific experiments that relate to the task at hand. Regardless, the notes given here all refer, to a greater or lesser extent, to the specific situations encountered in the day-to-day operation of the internal source MALDI-FTICR mass spectrometer at the University of Georgia; extension of these details to another instrumental set-up can be achieved seamlessly in some cases, or may turn out to be highly impractical in others. Omissions of favorite techniques should also be measured by this flexible guage.

The experiments detailed in the following chapters have some common features that deserve explanation. In a gross oversimplification, the experiments involve:

1. Preparation of the sample spot on the MALDI target,
2. Introduction of the MALDI target proximate to the FTICR-MS analyzer cell,
3. Illumination of the sample spot with a pulsed laser to produce gas phase ions,
4. Trapping of the ions within the ICR cell,
5. Manipulation of the ion population for isolation, energy control, or chemistry,

6. Excitation of the population followed by digitization of the image current, and

7. Extraction of the frequency spectrum and conversion to a mass spectrum.

Indeed, with the exception of step 2, this is the recipe for any MALDI-FTICR-MS experiment with the details of each step specifiable to wide varieties of problems. The qualities of the internal source MALDI-FTICR-MS alluded to in the introduction and the requirements of the analytical problems studied herein demand unique approaches to satisfying the above tasks.

PREPARATION OF THE SAMPLE SPOT

Matrix assisted laser desorption/ionization (MALDI), introduced by Hillencamp and Karas, uses a crystalline organic matrix to carry nonvolatile compounds into the gas phase.[1] An analyte is co-crystallized in the matrix from the solution phase so that crystals of the matrix are essentially doped with the analyte at about a 1000-to-1 to 10,000-to-1 matrix-to-analyte ratio.[2] Alternately, a thin film with a similar analyte doping ratio can be produced by electrospray deposition of a mixture of the matrix and analyte;[3] this second method is extremely useful for producing thin films which are much more homogeneous than those produced by the dried droplet technique that is widely used for most MALDI techniques.[3]

A number of matrices and sample preparations have been used in the following experiments. Solutions of water soluble polymers and peptides were most often mixed with saturated solutions of 3,5-dimethoxy-4-hydroxycinnamic acid (also known as “sinapinic acid” or abbreviated here as SIN) or "-cyano-4-hydroxycinnamic acid ("-CN),

or in 1 M 2,5-dihydroxybenzoic acid (DHB), each prepared in 50% aqueous acetonitrile. Trifluoroacetic acid is added (0.1% v/v) to lower the pH significantly below the pK of the acidic matrices; this has been shown to improve subsequent crystallization.[4, 5] The sample and matrix solutions are mixed to produce a suitable matrix-to-analyte ratio of approximately 1000:1. The selection of the matrix can seem quasi-Edisonian because the observable results do not always correspond to the reputation of the material. Some generalities that apply to this work include that the use of "-CN is common when screening a new sample for instrument sensitivity because "-CN "always" produces ions; it is also known as a "hot" matrix, i.e., one that imparts substantial internal energy to the analyte, often resulting in metastable fragmentation of the ions. SIN forms large crystals prone to ablation desorption which makes it a good matrix for cationized species (as in many synthetic polymers and in glycopeptides) and for larger proteins than are examined in the internal source MALDI-FTICR-MS. DHB is a relatively "cool" matrix (little fragmentation) and is compatible with many solvents; it is so soluble that it is easy to have too much DHB in a sample spot. That is, the matrix signal can overwhelm the signal due to the analyte ions or, worse, can competitively suppress the formation of analyte ions, altogether.[6, 7]

The analyte and matrix solutions are mixed either at the point of deposition using a pipet tip to repeatedly aspirate the two or in an Eppendorf tube just prior to deposition. If a cationic species is preferred, a solution carrying the cation of choice can be added, as well. Natural abundances of sodium and potassium contamination can often result in a mixed distribution of sodiated and potassiated ions, complicating the analysis. The addition of a preferred cation (in the form of a NaCl or KCl solution) at about a 10:1

molar ratio with respect to the analyte has a two-fold advantage: first, all the ions will have the same charge carrier thus reducing the spectrum complexity by half (or better) and, second, if the same total number of ions are formed the signal-to-noise is often increased for the remaining species by the amount of the other species in the non-doped sample.

Occasionally salts or other water soluble species interfere with ion production and must be removed. For robust samples such as most synthetic polymers, ion exchange is suitable; but, ion exchange columns are ineffective for these highly dilute (~0.001 M) samples because of sample loss to the column and the enormous dilution factors. However, addition of one or two beads of cation exchange resin to 1 mL of analyte solution can significantly reduce the cation load to a finished sample spot.

Desalting of samples with lower concentrations or that are prone to solution phase fragmentation in the presence of acidic media (like ion exchange gels) can be accomplished directly on the sample spot. Immobilization of proteolytic peptides on a thin nitrocellulose film followed by rinsing with cold, distilled water has proven effective.[8-10] In this lab, preparation involves dissolving 10 mg nitrocellulose in 1 mL 1:1 acetone:isopropanol solution and applying 1 µL to the puck (if "-CN or another relatively water insoluble matrix is to be used, it can be dissolved with the nitrocellulose prior to application). The contaminated analyte solution is applied to the dried nitrocellulose spot and also allowed to dry at which time the nitrocellulose will noncovalently immobilize the peptides or other polyamide. The sample is then washed by applying a 0.5 µL drop of 4EC deionized water to the sample, allowing 30 seconds for dissolution of contaminants and removal by aspiration. If a water soluble matrix is used,

it should be added last. This protocol has the added advantage of using the nitrocellulose as a co-matrix to provide collision cooling in the initial desorption.

Nonpolar analytes require different treatment. Direct application of matrix and/or analyte in organic solvent can be disastrous because the surface tension is often low and the sample can spread to contaminate the entire sample puck. Also, some matrices (e.g., SIN) form an amorphous, glasslike solid impervious to the laser when dried from solvents with a high organic ratio. Matrices used here that have proven compatible with nonpolar analytes include DHB, trans-3-indoleacrylic acid (IAA), and 1,8-dihydroxy-9[10H]-anthracenone (also known as "dithranol" or DITH), the latter of which has a high vapor pressure that precludes its leisurely use in the ultrahigh vacuum region of the FTICR-MS: spots of DITH must be analyzed quickly since it completely sublimates in about 20 minutes at UHV (thereby fouling the vacuum system for roughly the next 12 hours).

Application of these matrices with their nonpolar analytes is usually achieved via electrospray deposition. Starting with THF or acetone solutions comprising a matrix solution with either 1 M DHB or 0.2 M IAA, an analyte solution of approximately 1 mM, and a solution containing a cation source (usually sodium trichloroacetate, sodium iodide, cupric chloride, or silver trifluoroacetate, as noted in each of the following chapters), a vertically mounted, wire-constricted, 14 gauge stainless steel hypodermic needle is filled with sufficient volumes of each to produce an approximately 400:1:10 matrix:analyte:cation molar ratio. Figure 2.1 shows a schematic of electrospray deposition while Figure 2.2 shows a photograph of the electrospray rig in use. Further dilution (5X to 10X) with pure solvent facilitates the production of a thin, electrosprayed

film. A 4.5 kV DC potential between the needle tip and the sample puck (mounted perpendicular to the tip ~1cm away) is applied resulting in a diffuse powder of the matrix, analyte, and any cation coating the surface of the sample puck; location of the spray on the puck is controlled by covering the clean puck with aluminum foil and tearing off a small portion resulting in a crude mask at the point of desired deposition. An additional benefit of the electrospray deposition protocol for compatible analytes is the attenuation of shot-to-shot variation in ion abundance due to the uniformity of doping and crystal morphology.[3]

DELIVERY OF THE MALDI TARGET TO THE FTICR ANALYZER CELL

The instrument, shown in Figure 2.3, and its capabilities have been described in detail previously;[11-16] details on the delivery of the prepared sample puck from atmospheric pressure to the UHV chamber are presented here, for clarity. A prepared sample puck is mounted on a linear manipulator in a small vacuum chamber (referred to as the antechamber) which is then evacuated from ambient pressure to high vacuum (~10^{-8} torr), in turn, by a mechanical pump (to ~10^{-5} torr), a diffusion pump (to ~10^{-6} -10^{-7} torr), and finally by a high speed cryogenic pump. This sequence is essential to maintaining the integrity of the UHV analyzer chamber by elimination of water and other recalcitrant contaminants entering the antechamber when it is open to atmosphere; contamination is further minimized by maintaining a positive flow of dry nitrogen gas within the antechamber while loading the sample. Upon reaching sufficient vacuum, a gate valve separating the antechamber and the ultrahigh vacuum mass analyzer region, or "main chamber, is opened through which the puck is delivered to a long, linear-rotary

Figure 2.1: Typical set-up for electrospray deposition as performed in the Amster group. A flow restricted hypodermic needle filled with matrix, analyte, and cation solution and with a 4.5 kVDC power supply attached to it is brought to within about 2 cm of the grounded titanium puck. A thin, even film of the solutes is deposited.

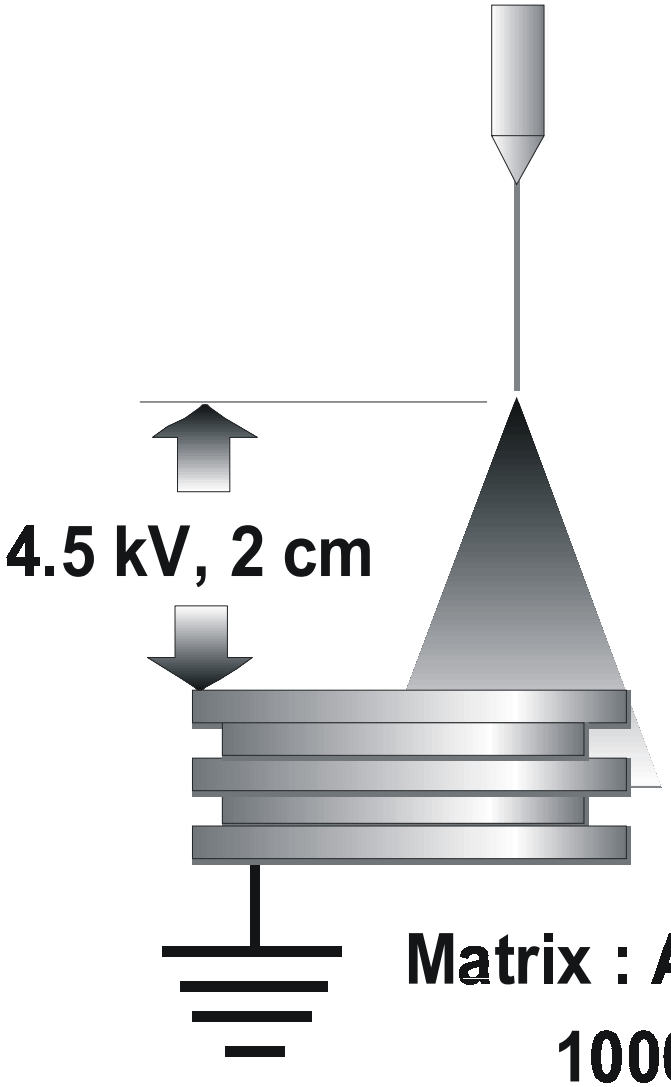

Matrix : Analyte : Cation

1000 : 1 : 10

Figure 2.2: a) Photograph of the electrospray sample apparatus in action. The sample is gravity fed by filling the needle with the solution to be deposited. The sample puck is mounted on an adjustable height, metal arm that is attached to the ground lead of a high voltage DC power supply. The inset shows the needle with the constricting wire that limits the flow rate. b) MALDI samples on the puck. (Dry drop and espray).

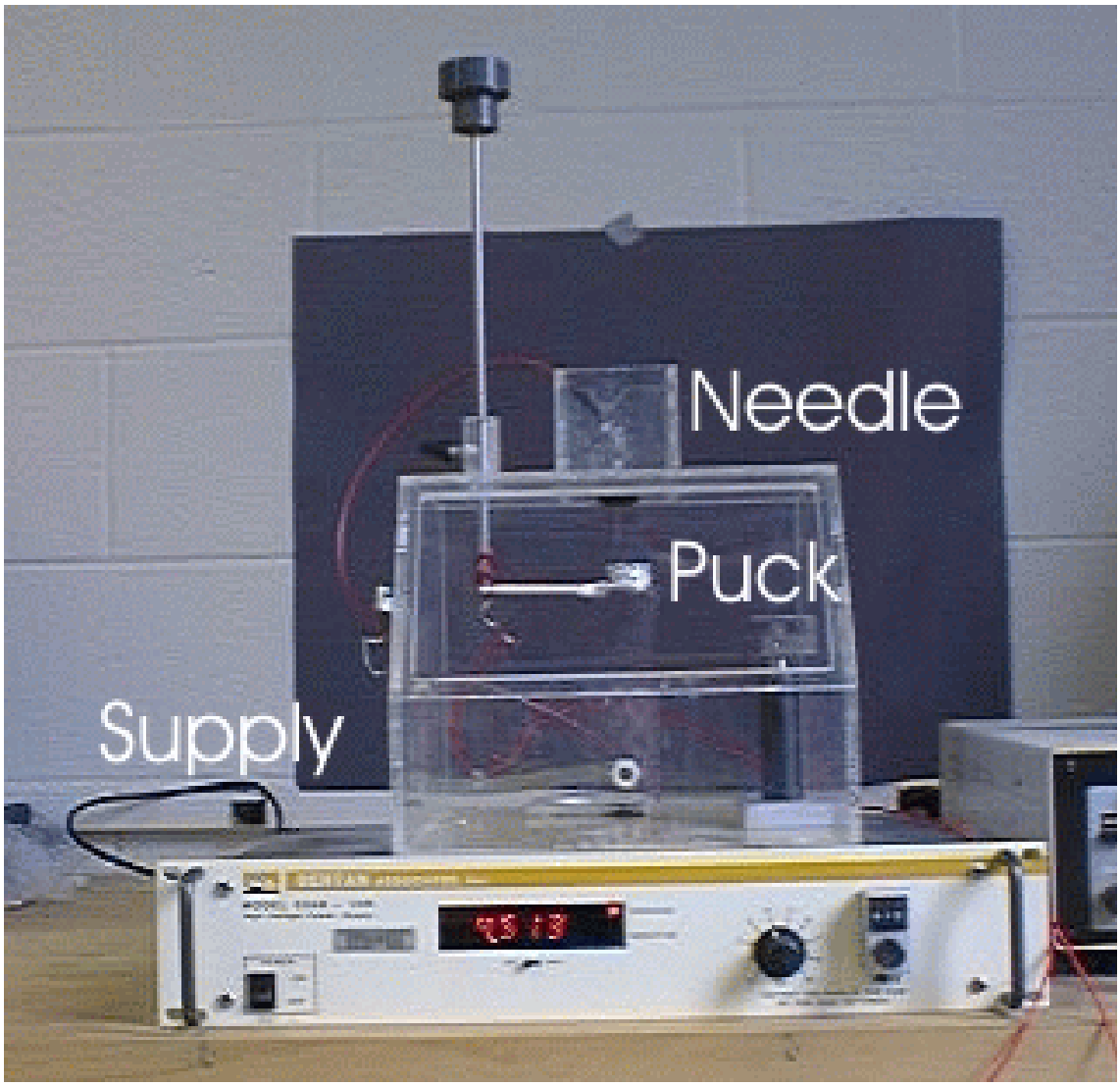
Needle
Puck
Supply

manipulator, the antechamber manipulator is retracted, and finally the gate valve closed to isolate the main chamber. The position of the linear-rotary manipulator is adjusted to align the edge of the target puck with the magnetic field axis at a point about 1 cm from the edge of the ICR cell front trapping electrodes. This puck alignment helps minimize the initial magnetron radius of the ions by having the MALD-ionization plume enter the cell as close to the center of the trapping field as possible and along the magnetic field axis to the V q B motion.

A 2.5 cm (1") cylindrical titanium puck is used throughout the following experiments. It has a low mass and no magnetic susceptibility and, therefore, helps minimize perturbation of the uniform magnetic field that is key to the FTICR experiment. And, it is incredibly durable fending off both physical and chemical attacks of all kinds. Careful application of the MALDI spots can easily result in 20 individual dried-droplet sample spots or 10 electrospray deposited regions, allowing researchers to perform many different experiments between sample loading cycles.

THE MALDI EVENT

A MALDI event involves training a focused laser pulse on the sample. The matrix characteristically should absorb strongly at the wavelength of the ionization laser, and usually absorbs much more strongly than the analyte so that internal excitation of the sample due to the laser is minimized. Ideally, in fact, the analyte would be transparent at the wavelength of the laser so that the only energy imparted to molecule is due to collisions in the resulting MALDI plume, although, in practice, there is often some laser

Figure 2.3: Schematic of the internal source MALDI-FTICR-MS.

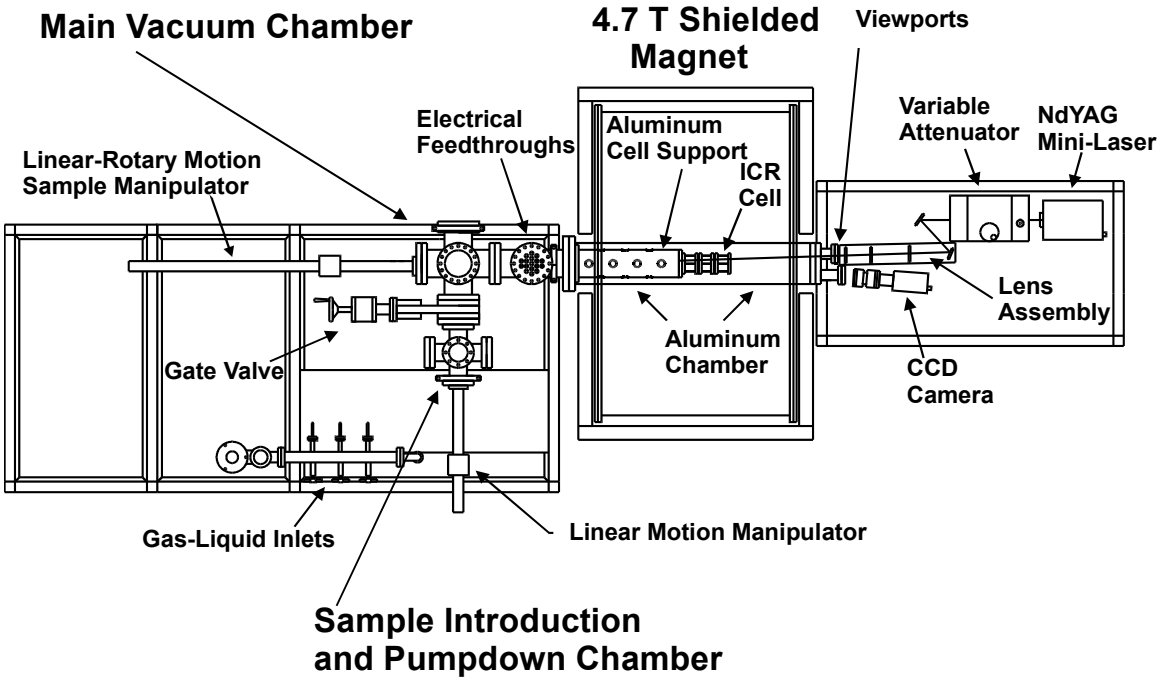
Main Vacuum Chamber
4.7 T Shielded Magnet
Viewports
Electrical Feedthroughs
Aluminum Cell Support
ICR Cell
Variable Attenuator
NdYAG Mini-Laser
Linear-Rotary Motion Sample Manipulator
Lens Assembly
Aluminum Chamber
CCD Camera
Gate Valve
Gas-Liquid Inlets
Linear Motion Manipulator
Sample Introduction and Pumpdown Chamber

excitation component; still, compared to the explosive tumult of the MALDI event itself, the laser absorption component of analyte internal energy is small. Figure 2.4 shows the UV-Vis absorbance spectra of 1 mM solutions of DHB, PEG 2K, and a polystyrene with an average molecular weight of 2000 Da; at 355 nm, the DHB absorbs much more strongly than the PEG sample, but would obviously compete with the chromophore rich polystyrene.

As Gluckmann et al. point out, a uniform MALDI theory that explains all mechanisms of ionization and introduction to the gas phase is unlikely to arise.[17] In fact, there are many valid pathways that sometimes occur simultaneously in a single ionization event. For instance, Nylon-6, a condensation polymer, ionized from DHB exhibits protonated ions (generally considered a gas phase ionization product) and alkali metal cationized ions (assumed to be preformed in the desorbed matrix cluster); for more on this example, refer to Chapter 7. The different mechanisms can be can be traced to the events of desorption.

TRAPPING MALDI IONS WITH THE OPEN CYLINDRICAL CELL

The internal MALDI-FTICR-MS takes advantage of the open cylinder design of its trapping cell to facilitate the MALD-ionization event. A frequency tripled Nd:YAG laser (355 nm) is fired through some attenuation and focusing optics, a MgF_2 viewport, and the ICR cell to its focal point: the centered sample on the offset puck. The laser spot position is determined by completely ablating an area of approximately 50 μm diameter with multiple laser shots at full power. Ablation progress is monitored on a video display

Figure 2.4: UV-Visable absorption spectra of a matrix and two analytes. a) DHB, b) PEG 2K, and c) polystyrene (M_n . 2000)

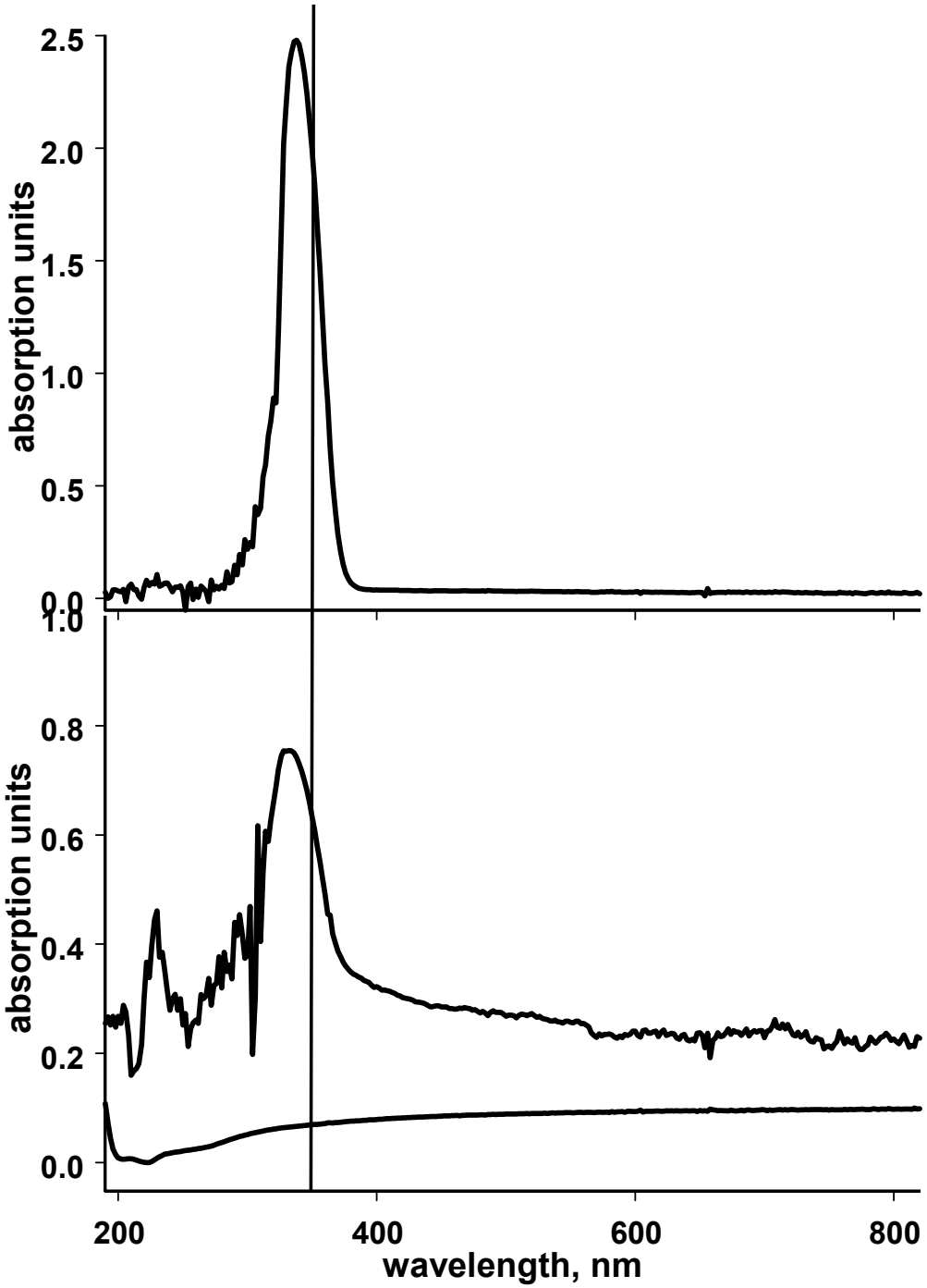
2.5
2.0
1.5
1.0
0.5
0.0
absorption units
1.0
0.8
0.6
0.4
0.2
0.0
absorption units
200
400
600
800
wavelength, nm

provided by a CCD camera mounted parallel to the laser optics and focused through a second viewport.

In MALDI, the desorbed ions and neutrals have narrow initial velocity distributions independent of mass.[18-21] This imparts a highly mass dependent initial kinetic energy (KE) distribution to the desorbed analyte ions. In a mixture of polyethylene glycols (PEG) as the analyte desorbed from DHB, one would expect an average velocity of 550 meters/second corresponding to KE for $PEG_7 + Na^+$ (m/z = 349.1838 Da) of 0.54 eV while $PEG_{78} + Na^+$ (m/z = 3475.0447 Da) enters the world at 5.4 eV. In order to trap a broad m/z range of ions thus produced, a scheme for deceleration of the ions is essential.

As mentioned earlier, the internal source MALDI-FTICR-MS was designed to minimize time-of-flight mass discrimination problems inherent in external source instruments. Ions produced at the cell and with no other applied field will enter the cell with about the same velocity profile. The back trapping potential need only exceed the maximum KE in the distribution to prevent the ions from passing completely through the cell. However, these ions are reversed in direction by the back trapping potential and attain a KE equal to their initial KE and will exit the cell at a corresponding velocity (minus that portion converted into radial kinetic energy) unless the front trapping potential is increased to match the back trapping potential. This is the essence of gated trapping.[12, 13, 22]

A few caveats are in order regarding this sufficient, if simplified, explanation of gated trapping. Higher trapping potentials reflect the ions earlier in the experiment and can exacerbate the time-of-flight "windowing" effect wherein the a slice of the

distribution is sampled and other ions lost; however, this can be minimized by judicious attention to the gated trap timing and application of a low pressure (~10^{-5} to ~10^{-6} torr) of neutral collision gas prior to desorption. Higher trapping potentials and collisions with neutrals also result in more rapid magnetron drift, so that optimization of these two parameters is essential; after about 100 milliseconds, the ion-neutral collisions should have reduced the energy components of the cyclotron and trapping motion of the ions to approximately thermal levels.[23] At this point in the experiment, any excess trapping potential can be ramped to a lower level, often less than 1 volt, while the excess buffer gas is pumped away; this lower trapping voltage is essential to minimization of radial ejection from accelerated magnetron expansion. Ion mass-to-charge distributions greater than 4000 Da wide can be trapped and simultaneously analyzed in this manner as can be seen in the "Gas Only" column of Figure 2.5a.

MANIPULATION OF THE ION POPULATION

Storage of ions in the cell is a straightforward matter of reducing the number of collisions experienced by ions already cooled to ambient energy levels. Ion storage in the cell can also degrade the quality of the measured transient because the population is more diffuse and the ions with greater initial magnetron radii face an increased likelihood of radial ejection upon expansion of the cyclotron radius for detection. Pumping delays prior to excitation and minimal application of collision gases are essential. Overall, radial losses due to magnetron expansion are often minimal at UHV because the main mechanism involves collisions with other gas phase molecules upsetting the equilibrium between the radial component of the trapping field and the force imposed on the ions by

the magnetic field, so the ion population can be stored virtually indefinitely when the trapping voltage is minimized.

At this point, the ions in the cell can be analyzed or they can be manipulated in several ways prior to mass analysis. Specific stored ions can be selected via several techniques including application of an inverse Fourier transform loaded to an arbitrary waveform generator (ARB),[24, 25] by applying a low voltage quadrupolar excitation (QE) event,[15, 23, 26-31] or by correllated sweep excitation.[32] MS^n experiments are possible on the selected ions by exciting them to a high radius–and, therefore, high kinetic energy–within the cell in the presence of a neutral collision gas. The overall population intensity can be reduced through temporary suspension of trapping potentials on a thermal population.[33, 34] Finally, remeasurement of ions, a tool that allows repeated efficient QE/measurement cycles on a single ion population,[11, 14, 15, 29, 34-36] can be applied to the problem of low abundance ions to help in accumulation of the products of multiple ionization events.[16]

Ion selection by SWIFT using an arbitrary waveform generator (AWG) is usually the preferable technique. The AWG takes a desired excitation profile (m/z domain) and applies an inverse Fourier transform to determine the corresponding time domain spectrum in an algorithm largely indistinguishable from the SWIFT experiment described in Chapter 1. The excitation profile includes the ranges of m/z to eject or excite and these ranges, in turn, can have notches of no excitation wherein ions should be retained. A properly designed AWG pulse can retain a single isotope peak without any net excitation of the retained ions.

Quadrupolar excitation, which can also be used for ion selection, is used to axialize and thermalize ions. In this body of work, two-plate azimuthal QE is used

Figure 2.5: Wide distributions achieved with a low pressure collision gas, alone, and greater coherence achieved by application of quadrupolar excitation and collision gas. a) A roughly equimolar mixture of three PEG samples trapped from a single laser shot without significant mass discrimination (left), and the same sample showing isolation of a single oligomer by QE. Also shown are an expansion (b) showing the isotope distribution of the isolated oligomer along with time domain signals that produce each of these spectra (c).

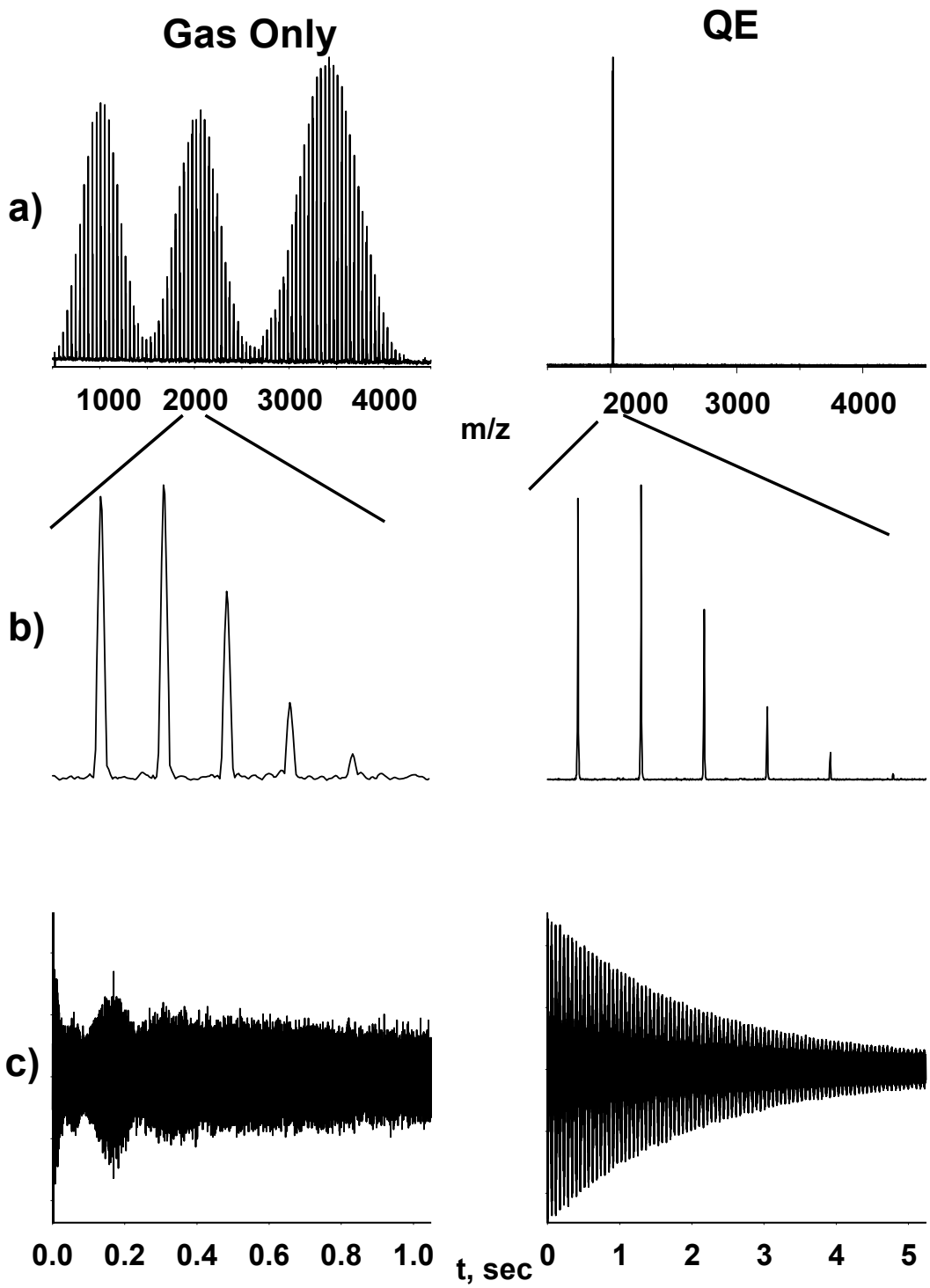
Gas Only
QE
a)
1000
2000
3000
4000
2000
3000
4000
m/z
b)
c)
0.0
0.2
0.4
0.6
0.8
1.0
t, sec
0
1
2
3
4
5

wherein an in phase rF pulse is applied to opposing cell plates while a collision gas is pulsed to 10^{-4} to 10^{-5} torr; though not a true quadrupolar field, this form of QE has been shown to approximate the desired field to a high degree of precision.[31] The combination of the quadrupolar electrical field, the energy exchange via collisions, and the high magnetic field cause the QE affected ions to collapse to the cell center while most off-resonant ions are ejected due to magnetron expansion and/or off-resonance excitation. An added advantage is that the ions are cooled from much of their internal energy as well as from most of the cyclotron, magnetron, and longitudinal kinetic energy.[27, 37, 38]

For narrow band ion selection by QE, a low voltage (typically 1-2 V), single frequency rF field is applied to the excite plates of the cell at the unperturbed cyclotron frequency of the ion of interest. The unperturbed frequency can be calculated from Equation 1.10. The corresponding measured (ie, perturbed) m/z at this unperturbed frequency for the present trapping conditions is used to program the QE pulse. In practice, this amounts to roughly 4-6 m/z units less than the measured m/z of the selected ion; this simple rule of thumb can be used since subsequent optimization of the ion isolation pulse (for either method) makes this option equivalent to calculation and application of the true unperturbed frequency. The remaining ions are typically within 5-10 m/z units of the perturbed m/z corresponding to the QE pulse, and will excite to a more durable period of coherence due to their minimally diffuse state, as shown earlier in Figure 2.5.

Ion selection can also be achieved through correlated sweep excitation. Since the sweep excitation is really a series of single frequency rF pulses of a given duration, the power spectrum of each of these is effectively a sinc function with nodes of zero net

energy spaced (2B + 2Bn) radians/second from the fundamental frequency and relative maxima of net energy at (B + 2Bn) radians/second (for n = 0,1, 2,...).[32] Creation of a chirp function that skips the selected ion fundamental frequency and spaces the remaining frequency steps so that nodes overlap at the selected ion frequency results in an ejection pulse that has a sharp drop to zero *net* excitation radius for ions with similar to the chosen notch frequency, minimizing selected ion excitation. This is critical for MS^n experiments targeting the initial kinetic energy of the target ion. It is worthwhile to note that the isolated ions do experience continual off-resonance excitation and de-excitation cycles throughout the correlated sweep experiment but the design of the sequence is such that the ions should return to a position of equivalent radius to that which they had at the start of the sweeps.

While QE can isolate very narrow distributions of ions, it can also axialize ions of broader distributions. Many variations have been explored,[15, 39-45] but in this work the primary broadband QE (BBQE) methods exploit either high amplitude, single frequency rF excitation or repetitive chirp excitation.[43, 45] Application of a high voltage single frequency rF field works because the power spectrum of the applied field becomes broader with amplitude and results in a broader ion envelope experiencing QE. There are a couple of minor drawbacks to this mode of BBQE. First, ions at or near the applied frequency are usually ejected and the window of ejection is qualitatively proportional to the amplitude of the applied field; still, this ejection window is only 2-3 Da wide at 20V QE and m/z 2025 and can usually be chosen such that ions of interest are unaffected. Second, while the width of the axialized ion envelope increases with QE amplitude, the quality of the axialization degrades (as demonstrated by remeasurement efficiency).[15, 45]

Repetitive chirp QE offers some advantages to high amplitude, single frequency QE although it is much harder to tune and requires an external signal generator and some simple support electronics. Frequency sweeps (or, "chirps") encompassing the m/z region of interest are programmed to the signal generator and allowed to run on a continuous loop throughout the 3 - 4 second QE cycle. A typical chirp will excite ions from 700 to 3000 m/z by stepping though 1000 evenly spaced frequencies corresponding to this range over the course of 1 msec with the amplitude high enough to excite the non-resonant frequencies between steps; that is, a nearly linear power spectrum is supplied. High remeasurement efficiencies on broad distributions of ions are possible, but an as yet unexplained notching effect wherein packets of ions at seemingly irregular spacing can be ejected or inefficiently axialized relegates the method to some very specific applications. An example, described in a Chapter 4, is broadband ion accumulation with the internal source MALDI.

EXCITATION OF THE IONS AND RECORDING THE IMAGE CURRENT

Excitation and detection have already been covered in some detail and are fairly standard for FTICR-MS experiments. Briefly, excitation is achieved by subjecting the ions contained in the cell to an azimuthal dipolar rF sweep through the resonant frequencies of the ion m/z range of interest. Given the starting and ending frequencies of the sweep, the resulting ion radii are proportional to the amplitude and duration of the sweep even though an uneven power spectrum is delivered for ions with frequencies at the extremes of the chirp.[46] The induced image current on each detector plate is converted to a voltage across a 5.1 MS resistor to ground at the input to a high speed

buffer mounted adjacent to the cell. This placement of the current-to-voltage converter helps correct impedence prior to subsequent amplification and minimizes noise pickup through the output conductors.[47] An external pre-amplifier boosts this signal from each of the opposing detector plates and feeds the two phases to a differential amplifier which, essentially, doubles the amplitude of the voltage representation of the image current signal while canceling any common mode noise. This signal is digitized and stored directly as a series of time dependent amplitudes representing the time-domain signal. The fast Fourier transform (FFT) of this data yields an analogous frequency domain data set corresponding to amplitudes as a function of frequency.

Conversion of this frequency domain spectrum to a mass spectrum is not a straightforward application of the cyclotron equation, but rather a matter of fitting the measured frequencies for some assignable peaks, either internally (from the spectrum to be calibrated) or externally (from other spectra). For most of the experiments here, calibration equations took a form that resulted in good correlation of mass-to-charge with the measured frequency by fitting a function that was derived from the cyclotron and magnetron equations; this required that external calibrant transient signals be measured with the ions at the same trapping voltage as the ions in the spectrum to be calibrated. This is still highly advisable despite newer calibration equations that purport to account for trapping differences; it is also necessary that the excitation parameters and the measured transient duration (digitization rate and number of data points) be equal in both spectra. Finally, as will be described in greater detail in Chapter 3, spectra with similar amounts of space charge are more compatible as the calibrant and the calibrated

(although the most recent versions of the calibration equations also take space charge related frequency shifts into account).

REFERENCES

(1) Karas, M.; Hillenkamp, F. *Anal. Chem.* **1988,** *60*, 2299.

(2) Schurenberg, M.; Schulz, T.; Dreisewered, K.; Hillenkamp, F. *Rapid Commun. Mass Spectrom.* **1996,** *10*, 1873-1880.

(3) Hensel, R. R.; King, R. C.; Owens, K. G. *Rapid Commun. Mass Spectrom.* **1997,** *11*, 1785-1793.

(4) Beavis, R. C.; Chait, B. T. *Chemical Physics Letters* **1991,** *181*, 479.

(5) Beavis, R.; Chait, B.;, 1997.

(6) Tang, X. D.; Dreifuss, P. A.; Vertes, A. *Rapid Commun. Mass Spectrom.* **1995,** *9*, 1141-1147.

(7) Blais, J. C.; Tessier, M.; Bolbach, G.; Remaud, B.; Rozes, L.; Guittard, J.; Brunot, A.; Marechal, E.; Tabet, J. C. *Int. J. Mass Spectrom. Ion Process.* **1995,** *144*, 131-138.

(8) Preston, L. M.; Murray, K. K.; Russell, D. H. *Biological Mass Spectrometry* **1993,** *22*, 544-550.

(9) Worrall, T. A.; Cotter, R. J.; Woods, A. S. *Anal. Chem.* **1998,** *70*, 750-756.

(10) Zaluzec, E. J.; Gage, D. A.; Allison, J.; Watson, J. T. *J. Am. Soc. Mass Spectrom.* **1994,** *5*, 230-237.

(11) Easterling, M. L.; Pitsenberger, C. C.; Kulkarni, S. S.; Taylor, P. K.; Amster, I. J. *Int. J. Mass Spectrom. Ion Process.* **1996,** *158*, 97-113.

(12) Easterling, M. L.; Pitsenberger, C. C.; Amster, I. J. *J. Am. Soc. Mass Spectrom.* **1997,** *8*, 195-198.

(13) Easterling, M. L.; Mize, T. H.; Amster, I. J. *Int. J. Mass Spectrom.* **1997,** *169*, 387-400.

(14) Pitsenberger, C. C.; Easterling, M. L.; Amster, I. J. *Anal. Chem.* **1996,** *68*, 4409-4413.

(15) Pitsenberger, C. C.; Easterling, M. L.; Amster, I. J. *Anal. Chem.* **1996,** *68*, 3732-3739.

(16) Mize, T. H.; Amster, I. J. *Anal. Chem.* **2000,** *72*, 5886-5891.

(17) Gluckmann, M.; Pfenninger, A.; Kruger, R.; Thierolf, M.; Karas, M.; Horneffer, V.; Hillenkamp, F.; Strupat, K. *Int. J. Mass Spectrom.* **2001,** *210*, 121-132.

(18) Berkenkamp, S.; Menzel, C.; Hillenkamp, F.; Dreisewerd, K. *J. Am. Soc. Mass Spectrom.* **2002,** *13*, 209-220.

(19) Gluckmann, M.; Karas, M. *J. Mass Spectrom.* **1999,** *34*, 467-477.

(20) Knobeler, M.; Wanczek, K. P. *Int. J. Mass Spectrom. Ion Process.* **1997,** *163*, 47-68.

(21) Bokelmann, V.; Spengler, B.; Kaufmann, R. *Eur. Mass Spectrom.* **1995,** *1*, 81-93.

(22) Vartanian, V. H.; Laude, D. A. *J. Am. Soc. Mass Spectrom.* **1995,** *6*, 812-821.

(23) Guan, S. G.; Marshall, A. G. *Rapid Commun. Mass Spectrom.* **1993,** *7*, 857-860.

(24) Guan, S. H.; Marshall, A. G. *Anal. Chem.* **1993,** *65*, 1288-1294.

(25) Guan, S. H.; Marshall, A. G. *International Journal Of Mass Spectrometry And Ion Processes,* **1996,** *158*, 5-37.

(26) Schweikhard, L.; Guan, S. H.; Marshall, A. G. *Int. J. Mass Spectrom. Ion Process.* **1992,** *120*, 71-83.

(27) Guan, S. H.; Wahl, M. C.; Wood, T. D.; Marshall, A. G. *Anal. Chem.* **1993,** *65*, 1753-1757.

(28) Marshall, A. G.; Guan, S. H. *Physica Scripta* **1995**, 155-164.

(29) Speir, J. P.; Gorman, G. S.; Pitsenberger, C. C.; Turner, C. A.; Wang, P. P.; Amster, I. J. *Anal. Chem.* **1993,** *65*, 1746-1752.

(30) Hendrickson, C. L.; Laude, D. A. *Anal. Chem.* **1995,** *67*, 1717-1721.

(31) Hendrickson, C. L.; Drader, J. J.; Laude, D. A. *J. Am. Soc. Mass Spectrom.* **1995,** *6*, 448-452.

(32) de Koning, L. J.; Nibbering, N. M. M.; van Orden, S. L.; Laukien, F. H. *Int. J. Mass Spectrom.* **1997,** *165*, 209-219.

(33) Laude, D.; Beu, S. *Anal. Chem.* **1989,** *61*, 2422-2427.

(34) Easterling, M. L.; Mize, T. H.; Amster, I. J. *Anal. Chem.* **1999,** *71*, 624-632.

(35) Guan, Z. Q.; Hofstadler, S. A.; Laude, D. A. *Anal. Chem.* **1993,** *65*, 1588-1593.

(36) Campbell, V. L.; Guan, Z. Q.; Laude, D. A. *J. Am. Soc. Mass Spectrom.* **1995,** *6*, 564-570.

(37) Pasatolic, L.; Huang, Y. L.; Guan, S. H.; Kim, H. S.; Marshall, A. G. *J. Mass Spectrom.* **1995,** *30*, 825-833.

(38) Reinhold, B. B.; Costello, C. E.; Guan, S. H.; Marshall, A. G. *Abstracts Of Papers Of The American Chemical Society* **1996,** *212*, 74-Anyl.

(39) Guan, S. H.; Gorshkov, M. V.; Marshall, A. G. *Chemical Physics Letters* **1992,** *198*, 143-148.

(40) Schweikhard, L.; Alber, G. M.; Marshall, A. G. *Physica Scripta* **1992,** *46*, 598-602.

(41) Guan, S. H.; Wahl, M. C.; Marshall, A. G. *Journal Of Chemical Physics* **1994,** *100*, 6137-6140.

(42) Pitsenberger, C. C.; Amster, I. J., Atlanta, GA, May 21-26, 1995 1995; 798.

(43) Marto, J. A.; Guan, S. H.; Marshall, A. G. *Rapid Commun. Mass Spectrom.* **1994,** *8*, 615-620.

(44) Oconnor, P. B.; Speir, J. P.; Wood, T. D.; Chorush, R. A.; Guan, Z. Q.; McLafferty, F. W. *J. Mass Spectrom.* **1996,** *31*, 555-559.

(45) Pitsenberger, C. C.; Amster, I. J. *Eur. Mass Spectrom.* **1997,** *3*, 1-9.

(46) Xiang, X. Z.; Guan, S. H.; Marshall, A. G. *J. Am. Soc. Mass Spectrom.* **1994,** *5*, 238-249.

(47) Hunter, R.; personal communications with author, 1998.

CHAPTER 3

MASS ACCURACY AND SPACE CHARGE

INTRODUCTION

Fourier transform ion cyclotron mass spectrometry (FTICR-MS) has demonstrated unprecedented mass resolution for both singly charged[1-3] and mutiply charged ions[4, 5] which allow identification of isobaric species. For FTICR-MS to become a widespread substitute – or better, replacement – for the other high mass, high accuracy forms of mass spectrometry such as time of flight (TOF) mass spectrometry, it must show a marked improvement in at least one of these two areas. FTICR-MS will not, soon, exceed the sensitivity at high mass of TOF-MS due to magnetic field limitations and trapping considerations; however, recent improvements to mass accuracy measurements, presented here and elsewhere,[6-8] have improved FTICR-MS as an analytical tool while the techniques used to confirm these mass accuracy results simultaneously help to extend the sensitivity of the internal source MALDI-FTICR-MS used for these experiments and those detailed in the subsequent chapters.

In mass spectrometry, measurements can be improved with increased mass accuracy.[9-11] While precise mass measurements have been used for decades to determine elemental compositions for low molecular weight materials,[12] the assignment of exact masses to high molecular weight substances has eluded the analytical community due to questions of resolution[13-17] and even peak shape[9, 10, 18] which can severely effect assignment of a given mass to a mass spectrometric peak. Takach et al have presented work demonstrating that the number of proteolytic fragment masses necessary for identification of the parent protein in a database search is inversely proportional to the mass accuracy of the peaks.[13] Exact assignment of repeat unit masses in synthetic

polymers requires accurate mass measurement which can, as a matter of course, effect the assignment of the endgroup chemical formulas for low mass polymers.[19]

High mass resolution, the undisputed domain of the FTICR mass spectrometer, is a prerequisite for accurate mass assignment.[14, 16, 20-24] Analysis of "unknown" samples by FTICR-MS has been demonstrated for a variety of naterials inclucing polymer analysis,[7, 19], identification of proteins and their proteolytic fragments,[25] elemental identification,[26] and collisional dissociation product characterization.[20, 27-29] FTICR-MS measures ion masses by determining their excited cyclotron frequencies, which can be measured to a high degree of precision (usually in the sub-ppb domain).[30]

Precision does not guarantee accuracy, though. Image current is created by coherent motion of a group of ions between a set of opposed electrodes in a magnetic field, resulting in a temporal signal defined by the equation $\omega_C = qB/m = 2\pi f_C$, in which the cyclotron frequency, f_C, or its measured analog the cyclotron angular velocity, ω_C (usually referred to as the cyclotron frequency, as well), are directly related to the applied magnetic field, B, and inversely proportional to the mass-to-charge ratio, m/q.[31] Complications arise from the convolution of the cyclotron frequency with other measureable oscillations caused by the requirements that the charged particles to be measured must be contained in a finite volume to be measured. The DC electric field commonly used to achieve the trapping effect within the analyzer section of the ICR cell influences the movement of the ions and their observed cyclotron frequency.[32] Moreover, the collective field of the ions trapped in the cell results in a phenomenon known as "space charge" which results in perturbations to the trapping field.[33] This frequency shift has also been noted in quadrupole ion trap mass spectrometers (QIT-MS).[34, 35]

Space-charge effects were first proposed as a limitation to ICR mass accuracy by Sommer et al. in their report describing the first ICR mass spectrometer, the omegatron.[36] Beauchamp later reported a reduction in the expected cyclotron frequency of ions in a drift cell due to space-charge,[37] and represented this symbolically by the relationship, $T_{obs} = T_c - T_m - *$, where T_m describes the magnetron frequency and * is a smaller magnitude term resulting from space-charge. The terms describing these effects are negative in magnitude since the force on an ion caused by these electric fields opposes the force induced by the magnetic field, thereby reducing the observed cyclotron frequency.

Radial electric field gradients described in terms of trap electrode geometry and ion cloud shape were used to describe shifts in the observed frequency of ions in analyzer cells.[33] However, the model used was defined for the scanning ICR experiment and its detection scheme in which ions reside near the center of the analyzer cell and are ejected to an ion multiplier sequentially by resonant rF excitation. On the other hand, FTICR-MS is performed by exciting ions coherently to a radius of gyration sufficient for their collective charge to induce a current on detector electrodes, and this current detected simultaneously (to be distributed amongst many channels with respect to frequency and magnitude of signal via the fast Fourier transform).[30] In the Jeffries treatment, the ions are located near the center of the analyzer cell, which is a reasonable assumption since the deviations from ideal behavior are lowest in the center of most cells.[18] The Jeffries' model of space charge has been used by several investigators to formulate relationships between observed frequency and expected mass for FT-ICR experiments.[7, 8, 38, 39] For

instance, McIver and co-workers applied Jeffries' equations to develop an expression relating observed frequencies to the mass-to-charge of the ion, Equation 3.1.[38]

$$\omega_{obs} = \frac{qB}{m} - \frac{2\alpha V}{a^2 B} - \frac{q\rho G_i}{\varepsilon_o B} \tag{3.1}$$

For ω_{obs}, the observed (or measured) cyclotron radial velocity, the first term (qB/m) is equal to the unperturbed cyclotron radial velocity and the second term ($2\alpha V/a^2B$) describes magnetron component of ω_{obs} (in a perfectly quadrupolar static trapping field with cell geometry factor, α, trapping voltage, V, trap spacing, a, and magnetic field, B. The last term ($q\rho G_i/\varepsilon_0 B$) describes the space charge component of the frequency shift, where q represents the elementary charge magnitude, ρ the density of the ion cloud with respect to charge, G_i the ion cloud geometry (a nebulous term that varies indirectly with trapping geometry and ρ), and ε_o, the permittivity of free space. McIver correlated the shift between the frequency of an ion with known mass and the measured mass of an unknown to demonstrate sub-ppm average mass accuracy for low mass-to-charge ions.[38] The results of Jeffries[33] and McIver[38] were used by Gross and coworkers to parameterize the mass-to-frequency relationship, as shown in Equation 3.2,

$$\frac{m}{z} = \frac{a}{f} + \frac{b}{f^2} \tag{3.2}$$

where f_C is the measured frequency of an ion, a and b are experimentally determined constants, and m/z is the mass-to-charge ratio. Until recently, this equation (and a derivation that includes a third expansion coefficient, c/f^3) has been in wide use.[39] The two (or three) constant terms in this calibration equation are determined by best fit to

derivations of Equation 2, with decreasing effect on the final calculation of m/z. However, b and c are functions of the ion density of the mass spectrum used to calibrate the instrument.[39] Variations between D for the analyte and D of the calibrant must be taken into account in order to maximize mass accuracy.

Chen and Comisarow explained the frequency shifts in the FTICR-MS as coulombic interactions between ions.[40, 41] The coulombic forces between ions of different mass-to-charge was used to calculate a reduction in magnetic force, which was used to explain some of the observed frequency differences. The model was expanded from a point charge calculation of coulombic interactions to the use of line charges and cylindrical charges, which yielded better approximations for the frequency shifts, but failed to explain space-charge induced frequency shifts for ions of similar mass-to-charge.[38] Coulombic interactions between an ion in the ICR cell and its induced image charge on the cell electrodes can also occur.[42, 43] The resultant force attracts the ion toward the cell plate in opposition to the magnetic force. This outward force is mass independent and has been described in terms of the cell geometry, position of the ions within the cell.[44]

Easterling et al have shown the utility of the open cylindrical cell for use in measuring molecular weight distributions for industrial polymers with moderate levels of polydispersity to greater than part-per-million mass accuracy.[7, 8] This chapter shall revisit that work in order to lay the foundations for the subsequent research. In particular, the mechanics of high mass accuracy using external calibrants will be examined along with the conditions necessary for measuring wide mass distributions. And, the technique of suspended trapping,[45] used here to systematically lower overall ion abundances to

examine the parameter D of Equation 1, will also be used to lower the space charge coalescence of isobaric peaks (see Chapters 5 and 6) and serves as the basis for ion retention in accumulated trapping (Chapter 4).

EXPERIMENTAL

All experiments were performed with the 4.7 tesla FTICR mass spectrometer with an internal source for matrix assisted laser desorption/ionization (MALDI) that was designed and fabricated at the University of Georgia, and that has been described previously.[1, 46] MALDI samples were applied to a target that was positioned within 1 cm of an open cylindrical cell.[47] The 355 nm line of a Nd:YAG laser (ACL-1, New Wave, Sunnyvale, CA) was focused through the cell and onto the sample. Ions formed by MALDI were captured by using gated trapping[48-50] with a 200-400 μs delay between ionization and restoration of the symmetric trapping potential. Prior to detection, nitrogen was introduced into the analyzer region at a pressure of ca. $1x10^{-5}$ Torr through a pulsed valve for 1-3 ms to reduce the amplitude of the axial oscillation of the ions by collisional damping. After trapping the ions with a 20-30 V potential, the end electrode voltages are lowered to 250-1000 mV prior to detection. Capacitive coupling of the RF excitation to the trap plates during dipolar excitation is used to reduce the axial ejection of ions.[47, 51] A previously described circuit was used to disengage capacitive coupling during the gated trapping event.[46]

Reduction in the number of trapped ions was performed with alternating cycles of quadrupolar excitation (QE) and suspended trapping.[45] Following detection, the trapping electrodes were brought to ground potential for about 1 ms to allow axial ion loss via suspended trapping; the trapping potential was then restored to 1 V and a narrowband QE

pulse was applied. For narrowband QE, a 1 V_{p-p} burst excitation pulse was applied at a frequency that was slightly higher than the observed frequency of the ion. Broadband remeasurement used a 10 V_{p-p} arbitrary waveform with a bandwidth that covered the frequency range of interest. QE signals were usually applied for 2-3 s in the presence of nitrogen admitted through a pulse valve, providing a peak background pressure of approximately $1x10^{-4}$ Torr. Reduction in the abundance of a single mass-to-charge from a distribution of trapped masses was accomplished by collisionally activated dissociation, in which nitrogen buffer gas was admitted through a pulsed valve at a peak pressure of $1x10^{-7}$ Torr, followed by resonant excitation of the target ion with a 5.3 V_{p-p} signal for 1 ms. Experiments requiring single ion isolation used an arbitrary waveform pulse for resonant ejection of the isotope ions.

Poly(ethylene glycol) (PEG) samples were prepared for MALDI analysis using the dried droplet method by placing 1 μL of a 0.1 M PEG solution on the probe followed by 1 μL of a saturated sinipinic acid (Sigma, St. Louis, MO) solution. Both matrix and analyte were dissolved in 50% aqueous acetonitrile containing 0.1% trifluoroacetic acid (TFA) and a 0.5 μL amount of a 1 mM NaCl (aq) solution was added to promote sodium ion adduction. Poly(methyl) methacrylate (PMMA) samples were dissolved in acetone (0.1 M) and mixed 60:40 (v:v) with a 0.2 M solution of trans-3-indoleacrylic acid (IAA) in acetone. About 70-100 μL of the mixture was applied to the sample target by electrospray deposition to create a homogenous thin film.[52] Insulin B-chain was prepared in the same manner as for the PEG samples, but without salt addition. Both calibrant and analyte were applied to the same target. External calibration was performed by rotating the sample target to bring first the analyte and then the calibrant under the focal point of

the laser. All analytes and matrices were obtained from commercial suppliers and used without modification.

RESULTS AND DISCUSSION

Previous studies of the effect of ion number on observed ICR frequency used electron ionization, which allowed the number of trapped ions to be calculated from the neutral gas pressure and electron beam geometry.[38, 39] Although less rigorous theoretical quantitation exists for ion generation using MALDI, random fluctuations in ion intensity prevent practical prediction of ion number from the parameters of the ionization event. However, signal intensity in FTICR is a linear function of population for ions of similar charge,[31] allowing the absolute number of charges to be determined from the measured ion current in a detection circuit of precisely known capacitance,[53] although the uncertainty in cyclotron radius at detection time has limited the accuracy of this type of measurement to about ±10%.[54] It is therefore difficult to determine the absolute number of ions in the cell for the measurements reported here. However, since signal intensity is directly proportional to the number of ions (for singly charged ions), the absolute intensity of the signal can be used as a measure of the ion density, provided that the experimental conditions are identical for all mass spectra.[31]

The frequency shift observed by variation of the abundance of ions in a mass spectrum that contains ions of only one mass-to-charge is shown in Figure 3.1. Several successive laser shots produced varying numbers of ions, and the mass spectra that were obtained show a linear correlation between observed frequency, T_o, and ion intensity, with a negative slope. The total frequency change associated with the variation in absolute ion intensity in this example was about 7.5 Hz, which would cause a 110 ppm

frequency error if ignored. This trend agrees with the theoretical models of space-charge behavior that predict a linear relationship between ion population and frequency shift, for example the work of McIver, Equation 3.1.[38]

The statistical scatter seen in Figure 3.1 is characteristic of the polychromatic nature of MALDI ion production.[55-57] This is largely due to the residual kinetic energy from the desorption event, which is distributed to the ion as radial displacement (which effects the cyclotron frequency) and the longitudinal oscillation which, while exerting a much lower effect on the observed frequency with respect to its total magnitude, can be significant with respect to the relatively small changes in frequency measured here. Ions of lower kinetic energy relax to a smaller radius closer to the magnetic axis that leads to higher ion densities and increased inter-coulombic interactions;[9] that is, they will remain coherent longer post-excitation thereby lessening one of the effects that cause scatter. Also, in spite of the application of capacitive coupling, ions sample different electric field gradients as a function of their position in the analyzer cell because the cell is not perfectly quadrupolar along the magnetic axis, creating variations in the observed cyclotron frequency. These effects produce deviations from the expected linear model in the frequency versus intensity plot, as observed for the data displayed in 2a, from measurements of substance P ionized by MALDI.

The experimental error caused by the random nature of desorption can be reduced in part by relaxation of the trapping oscillation, as shown in Figure 3.2b. Here, ions were allowed to undergo collisions with a pulse of nitrogen prior to detection, to allow damping of the trapping motion. The scatter of the individual frequency measurements

Figure 3.1: Frequency shift as a function of ion population for the monoisotopic peak of bradykinin, showing the change in observed frequency as a function of total ion intensity as ions from a single laser shot are remeasured.

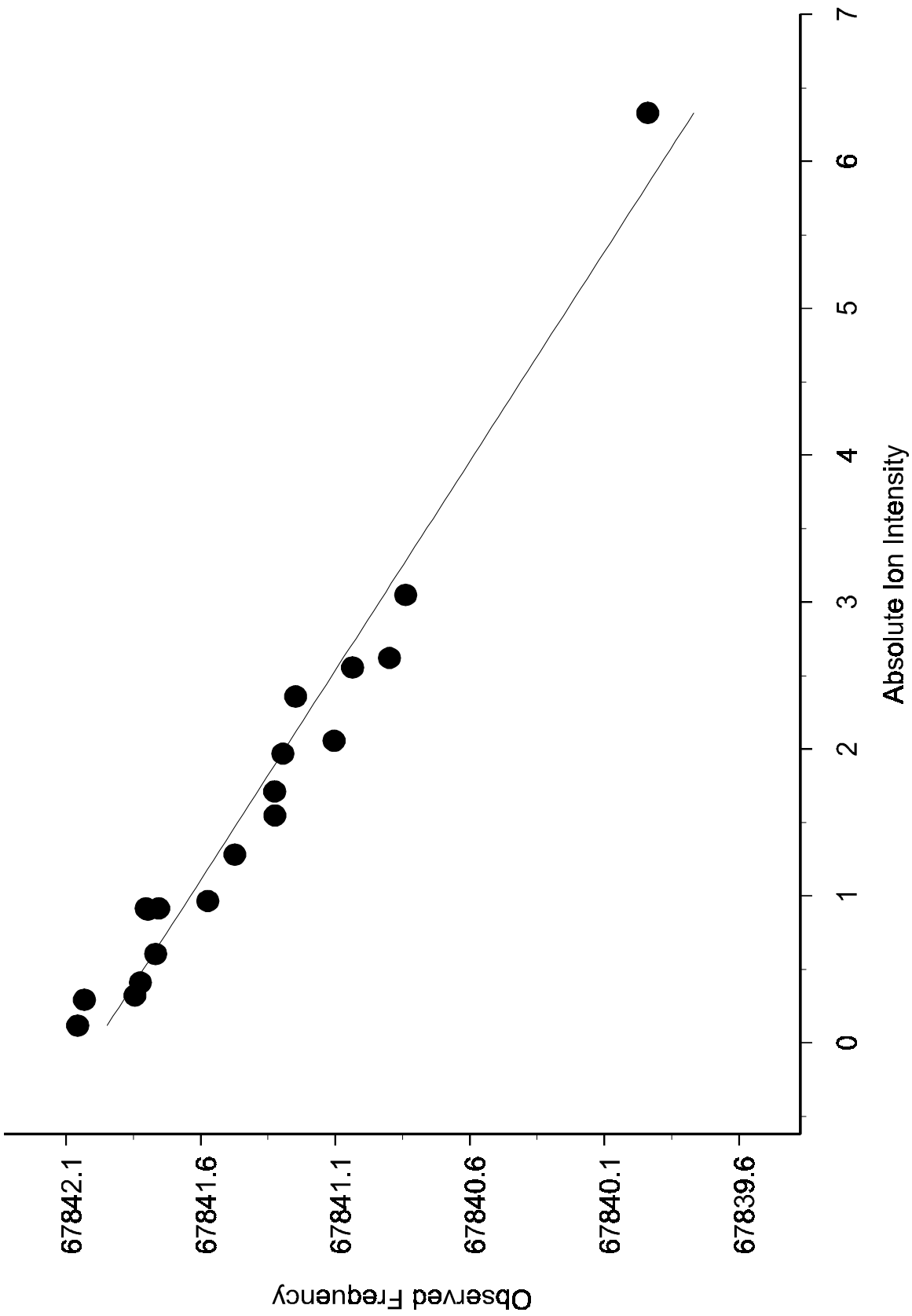
Observed Frequency
67842.1
67841.6
67841.1
67840.6
67840.1
67839.6
0
1
2
3
4
5
6
7
Absolute Ion Intensity

Figure 3.2: Plot of observed frequency as a function of ion intensity for substance P measured over 19 laser shots. (a) Ions captured with gated trapping. (R^2 = 0.73) (b) Ions captured with gated trapping and collisional cooling with a pulsed buffer gas show improved linearity due to damping of the trapping motion. (R^2 = 0.90) (c) Addition of quadrupolar excitation to the experimental sequence creates uniform pre-excitation conditions and provides the highest linearity in frequency versus intensity for MALDI generated ions. (R^2 = 0.99)

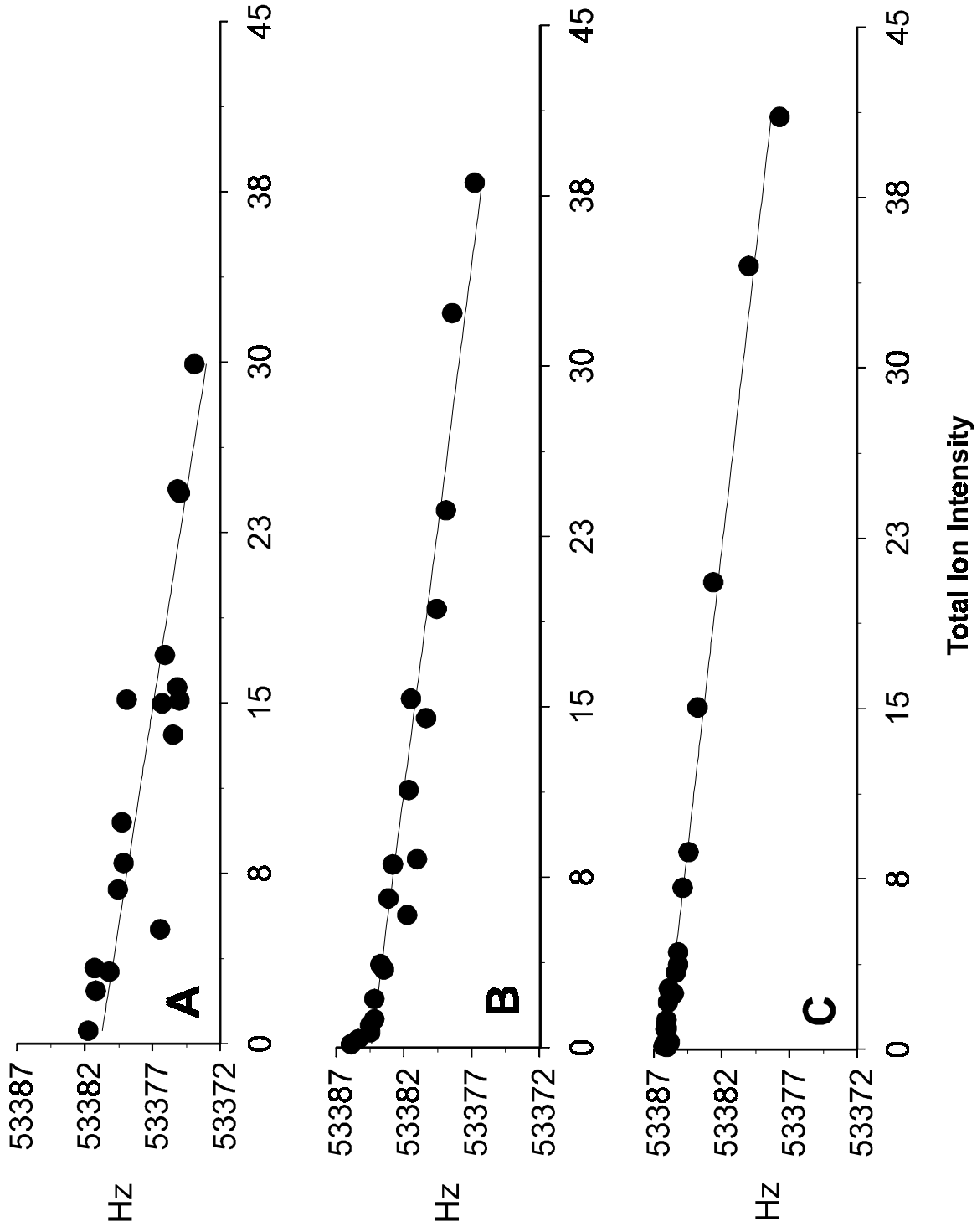
53387
53382
53377
53372
Hz
A
B
C
0
8
15
23
30
38
45
Total Ion Intensity

from the best-fit line has improved significantly compared to the data of Figure 3.2a. The least scatter is obtained by axialization of the ions before measurement, as shown in Figure 3.2c. With the application of quadrupolar excitation,[58] magnetron motion is damped along with the minimization of the trapping oscillation and cyclotron frequency. This is important because using QE to minimize the effects of magnetron expansion (which occurs due to collisions in the absence of QE) leads to greater signal linearity. This decoupling of ion generation effects from detection is important for the internal MALDI ion source which provides a wide distribution of ion populations and initial velocities.[56, 57, 59, 60]

Figure 3.3 shows a similar plot for three different ions from a PEG 3400 sample that exhibit a wider range of masses and frequencies than in the previous example. For these experiments, a set of ions was trapped from a single laser pulse, and then remeasured with alternate applications of quadrupolar axialization for ion centering, and brief (# $1x10^{-3}$ s) suspended trapping[45] events between remeasurement cycles to reduce the overall ion population in a controlled fashion. The observed range of ion densities is comparable to the range of values that might be observed during the acquisition of a mass spectrum of an analyte and a standard used as an external calibrant. Measured frequency, when plotted as a function of the total ion abundance, is linear with a negative slope, and exhibits R^2 values greater than 0.98 and slopes with values that agree within 5% of each other. These deviations provide empirical evidence that ion density produces a predictable, systematic error in accuracy for FT-ICR. In this example, the magnitude of the observed cyclotron frequency shift could produce an error as large as 150 ppm for mass determination using external calibration if the effect of space-charge is ignored.

Figure 3.3: Plot of observed frequency as a function of total ion intensity for the sodium cationized peaks of a PEG 3400 sample at n=77 (m/z 3431), n=82 (m/z 3651) and the A+1 peak of n=90 (m/z 3962) taken from the same spectrum. Linear fits of all three data set yielded a slope of about -0.19 Hz/IU. Repeated suspended trapping followed by quadrupolar excitation cycles of the polymer distribution provided a constant decrease in total ion number between measurements. The peak at m/z 3962 was about an order of magnitude less intense at than the other peaks examined.

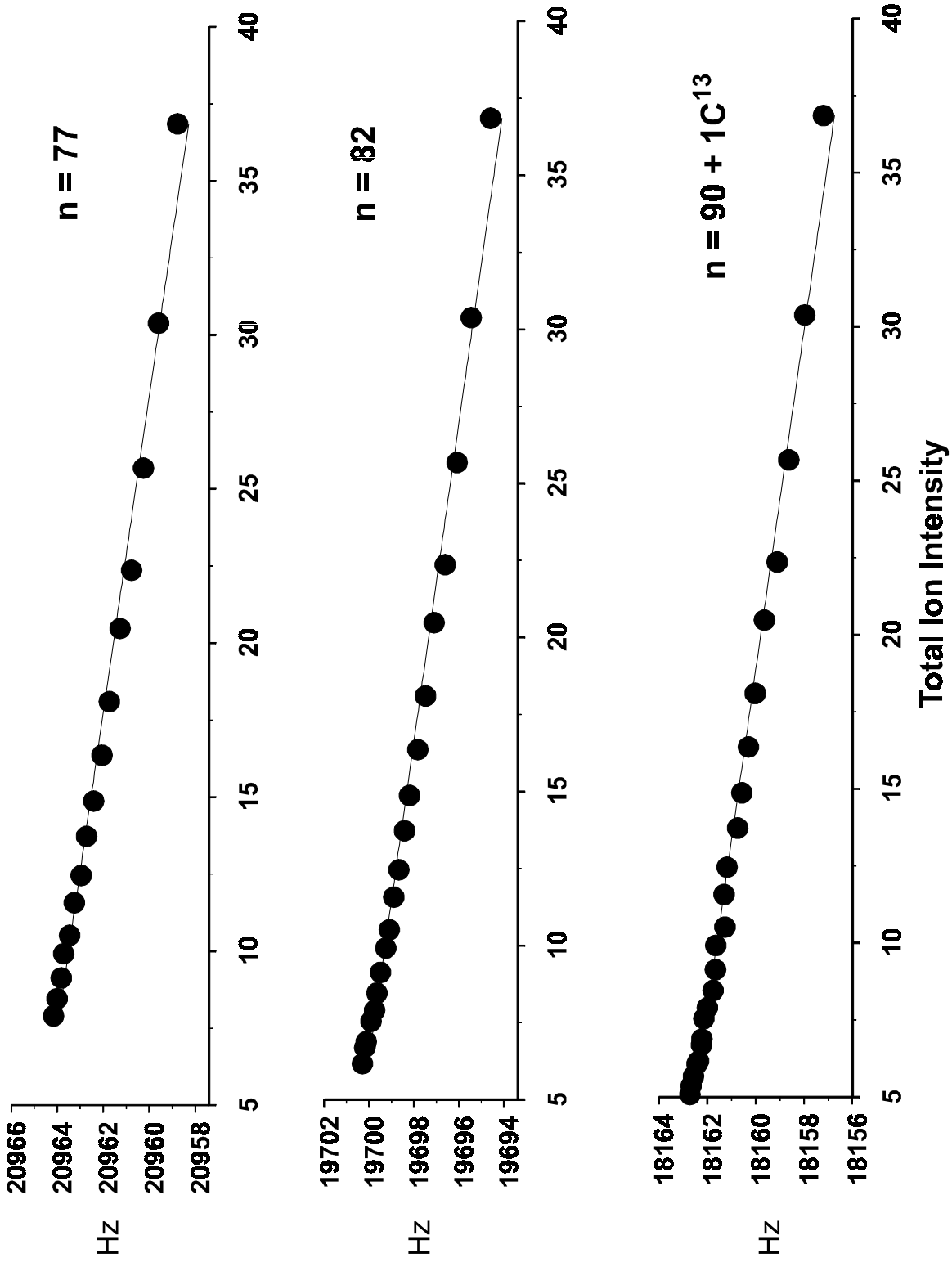
n = 77
n = 82
n = 90 + 1C13
Hz
Hz
Hz
20966
20964
20962
20960
20958
19702
19700
19698
19696
19694
18164
18162
18160
18158
18156
5
10
15
20
25
30
35
40
Total Ion Intensity

Prior studies of space-charge have not explored whether the magnitude of the displacement between ions' mass-to-charge values have an effect on the degree to which the space charge-induced frequency shift occurs. Ion coalescence, a severe space-charge effect wherein different ion species lock phase witheach other, occurs for ions that are closely spaced in frequency and that are present at high ion density.[61-63] To examine whether space-charge induced frequency shifts are more pronounced for ions that are close in mass, a group of closely-spaced isotope peaks were significantly reduced in intensity, while other ions in the mass spectrum were reduced only marginally. We then looked for differences between the space-charge induced frequency shift of the closely-spaced ions versus ions that were well removed in mass-to-charge from those that were reduced in intensity. To achieve this result, the experiment of Figure 3.3 was repeated, but the suspended trapping event was replaced by a resonant collisional activation pulse directed at one oligomer and its isotopes in the polymer distribution. Collisional dissociation reduced the population of the target oligomer by a few percent upon each application either by removal of the adducted alkali metal cation (neutralization), or by fragmentation of the molecule to produce lower mass ions outside the broadband axialization window. Following multiple remeasurements of ions generated from a single MALDI event,[64] the absolute intensity of the target oligomer at m/z 2066 and its isotopes (m/z 2067-2070) are observed to decrease over an order of magnitude while the total ion intensity is reduced by only 25% during 13 remeasurement cycles. The top panel of Figure 3.4 shows the polymer mass distribution after the first axialization event and before collisionally activated dissociation (CAD), in which the peaks show the expected distribution with a number average of approximately 2000 Da. The lower panel shows a

decrease in the intensity of the target ion at m/z 2068, and its isotopes, after 13 remeasurement cycles. A comparison of the absolute intensities of the target ion versus that of the overall polymer distribution is plotted in Figure 3.5. As can be seen, the intensity of the ions near m/z 2068 are reduced much more significantly than the other ions that are present. Figure 3.6a shows the measured frequency plotted as a function of the total ion intensity for the n=41 PEG oligomer at m/z 1846. The shift in measured frequency is nearly 8 Hz over the extremes of this experiment representing a maximum mass error of about 200 ppm for an ion at m/z 1846. A linear fit of these data points indicates a slope of about - 0.26 Hz per arbitrary unit of total ion intensity. This data is plotted in an identical fashion for the reduced target ion in Figure 3.6b, for which an identical frequency shift is observed for the change in total ion intensity, demonstrating that the space charge induced frequency shift is independent of mass (frequency) separations of ions in the mass spectrum.

As a test of the ability to correct for ion population effects on mass accuracy, a PEG 3400 sample was used to externally calibrate a single peptide mass, with the results shown in Figure 3.7. The mass channel multiplicity of the PEG 3400 distribution required he ion population to be reduced in the same manner as the experiments in Figure 3.3 so that the calibrant and analyte had nearly similar total ion intensities, although the base peak of the polymer sample is less than 1.25% as intense as that of the peptide. The accuracy of the externally calibrated mass measurement for the monoisotopic peak of insulin B-chain is about 1.6 ppm. The initial polymer (calibrant) mass spectrum yielded a total ion intensity that was about three times greater than that of the peptide. Ignoring

Figure 3.4: Mass spectra of a PEG 2000 distribution before (top) and after CAD of the ions at m/z 2066 (bottom). The CAD experiment was performed so that only a portion of the target ions were lost in between each remeasurement cycle to provide a small decrease per cycle in the ion population at that mass.

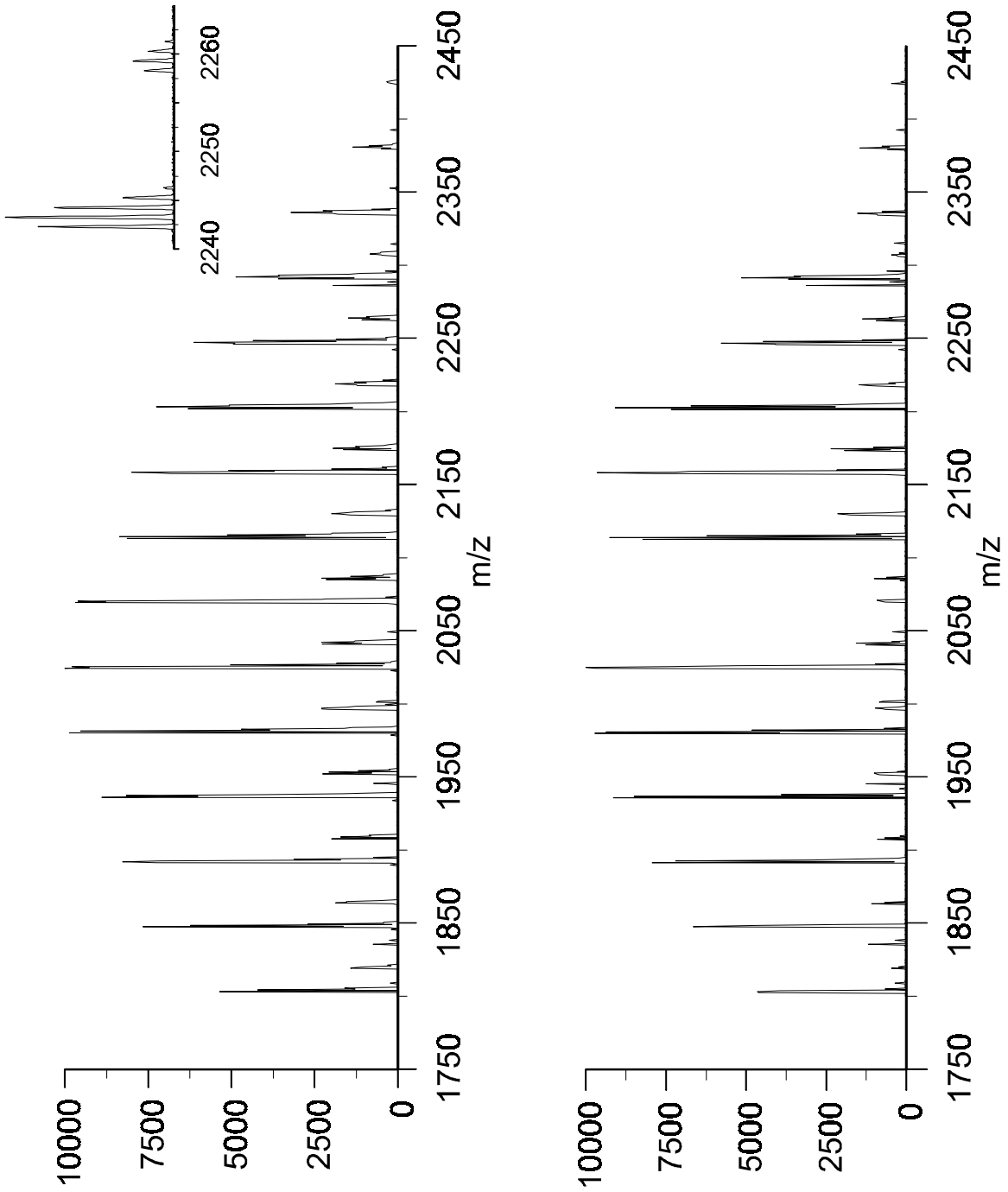
10000
7500
5000
2500
0
1750
1850
1950
2050
2150
2250
2350
2450
m/z
2240
2250
2260

Figure 3.5: Intensities of peaks at m/z 2066 and m/z 1848 from a PEG 2000 distribution in which CAD was used to reduce the intensity of the m/z 2066 ion over an order of magnitude while the total ion intensity decreased by about 25%.

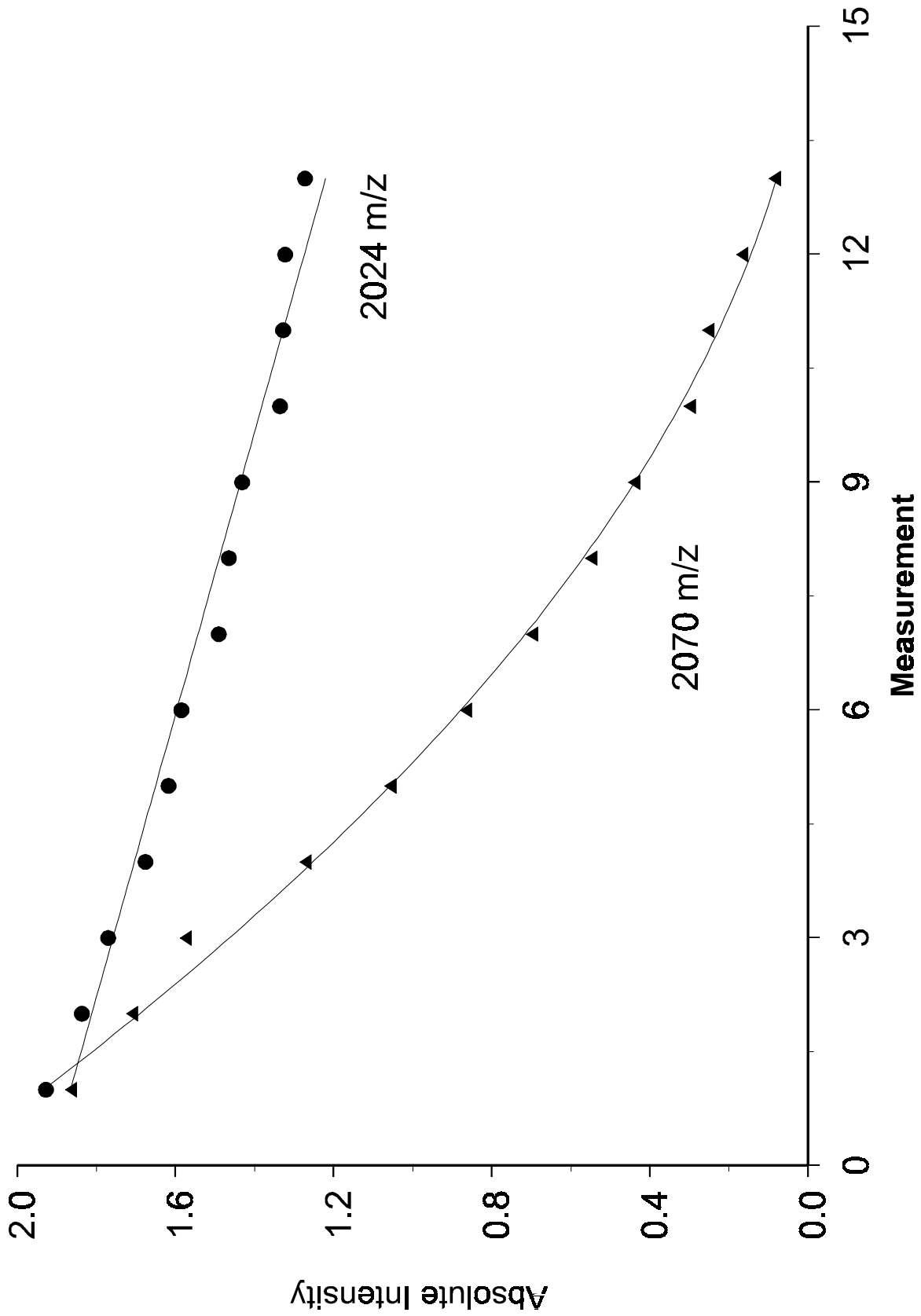
Absolute Intensity
2.0
1.6
1.2
0.8
0.4
0.0
0
3
6
9
12
15
Measurement
2024 m/z
2070 m/z

Figure 3.6: (a) Linear fit of measured frequency is plotted as a function of total ion intensity for the n=41 oligomer of the PEG 2000 distribution shown in Figure 3.3. (b) Linear fit of the measured frequency is plotted as a function of total ion intensity for the oligomer peak undergoing a systematic reduction in intensity. The calculated slope of -0.26 Hz per absolute intensity unit is less than a 3% deviation from the slope of the non-reduced peak.

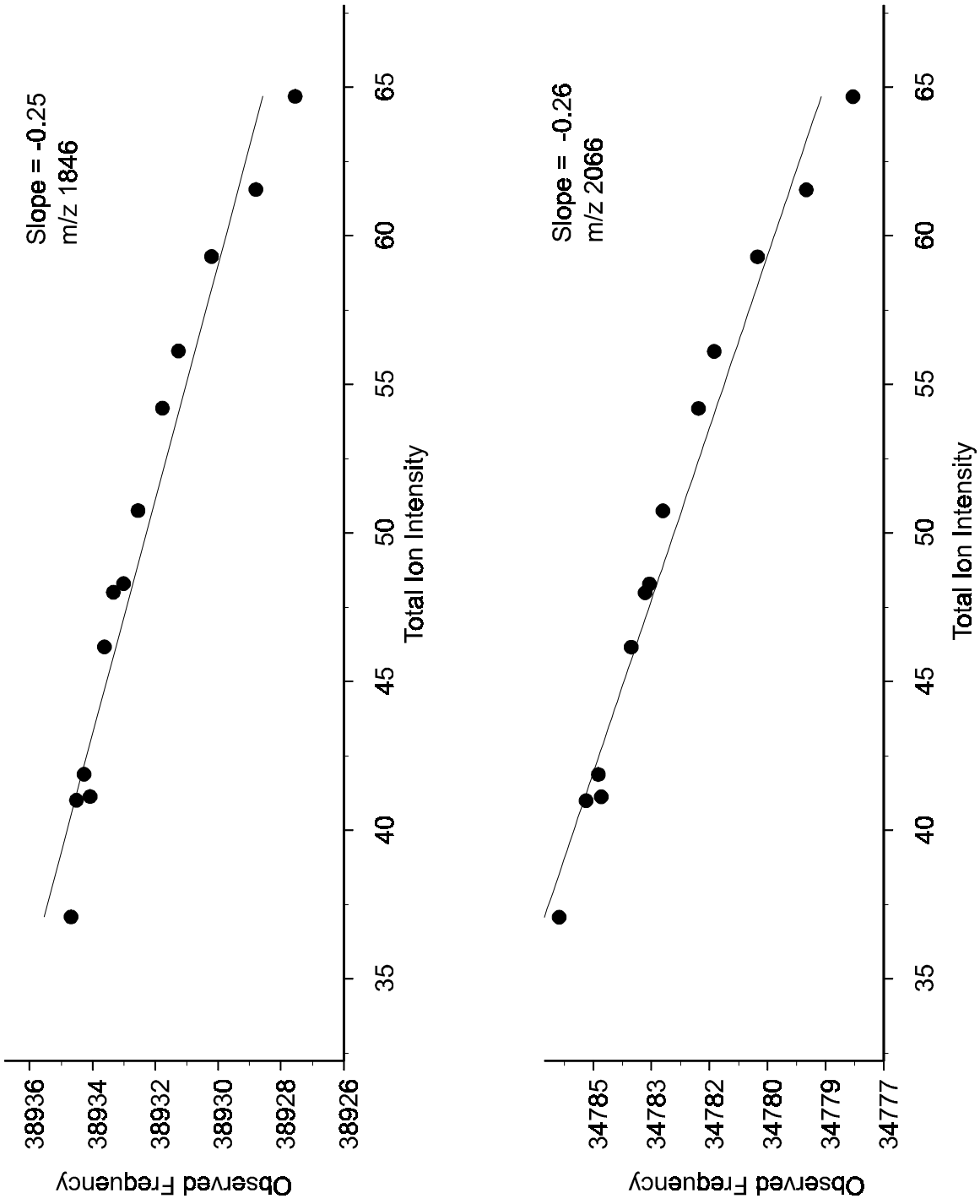
Slope = -0.25
m/z 1846
Observed Frequency
38936
38934
38932
38930
38928
38926
35
40
45
50
55
60
65
Total Ion Intensity
Slope = -0.26
m/z 2066
Observed Frequency
34785
34783
34782
34780
34779
34777
35
40
45
50
55
60
65
Total Ion Intensity

Figure 3.7: (a) MALDI mass spectrum of bovine insulin B-chain externally calibrated by the PEG 3400 distribution shown in (b). Systematic reduction of the total ion intensity of the polymer distribution to match that of the protein provided external mass accuracy of 1.63 ppm

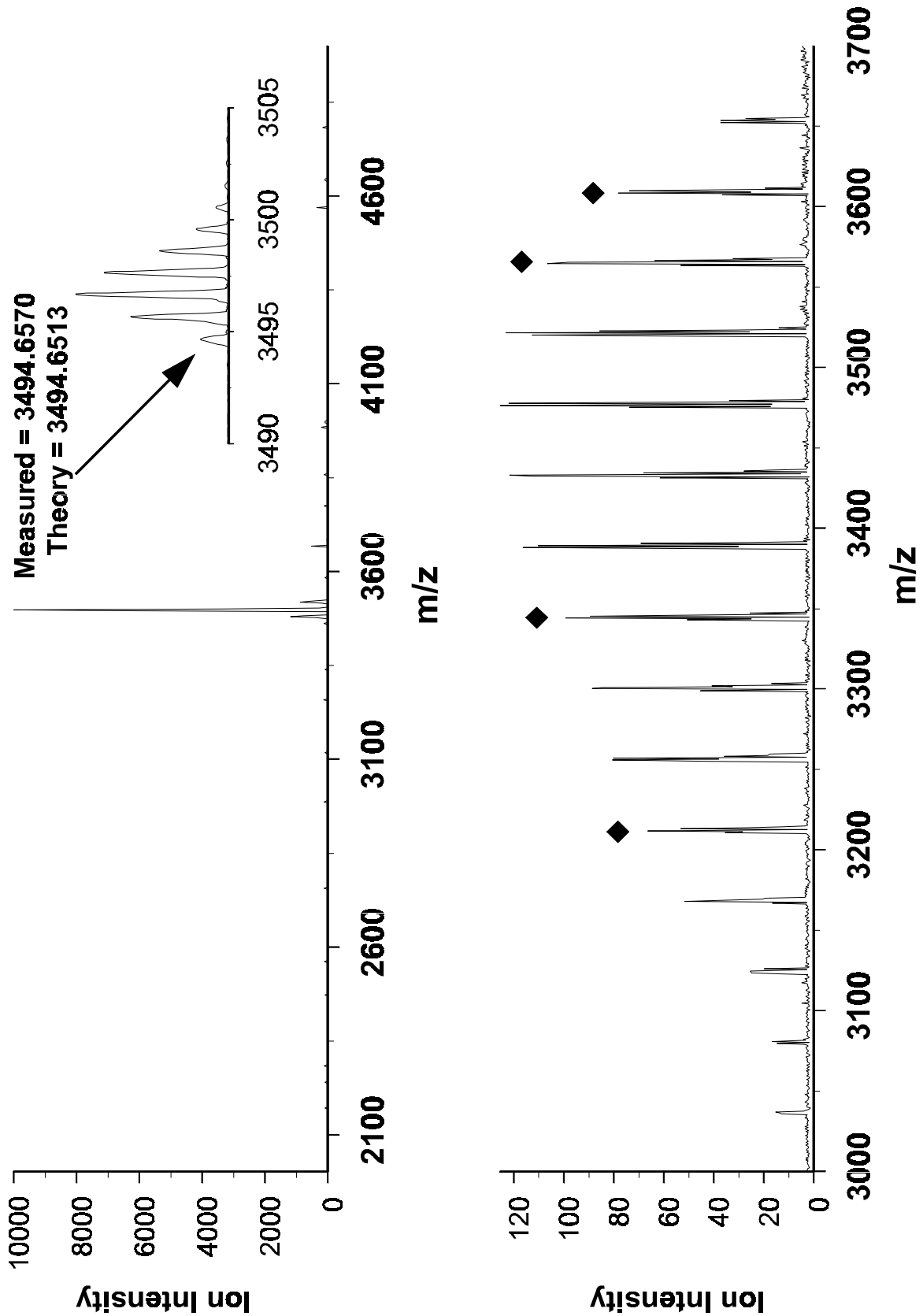
Measured = 3494.6570
Theory = 3494.6513
Ion Intensity
m/z
Ion Intensity
m/z

space-charge and applying the initial polymer mass spectrum as a calibrant for the peptide sample resulted in a mass measurement error of 220 ppm. This result is particularly remarkable in that the desorption dynamics of cation-attached polymers and protonated peptides are quite different, and thus polymers are considered to be poor standards for calibration of peptide samples when using time-of-flight mass spectrometry, which is sensitive to the initial kinetic energy of desorbed ions.

For polymer samples, these techniques have an obvious use in the accurate determination of the masses of the components of the molecular weight distribution; in most polymers discussed here, however, the high resolution of the FTICR is an unnecessary luxury. But, in addition to the molecular weight information obtained from the polymer distribution, the mass of the repeat unit and of the end group of a polymer can be determined by linear regression methods.[65-67] A linear least squares fit of the plot of the molecular weights of the oligomers against the degree of polymerization yields the mass of the monomer unit obtained as the slope of the line, and the residual mass of the end group and cation obtained as the intercept. Accurate mass measurement is imperative for successful calculations. Figure 3.8 shows implementation of this method with data obtained from the MALDI-FTMS mass spectrum of PEG 2K. The mass spectrum used to generate this plot was internally calibrated using three peaks at the low end of the oligomer distribution, and three peaks at the high end mass. The calibrant points are not use in the linear regression fit. The average absolute error for the masses of the monoisotopic peaks is 2.00 ppm (mean square error = 0.52 ppm). The least squares fit of these peaks yields a slope of 44.0261 amu, versus a calculated oligomer mass of 44.0262 amu, in error by 0.1 mmu, i.e.2.27 ppm. The intercept, 41.0055 amu,

represents the residual mass, that of H_2O plus Na^+. The measured value is in error by 1.7 mmu from the calculated value of 41.0038 amu. These data show that internal calibration produces highly accurate data from which the repeat mass and the end group mass can be determined with great certainty.

External calibration of polymer samples was tested using PEG 2K as the calibrant and PMMA 2K as the analyte. The monoisotopic peak masses were measured with an average absolute error of 4.00 ppm (1.80 MSE). The least squares fit of the data yields an oligomer mass of 100.0517 amu which is a 7.00 ppm difference from the calculated value of 100.0524 amu, and a residual mass of 25.0248 amu which is 22.3 mmu different than the calculated mass of the end group, $H_{2,}$ plus the mass of Na^+ (25.0025 amu). This example illustrates an important point in determination of the end group mass by the linear regression method. A very small error in the slope as determined by the least squares fit of the data is amplified as the line is extrapolated over a large mass range to determine the y-intercept. This error becomes larger as the molecular weight of the polymer increases.

An alternative method of determining residual mass is to use the measured mass of the repeat unit to assign an elemental composition, and then to use the calculated exact mass of the repeat unit to calculate the residual mass for each oligomer; these individual residual masses are then averaged. For example, the data of Figure 3.9 yields a repeat mass of 100.0517 Da, suggesting $C_5H_8O_2$ as the elemental composition. Using the calculated exact mass of $C_5H_8O_2$, 100.0524, the average calculated residual mass is 25.0097 amu, only 7.2 mmu from the actual value, a much more accurate value than that resulting from only the least squares fit to the data.

Figure 3.8: A plot of the measures masses of the oligomers of PEG 2000, internally calibrated, versus degree of polymerization. Linear regression of the data indicates an oligomeric repeat mass of 44.0261 Da (C2H4O)n and end-group mass of 41.0055 Da. (H2O+Na)+. These values represent mass measurement errors of 44.0262 - 44.0261 = .0001 Da. (2.27 ppm) for the repeat mass and |41.0038 - 41.0055| = .0017 Da (41.5 ppm) for the repeat group. The inset shows the oligomer distribution from which the mass values were obtained.

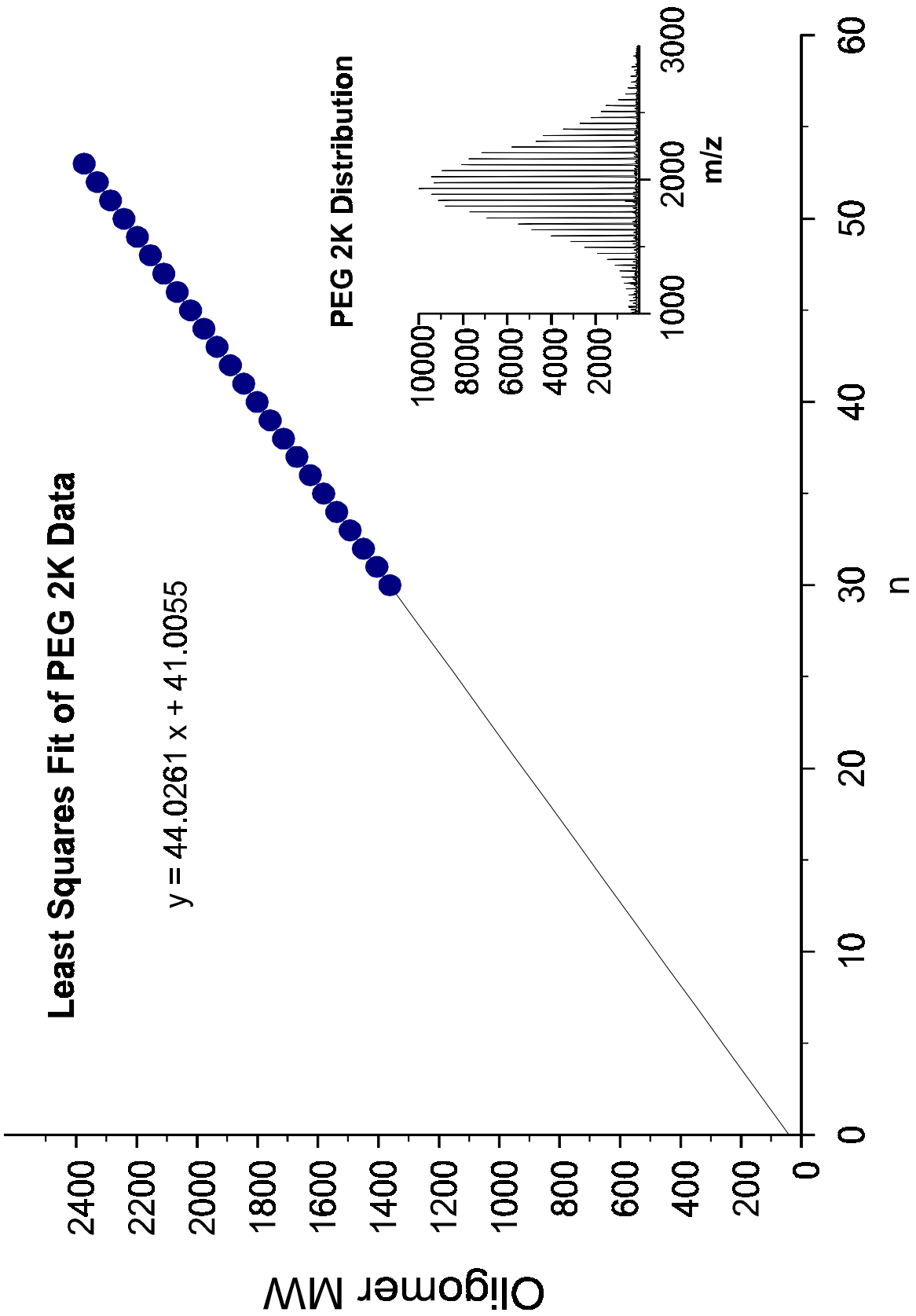
Least Squares Fit of PEG 2K Data
y = 44.0261 x + 41.0055
Oligomer MW
n
PEG 2K Distribution
m/z

At higher mass-to-charge, small frequency changes are much more significant due to the inverse relationship between m/z and cyclotron frequency. Table 3.1 shows the error obtained for the masses measured for each of the A+1 peaks ($^{13}C_1$-containing ions) of the Na^+ cationized series in an internally calibrated PEG 6K mass spectrum, and for the peaks in two mass spectra of PMMA 6K that were externally calibrated from the PEG 6K data. The average absolute error for the internally calibrated data is 1.8 ppm (0.5 ppm MSE), and is typical of the errors obtained when using internal calibration. Since the analyte and calibrant ions are present together in the analyzer cell with internal calibration, there is no expected space charge problem in this case. However, the total ion intensity of one PMMA mass spectrum is half that of the calibrant mass spectrum, while the second mass spectrum has a total ion intensity that is very close to that of the calibrant. The mean square error for the latter data is 15-fold less than for the initial data.

By accounting for the space-charge effect with externally calibrated data, extremely accurate values can be obtained for the repeat mass and end-group mass of polymers at high mass-to-charge, such as PMMA 6K. Using linear regression to fit the plot of the mass of the A+1 peaks of PMMA 6000 versus the degree of polymerization yields a value for the repeat mass of 100.0605 Da, different from the calculated value of 100.0524 Da by 8.1 mmu. The end-group mass determined by linear regression is 25.4861 Da, in error by 520 mmu from the calculated value of 26.0059 Da ($H_2 + Na^+ + {}^{13}C - {}^{12}C$). By using the calculated value of the repeat mass, the end-group mass is determined to be 26.0295 Da, different from the calculated value by only 23.6 mmu.

Table 3.1: List of observed masses (MW_{MEAS}), expected masses (MW_{CALC}), and mass measurement errors (in ppm) for the external calibration standard (PEG 6K) and PMMA 6K spectra acquired with total ion intensities similar to (right columns) and lower than (middle columns) that of the calibrant. These results show the effect of space charge on the mass accuracy measurement of ions.

PEG 6K total ion int = 18.84			PMMA 6K total ion int = 8.952			PMMA 6K total ion int = 17.29		
MW_{meas}		MW_{calc}	MW_{meas}		MW_{calc}	MW_{meas}		
ppm			ppm			MW_{calc}	ppm	
6337.750	6337.752	0.40	6129.475	6129.207	-44	6329.303	6329.311	1.3
6381.774	6381.778	0.65	6229.621	6229.259	-58	6429.372	6429.364	-1.2
6425.816	6425.804	-1.8	6329.703	6329.311	-62	6529.409	6529.416	1.2
6469.850	6469.831	-3.0	6429.790	6429.364	-66	6629.471	6629.469	-0.42
6513.859	6513.857	-0.31	6529.868	6529.416	-69	6729.537	6729.521	-2.4
6557.874	6557.883	1.4	6629.934	6629.469	-70	6829.597	6829.573	-3.5
6601.902	6601.909	1.0	6730.018	6729.521	-74	6929.659	6929.626	-4.7
6645.943	6645.935	-1.2	6830.085	6829.573	-75	7029.730	7029.678	-7.3
6689.979	6689.962	-2.6	6930.117	6929.626	-71	7129.786	7129.731	-7.7
6734.004	6733.988	-2.4	MSE = 22 ppm			MSE = 1.4 ppm		
6778.026	6778.014	-1.7						
6822.057	6822.041	-2.4						
6866.061	6866.066	0.80						
6910.100	6910.092	-1.2						
6954.116	6954.119	0.41						
6998.151	6998.145	-0.77						
7042.203	7042.171	-4.6						
7086.164	7086.198	4.8						
7130.251	7130.224	-3.8						
7174.260	7174.250	-1.4						
MSE = 0.50 ppm								

Figure 3.9: MALDI-FTMS mass spectrum of PMMA 6000 show a series of sodium and potassium attached oligomers. The inset shows the mass resolution that is typical for all the oligomer peaks (RP = 28,000). With external calibration, the mean squared error in mass measurement was determined to be 1.4 ppm.

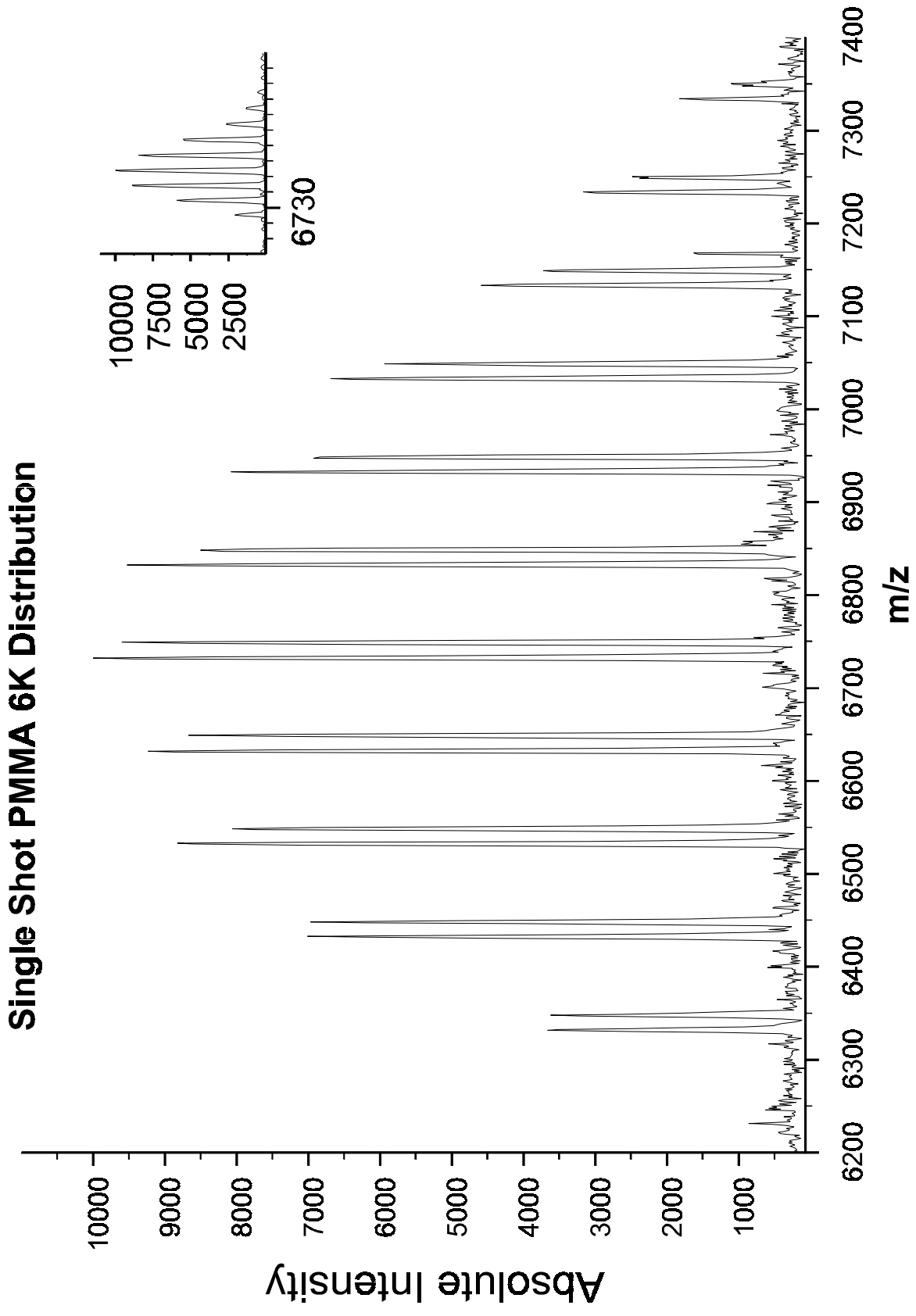
Single Shot PMMA 6K Distribution
Absolute Intensity
m/z
10000
9000
8000
7000
6000
5000
4000
3000
2000
1000
6200
6300
6400
6500
6600
6700
6800
6900
7000
7100
7200
7300
7400
10000
7500
5000
2500
6730

CONCLUSIONS

We have shown that the mass accuracy obtained by FTICR can be improved by correcting for the differences in the number of trapped ions when using external calibration methods. Mass accuracy less than 2 ppm can be obtained for ions up to m/z 6K when using external calibration. This improvement is important for ions formed by MALDI, as the chaotic nature of laser desorption often produces wide shot-to-shot variations in the number of ions that are produced. Sample characteristics such as mass distribution are also an important factor for analytes or calibrants such as polymers in which small changes in the abundance of peaks in the mass spectrum (and in their signal-to-noise) produce large changes in the overall number of trapped charges. For a given signal-to-noise ratio, the total ion intensity increases as the number of components in the sample increases. Thus complex mixtures such as polymers, tryptic digests, or combinatorial libraries will exhibit a much greater total ion intensity than a single component sample, for a given value of signal-to-noise. By accounting for the total number of ions in the cell, samples of any type can be examined with ppm mass accuracy.

REFERENCES

(1) Easterling, M. L.; Pitsenberger, C. C.; Kulkarni, S. S.; Taylor, P. K.; Amster, I. J. *International Journal Of Mass Spectrometry And Ion Processes* **1996,** *158*, 97-113.

(2) Li, Y. Z.; Hunter, R. L.; McIver, R. T. *International Journal Of Mass Spectrometry And Ion Processes, Dec* **1996,** *158*, 175-188.

(3) Pasatolic, L.; Huang, Y. L.; Guan, S. H.; Kim, H. S.; Marshall, A. G. *J. Mass Spectrom.* **1995,** *30*, 825-833.

(4) Hofstadler, S. A.; Severs, J. C.; Smith, R. D.; Swanek, F. D.; Ewing, A. G. *Hrc-Journal Of High Resolution Chromatography* **1996,** *19*, 617- 621.

(5) Shi, S. D. H.; Hendrickson, C. L.; Marshall, A. G.; Simonsick, W. J.; Aaserud, D. J. *Analytical Chemistry* **1998,** *70*, 3220-3226.

(6) Mize, T. H.; Amster, I. J. *Analytical Chemistry* **2000,** *72*, 5886-5891.

(7) Easterling, M. L.; Mize, T. H.; Amster, I. J. *Int. J. Mass Spectrom.* **1997,** *169*, 387-400.

(8) Easterling, M. L.; Mize, T. H.; Amster, I. J. *Analytical Chemistry* **1999,** *71*, 624-632.

(9) Guan, S. H.; Wahl, M. C.; Marshall, A. G. *Analytical Chemistry* **1993,** *65*, 3647-3653.

(10) Campbell, V. L.; Guan, Z. Q.; Laude, D. A. *Journal Of The American Society For Mass Spectrometry* **1995,** *6*, 564-570.

(11) Nikolaev, E. N.; Miluchihin, N. V.; Inoue, M. *International Journal Of Mass Spectrometry And Ion Processes* **1995,** *148*, 145-157.

(12) McLafferty, F. W.; Turacek, F. *Interpretation of Mass Spectra*, 4 ed.; University Science Books: Sausalito, CA, 1993.

(13) Takach, E. J.; Hines, W. M.; Patterson, D. H.; Juhasz, P.; Falick, A. M.; Vestal, M. L.; Martin, S. A. *J. Protein Chem.* **1997,** *16*, 363-369.

(14) Dey, M.; Castoro, J. A.; Wilkins, C. L. *Analytical Chemistry* **1995,** *67*, 1575-1579.

(15) Kelleher, N. L.; Senko, M. W.; Little, D. P.; Oconnor, P. B.; McLafferty, F. W. *Journal Of The American Society For Mass Spectrometry* **1995,** *6*, 220-221.

(16) Aaserud, D. J.; Kelleher, N. L.; Little, D. P.; McLafferty, F. W. *Journal Of The American Society For Mass Spectrometry* **1996,** *7*, 1266-1269.

(17) Zaluzec, E. J.; Gage, D. A.; Allison, J.; Watson, J. T. *Journal of the American Society for Mass Spectrometry* **1994,** *5*, 230-237.

(18) Guan, S. H.; Marshall, A. G. *International Journal Of Mass Spectrometry And Ion Processes, Aug* **1995,** *146*, 261-296.

(19) Dekoster, C. G.; Duursma, M. C.; Vanrooij, G. J.; Heeren, R. M. A.; Boon, J. J. *Rapid Communications In Mass Spectrometry* **1995,** *9*, 957-962.

(20) Wu, Q. Y.; Vanorden, S.; Cheng, X. H.; Bakhtiar, R.; Smith, R. D. *Analytical Chemistry* **1995,** *67*, 2498-2509.

(21) Hettich, R. L.; Stemmler, E. A. *Rapid Communications In Mass Spectrometry* **1996,** *10*, 321-327.

(22) Winger, B. E.; Hofstadler, S. A.; Bruce, J. E.; Udseth, H. R.; Smith, R. D. *Journal Of The American Society For Mass Spectrometry* **1993,** *4*, 566-577.

(23) Hofstadler, S. A.; Bruce, J. E.; Rockwood, A. L.; Anderson, G. A.; Winger, B. E.; Smith, R. D. *International Journal Of Mass Spectrometry And Ion Processes* **1994,** *132*, 109-127.

(24) Gorshkov, M. V.; Marshall, A. G.; Nikolaev, E. N. *Journal Of The American Society For Mass Spectrometry* **1993,** *4*, 855-868.

(25) Mortz, E.; Oconnor, P. B.; Roepstorff, P.; Kelleher, N. L.; Wood, T. D.; McLafferty, F. W.; Mann, M. *Proceedings Of The National Academy Of Sciences Of The United States Of America Aug* **1996,** *93*, 8264-8267.

(26) Watson, C. H.; Wronka, J.; Laukien, F. H.; Barshick, C. M.; Eyler, J. R. *Analytical Chemistry* **1993,** *65*, 2801-2804.

(27) Speir, J. P.; Senko, M. W.; Little, D. P.; Loo, J. A.; McLafferty, F. W. *J. Mass Spectrom.* **1995,** *30*, 39-42.

(28) Little, D. P.; Aaserud, D. J.; Valaskovic, G. A.; McLafferty, F. W. *Journal Of The American Chemical Society* **1996,** *118*, 9352- 9359.

(29) Wu, J. Y.; Fannin, S. T.; Franklin, M. A.; Molinski, T. F.; Lebrilla, C. A. *Analytical Chemistry* **1995,** *67*, 3788-3792.

(30) Comisarow, M. B.; Marshall, A. G. *J. Chem. Phys.* **1976,** *64*, 110-119.

(31) Comisarow, M. B. *J. Chem. Phys.* **1978,** *69*, 4097-4104.

(32) Dunbar, R. C.; Chen, J. H.; Hays, J. D. *International Journal of Mass Spectrometry and Ion Processes* **1984,** *57*, 39-56.

(33) Jeffries, J. B.; Barlow, S. E.; Dunn, G. H. *International Journal of Mass Spectrometry and Ion Processes* **1983,** *54*, 169-187.

(34) Cox, K. A.; Cleven, C. D.; Cooks, R. G. *International Journal of Mass Spectrometry and Ion Processes* **1995,** *144*, 47-65.

(35) Cleven, C. D.; Cox, K. A.; Cooks, R. G.; Bier, M. E. *Rapid Communications in Mass Spectrometry* **1994,** *8*, 451-454.

(36) Sommer, H.; Thomas, H. A.; Hipple, J. A. *Phys. Rev.* **1949,** *76*, 1877.

(37) Beauchamp, J. L.; Armstrong, J. T. *Rev. Sci. Instrum.* **1969,** *40*, 123-&.

(38) Francl, T. J.; Sherman, M. G.; Hunter, R. L.; Locke, M. J.; Bowers, W. D.; McIver, R. T. *International Journal of Mass Spectrometry and Ion Processes* **1983,** *54*, 189-199.

(39) Ledford, E. B.; Rempel, D. L.; Gross, M. L. *Analytical Chemistry* **1984,** *56*, 2744-2748.

(40) Chen, S.-P.; Comisarow, M. B. *Rapid Communications in Mass Spectrometry* **1991,** *5*, 450-455.

(41) Chen, S. P.; Comisarow, M. B. *Rapid Communications In Mass Spectrometry* **1992,** *6*, 1-3.

(42) Wineland, D. J.; Dehmelt, H. G. *J. Appl. Phys.* **1975,** *46*, 919-930.

(43) Wineland, D.; Dehmelt, H. *Bulletin of the American Physical Society* **1974,** *19*, 642-643.

(44) Xiang, X. Z.; Grosshans, P. B.; Marshall, A. G. *International Journal Of Mass Spectrometry And Ion Processes* **1993,** *125*, 33-43.

(45) Laude, D.; Beu, S. *Anal. Chem.* **1989,** *61*, 2422-2427.

(46) Easterling, M. L.; Pitsenberger, C. C.; Amster, I. J. *Journal Of The American Society For Mass Spectrometry* **1997,** *8*, 195-198.

(47) Beu, S. C.; Laude, D. A. *International Journal of Mass Spectrometry and Ion Processes* **1992,** *112*, 215-230.

(48) Koster, C.; Castoro, J. A.; Wilkins, C. L. *Journal Of The American Chemical Society* **1992,** *114*, 7572- 7574.

(49) Alford, J. M.; Williams, P. E.; Trevor, D. J.; Smalley, R. E. *International Journal of Mass Spectrometry and Ion Processes* **1986,** *72*, 33-51.

(50) Kofel, P.; Allemann, M.; Kellerhals, H.; Wanczek, K. P. *International Journal of Mass Spectrometry and Ion Processes* **1986,** *72*, 53-61.

(51) Beu, S. C.; Laude, D. A. *Analytical Chemistry* **1992,** *64*, 177-180.

(52) Hensel, R. R.; King, R. C.; Owens, K. G. *Rapid Communications in Mass Spectrometry* **1997,** *11*, 1785-1793.

(53) Limbach, P. A.; Grosshans, P. B.; Marshall, A. G. *Analytical Chemistry* **1993,** *65*, 135-140.

(54) Chen, R. D.; Cheng, X. H.; Mitchell, D. W.; Hofstadler, S. A.; Wu, Q. Y.; Rockwood, A. L.; Sherman, M. G.; Smith, R. D. *Analytical Chemistry* **1995,** *67*, 1159-1163.

(55) Schurenberg, M.; Schulz, T.; Dreisewered, K.; Hillenkamp, F. *Rapid Communications In Mass Spectrometry* **1996,** *10*, 1873-1880.

(56) Juhasz, P.; Vestal, M. L.; Martin, S. A. *Journal of the American Society For Mass Spectrometry* **1997,** *8*, 209-217.

(57) Beavis, R. C.; Chait, B. T. *Chemical Physics Letters* **1991,** *181*, 479.

(58) Schweikhard, L.; Guan, S. H.; Marshall, A. G. *International Journal Of Mass Spectrometry And Ion Processes* **1992,** *120*, 71-83.

(59) Zhou, J.; Ens, W.; Standing, K. G.; Verentchikov, A. *Rapid Communications in Mass Spectrometry* **1992,** *6*, 671-678.

(60) Zhang, W. Z.; Chait, B. T. *International Journal of Mass Spectrometry and Ion Processes* **1997,** *160*, 259-267.

(61) Huang, J. Y.; Tiedemann, P. W.; Land, D. P.; McIver, R. T.; Hemminger, J. C. *International Journal Of Mass Spectrometry And Ion Processes* **1994,** *134*, 11-21.

(62) Naito, Y.; Inoue, M. *International Journal Of Mass Spectrometry And Ion Processes, Dec* **1996,** *158*, 85-96.

(63) Stults, J. T. *Analytical Chemistry* **1997,** *69*, 1815-1819.

(64) Speir, J. P.; Gorman, G. S.; Pitsenberger, C. C.; Turner, C. A.; Wang, P. P.; Amster, I. J. *Analytical Chemistry* **1993,** *65*, 1746-1752.

(65) Vanrooij, G. J.; Duursma, M. C.; Heeren, R. M. A.; Boon, J. J.; Dekoster, C. G. *Journal Of The American Society For Mass Spectrometry* **1996,** *7*, 449-457.

(66) Montaudo, G.; Montaudo, M. S.; Puglisi, C.; Samperi, F. *Rapid Communications In Mass Spectrometry* **1994,** *8*, 981-984.

(67) Montaudo, G.; Montaudo, M. S.; Puglisi, C.; Samperi, F. *Analytical Chemistry* **1994,** *66*, 4366-4369.

CHAPTER 4

BROADBAND ION ACCUMULATION WITH AN INTERNAL SOURCE MALDI-FTICR-MS[†]

[†] Reproduced with permission from Mize, Todd H. and Amster, I. Jonathan, *Analytical Chemistry*, **2000**, *72*, 5886-5891. Copyright 2000, American Chemical Society.

ABSTRACT

A new method is described which allows a broad mass range of ions from multiple MALDI events to be accumulated in an FTICR analyzer cell prior to detection. Signal intensity and signal-to-noise are observed to grow in direct proportion to the number of laser shots, providing a substantial improvement to the analysis of low level samples compared to more commonly used signal averaging methods. In addition, calibrant ions desorbed from a separate sample spot can be added to the analyzer cell after an analyte population has been accumulated, providing an internal mass standard without the necessity of mixing calibrant and analyte. This method provides excellent mass accuracy by eliminating mass errors due to space charge effects.

INTRODUCTION

Fourier transform ion cyclotron resonance mass spectrometry (FTICR-MS) provides ultra high mass resolution for high mass ions.[1-4] This makes it an ideal tool for the analysis of proteins and peptides,[5] synthetic polymers,[6] oligonulcleotides,[7] and oligosaccharides.[8] Complex mixtures such as polymer distributions or proteolytic digestion fragments can be analyzed with or without prior fractionation, especially if the complexity is not exacerbated by multiple charge states. Performed carefully, it is a nondestructive technique that allows for multiple measurements,[9] MS/MS,[10, 11] and gas phase reactions [12] of a handful of ions. Matrix assisted laser desorption/ionization (MALDI) [13, 14] is particularly useful as an ionization method for complex mixtures of nonvolatile compounds. In contrast to electrospray ionization, it primarily produces singly charged ions thereby minimizing the complexity of the resultant spectra. Also, mass discrimination effects from sample ionization are far less pronounced than for electrospray ionization.[15, 16]

In order to efficiently detect ions by MALDI-FTICR-MS, gated trapping is generally employed.[17, 18] After the ionization event, ions of all masses have approximately the same velocity, which is generally directed along the central axis of the FTICR analyzer cell. The trapping potential must be high enough to stop the most massive ions that are to be measured as these have the greatest kinetic energy. With gated trapping, the potential of the trapping plate on the front side of the analyzer (i. e., the side from which ions enter) is briefly reduced to allow the desorbed ions to enter the cell, while the potential of the rear trapping electrode is raised high enough to stop and turn around the ions. The front trapping potential is then raised to create a symmetric

trapping potential before the reflected ions can exit the cell. This technique has been demonstrated to efficiently trap MALDI-formed ions over a wide mass range, particularly when implemented with an open-ended analyzer cell.[19]

Low abundance sample analysis, whether due to low ionization response for difficult compound classes, or to low sample concentration and interferences (e. g., in-gel proteolytic digests), can benefit greatly from accumulation of a number of ionization events in the ICR cell prior to mass analysis. Ion signal, measured as the image current of the excited ions, is linearly related to the number of ions analyzed.[20] At low ion numbers, the image current will produce less signal than the ambient electronic noise. Two approaches have been described to improve signal-to-noise. One is to co-add the time domain signal from several acquisitions. This improves signal-to-noise at a rate proportional to the square root of the number of acquisitions. However, shot-to-shot variations in ion number characteristic of MALDI can lead to peak broadening or peak splitting in the signal-averaged spectrum due to space charge frequency shifts in the individual acquisitions.[21] A second approach to improving signal-to-noise is to remeasure a single ion population.[9, 22-24] Signal averaging of efficiently remeasured ions by using quadrupolar excitation (QE) eliminates the shot-to-shot variation in population which causes this line broadening and is therefore a preferable alternative to co-addition of separate MALDI generated ion clouds. In very low ion abundance experiments, the population is often too small to yield isotope distributions similar to those statistically predicted from the molecular composition, thus making identification of the ions more difficult. [25] While remeasurement can increase the signal-to-noise ratio for a single ionization event, it will not change the statistical anomaly in isotope distribution. Also,

any scheme for co-addition of spectra is plagued by diminishing returns because signal averaging *n* measurements only results in $n^{1/2}$ improvement in signal-to-noise. For these reasons, we have developed a method for accumulation of ions from several laser shots in the FTICR analyzer cell which can be detected after a substantial ion population is present. Hasse and co-workers[26] have demonstrated the accumulation of ions of a single mass-to-charge from several laser desorption events. Here, we extend this concept to distributions of ions over a broad mass range, and apply this to examining the products of a tryptic digest of a protein and to polymer distributions. Ion accumulation is shown to cause signal-to-noise to improve in direct proportion to the number of laser shots.

EXPERIMENTAL

Experiments were performed with a 4.7 Tesla FTICR-MS with an internal MALDI source designed and fabricated in-house. The details of this instrument have been published previously.[27] A 1" diameter sample puck carrying up to 20 MALDI samples is mounted on a linear-rotary manipulator ~1 cm from the front trap of an 2-1/4" diameter open cylindrical FTICR cell with 2-1/4" long trapping electrodes and 3-3/8" excite/detect electrodes. For MALDI, the 355nm line of a Nd:YAG laser is focused onto the sample puck at a point that lies on the central axis of the cell. The cell is equipped with capacitive coupling for reducing axial ejection. Capacitive coupling can be disabled during the experimental sequence to improve gated trapping. A trapping potential of 0.25 volts is applied at the beginning of the experiment sequence. After the laser pulse, the ions formed by MALDI cross this small potential at the front trap. The rear trap is stepped up to an acceptable, higher stopping potential, on the order of 5 volts ~200 μsec

after the laser is fired. After a short (~100 μsec) delay to allow the full velocity distribution of ions to enter the cell, the front trap is then rapidly raised to the same potential as the rear trap as in normal gated trapping, and quadrupolar excitation (QE) is applied to center the ions in the cell. After a short pump down period during which the trapping plates are ramped back to 0.25 V in 500 msec, another round of ion accumulation is performed or a sweep excitation pulse is applied and the ions are detected. Ion retention times for thermalized ions and for incoming MALDI ions were calculated during the accumulating trapping event using SimIon modeling software.[28]

Bovine serum albumin (BSA), carbonic anhydrase (CAH), horse heart myoglobin (MYO), polyethylene glycol (PEG) 1K and 2K, sinapinic acid (SA), trans-3-indole acrylic acid (IAA), and dihydroxy benzoic acid (DHB) were obtained from Sigma Chemical Company, St. Louis. Polymethyl methacrylate (PMMA) 2K was obtained from Rohm and Haas. Proteins were dissolved at 0.1 mg/mL in 0.05 M NH_4HCO_3, denatured for 5 minutes in 95EC water bath, and digested overnight with 2 Fg trypsin at room temperature. In gel digestion of BSA was performed after isolation of 1Fmol BSA in a polyacrilamide gel (SDS-PAGE). Digestion and recovery of the peptides was accomplished using the procedure of Arnott et al.[29] All cysteines were reduced and derivatized with iodoacetamide. PEGs and matrices were dissolved in 50% aqueous acetonitrile with 0.1% trifluoroacetic acid. Peptides were applied to the sample puck with an equal volume of 1 M DHB, and a 1 mM solution of the PEGs applied with an equal volume of saturated SA.

Radial and axial ion motion was relaxed prior to accumulation and analysis via repetitive chirp quadrupolar excitation (QE). [22, 30] Chirp QE was accomplished using a

Stanford Research Systems DS335 3.1 MHZ Synthesized Function Generator running at 1000 chirps per second with a range of 72-30 kHz (corresponding to an m/z range of 1000-2400) in logarithmic, bidirectional mode. The excitation waveform was amplified by an IonSpec RF amplifier to 25 V and delivered to the cell as a two plate quadrupolar field. The QE field was applied for 3.5 seconds while nitrogen buffer gas was introduced via a pulsed valve to a pressure of approximately 10^{-5} torr. QE has the added benefit of mass selection which serves to eliminate the abundant matrix ions that can contribute to space charge related frequency shifts and coulombic line broadening and that can limit the cell's ion capacity.[21, 31, 32] Ions were then excited using a 1 msec, 40 V chirp followed by broadband detection at 500 kHz digitization rate.

RESULTS AND DISCUSSION

FTICR-MS instruments have been described with MALDI ion sources that are either external or internal to the high magnetic field region. In external source instruments, ion optics are required to efficiently transfer ions into the high magnetic field region. A time-of-flight mass separation of ions occurs during this transfer which can result in a bandpass mass discrimination in the collection of ions in the analyzer, i. e., only ions over a narrow mass range are captured.[33-35] A number of solutions to the mass separation have been proposed utilizing external ion accumulation in an additional optical element (such as in an octopole or hexapole). [36-40] Other solutions include off-axis injection[41] and sidekick injection[42] both of which involve increasing the magnetron radii of the ions to decrease the chance of an ion exiting any entrance orifice.

Alternatively, the time-of-flight effects can be minimized by shortening the transfer distance between the source and the ICR cell. An internal MALDI source produces ions at the edge of the ICR cell making the time-of-flight only subject to the initial ion velocities and the length of the cell. Wide distributions of ions can be trapped by introducing a low pressure collision gas to damp this initial kinetic energy.[19] The internal source uses gated trapping [43-45] for ion collection in which, generally, the trapping electrodes near the source (front trap) start at ground potential and the far (rear trap) electrodes are held at a potential sufficient to stop the ions with the highest kinetic energy in the ion plume distribution. After the laser pulses, ions enter the analyzer, passing the front trapping electrode. Before the ions that are reflected by the rear trapping potential can exit the cell, the front trapping electrodes are raised to the stopping potential and the ions are trapped in the resulting symmetric potential well. The gated trapping method provides an efficient means to trap MALDI-formed ions over a wide mass range.

To accumulate ions from several laser shots, it is necessary to modify the gated trapping parameters so that ions that are already trapped in the analyzer cell are not ejected by the asymmetric trapping potentials used to capture ions from subsequent MALDI events. Suspended trapping experiments in which both front and back traps are lowered to ground potential show that ions that have been axialized by QE remain in the cylindrical cell for 200-300 Fs without any trapping potential before they diffuse out along the magnetic field axis. [21, 46] Initial experiments to accumulate ions used such an event during the MALDI process and then raised both trapping potentials simultaneously to capture the ions that had entered the analyzer. However, the incoming cloud of ions and neutrals was found to eject the ions that were already present in the analyzer. A

more successful approach has been to use a small potential on the front trapping plate over which incoming ions may pass but which retains previously trapped ions. The previously accumulated ions will be accelerated by the asymmetric trapping potential that is briefly applied to stop incoming ions. Table 4.1 compares the calculated residence times of accumulated ions in the asymmetric trapping potential used for gated trapping and that have thermal kinetic energy (0.03 eV), with those entering the cell with a uniform velocity of 450 m/s, typical of MALDI produced ions.[47] Previously accumulated ions remain in the cell for 400 Fs or longer, while newly desorbed ions enter the cell within 130 Fs, traverse the cell, and are reflected by the rear trap potential to exit the front of the cell in > 750 Fs. The residence times depend on their mass-to-charge. Their flight times provide a substantial window that allows the full velocity distribution of the MALDI plume to enter the trapping region prior to gating the front trap to 12 V. Based on these data, the delay for gated trapping was selected to be 300 Fs after ionization.

Broadband gated ion accumulation was performed on peptides from a BSA tryptic digest for 50 cycles to demonstrate the linearity of increase in ion abundance shown in Figure 4.1. The accumulation/detection range was from m/z 1000-2500, as determined by the frequency range of the repetitive chirp QE. Excite parameters and transient duration were the same in each repetition. As can be seen, the signal and signal-to-noise grow linearly with the number of laser shots, n. The shot-to-shot variations in ion production inherent to MALDI serve to explain the scatter in the data. By way of comparison, the theoretical apparent increase in S/N ($n^{1/2}$) for 100% efficient remeasurement of the average accumulation signal is also plotted. Clearly, accumulation provides a substantially better way to improve signal-to-noise.

Table 4.1: Retention times for ions of various mass-to-charge, both those already in the trapping/detection region with thermal kinetic energy (thermalized ions) and those entering the cell with initial velocity of 450 m/s (MALDI formed ions). Calculations were made with SIMION, using experimental conditions described in the text.

m/z	MALDI formed ions		Thermalized ions
	t_{in}, Fsec	t_{out}, Fsec	$t_{retention}$, Fsec
500	128	775	434
1000	112	770	610
2500	106	824	1045
5000	104	918	1640

Figure 4.1: Signal intensity (right axis) and signal-to-noise (left axis) increase linearly with the number of accumulation cycles. By means of comparison, the predicted signal-to-noise for 50 remeasurement cycles of similar single shot intensity is also shown.

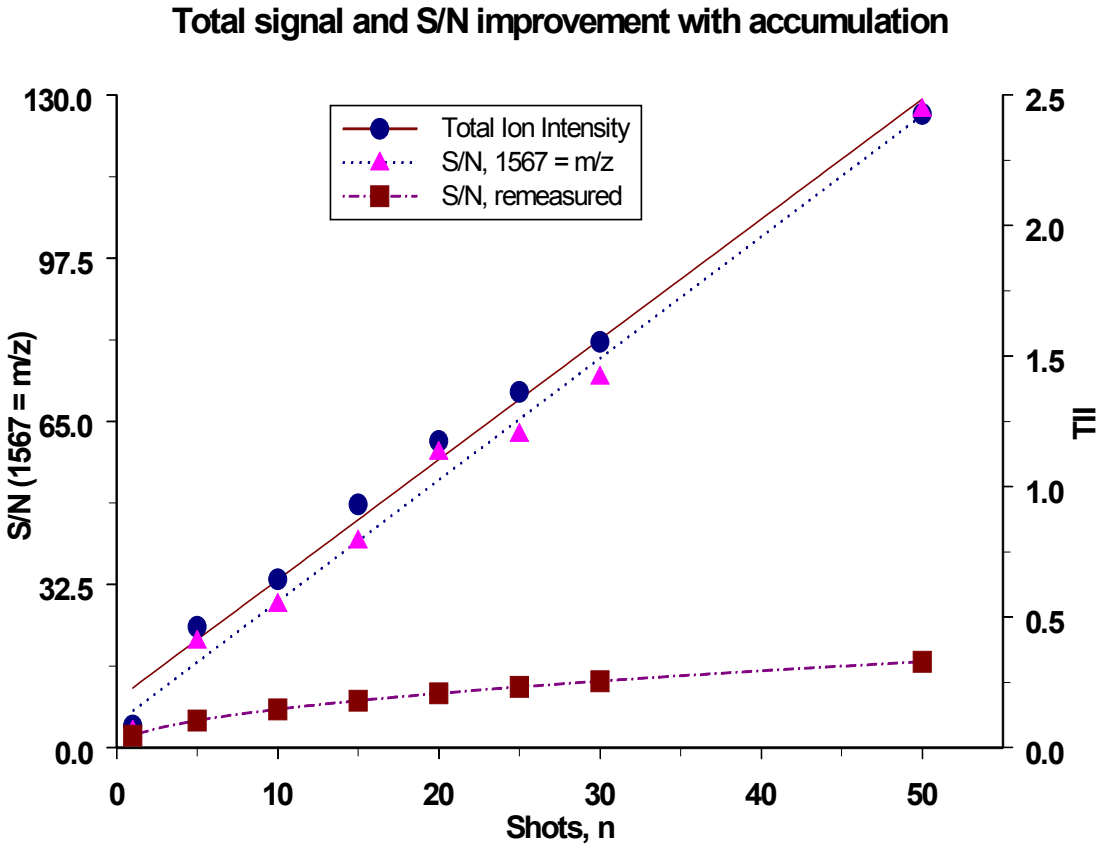
Total signal and S/N improvement with accumulation
Total Ion Intensity
S/N, 1567 = m/z
S/N, remeasured
S/N (1567 = m/z)
TII
Shots, n
130.0
97.5
65.0
32.5
0.0
2.5
2.0
1.5
1.0
0.5
0.0
0
10
20
30
40
50

The utility of this technique for increasing signal-to-noise is illustrated in Figure 4.2 which compares the mass spectra resulting from a single shot, five accumulations, and ten accumulations of ions from MALDI of an in-gel tryptic digest of bovine serum albumin. In the single shot spectrum only ions of a single peptide are observed. Accumulating ions from five laser shots improves the signal-to-noise for this set of peaks while also rescuing some other peaks from the noise. The coincident increase in coulombic interactions with and, thereby, sympathetic cooling by ions of similar mass previously cooled via QE helps increase the broadband trapping efficiency, as well. The relaxation mechanism is similar to that described by Li and coworkers for improved trapping of negative ions using electrons, but the relaxation time constant is decreased two- to three-fold in the m/z range 1000-2000 for ions cooled by similar sized ions.[48, 49] Moreover, relaxation speed is inversely proportional to ion (or electron) number density making subsequent accumulations more efficient, still.[49] After ten laser shots, many peaks that were lost in the noise in the first spectrum exist at an ion current approximately twice that of the original base peak. By comparison, conventional signal averaging would have required 100 laser shots to achieve the same improvement.

A second examination of this sample illustrates another important aspect of increasing ion number in low abundance samples. Isotope distributions are predicted based on their statistical natural abundances and are used to help identify the atomic composition and monoisotopic peak of the ions . This requires a representative sample of the global population. Samples with low ion abundance can be expected to deviate from ideal statistical behavior such as the base peak ions in the single shot spectrum of in-gel BSA digest, Figure 4.3, top. Accumulation of 25 shots increases the population

Figure 4.2: Accumulation of peptide ions from an in-gel tryptic digest of BSA. Ions below the threshold of detection after one shot are easily assignable after ten. The insets demonstrate the increase in signal-to-noise for the base peak.

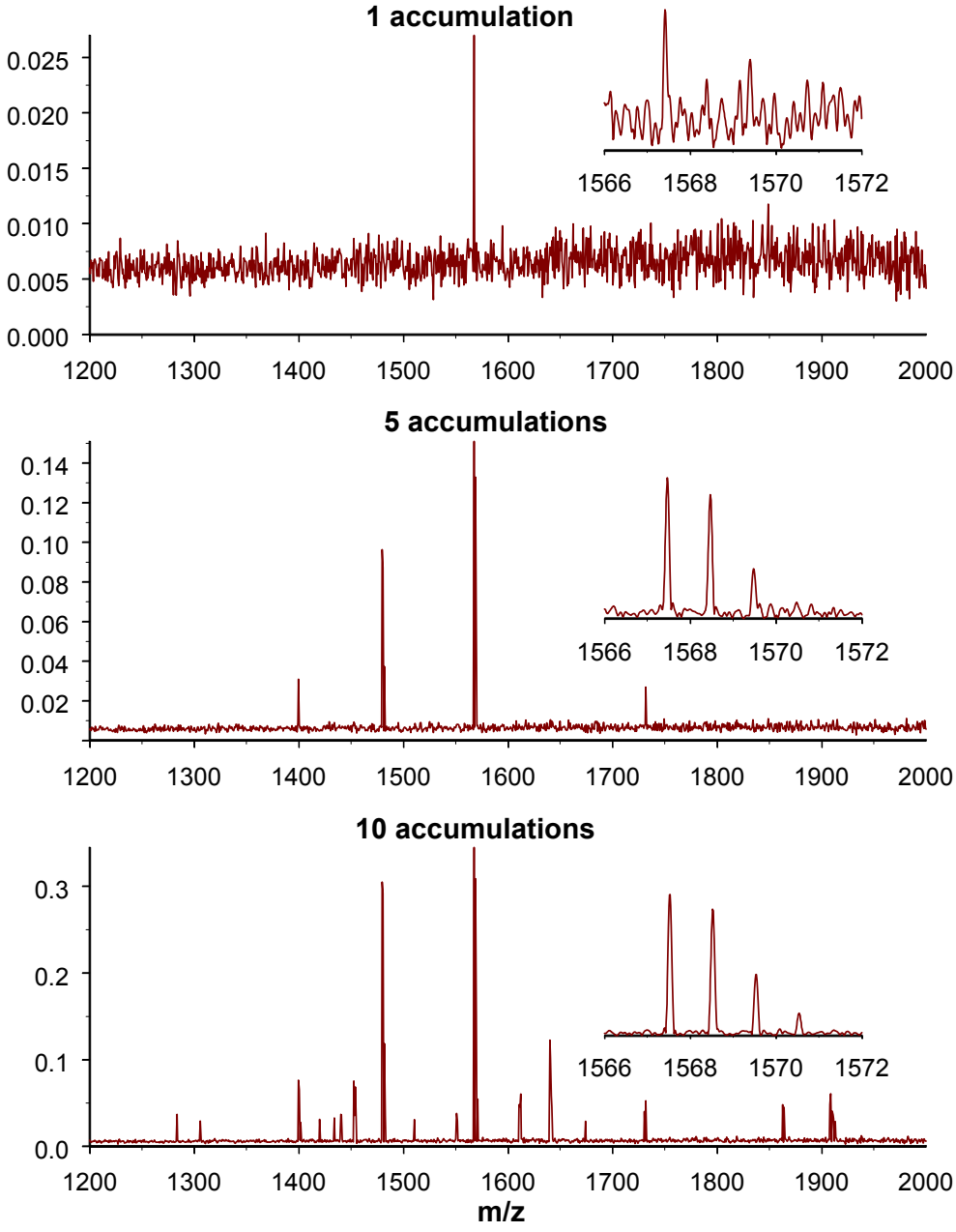
1 accumulation
0.025
0.020
0.015
0.010
0.005
0.000
1566
1568
1570
1572
1200
1300
1400
1500
1600
1700
1800
1900
2000
5 accumulations
0.14
0.12
0.10
0.08
0.06
0.04
0.02
10 accumulations
0.3
0.2
0.1
0.0
m/z

sufficiently so that the expected isotope pattern can clearly be recognized. To achieve the same S/N improvement via remeasurement would require 784 remeasurement cycles, but would not change the anomalous isotope distribution since the same, poorly sampled population would be coaveraged.

Signal averaging many individual single shots is another option that can improve population sampling; however, shot-to-shot variations in MALDI signal intensities can lead to space charge induced peak broadening. Figure 4.4 shows the difference between the coaveraged spectrum of 50 MALDI-FTICR shots (top) and a single measurement after 50 accumulations (bottom). The differences in space charge from one shot to the next result in a proportional shift in the apparent (measured) cyclotron frequencies and, by extension, the mass-to-charge ratios of the ions.[50, 51] These shifts are also coaveraged in the final spectrum resulting in erroneous peak shapes that will have a deleterious effect on calibrated mass and slow the improvement of signal-to-noise. The destructive interference of these small frequency shifts is further demonstrated in the structure of the raw signals (insets, Figure 4.4); the signal for the averaged spectrum disappears in the background

Broadband accumulation can also be used to improve mass accuracy on true unknowns. Methods to correct the space charge effects on external calibration have been developed, but the best way to eliminate space charge induced frequency shifts between calibrant and analyte spectra is to use internal calibration. Normally, this can only be achieved if the calibrant and analyte are co-crystallized on the same MALDI spot. With accumulation, the calibrants can be introduced from a separate sample spot subsequent to the desorption of the analyte. In this manner, the calibrant can be chosen to fit the

Figure 4.3: The unrepresentative ion population obtained from a single shot at an in-gel BSA tryptic digest (top panel, zoom on base peak) can result in poor statistical isotope distributions. This can be corrected by continued sampling; for instance, 25 accumulations provides a statistically relevant ion population thus easing assignment of the monoisotopic peak.

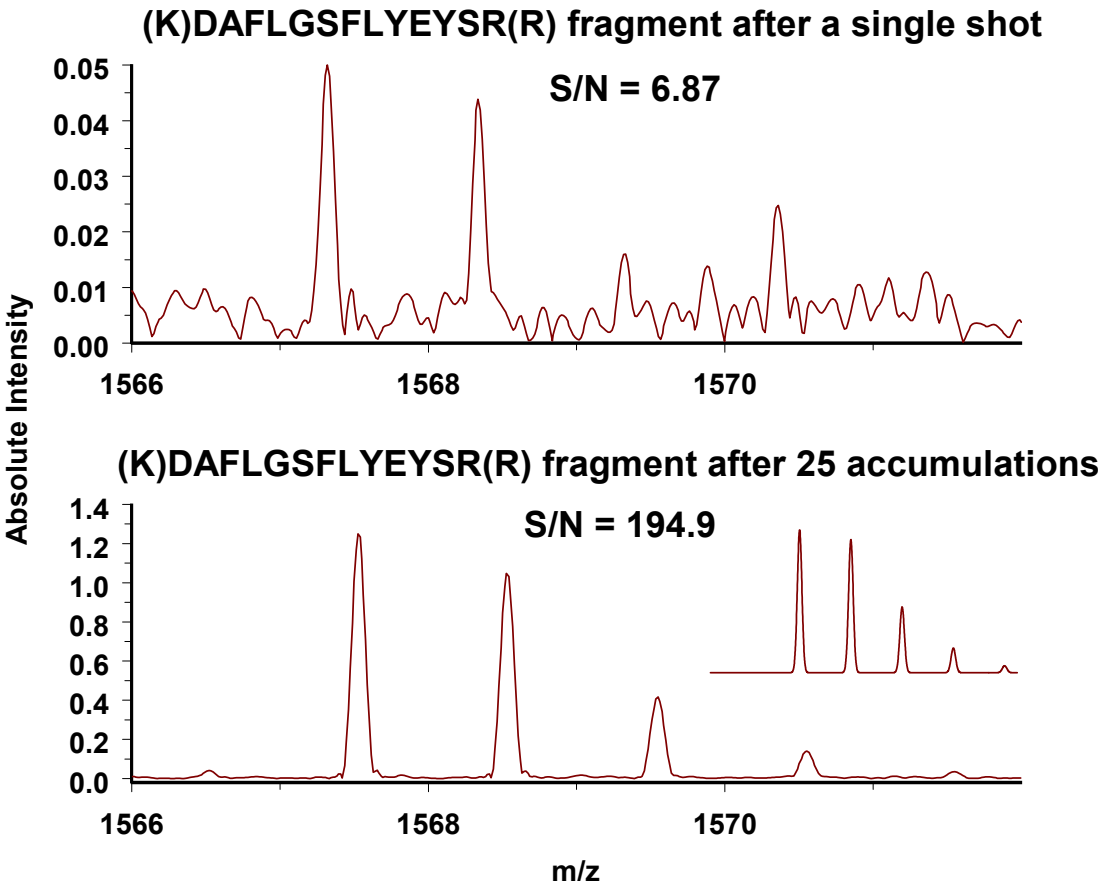
(K)DAFLGSFLYEYSR(R) fragment after a single shot
S/N = 6.87
0.05
0.04
0.03
0.02
0.01
0.00
1566
1568
1570
(K)DAFLGSFLYEYSR(R) fragment after 25 accumulations
S/N = 194.9
1.4
1.2
1.0
0.8
0.6
0.4
0.2
0.0
1566
1568
1570
Absolute Intensity
m/z

Figure 4.4: Space charge induced peak broadening due to shot-to-shot variations in total ion density in a 50 shot signal averaged spectrum of in-gel BSA tryptic digest (top panel) are eliminated in the single measurement spectrum of fifty broadband accumulations from the same sample. The insets show the destructive interference due to small space charge induced frequency shifts in the averaged spectrum versus the beating structure clearly visible in the accumulated spectrum. noise while the signal from the 50 accumulated shots measured shows beating structurefor the duration of the transient.

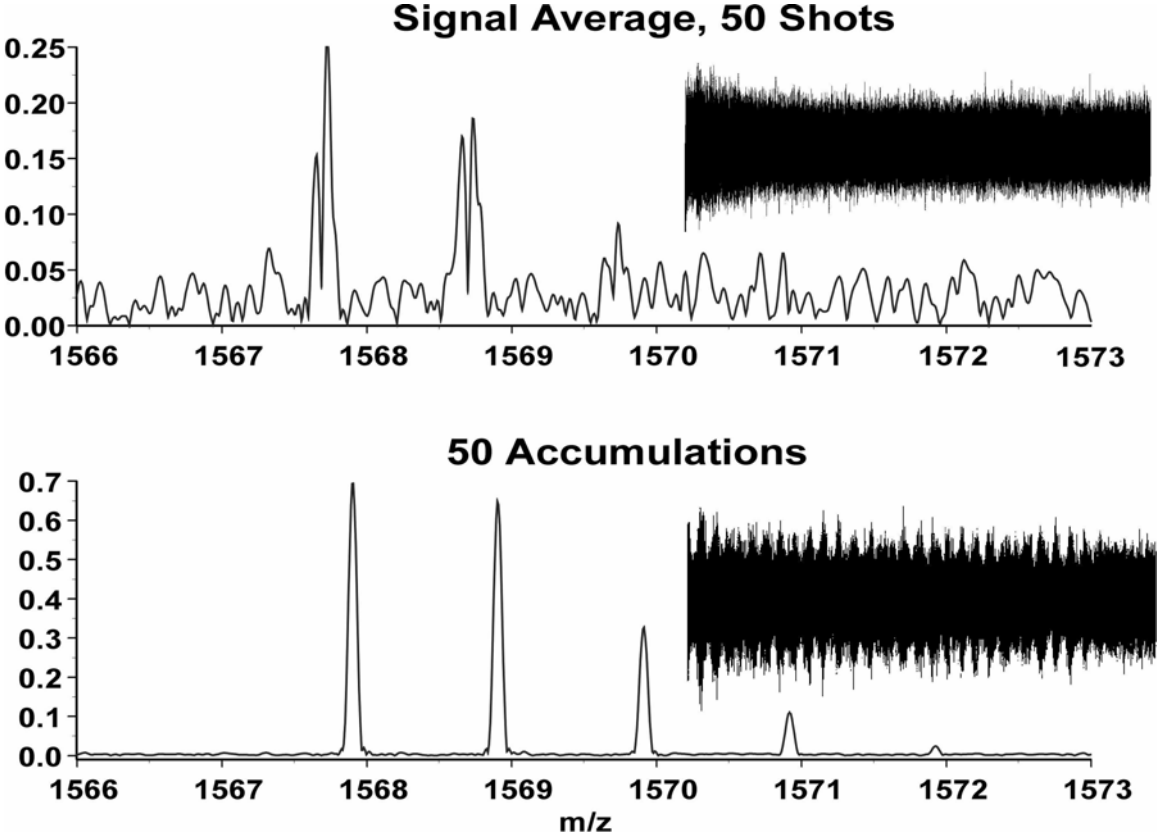
Signal Average, 50 Shots
0.25
0.20
0.15
0.10
0.05
0.00
1566
1567
1568
1569
1570
1571
1572
1573
50 Accumulations
0.7
0.6
0.5
0.4
0.3
0.2
0.1
0.0
1566
1567
1568
1569
1570
1571
1572
1573
m/z

analytes' mass range from among a variety preloaded on the same sample holder, thus facilitating the analysis of the unknowns. Figure 4.5 shows ten accumulation spectrum of an in-gel BSA digest before and after addition of a mixture of polyethylene glycol (PEG) 1K and 2K. Not only are the analyte and calibrant ions from separate matrices, but the mode of ionization is markedly different; i.e., the peptide ions are all protonated species while the PEG ions are exclusively sodiated. Use of polymer distributions like this increases the coverage of the calibrant across the spectrum, improving mass accuracy. Space charge related frequency shifts between calibrant and analyte spectra are eliminated by this procedure.[21]

A mixed sample of BSA, myoglobin, and carbonic anhydrase was digested in trypsin and analyzed by this method. After 10 accumulations of the peptide, PMMA 2K was added as an internal calibrant. Its wide repeat unit spacing of 100 m/z units results in little overlap of the peptide peaks of the mixed digest. The calibrated, non-PMMA peaks were then submitted to MS-Fit [52] for protein identification. BSA and myoglobin were returned with high correlation factors (MOWSE scores greater than 4.4×10^5). Table 4.2 shows the mass errors for 20 of the peaks in the mass spectrum; the average absolute error by this method is 2.9 ppm with a standard deviation of 1.9 ppm. Since there is only a single shot spectrum, there is no peak broadening due to shot-to-shot space charge differences and isobaric peaks of nominally the same mass-to-charge can be separated as seen in Figure 4.6. The peaks measured at m/z 1479.7274 (myoglobin residues 51-63) and 1479.8055 (BSA residues 421-433) are discernable although their isotopes are overshadowed by the more abundant peptide measured at m/z 1480.7794 (BSA residues

Figure 4.5: Ten accumulations of an in-gel BSA tryptic digest before (top) and after (bottom) addition of PEG 1K and 2K ions as an internal standard.

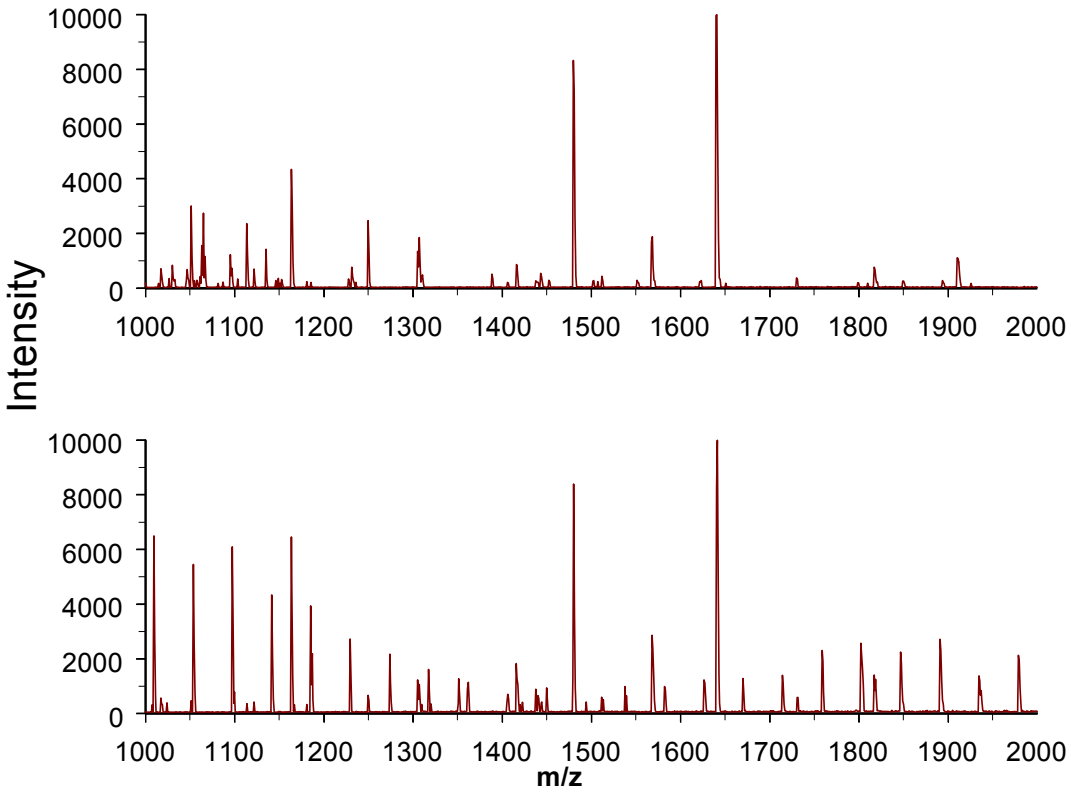
Intensity
10000
8000
6000
4000
2000
0
1000
1100
1200
1300
1400
1500
1600
1700
1800
1900
2000
m/z

Table 4.2: Error in mass accuracy for the 20 most abundant monoisotopic peptide ions in the MALDI-FTICR mass spectrum of a tryptic digest of BSA, myoglobin, and carbonic anhydrase after thirty accumulations and the insertion of one MALDI pulse of polymethylmethacrylate ions as an internal calibrant.

Measured m/z	Parent protein	Calculated m/z	Error, ppm
1193.6058	BSA	1193.6027	2.6
1271.6650	Myoglobin	1271.6636	1.1
1283.7105	BSA	1283.7112	-0.55
1305.7128	BSA	1305.7167	-3.0
1378.8381	Myoglobin	1378.8422	-3.0
1419.6982	BSA	1419.6942	2.8
1479.7274	Myoglobin	1479.7365	-6.2
1479.8055	BSA	1479.7960	6.4
1480.7794	BSA	1480.7800	-0.41
1511.8409	BSA	1511.8433	-1.6
1553.7913	Myoglobin	1553.7964	-3.3
1554.6530	BSA	1554.6535	-0.32
1567.7476	BSA	1567.7433	2.7
1576.7647	BSA	1576.7681	-2.2
1581.8109	Carbonic Anhydrase	1581.8178	-4.4
1657.7172	BSA	1657.7280	-6.5
1724.8299	BSA	1724.8352	-3.1
1816.8810	Myoglobin	1816.8870	-3.3
1853.9643	Myoglobin	1853.9622	1.1
2199.1971	Carbonic Anhydrase	2199.2025	-2.5
Average absolute error, ppm			2.9
Absolute error standard deviation, ppm			1.9

Figure 4.6: Isobaric separation of two peptides from a mixed trypsin digestion of BSA, myoglobin, and carbonic anhydrase. The spectrum represents 30 accumulations of peptide ions followed by one accumulation of PMMA 2K as an internal standard. This mass resolution is important in characterization of complex mixtures by mass spectrometry.

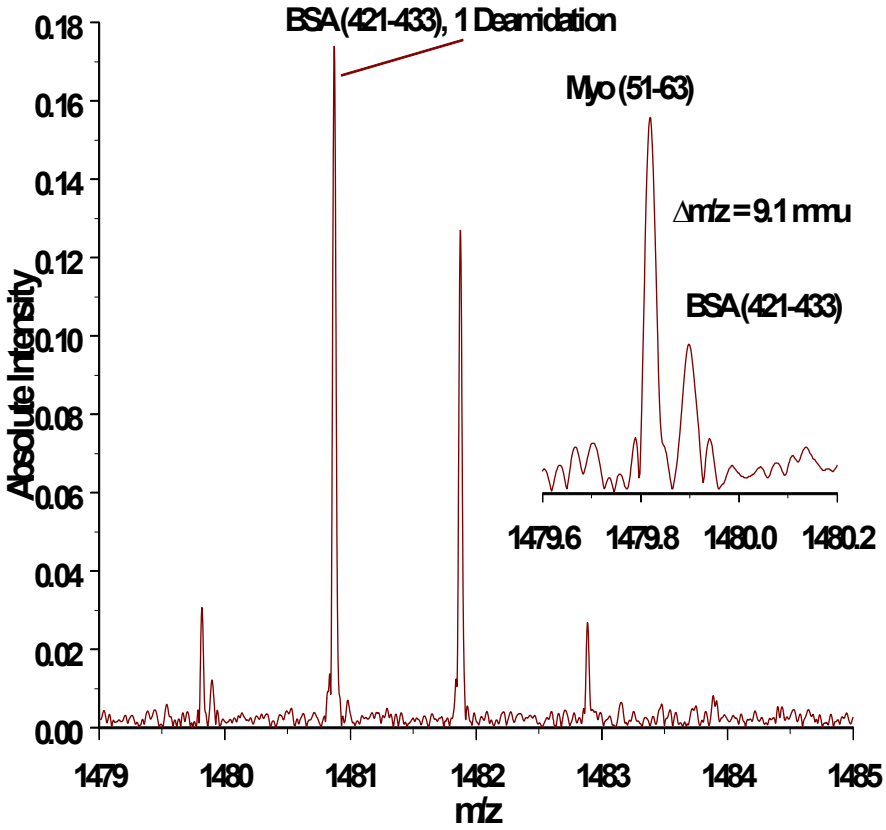
BSA (421-433), 1 Deamidation
Myo (51-63)
Δm/z = 9.1 mmu
BSA (421-433)
1479.6
1479.8
1480.0
1480.2
Absolute Intensity
0.18
0.16
0.14
0.12
0.10
0.08
0.06
0.04
0.02
0.00
1479
1480
1481
1482
1483
1484
1485
m/z

421-433 with one site of glutamine or asparagine deamidation).[53] While new time-of-flight instruments report similar mass accuracy as shown here,[54] their mass resolution does not allow such isobaric peaks to be distinguished.

CONCLUSIONS

Broadband accumulated trapping extends the utility of the internal MALDI source FTICR-MS by improving the signal to noise ratio and population statistics for low abundance samples. Signal-to-noise increases in direct proportion to the number of accumulation steps. Ions originally lost in the noise can be observed after only ten laser shots, a vast improvement over conventional signal averaging.

Insertion of external calibrants as internal standards provide the highest degree of mass accuracy by eliminating space charge differences between the calibrant and analyte spectra. This will be useful for the identification of the components of complex mixtures of proteins digested together without further separation of the resultant peptides. It is also useful in the case of true unknowns where the mass range to be calibrated can only be determined after initial mass analysis.[55, 56] This method will be useful for the analysis of complex proteomic mixtures where both high mass resolution and mass accuracy will be required in addition to high sensitivity.

ACKNOWLEDGEMENTS

The authors would like to thank Dr. Pete O'Connor of Boston University for sharing his results on related work in advance of publication. We gratefully acknowledge funding provided by the National Science Foundation (CHE-9974579).

REFERENCES

1. Smith, R. D.; Cheng, X.; Bruce, J. E.; Hofstadler, S. A.; Anderson, G. A. *Nature* **1994,** *369*, 137-139.
2. Shi, S. D. H.; Hendrickson, C. L.; Marshall, A. G. *Proc. Natl. Acad. Sci. U. S. A.* **1998,** *95*, 11532-11537.
3. Zhang, Z. Q.; Guan, S. H.; Marshall, A. G. *J. Am. Soc. Mass Spectrom.* **1997,** *8*, 659-670.
4. Beu, S. C.; Senko, M. W.; Quinn, J. P.; McLafferty, F. W. *J. Am. Soc. Mass Spectrom.* **1993,** *4*, 190-192.
5. Winger, B. E.; Hofstadler, S. A.; Bruce, J. E.; Udseth, H. R.; Smith, R. D. *J. Am. Soc. Mass Spectrom.* **1993,** *4*, 566-577.
6. Castoro, J. A.; Koster, C.; Wilkins, C. *Rapid Commun. Mass Spectrom.* **1992,** *6*, 239-241.
7. Stemmler, E. A.; Hettich, R. L.; Hurst, G. B.; Buchanan, M. V. *Rapid Commun. Mass Spectrom.* **1993,** *7*, 828-836.
8. Penn, S. G.; Cancilla, M. T.; Lebrilla, C. B. *Anal. Chem.* **1996,** *68*, 2331-2339.
9. Speir, J. P.; Gorman, G. S.; Pitsenberger, C. C.; Turner, C. A.; Wang, P. P.; Amster, I. J. *Anal. Chem.* **1993,** *65*, 1746-1752.
10. Anders, L. R.; Beaucham.Jl; Dunbar, R. C.; Baldesch.Jd *J. Chem. Phys.* **1966,** *45*, 1062-&.
11. Gauthier, J. W.; Trautman, T. R.; Jacobson, D. B. *Anal. Chim. Acta* **1991,** *246*, 211-225.

12. Freiser, B. S. In *Techniques for the Study of Ion-Molecule Reactions*; Farrar, J. M., Saunders, W. H., Eds.; Wiley-Interscience: New York, 1988, pp Chapter 2.

13. Karas, M.; Bachmann, D.; Bahr, U.; Hillenkamp, F. *Int. J. Mass Spectrom. Ion Processes* **1987,** *78*, 53-68.

14. Karas, M.; Hillenkamp, F. *Anal. Chem.* **1988,** *60*, 2301-2303.

15. Larsen, B. S.; Simonsick, W. J.; McEwen, C. N. *J. Am. Soc. Mass Spectrom.* **1996,** *7*, 287-292.

16. McEwen, C. N.; Simonsick, W. J.; Larsen, B. S.; Ute, K.; Hatada, K. *J. Am. Soc. Mass Spectrom.* **1995,** *6*, 906-911.

17. Castoro, J. A.; Wilkins, C. L. *Anal. Chem.* **1993,** *65*, 2621-2627.

18. Hofstadler, S. A.; Laude, D. A. *Int. J. Mass Spectrom. Ion Processes* **1990,** *101*, 65-78.

19. Easterling, M. L.; Mize, T. H.; Amster, I. J. *Int. J. Mass Spectrom.* **1997,** *169*, 387-400.

20. Grosshans, P. B.; Marshall, A. G. *Anal. Chem.* **1991,** *63*, 2057-2061.

21. Easterling, M. L.; Mize, T. H.; Amster, I. J. *Anal. Chem.* **1999,** *71*, 624-632.

22. Pitsenberger, C. C.; Amster, I. J. *Eur. Mass Spectrom.* **1997,** *3*, 1-9.

23. Easterling, M. L.; Pitsenberger, C. C.; Amster, I. J. *J. Am. Soc. Mass Spectrom.* **1997,** *8*, 195-198.

24. Pitsenberger, C. C.; Easterling, M. L.; Amster, I. J. *Anal. Chem.* **1996,** *68*, 3732-3739.

25. Millington, D. S.; Unsworth, W. D. In *Isotopes: Essential Chemistry and Applications*; Elvidge, J. A., Jones, J. R., Eds.; The Chemical Society: London, 1980; Vol. 35, pp 195-231.

26. Hasse, H. U.; Becker, S.; Dietrich, G.; Klisch, N.; Kluge, H. J.; Lindinger, M.; Lutzenkirchen, K.; Schweikhard, L.; Ziegler, J. *Int. J. Mass Spectrom. Ion Processes* **1994,** *132*, 181-191.

27. Easterling, M. L.; Pitsenberger, C. C.; Kulkarni, S. S.; Taylor, P. K.; Amster, I. J. *Int. J. Mass Spectrom. Ion Processes* **1996,** *158*, 97-113.

28. Dahl, D. A.; Delmore, J. E.; Appelhans, A. D. *Rev. Sci. Instrum.* **1990,** *61*, 607-609.

29. Arnott, D.; O'Connell, K. L.; King, K. L.; Stults, J. T. *Anal. Biochem.* **1998,** *258*, 1-18.

30. Oconnor, P. B.; Speir, J. P.; Wood, T. D.; Chorush, R. A.; Guan, Z. Q.; McLafferty, F. W. *J. Mass Spectrom.* **1996,** *31*, 555-559.

31. Guan, S. H.; Wahl, M. C.; Wood, T. D.; Marshall, A. G. *Anal. Chem.* **1993,** *65*, 1753-1757.

32. Campbell, V. L.; Guan, Z. Q.; Laude, D. A. *J. Am. Soc. Mass Spectrom.* **1995,** *6*, 564-570.

33. Dey, M.; Castoro, J. A.; Wilkins, C. L. *Anal. Chem.* **1995,** *67*, 1575-1579.

34. Oconnor, P. B.; Duursma, M. C.; vanRooij, G. J.; Heeren, R. M. A.; Boon, J. J. *Anal. Chem.* **1997,** *69*, 2751-2755.

35. Sze, T. P. E.; Chan, T. W. D. *Rapid Commun. Mass Spectrom.* **1999,** *13*, 398-406.

36. Senko, M. W.; Hendrickson, C. L.; Emmett, M. R.; Shi, S. D. H.; Marshall, A. G. *J. Am. Soc. Mass Spectrom.* **1997,** *8*, 970-976.

37. Hofstadler, S. A.; Wu, Q. Y.; Bruce, J. E.; Chen, R. D.; Smith, R. D. *Int. J. Mass Spectrom. Ion Processes* **1995,** *142*, 143-150.

38. Beu, S. C.; Laude, D. A. *Int. J. Mass Spectrom. Ion Processes* **1990,** *97*, 295-310.

39. Bruce, J. E.; Anderson, G. A.; Hofstadler, S. A.; Vanorden, S. L.; Sherman, M. S.; Rockwood, A. L.; Smith, R. D. *Rapid Commun. Mass Spectrom.* **1993,** *7*, 914-919.

40. Bruce, J. E.; Vanorden, S. L.; Anderson, G. A.; Hofstadler, S. A.; Sherman, M. G.; Rockwood, A. L.; Smith, R. D. *J. Mass Spectrom.* **1995,** *30*, 124-133.

41. Guan, S. H.; Pasatolic, L.; Marshall, A. G.; Xiang, X. Z. *Int. J. Mass Spectrom. Ion Processes* **1994,** *139*, 75-86.

42. Caravatti, P.,United States Patent 4,924,089, **1990**.

43. Kofel, P.; Allemann, M.; Kellerhals, H.; Wanczek, K. P. *Int. J. Mass Spectrom. Ion Processes* **1985,** *65*, 97.

44. Koster, C.; Castoro, J. A.; Wilkins, C. L. *Journal Of The American Chemical Society* **1992,** *114*, 7572- 7574.

45. Alford, J. M.; Williams, P. E.; Trevor, D. J.; Smalley, R. E. *Int. J. Mass Spectrom. Ion Processes* **1986,** *72*, 33-51.

46. Hogan, J. D.; Laude, D. A. *Anal. Chem.* **1990,** *62*, 530-535.

47. Gluckmann, M.; Karas, M. *J. Mass Spectrom.* **1999,** *34*, 467-477.

48. Li, G. Z.; Guan, S. H.; Marshall, A. G. *J. Am. Soc. Mass Spectrom.* **1997,** *8*, 793-800.

49. Spizer, L. *Physics of Fully Ionized Gases*; Interscience: New York, 1962.

50. Francl, T. J.; Sherman, M. G.; Hunter, R. L.; Locke, M. J.; Bowers, W. D.; McIver, R. T. *Int. J. Mass Spectrom. Ion Processes* **1983,** *54*, 189-199.

51. Ledford, E. B.; Rempel, D. L.; Gross, M. L. *Anal. Chem.* **1984,** *56*, 2744-2748.

52. Baker, P. R.; Clauser, K. R., MS Fit, http://prospector.ucsf.edu.

53. Stults, J. T. *Anal. Chem.* **1997,** *69*, 1815-1819.

54. Davis, S. C.; Makarov, A. A.; Cameron, G., Long Beach, CA, June 11-15, 2000 2000; ASMS.

55. Gygi, S. P.; Rist, B.; Gerber, S. A.; Turecek, F.; Gelb, M. H.; Aebersold, R. *Nat. Biotechnol.* **1999,** *17*, 994-999.

56. Goodlett, D. R.; Bruce, J. E.; Anderson, G. A.; Rist, B.; Pasa-Tolic, L.; Fiehn, O.; Smith, R. D.; Aebersold, R. *Anal. Chem.* **2000,** *72*, 1112-1118.

CHAPTER 5

CHARACTERIZATION OF POLYESTERS BY MATRIX ASSISTED LASER DESORPTION/IONIZATION AND FOURIER TRANSFORM MASS SPECTROMETRY [†]

[†]Mize, T. H., Simonsick, W. H., and Amster, I. J. To be submitted to *Macromolecules*.

ABSTRACT

Two homopolyesters, poly(neopentyl glycol-alt-isophthalic acid) and poly(hexanediol-alt-azelaic acid), and two copolyesters, poly(dipropoxylated bisphenol-A-*alt*-(isophthalic acid-*co*-adipic acid)) and poly(neopentyl glycol-*alt*-(adipic acid-*co*-isophthalic acid)) were analyzed by matrix assisted laser desorption/ionization Fourier transform mass spectrometry (MALDI-FTMS). The high resolution and high mass accuracy provided by FTMS greatly facilitated the characterization of these copolyesters. Assignment of spectral peaks can be automated given isobaric resolution allowing even the ion abundances of overlapping isotopic envelopes to be assessed. Repeat units were confirmed and end functionality assigned. Single shot mass spectra of the entire polymeric distribution demonstrate that the dynamic range of this internal MALDI source instrument and the analyzer cell exceeds the performance of those previously reported for higher field instruments. Corrections of space charge mass shift effects are demonstrated for the analytes using an external calibrant and (subsequent to confirmation of structure) via internal calibration which removes ambiguity due to space charge differences in calibrant and analyte spectra. Capillary gel permeation chromatography was used to prepare low polydispersity samples from a high polydispersity polyester, improving the measurement of molecular weight distribution two-fold while retaining the benefits of high resolution mass spectrometry for elucidation of oligomer identity.

INTRODUCTION

Many of the macroscopic physical properties (e.g., mechanical strength, viscosity,) of synthetic polymers depend upon the distribution of individual oligomers in the polymer, often expressed as number average ($M_n = \Sigma M_i n_i / \Sigma n_i$) or weight average ($M_w = \Sigma M_i^2 n_i / \Sigma M_i n_i$) molecular weights and polydispersity ($D = M_w/M_n$). Currently the tool of choice for elucidation of molecular weight distributions in synthetic polymers is gel permeation chromatography (GPC).[1] Separation in GPC is based on differential retention of molecules based on their size, which roughly correlates to the molecular weight. Calibration is achieved by running mass standards under the same elution conditions as the analyte. Differences in three dimensional structure between an analyte and calibrant can lead to significant errors in the assignment of molecular weight by externally calibrated GPC.[2] For example, in some polymers cyclization produces molecules that elute much later than their linear counterparts with the same number of repeat units.[2] Other analytical techniques such as nuclear magnetic resonance, like GPC, only yield molecular weight averages and bulk composition without distinguishing any of the fine compositional detail of polymer mixtures. Alternate methods that allow the simultaneous elucidation of the masses of cyclic and linear oligomers represent a great step forward in the ability to fully characterize complex polymer samples. Matrix assisted laser desorption/ionization (MALDI) mass spectrometry, first introduced by Karas and Hillenkamp, achieves this goal and, coupled to a Fourier transform ion cyclotron resonance mass spectrometer (FTICR-MS), allows the determination of individual monomer distributions. [3-9]

Characterization of the repeat units and end groups of polymers by mass spectrometry requires a high degree of mass accuracy for homopolymers such as polyethylene glycol (or, PEG) and poly(methyl methacrylate) (or, PMMA).[10, 11] This requirement is even more important for simple alternating copolymers and is an absolute necessity in polymers with even a small degree of randomness. The presence of oligomeric species with overlapping isotope envelopes (resulting in spectral peaks differing by less than a mass unit, known as isobaric peaks) demands that high mass accuracy also be accompanied by high mass resolution.[12-14]

The analysis of synthetic polymers has benefitted greatly from the development of matrix assisted laser desorption/ionization mass spectrometry (MALDI-MS).[3] Application of this soft ionization technique to Fourier transform ion cyclotron resonance (FTICR) mass spectrometry allows for unprecedented mass accuracy and high resolution.[15, 16] These capabilities permit determination of molecular properties of polymers such as mass distribution,[9, 17-20] repeat unit masses,[21-26] end group elemental composition,[9, 21-23, 27] oligomer configurations, [21, 28, 29] and (in multicomponent polymers) relative concentrations of the various components.[30-36] Accurate mass determination over a broad mass range requires calibration that accounts for frequency shifts due to space charge effects. The successful characterization of space-charge effects on mass accuracy coupled with recent advances in instrumentation, make MALDI-FTICR MS a powerful tool for polymer characterization.[37] MALDI coupled with time-of-flight (TOF) mass spectrometry has been frequently used for polymer analysis.[38-41] However, the resolution and mass accuracy of TOF-MS are insufficient for definitive assignment of repeat unit

and end group masses.[42-44] We show here that the use of FTICR-MS coupled with a MALDI source provides the resolution and mass accuracy thus needed.

The development and application of FTICR-MS for polymer analysis has been an active area of research, although much of the work has focused on simple polymers (i.e., those containing a single monomer repeat unit) that accept a charge readily and that are stable under a wide variety of ionization conditions.[20, 25, 45-56] Polymers that have several oligomer configurations and copolymers (especially random copolymers) have rarely been examined this way. Koster and coworkers recently examined individual hyperbranched polyester-amide oligomer structures by electron capture dissociation,[57] and a number of synthetic polymers have been analyzed by ultrahigh resolution electrospray ionization (ESI) FTICR-MS after GPC fractionation.[2, 14, 58] This approach provides a less disperse mass range that reduces complexity of the spectrum and attenuates the mass discrimination inherent in ESI.[2, 59]

The capabilities of MALDI-FTICR MS for direct measurement of polydispersity and end group and repeat unit masses are demonstrated for a "simple" polyester, poly(neopentyl glycol-*alt*-isophthalic acid), and two copolyesters, poly(dipropoxylated bisphenol-A-*alt*-(isophthalic acid-*co*-adipic acid)) and poly(neopentyl glycol-*alt*-(adipic acid-*co*-isophthalic acid)). Space charge effects on mass accuracy are demonstrated and their attenuation is achieved by manipulation of the ion intensity of the external calibrant and, alternately, by internal calibration, to achieve low ppm mass accuracy in the measurement of the molecular weights of the oligomers. Auxiliary use of capillary GPC to provide lower dispersity samples for analysis when confronted with a highly disperse polyester is also demonstrated.

EXPERIMENTAL

A 4.7 tesla MALDI FTICR-MS that was constructed in-house has been used for all experiments.[37] Samples are applied to a 2.5 cm (1") diameter titanium puck that is positioned in the vacuum chamber by a magnetically coupled linear-rotary manipulator to within 1 cm of the ICR cell to reduce time-of-flight mass discrimination effects.[11, 37, 60-62] The cell is of open-ended cylindrical design. For most of the experiments, the detection region of the cell was 5.6 cm (2-1/4") long and 5.6 cm (2-1/4") diameter; as noted below, several of the experiments utilized a longer 8.5 cm (3-3/8") cell designed to further attenuate the effects of space charge. Working pressure for the mass spectrometer is 10^{-9} to 10^{-10} torr; during quadrupolar excitation (QE), the pressure is temporarily pulsed to $\sim 10^{-4}$ torr using nitrogen to provide neutral collisions. The spectrometer is controlled by a commercially obtained data station (Ionspec Corporation, Irvine, California).

Poly(neopentyl glycol-alt-isophthalic acid) (NPG-IPA) and poly(hexanediol-alt-azelaic acid) (HEX-AZ) were synthesized at DuPont Marshall Laboratories in Philadelphia, PA. The copolyesters poly(neopentyl glycol-alt-(adipic acid-co-isophthalic acid)) (U3NEO) and poly(dipropoxylated bisphenol-A-alt-(adipic acid-co-isophthalic acid)) (U415) were provided by Rohm and Haas Company. The polymer molecular weight distributions were characterized by gel permeation chromatography externally calibrated with narrow mass range polystyrene standards prior to delivery. Naming conventions for the analytes in this paper will be the above abbreviations for the homopolymers and the following for the individual monomer components: adipic acid (AA), isophthalic acid (IPA), dipropoxylated bisphenol-A (PBPA), and neopentyl glycol (NPG).

Polyester solutions were prepared in acetone at a concentration of 1 mM. MALDI samples were prepared for analysis by mixing 25 μL of polymer solution with 40 μL of 0.2 M *trans*-3-indole acrylic acid (IAA) in acetone and 10 μL of a saturated solution (ca. 5 mM) of sodium trichloroacetate in acetone and applying this solution to the sample puck by electrospray deposition via a charged metal hypodermic needle at 4.5 kV across 1 cm gap onto a grounded titanium target.[63] Polyethylene glycol (PEG) standards (1 mg/mL) and saturated sinapinic acid matrix were both dissolved in 50% acetonitrile with 0.1% trifluoroacetic acid and aqueous NaCl solution is added to the PEG in a 10:1 molar ratio; 1 μL of each solution was mixed on the sample puck and allowed to air dry.

The HEX-AZ polyester was also subjected to fractionation by capillary GPC in preparation for MALDI-FTMS analysis. A 25 cm glass capillary (220 μm i.d., SGE Analytical Products, Austin, TX) was slurry packed at 1600 psi (115 atm) using PLGel 3 μm Mixed-E GPC material (Polymer Laboratories, Amherst, MA) that had been resuspended overnight in THF. A 10 mM poly(HEX-AZ) solution in THF was loaded onto the column via a 0.5 μL injection loop and eluted at 60 μL/hour using THF supplied from a syringe pump (Model 55-1111, Harvard Apparatus, South Natick, MA). The matrix (IAA) and cation source (NaTCA) were sprayed onto the target through a slit in a grounded metal mask prior to GPC fractionation, as described above; column effluent was electrosprayed at 4.5 kV onto the prepared matrix spots, also through the slit in the metal mask. Each fraction was collected in this manner for one minute prior to rotation of the target to the next matrix spot.

Ions are formed by desorption with a frequency tripled (8 = 355 nm) Nd:YAG laser (ACL-MS-355, New Wave Research, Sunnyvale, CA) and are captured in the analyzer cell by gated trapping.[64, 65] The rear trapping plate of the cell is held at the desired initial trapping potential (optimized for each matrix and analyte combination) while the trapping plates nearest the puck is held at ground potential to allow the desorbed ions to enter. The front trapping potential is then raised to match the rear potential 400-600 μsec after the 1 ns laser pulse. A neutral collision gas is introduced to the instrument via a 3 ms pulse from a solenoid controlled valve, raising the pressure to a peak of 10^{-6} torr to attenuate the initial kinetic energy of the ions formed in the MALDI process.[62] After a delay of approximately 14 s to allow the system pressure to return to approximately 5 x 10^{-10} torr, an excitation pulse consisting of a linear sweep of the cyclotron frequencies of the mass-to-charge range of interest is applied to two opposing cell plates and, through capacitive coupling, to the adjacent trapping electrodes.[66] The ions' radii expand toward the edge of the ICR cell as the frequency sweep passes through their respective resonant frequencies and, after the excitation is finished, the entire suite of ions continues to orbit the center of the cell at the new radius. The motion of the ions induces an image current on the remaining two cell plates that is digitized and converted from time domain to frequency domain data by Fourier transformation. Application of a calibration equation converts the frequency spectrum to a mass spectrum.

RESULTS AND DISCUSSION

The internal MALDI FTICR-MS instrument at the University of Georgia has been proven effective for wide mass distributions in previous work.[11, 37, 67-69] Figures 5.1a

and 5.1b show full distributions of the copolyesters U415 and U3NEO obtained from single laser shots. Signal-to-noise for the most abundant peaks in the two polymer mass spectra are 430:1 and 520:1, respectively, with resolution ($m/\ m_{1/2}$) of 36,000 at m/z 969 (U415) and 21,000 at m/z 1793 (U3NEO). The experimental set-up was tuned using equimolar mixes of polyethylene glycol with average molecular weights of 1000, 2000, and 3400; this tune-up spectrum showed no mass discrimination over the detection range of m/z 300-4000. The number average and weight average molecular weights derived from these spectra were M_n = 1752 and M_w = 1913 for U3NEO (as compared to M_w = 2070 by GPC), and M_n = 1763 and M_w = 1991 for U415 (M_w = 2150 by GPC).

Typically, MALDI produces both sodium and potassium cationized polymer ions. The presence of potassium cationized ions 16 mass-to-charge units above the predominant sodium cationized peaks can cause uncertainty in the analysis of the mass spectrum due to the overlap of the isotope peaks of the potassiated ions of one component with those of the sodiated ions ofa different component, as shown in Figure 5.2a for U415. This problem can be significantly reduced by doping the sample with sodium ions to decrease the relative intensity of peaks arising from potassium ions. As shown in Figure 5.2b, the additional sodium ions competitively mute the interfering K^+ peaks without significantly deteriorating the signal-to-noise ratio. The attenuation of the K^+ attached ions allows clear assignment of the various oligomer types.

Figure 5.3 shows an FTICR mass spectrum of a simple polyester of neopentyl glycol and adipic acid (NPG-IPA). Even for this simple alternating copolymer, the mass spectrum shows some complexity from the overlap of two types of linear oligomers as

Figure 5.1. Mass spectra of the full distributions of the copolyesters U3NEO (A) and U415 (B). Insets show the base peak and its isotopes for each spectrum.

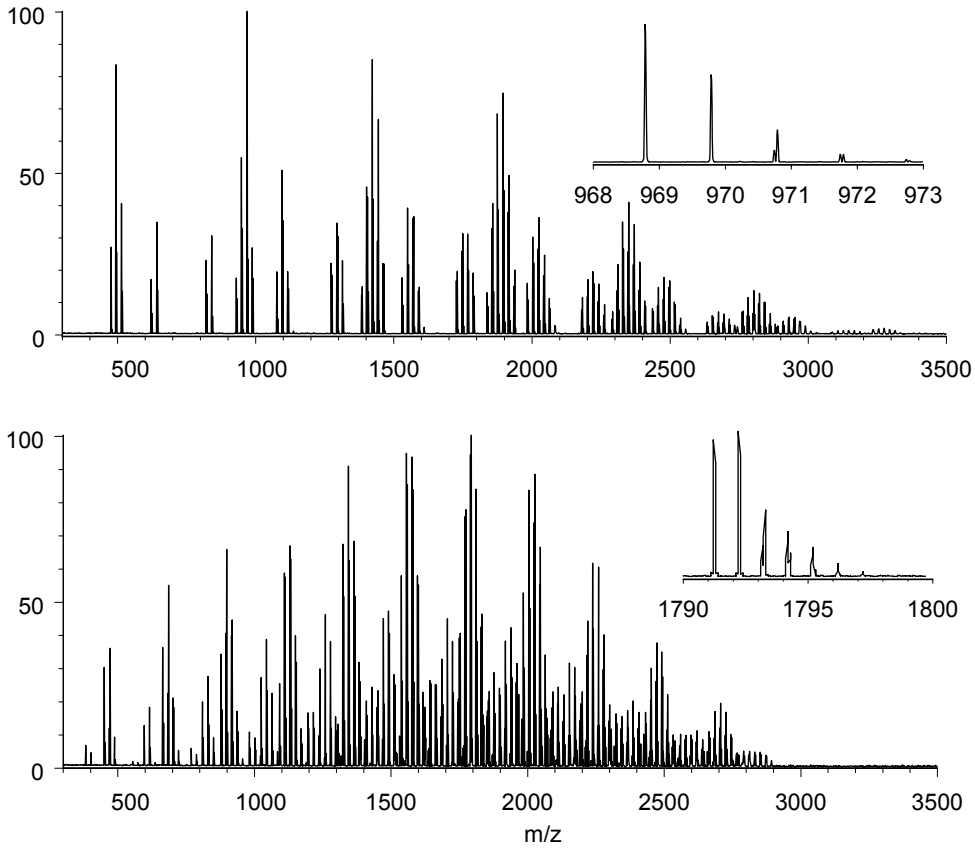
100
50
0
500
1000
1500
2000
2500
3000
3500
968
969
970
971
972
973
100
50
0
500
1000
1500
2000
2500
3000
3500
1790
1795
1800
m/z

Figure 5.2. A) Multiple cations in "native" copolyester (U415) samples result in signal overlap in the copolyester mass spectra. This example shows sodiated species (○) with overlapping potassiated (■) that complicate analysis and can dilute signal strength. B) Addition of excess Na^+ results in a cleaner spectrum. Cyclic oligomers appear 18 Da below linear counterparts below linear counterparts of same monomer composition. Variations in the acid species composition result in species overlapping with a spacing of 20 Da.

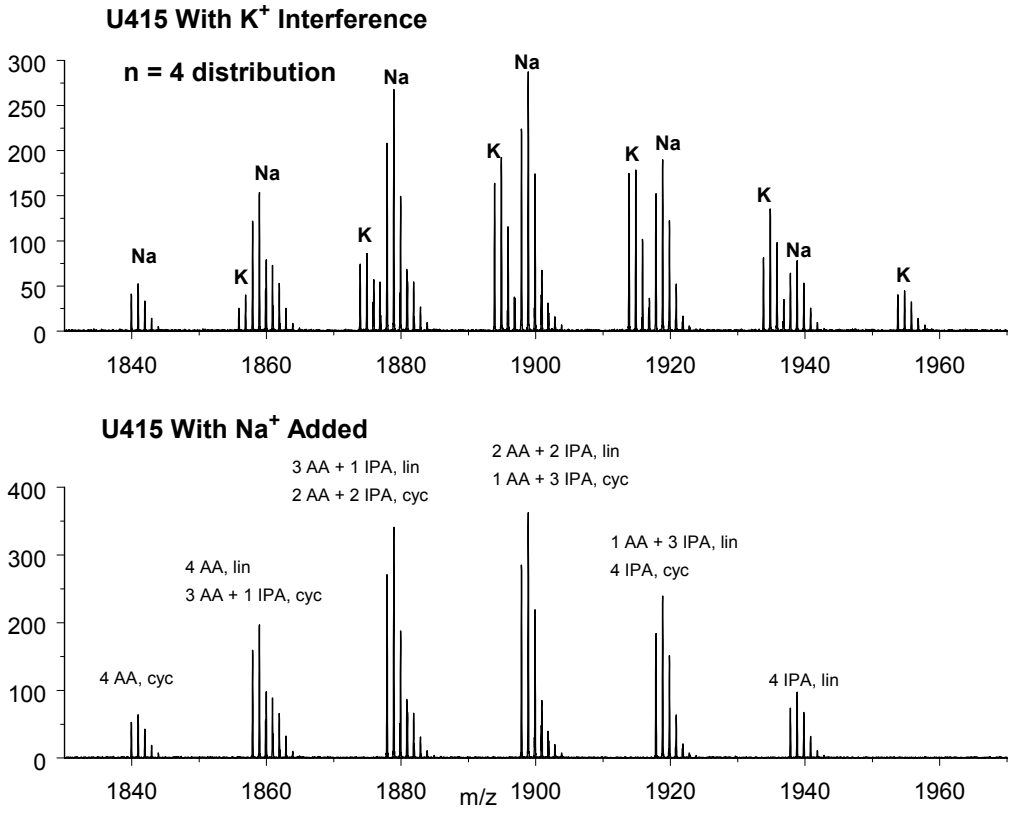
U415 With K+ Interference
n = 4 distribution
Na
K
Na
K
Na
K
Na
K
Na
K
Na
K
300
250
200
150
100
50
0
1840
1860
1880
1900
1920
1940
1960
U415 With Na+ Added
3 AA + 1 IPA, lin
2 AA + 2 IPA, cyc
2 AA + 2 IPA, lin
1 AA + 3 IPA, cyc
1 AA + 3 IPA, lin
4 IPA, cyc
4 AA, lin
3 AA + 1 IPA, cyc
4 AA, cyc
4 IPA, lin
400
300
200
100
0
1840
1860
1880
m/z
1900
1920
1940
1960

Figure 5.3. Poly(neopentyl glycol-alt-isophthalic acid) homopolyester mass spectrum synthesized with 2:1 alcohol:acid ratio. This results in linear oligomers with alcohol end caps ([ ) as well as normal linear oligomers with H- and -OH end groups (■) and cyclic species (○). A) The complete spectrum with insert demonstrating typical resolution at m/z = 3405. B) An expansion of the spectrum showing cyclic and normal linear species at n=7 and 8 and the alcohol end capped oligomer at n=7.

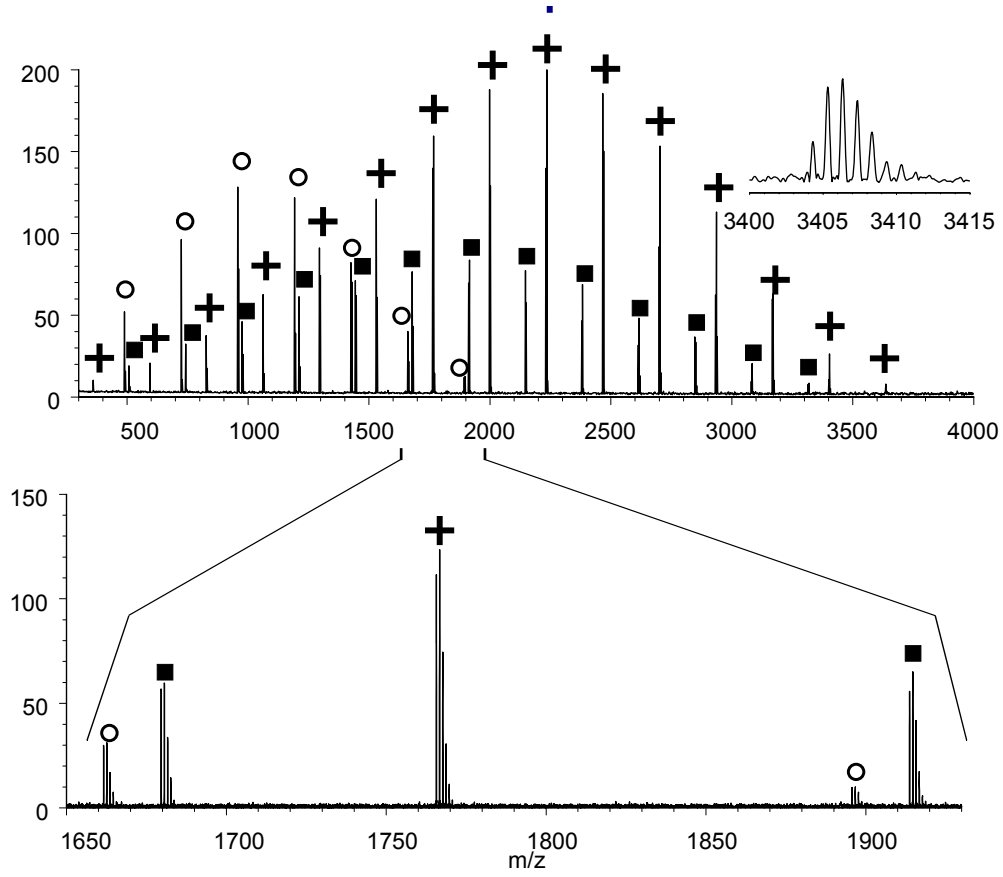
200
150
100
50
0
500
1000
1500
2000
2500
3000
3500
4000
3400
3405
3410
3415
150
100
50
0
1650
1700
1750
1800
1850
1900
m/z

well as cyclic oligomers. As can be seen in Figure 5.3, cyclic oligomers are clearly differentiated from their linear counterparts so that accurate assignment of each oligomer's monoisotopic mass can be derived. Linear regression analysis of the derived molecular weights versus the corresponding oligomer's degree of polymerization yields the repeat unit mass as the slope of the regression line and a residual mass equal to the end group mass plus that of the cationized species as the intercept.[10] In this case, we extract residual masses of 22.9889 (Na^+), 41.0006 ($H_2O + Na^+$),127.0735 Da ($C_5H_{12}O_2 + Na^+$) for the cyclic, linear, and alcohol saturated forms (calculated values = 22.9898, 41.0004, and 127.0735 Da, respectively) and a repeat unit of 234.0892 Da ($C_{13}H_{14}O_3$, calculated value = 234.0892 Da).

By comparison, Figure 5.4 illustrates the increased complexity of a copolyester mass spectrum as well as the variety of information that can be extracted from the data. In addition to the cyclic and "normal" linear oligomers that make up the neopentyl glycol/adipic acid/isophthalic acid copolyester shown in Figure 5.4a, where the total number of diacid monomers equals the total number of glycols, this particular copolyester also has the possibility of having diacid groups or glycol groups capping both ends, as seen in Figure 5.4b. As in simple polyesters, the alcohol (PBPA in the one polymer or NPG in the other) alternates with an acid; in this case each acid in a chain is either of the two available (IPA or AA). Thus, there is randomness inherent in the substance with respect to composition of the diacid monomers. For a given chain made up of n alcohols and n acids, there results a binomial distribution of n+1 components with a mass separation equal to the difference in the masses of the two diacids (in this

Figure 5.4. A) Segment from high resolution mass spectrum of poly(NPG-alt-(AA-co-IPA)). Linear species are denoted "L" and cyclic species, "C," with "x, y, z" referring to number of AA, IPA, and NPG, respectively. The mass separation between acid and alcohol monomers (42 and 62 Da) is on the same order as the difference between acid monomers (20 Da) resulting in mass overlays in the mass spectra at low degree of polymerization. B) Expansion of the mass scale allows assignment of the overlapping acid end capped species (L 4, 4, 7 and L 3, 5, 7) and alcohol end capped oligomers (L 8, 0, 9 through L 6, 2, 9).

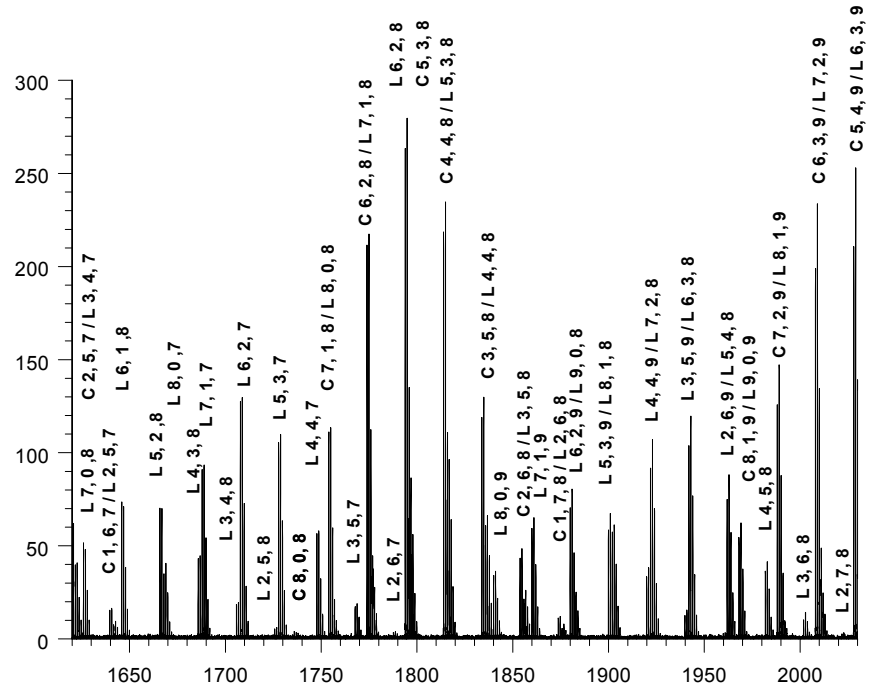
300
250
200
150
100
50
0
1650
1700
1750
1800
1850
1900
1950
2000
C 8, 0, 8
L 7, 0 ,8
C 2, 5, 7 / L 3, 4, 7
C 1, 6, 7 / L 2, 5, 7
L 6, 1 ,8
L 5, 2 ,8
L 8, 0 ,7
L 4, 3, 8
L 7, 1, 7
L 3, 4, 8
L 6, 2, 7
L 2, 5, 8
L 5, 3, 7
L 4, 4, 7
C 7, 1, 8 / L 8, 0, 8
L 3, 5, 7
C 6, 2, 8 / L 7, 1, 8
L 2, 6, 7
L 6, 2, 8
C 5, 3, 8
C 4, 4, 8 / L 5, 3, 8
C 3, 5, 8 / L 4, 4, 8
L 8, 0, 9
C 2, 6, 8 / L 3, 5, 8
L 7, 1, 9
C 1, 7, 8 / L 2, 6, 8
L 6, 2, 9 / L 9, 0, 8
L 5, 3, 9 / L 8, 1, 8
L 4, 4, 9 / L 7, 2, 8
L 3, 5, 9 / L 6, 3, 8
L 2, 6, 9 / L 5, 4, 8
C 8, 1, 9 / L 9, 0, 9
L 4, 5, 8
C 7, 2, 9 / L 8, 1, 9
L 3, 6, 8
C 6, 3, 9 / L 7, 2, 9
L 2, 7, 8
C 5, 4, 9 / L 6, 3, 9

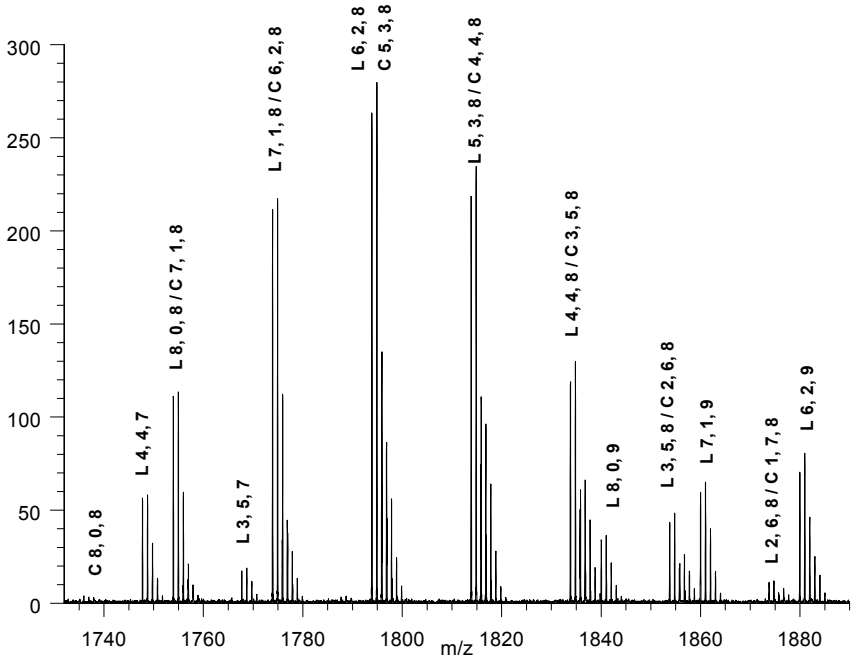
300
250
200
150
100
50
0
1740
1760
1780
1800
m/z
1820
1840
1860
1880
C 8, 0, 8
L 4, 4, 7
L 8, 0, 8 / C 7, 1, 8
L 3, 5, 7
L 7, 1, 8 / C 6, 2, 8
L 6, 2, 8
C 5, 3, 8
L 5, 3, 8 / C 4, 4, 8
L 4, 4, 8 / C 3, 5, 8
L 8, 0, 9
L 3, 5, 8 / C 2, 6, 8
L 7, 1, 9
L 2, 6, 8 / C 1, 7, 8
L 6, 2, 9

case 19.9687 Da). Figure 5.4b shows an expansion of the mass range between m/z 1730-1890. Starting at m/z 1736, a series of peaks appear at 20 mass unit intervals (the difference in mass between masses of the two acids) corresponding to cyclic oligomers. At about m/z 1754, another series of ions appears to grow into the distribution, as well, overlapping with the cyclic oligomers; these are the linear oligomers with the same monomer composition as the cylcic variants, plus HO- and -H as the end groups. Regression analysis on the monoisotopic peaks of the two series (with corresponding series across the spectrum) reveals that the distribution corresponds to the condensation products of 8 NPGs with 8 of the acids and having either Na^+ (for the cylcic oligomers) or $H_2O + Na^+$ (for linear oligomers) as the endgroup.

The polyester can also grow with alcohol or acid endcapping. Figure 5.4a shows the four types of oligomers that can occur in this polyester, some of which can be seen in the cyclic and linear panel below. The prominence of the alcohol- and acid-saturated peaks indicates that the monomers can condense directly onto the chain rather than first forming a ester intermediate, as well as indicating the relationship between the initial feed stock concentrations and the condensation reaction kinetics.

Calibration of the mass spectra can be accomplished with external calibrants or internally using the known masses of peaks within the distribution. Space charge can cause frequency shifts as large as 100 ppm. With internal calibration the systematic error due to space charge cancels fully,[11, 34] making this the preferred technique. For external calibration, a space charge correction can be applied to the calibration equation to account for the frequency shifts thus improving the repeat and endgroup mass determination by up to two orders of magnitude.[11] Elemental compositions of the

endgroup and repeat units assigned from the externally calibrated data can be used to calculate the exact masses of the corresponding oligomers and a subsequent calibration applied to demonstrate the limits of mass accuracy for a given mass spectrum. Table 5.1 compares external versus internal calibration for determining the repeat mass by linear regression analysis. Without accounting for space charge, the externally calibrated data show errors of approximately 10 ppm for the derivation of the repeat mass. Accounting for space charge reduces the error to ~5 ppm. Internal calibration reduces the error further to 1 ppm.

Since the analysis involves linear regression of the measured oligomer exact masses against the degree of polymerization, the slope of the line is typically within the same order of mass error as that of the oligomer masses. However, extrapolation of the line to n = 0 often results in unacceptably high mass error for the end group mass due to the extrapolation from high molecular weight to zero repeat units, whereby small errors at higher degrees of polymerization are magnified. If the error is due to random scatter, end group analysis can be improved by first using the mass found from the slope of the regression line to assign the exact chemical composition of the repeat unit and then calculating the exact mass of the repeat unit from the assigned elemental composition and forcing lines with this *corrected* slope through each of the original data points,[10] as shown in Figure 5.5 for the neopentyl glycol endcapped oligomers. For the data of Figure 5.3, simple regression analysis yielded an intercept of 127.0824 Da for -38.0 ppm mass error compared to the calculated mass of 127.0776 for $C_5H_{12}O_2Na^+$. The derived slope (214.119 Da) confirms the assignment of the monomer as $C_{11}H_{18}O_4$ (mass 214.121

Table 5.1: Linear regression analysis of the data from the mass spectrum of Figure 5.3. Correction for space charge frequency shifts due to differences in the polyethylene glycol standard's and the copolyester analytes' signal intensities improves accuracy to approach the instrument's capability (indicated by the internal calibration). Mass accuracy for the $(PBPA\text{-}AA)_n$ oligomers suffers due to convolution of the monoisotopic peaks with the M+2 peaks of cyclic $[PBPA_{(n+1)}\text{-}AA_n\text{-}IPA_1]$ oligomers.

Acid	Calculated Repeat	External Repeat	ERR (ppm)	Space Chg. Repeat	ERR (ppm)	Internal Repeat	ERR (ppm)
IPA-NPG	234.089	234.087	11	234.088	4	234.089	1
AA-NPG	214.121	214.118	12	214.120	4	214.120	1
IPA-PBPA	474.204	474.200	10	474.202	5	474.204	0.7
AA-PBPA	454.236	454.230	11	454.233	6	454.235	2

Figure 5.5. Linear regression of alcohol end capped linear oligomers of U3NEO using measured mass-to-charge versus degree of polymerization (inset) yields repeat unit mass of sufficient accuracy to assign elemental composition but not for the end group mass. Forcing lines with slope equal to the calculated mass of the correctly assigned repeat unit mass through the data points results in several intercepts (inset) which are averaged to yield an order of magnitude better mass accuracy.

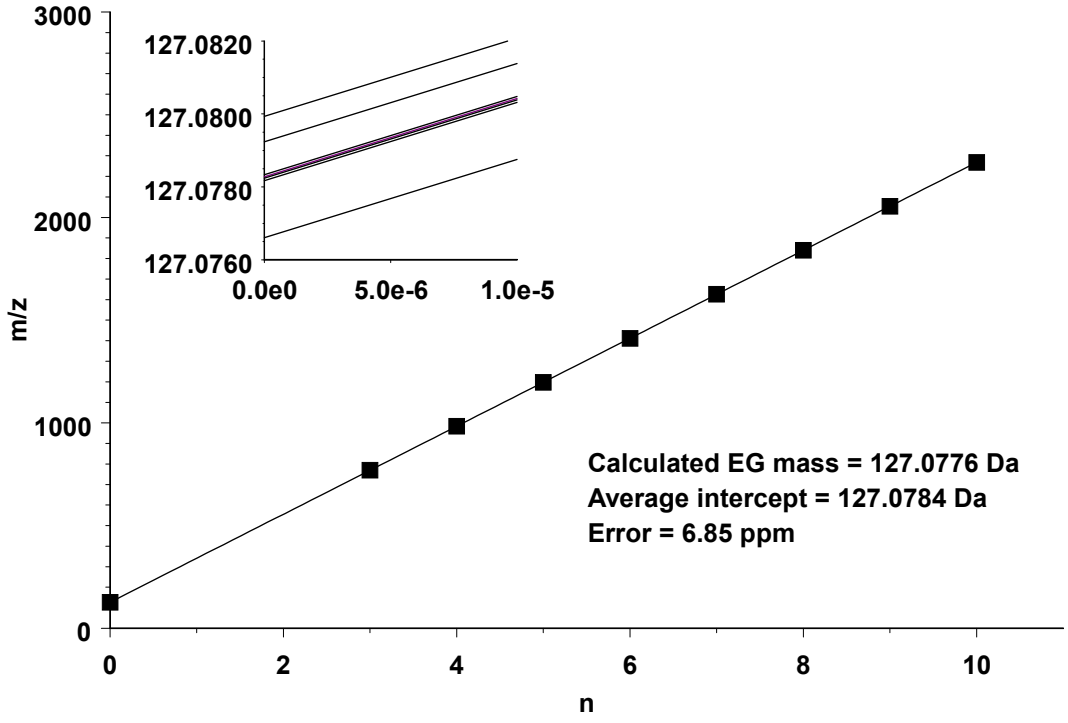
3000
2000
1000
0
m/z
0
2
4
6
8
10
n
127.0820
127.0800
127.0780
127.0760
0.0e0
5.0e-6
1.0e-5
Calculated EG mass = 127.0776 Da
Average intercept = 127.0784 Da
Error = 6.85 ppm

Da) within 9 ppm mass error. Using a value of slope calculated for the assigned elemental composition, the end group mass is derived by calculating the intercept of the lines that pass through each data point. The intercepts of these pseudo-regression lines are averaged to yield an end group mass of 127.078 Da, in exact agreement with the known end group mass. Table 5.2 compares end group masses for all the neopentyl glycol-alt-(adipic acid-co-isophthalic acid) components derived with and without the constraint of fixed repeat mass. These data clearly demonstrate the improved accuracy in determining end groups by constraining the repeat mass to its calculated value.

As mentioned earlier, examination of Table 5.1 shows higher mass error in the assignment of the so-called "normal" linear oligomers compared to the cyclic, alcohol saturated, and acid saturated species. Mere isotopic resolution results in the convolution of the M+2 isotope peak of cyclic oligomer ions with the monoisotopic peaks of the normal linear oligomers with one fewer IPA but the same nominal chain length, as seen in Figure 5.6a. This can occur due to something as simple as low spectral resolution causing the peaks to coalesce; alternately, at high total ion abundance, ions with close cyclotron frequencies can phase lock resulting in a larger ion packet traveling at an average frequency of the two.[14, 70, 71] In either case, it is necessary to increase the resolution with a longer transient and/or decreased total ion abundance, as necessary. Figure 5.6b shows an expansion of the mass scale for a high resolution mass spectrum of the copolyester, U415, for which the cyclic version (2 AA and 2 IPA) overlaps with the isotope peaks of the linear component (1 AA and 3 IPA). The two components are resolved to the baseline, permitting the exact masses to be determined, as well as their

Figure 5.6. Examples of high resolution (A) and ultrahigh resolution (B) mass spectra of U415. At the higher level of resolution, assignment of the cyclic and linear oligomers is straightforward and can be easily automated. Inset shows the whole spectrum from which the example was culled.

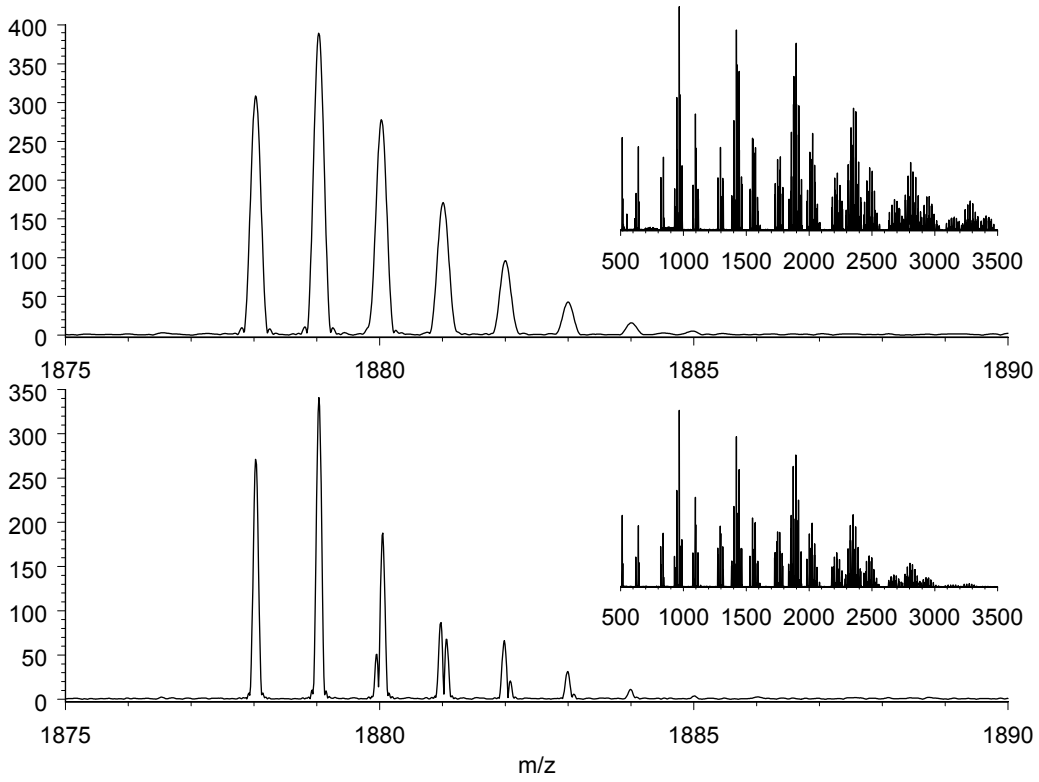
400
350
300
250
200
150
100
50
0
1875
1880
1885
1890
500 1000 1500 2000 2500 3000 3500
350
300
250
200
150
100
50
0
1875
1880
1885
1890
500 1000 1500 2000 2500 3000 3500
m/z

Table 5.2: Residual masses (RM) of the poly[NPG-alt-(AA-co-IPA)] copolyester (includes 22.9898 Da for the Na+ charge carrier and the calculated mass of the end groups). Corrected RM are obtained by assignment of elemental composition of the repeat unit from the slope of the regression line then forcing lines with the slope of these repeat units' *calculated* masses through the data points representing the measured RM of the oligomers and averaging the resulting intercepts. As in the repeat mass analysis, the linear oligomers suffer from convolution of their measured masses with those of the isotopes of the cyclic oligomers as well as demonstrating the dangers of systematic error in this endgroup analysis correction.

Acid	Chain Type	Calculated RM	Measured RM	ERR (ppm)	Corrected RM	ERR (ppm)
IPA	Cyclic	22.990	22.990	-4	22.990	-0.6
AA	Cyclic	22.990	22.990	13	22.990	7
IPA	Linear	41.004	41.002	51	41.005	-18
AA	Linear	41.004	41.001	77	41.006	-40
IPA	NPG	127.078	127.075	22	127.077	4
AA	NPG	127.078	127.082	-38	127.078	-7
IPA	IPA	189.020	189.014	34	189.019	8
AA	AA	169.052	169.045	38	169.050	11

abundances. Table 5.3 compares calculated repeat masses with those derived from isobarically resolved mass spectra.

While GPC can give us absolute molecular weight distribution information, the relatively poor resolution precludes determination of individual component distributions. However, with FTICR-MS, the number of each acid and alcohol component in a given oligomer is immediately apparent. Given an isobarically resolved spectrum and knowledge of the repeat and endgroup elemental compositions, it is elementary to assign each peak by a straightforward algorithm that systematically calculates the exact mass of each possible isotope and interrogates the measured peak masses with these calculated masses to find the best matches. The sum of the isotope ion intensities for each oligomer can be used to calculate number- and weight-average alcohol, AA, and IPA distributions, as shown in Table 5.4. While the overall molecular weight distribution is marginally lower for MALDI FTICR-MS compared to GPC ($M_{w\text{-}MALDI} / M_{w\text{-}GPC} = 0.93$ for U415, 0.92 for U3NEO, probably due to MALDI's well known mass discrimination toward lower molecular weights), the component distributions are impossible at the resolution offered by GPC.[18, 19, 29, 72-78]

While MALDI-FTMS yields acceptable molecular distribution information for polymers with low polydispersity indices ($D < 1.2$) and has been shown here to do so for mass ranges greater than two orders of magnitude, discrimination toward lower masses in mass spectra of more polydisperse samples is still problematic. This is illustrated in Figure 5.7a for the poly(HEX-AZ) homopolymer. Figure 5.7a shows a MALDI-FTMS mass spectrum of the polymer prepared and recorded as described for the other samples presented above. The peaks are all isotopically resolved and the calculated molecular

Table 5.3: Comparison of errors in deriving repeat unit masses for isotopically resolved versus isobarically resolved mass spectra. The data is for oligomers with equal numbers of alcohols and acids. Although both spectra were internally calibrated and the individual mass-to-charge ratios averaged 1.1 ppm error, the ultrahigh resolution repeat units differ by only 0.02 to 0.16 mDa from the calculated masses (masses shown to 10 μDa to demonstrate this detail).

(a) Data obtained at mass resolving power of 18,000 at m/z 2025.

(b) Data obtained at mass resolving power of 88,000 at m/z 2025.

	Calculated Repeat	High Res[a] Repeat	ERR (ppm)	Ultrahigh Res[b] Repeat	ERR (ppm)
IPA-NPG	234.08924	234.08901	1.0	234.08914	0.44
AA-NPG	214.12054	214.12032	1.1	214.12070	-0.75
IPA-PBPA	474.20424	474.20392	0.72	474.20417	0.15
AA-PBPA	454.23554	454.23464	2.1	454.23552	0.055

Table 5.4: Component- and molecular-weight distributions of the copolyesters. Initial reactant ratios were 51:34:15 (PBPA:AA:IPA) and 51:38:11 (NPG:AA:IPA) and the GPC derived weight-average molecular weights were 2150 and 2070, respectively.

	Alc = PBPA	AA	IPA	Mn	Mw
Nn =	3.8	2.2	1.6	1763	1991
Nw =	4.3	3.1	2.6	D = 1.1	

	Alc = NPG	AA	IPA	Mn	Mw
Nn =	7.8	5.3	2.6	1752	1913
Nw =	8.6	6.0	3.9	D = 1.1	

Figure 5.7. A) Single shot mass spectrum of poly(HEX-AZ). B) Mass spectrum reconstructed from the sum of 15 mass spectra, each representing ions from one minute fractions of a 15 minute capillary GPC separation. Insets show typical resolution as well as the presence of lower abundance and higher mass-to-charge species than detected in the unfractionated sample.

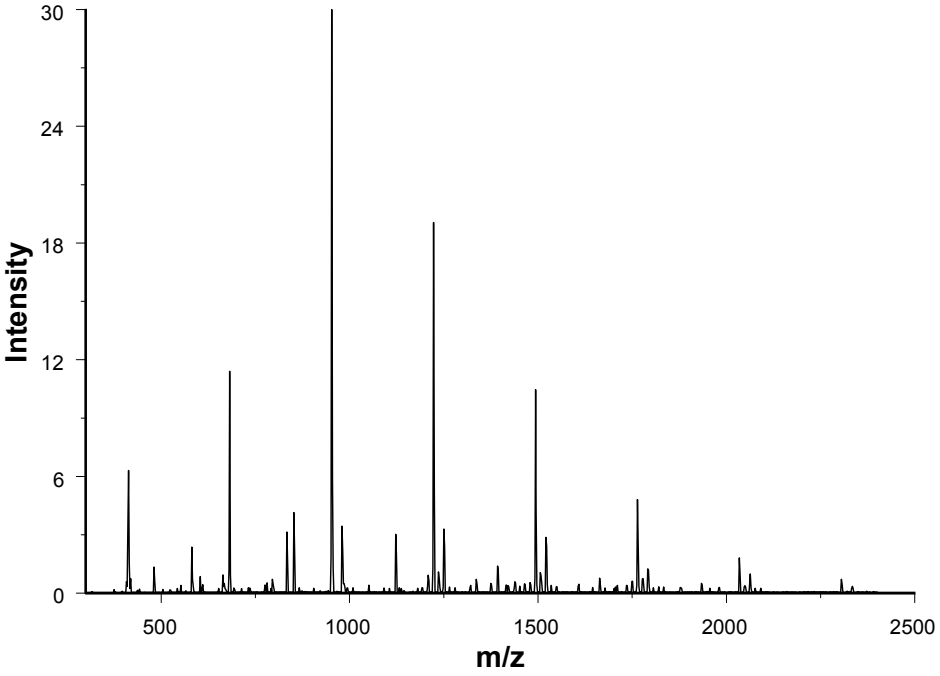
30
24
18
12
6
0
Intensity
500
1000
1500
2000
2500
m/z

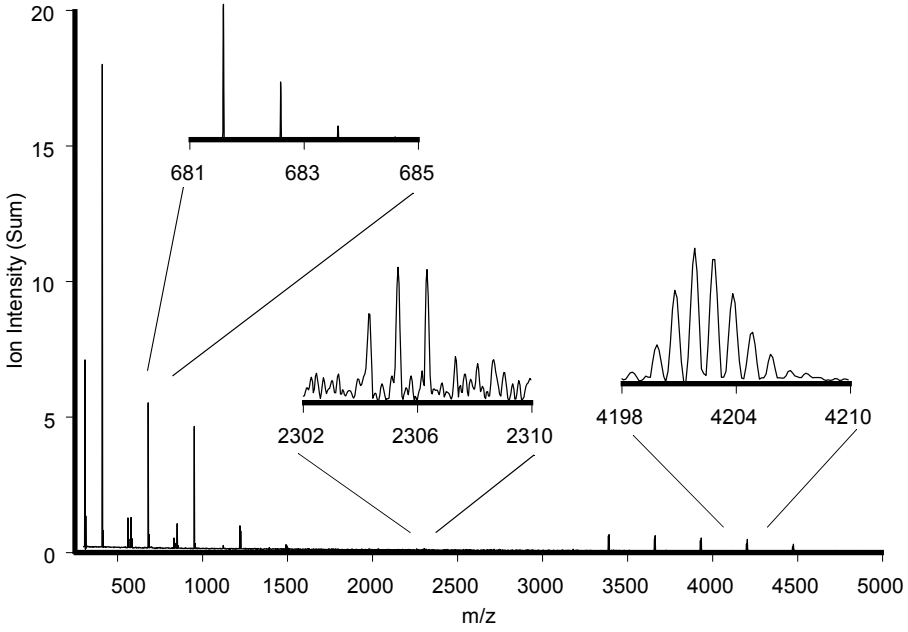
20
15
10
5
0
Ion Intensity (Sum)
681
683
685
2302
2306
2310
4198
4204
4210
500
1000
1500
2000
2500
3000
3500
4000
4500
5000
m/z

weight distribution parameters are Mn = 1083, Mw 1210, and D = 1.12 (compared to GPC from the supplier of 1040, 2590, and 2.5, respectively). It is well known that MALDI is not well suited for polymers of high polydispersity.[18, 79] Figure 5.7b shows a mass spectrum of the same polymer reconstructed from 15 mass spectra of one minute capillary GPC fractions electrosprayed directly onto a prepared MALDI target and subsequently analyzed. Peaks with resolved isotopes are discernible at close to the level of the noise and, more importantly, at approximately twice the mass-to-charge found in the unfractionated sample. The inset of Figure 5.8 shows that the column provided consistently low polydispersity samples for mass spectral analysis without significant dilution of the sample. The pseudo-chromatogram in Figure 5.8 is derived from the measured ion intensity, average elution time, and a standard deviation elution time (from a best fit of the cumulative normal distribution) for each oligomeric specie.

CONCLUSIONS

High mass resolution and high mass accuracy facilitate the assignment of peaks in copolymer mass spectra. The determination of repeat unit and endgroup elemental compositions and various calibration corrections were explored to improve the analysis. Isobaric resolution was shown to further enhance the assignment of overlapping species. Molecular weight and component distributions were calculated from single shot spectra and the component distributions found to be consistent with the expected composition. The preparatory application of capillary GPC for providing low polydispersity fractions of a high polydispersity sample proved crucial to its mass spectral characterization; the technique is simple to implement and could find use in the preparation for analysis of other complex mixtures by MALDI.

Figure 5.8. A capillary GPC-MALDI-FTMS pseudo-chromatogram calculated from the 15 time resolved mass spectra shown in the inset. The average elution time and cumulative abundances are integral to the mass spectra; fitting this data to a cumulative normal distribution for each peak yields the standard deviation of the elution time, from which the gaussian curves were calculated.

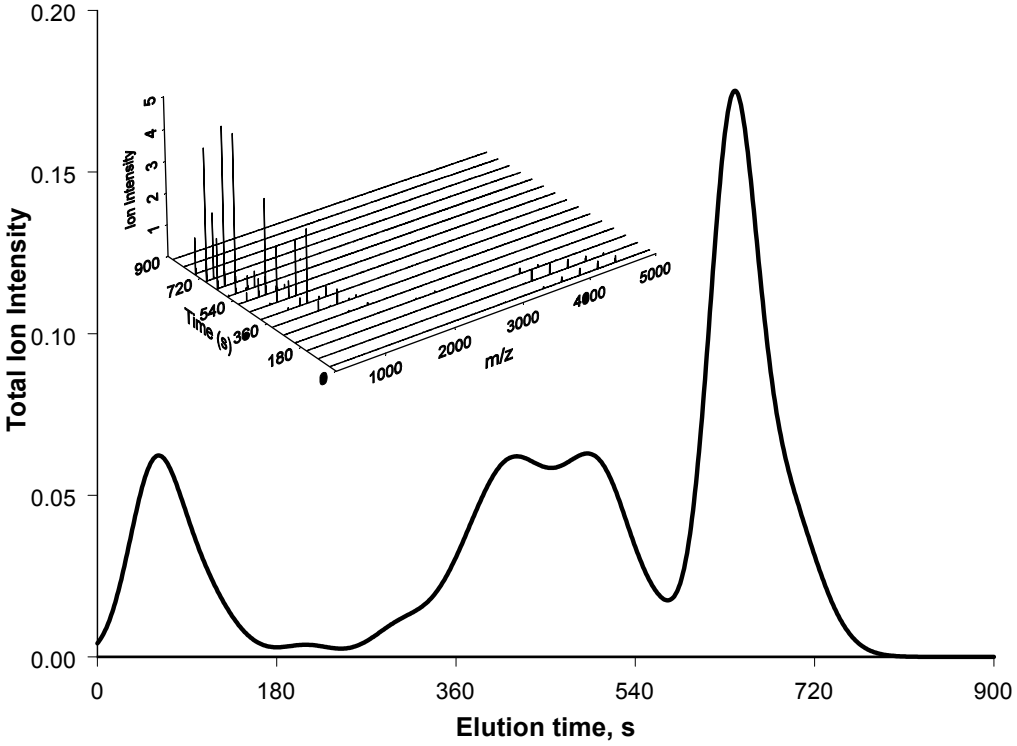
Total Ion Intensity
0.20
0.15
0.10
0.05
0.00
0
180
360
540
720
900
Elution time, s
Ion Intensity
1
2
3
4
5
Time (s)
900
720
540
360
180
0
m/z
1000
2000
3000
4000
5000

These features of MALDI-FTMS polymer analysis serve as a general first step toward full exploitation of the capabilities of trapped ion analysis. Future work will build on the MS/MS experiments for determining the sequence of terpolyesters, dendrimers, and, most challenging of all, random copolymers.[6, 57, 80, 81]

REFERENCES

(1) Yau, W.; Kirkland, J.; Bly, D. *Modern size-exclusion liquid chromatography*; John Wiley and Sons: New York, 1979.

(2) Aaserud, D. J.; Prokai, L.; Simonsick, W. J. *Analytical Chemistry* **1999,** *71*, 4793-4799.

(3) Karas, M.; Hillenkamp, F. *Anal. Chem.* **1988,** *60*, 2299.

(4) Montaudo, G.; Montaudo, M. S.; Puglisi, C.; Samperi, F.; Sepulchre, M. *Macromolecular Chemistry and Physics* **1996,** *197*, 2615-2625.

(5) Montaudo, G.; Montaudo, M. S.; Puglisi, C.; Samperi, F. *Journal of Polymer Science Part a-Polymer Chemistry* **1996,** *34*, 439-447.

(6) Montaudo, M. S. *Polymer* **2002,** *43*, 1587-1597.

(7) Sato, H.; Ohtani, H.; Tsuge, S.; Hayashi, N.; Katoh, K.; Masuda, E.; Ohnishi, K. *Rapid Communications in Mass Spectrometry* **2001,** *15*, 82-88.

(8) Jackson, A. T.; Jennings, K. R.; Scrivens, J. H. *Journal of the American Society for Mass Spectrometry* **1997,** *8*, 76-85.

(9) Dekoster, C. G.; Duursma, M. C.; Vanrooij, G. J.; Heeren, R. M. A.; Boon, J. J. *Rapid Communications In Mass Spectrometry* **1995,** *9*, 957-962.

(10) Vanrooij, G. J.; Duursma, M. C.; Heeren, R. M. A.; Boon, J. J.; Dekoster, C. G. *Journal Of The American Society For Mass Spectrometry* **1996,** *7*, 449-457.

(11) Easterling, M. L.; Mize, T. H.; Amster, I. J. *International Journal of Mass Spectrometry* **1997,** *169*, 387-400.

(12) Heeren, R. M. A.; Dekoster, C. G.; Boon, J. J. *Analytical Chemistry* **1995,** *67*, 3965-3970.

(13) Montaudo, G.; Montaudo, M. S.; Puglisi, C.; Samperi, F.; Sepulchre, M. *Macromolecular Chemistry And Physics* **1996,** *197*, 2615-2625.

(14) Shi, S. D. H.; Hendrickson, C. L.; Marshall, A. G.; Simonsick, W. J.; Aaserud, D. J. *Analytical Chemistry* **1998,** *70*, 3220-3226.

(15) Marshall, A. G.; Comisarow, M. B.; Parisod, G. *J. Chem. Phys.* **1979,** *71*, 4434.

(16) Marshall, A. G.; Wang, T. C. L.; Ricca, T. L. *Journal of the American Chemical Society* **1985,** *107*, 7893.

(17) Brenna, J. T.; Creasy, W. R.; Zimmerman, J. *Advances In Chemistry Series* **1993**, 129-154.

(18) Hogan, J. D.; Laude, D. A. *Analytical Chemistry* **1992,** *64*, 763-769.

(19) Dey, M.; Castoro, J. A.; Wilkins, C. L. *Analytical Chemistry* **1995,** *67*, 1575-1579.

(20) Dey, M.; Castoro, J. A.; Wilkins, C. L. *Analytical Chemistry* **1995,** *67*, 1575-1579.

(21) Montaudo, G.; Montaudo, M. S.; Puglisi, C.; Samperi, F. *Journal Of Polymer Science Part A-Polymer Chemistry* **1996,** *34*, 439-447.

(22) Montaudo, G.; Montaudo, M. S.; Puglisi, C.; Samperi, F. *Macromolecules* **1995,** *28*, 4562-4569.

(23) Montaudo, G.; Montaudo, M. S.; Puglisi, C.; Samperi, F. *Rapid Communications In Mass Spectrometry* **1995,** *9*, 453-460.

(24) Smith, R. D.; Cheng, X.; Bruce, J. E.; Hofstadler, S. A.; Anderson, G. A. *Nature* **1994,** *369*, 137-139.

(25) Omalley, R. M.; Randazzo, M. E.; Weinzierl, J. E.; Fernandez, J. E.; Nuwaysir, L. M.; Castoro, J. A.; Wilkins, C. L. *Macromolecules* **1994,** *27*, 5107-5113.

(26) Danis, P. O.; Huby, F. J. *Journal Of The American Society For Mass Spectrometry* **1995,** *6*, 1112-1118.

(27) Heeren, R. M. A.; Boon, J. J. *International Journal Of Mass Spectrometry And Ion Processes* **1996,** *158*, 391-403.

(28) Wu, J. Y.; Chen, C. X.; Kurth, M. J.; Lebrilla, C. B. *European Mass Spectrometry* **1995,** *1*, 363-370.

(29) Oconnor, P. B.; McLafferty, F. W. *Journal Of The American Chemical Society* **1995,** *117*, 12826- 12831.

(30) Spickermann, J.; Martin, K.; Rader, H. J.; Mullen, K.; Schlaad, H.; Muller, A. H. E.; Kruger, R. P. *European Mass Spectrometry* **1996,** *2*, 161-165.

(31) Mitchell, D. W.; Smith, R. D. *Journal Of Mass Spectrometry* **1996,** *31*, 771-790.

(32) Guan, S. H.; Marshall, A. G. *Journal Of The American Society For Mass Spectrometry* **1994,** *5*, 64-71.

(33) Jeffries, J. B.; Barlow, S. E.; Dunn, G. H. *International Journal of Mass Spectrometry and Ion Processes* **1983,** *54*, 169-187.

(34) Ledford, E. B.; Rempel, D. L.; Gross, M. L. *Analytical Chemistry* **1984,** *56*, 2744-2748.

(35) Peurrung, A. J.; Kouzes, R. T. *International Journal Of Mass Spectrometry And Ion Processes* **1995,** *145*, 139-153.

(36) Uechi, G. T.; Dunbar, R. C. *Journal Of The American Society For Mass Spectrometry* **1992,** *3*, 734-741.

(37) Easterling, M. L.; Pitsenberger, C. C.; Kulkarni, S. S.; Taylor, P. K.; Amster, I. J. *International Journal Of Mass Spectrometry And Ion Processes* **1996,** *158*, 97-113.

(38) Danis, P. O.; Karr, D. E. *Organic Mass Spectrometry* **1993,** *28*, 923-925.

(39) Wilczekvera, G.; Danis, P. O.; Eisenberg, A. *Macromolecules* **1996,** *29*, 4036-4044.

(40) Danis, P. O.; Saucy, A.; Huby, F. J. *Abstracts Of Papers Of The American Chemical Society* **1996,** *211*, 368-Poly.

(41) Danis, P. O.; Karr, D. E.; Simonsick, W. J.; Wu, D. T. *Macromolecules* **1995,** *28*, 1229-1232.

(42) Katayama, H.; Kitaguchi, H.; Kamigaito, M.; Sawamoto, M. *Journal of Polymer Science Part a-Polymer Chemistry* **2000,** *38*, 4023-4031.

(43) Thomson, B.; Suddaby, K.; Rudin, A.; Lajoie, G. *European Polymer Journal* **1996,** *32*, 239-256.

(44) vanderHage, E. R. E.; Duursma, M. C.; Heeren, R. M. A.; Boon, J. J.; Nielen, M. W. F.; Weber, A. J. M.; deKoster, C. G.; deVries, N. K. *Macromolecules* **1997,** *30*, 4302-4309.

(45) Nuwaysir, L. M.; Wilkins, C. L. *Analytical Chemistry* **1988,** *60*, 279.

(46) Brown, C. E.; Kovacic, P.; Wilkie, C. A.; Cody, R. B.; Kinsinger, J. A. *Journal of Polymer Science Part C-Polymer Letters* **1985,** *23*, 453-463.

(47) Brown, C. E.; Kovacic, P.; Cody, R. B.; Hein, R. E.; Kinsinger, J. A. *Journal of Polymer Science Part C-Polymer Letters* **1986,** *24*, 519-528.

(48) Brown, R. S.; Weil, D. A.; Wilkins, C. L. *Macromolecules* **1986,** *19*, 1255-1260.

(49) Brown, C. E.; Kovacic, P.; Wilkie, C. A.; Kinsinger, J. A.; Hein, R. E.; Yaniger, S. I.; Cody, R. B. *Journal of Polymer Science Part a-Polymer Chemistry* **1986,** *24*, 255-267.

(50) Miller, L. L.; Thomas, A. D.; Wilkins, C. L.; Weil, D. A. *Journal of the Chemical Society-Chemical Communications* **1986**, 661-663.

(51) Brown, C. E.; Kovacic, P.; Welch, K. J.; Cody, R. B.; Hein, R. E.; Kinsinger, J. A. *Polymer-Plastics Technology and Engineering* **1988,** *27*, 487-507.

(52) Johlman, C. L.; Wilkins, C. L.; Hogan, J. D.; Donovan, T. L.; Laude, D. A.; Youssefi, M. J. *Analytical Chemistry* **1990,** *62*, 1167-1172.

(53) Castoro, J. A.; Koster, C.; Wilkins, C. *Rapid Communications in Mass Spectrometry* **1992,** *6*, 239-241.

(54) Kahr, M. S.; Wilkins, C. L. *Journal of the American Society for Mass Spectrometry* **1993,** *4*, 453-460.

(55) Yan, W. Y.; Ammon, D. M.; Gardella, J. A.; Maziarz, E. P.; Hawkridge, A. M.; Grobe, G. L.; Wood, T. D. *European Mass Spectrometry* **1998,** *4*, 467-474.

(56) Maziarz, E. P.; Baker, G. A.; Wood, T. D. *Macromolecules* **1999,** *32*, 4411-4418.

(57) Koster, S.; de Koster, C. G.; van Benthem, R.; Duursma, M. C.; Boon, J. J.; Heeren, R. M. A. *International Journal of Mass Spectrometry* **2001,** *210*, 591-602.

(58) McEwen, C. N.; Simonsick, W. J.; Larsen, B. S.; Ute, K.; Hatada, K. *Journal of the American Society for Mass Spectrometry* **1995,** *6*, 906-911.

(59) Guittard, J.; Tessier, M.; Blais, J. C.; Bolbach, G.; Rozes, L.; Marechal, E.; Tabet, J. C. *Journal Of Mass Spectrometry* **1996,** *31*, 1409-1421.

(60) Hasse, H. U.; Becker, S.; Dietrich, G.; Klisch, N.; Kluge, H. J.; Lindinger, M.; Lutzenkirchen, K.; Schweikhard, L.; Ziegler, J. *International Journal of Mass Spectrometry and Ion Processes* **1994,** *132*, 181-191.

(61) Pan, Y.; Cotter, R. J. *Organic Mass Spectrometry* **1992,** *27*, 3-8.

(62) Beavis, R. C.; Chait, B. T. *Chemical Physics Letters* **1991,** *181*, 479.

(63) Hensel, R. R.; King, R. C.; Owens, K. G. *Rapid Communications in Mass Spectrometry* **1997,** *11*, 1785-1793.

(64) Hofstadler, S. A.; Laude, D. A. *International Journal of Mass Spectrometry and Ion Processes* **1990,** *101*, 65-78.

(65) Beu, S. C.; Laude, D. A. *International Journal of Mass Spectrometry and Ion Processes* **1990,** *97*, 295-310.

(66) Beu, S. C.; Laude, D. A. *Analytical Chemistry* **1992,** *64*, 177-180.

(67) Easterling, M. L.; Pitsenberger, C. C.; Amster, I. J. *Journal Of The American Society For Mass Spectrometry* **1997,** *8*, 195-198.

(68) Pitsenberger, C. C.; Easterling, M. L.; Amster, I. J. *Analytical Chemistry* **1996,** *68*, 4409-4413.

(69) Pitsenberger, C. C.; Easterling, M. L.; Amster, I. J. *Analytical Chemistry* **1996,** *68*, 3732-3739.

(70) Stults, J. T. *Current Opinion in Structural Biology* **1995,** *5*, 691-698.

(71) Anderson, J. S.; Laude, D. A. *International Journal Of Mass Spectrometry And Ion Processes* **1996,** *158*, 163-174.

(72) Guan, Z. Q.; Campbell, V. L.; Drader, J. J.; Hendrickson, C. L.; Laude, D. A. *Review Of Scientific Instruments* **1995,** *66*, 4507-4515.

(73) Larsen, B. S.; Simonsick, W. J.; McEwen, C. N. *Journal Of The American Society For Mass Spectrometry* **1996,** *7*, 287-292.

(74) Little, D. P.; Speir, J. P.; Senko, M. W.; Oconnor, P. B.; McLafferty, F. W. *Analytical Chemistry* **1994,** *66*, 2809-2815.

(75) Nielen, M. W. F. *Mass Spectrometry Reviews* **1999,** *18*, 309-344.

(76) Schriemer, D. C.; Li, L. A. *Analytical Chemistry* **1997,** *69*, 4176-4183.

(77) van Rooij, G. J.; Duursma, M. C.; de Koster, C. G.; Heeren, R. M. A.; Boon, J. J.; Schuyl, P. J. W.; van der Hage, E. R. E. *Analytical Chemistry* **1998,** *70*, 843-850.

(78) Shimada, K.; Lusenkova, M. A.; Sato, K.; Saito, T.; Matsuyama, S.; Nakahara, H.; Kinugasa, S. *Rapid Communications in Mass Spectrometry* **2001,** *15*, 277-282.

(79) Jackson, C.; Larsen, B.; McEwen, C. *Analytical Chemistry* **1996,** *68*, 1303-1308.

(80) Walker, K. L.; Kahr, M. S.; Wilkins, C. L.; Xu, Z. F.; Moore, J. S. *Journal Of The American Society For Mass Spectrometry* **1994,** *5*, 731-739.

(81) Leon, J. W.; Frechet, J. M. J. *Polymer Bulletin* **1995,** *35*, 449-455.

CHAPTER 6

BLOCK LENGTH ANALYSIS OF POLYSTYRENE-BLOCK-POLY(METHYLSTYRENE) BY INTERNAL MALDI-FTICR-MS [†]

[†]Mize, T. H., Wilczek-Vera, G., Terreau, O., Eisenberg, A., and Amster, I. J. Submitted to *Analytical Chemistry*.

ABSTRACT

Three poly(styrene-block-methylstyrene) copolymers were analyzed by ultrahigh resolution MALDI-FTICR mass spectrometry to determine their molecular weight distributions, block length distributions, and end group compositions. Prior reports of the mass spectrometry analysis of these type of compounds were not able to distinguish distributions of differing block compositions which produced overlapping oligomer species. Here is demonstrated resolution of isobaric species ($m/\Delta m$ = 175,000 at m/z = 2300), removing analytical ambiguity caused by overlapping block distributions. The reconstructed mass spectra allowed unequivocal identification of the relative abundances of the oligomeric species in the distribution, and the assignment of block length distributions for $(C_8H_8)_n$ - $(C_9H_{10})_m$.

INTRODUCTION

Block copolymers are valued for their mechanical,[1-3] rheological,[4] phase stability,[5] and electrical conductivity properties.[5, 6] While most blends of homopolymers are not compatible and show phase separation, block copolymers can only phase separate on a microscopic scale due to the connectivity of blocks. Depending on block composition a large variety of micro-phase separated structures may be obtained. The microphase separation transition and ordering properties of block copolymers make them ideal masking material for microlithography, for example.[5] An important detail of this sort of copolymer is the density profile which is highly dependent on molecular weight and individual block lengths. Control of the block lengths can also dramatically effect the mechanical properties. The conformation of a polymer in the solid phase is directly related to the solution phase microscopic structure which in turn is dependent on the block length ratio.[3] Other examples of block-length related properties can be found in fields as diverse as manufacture of elastomers for golf ball cores and in polyelectrolytes used in Langmuir thin film analysis, which tend to form different micellar structures depending on the relative ionic block length.[7]

A complete understanding of the synthetic pathways requires the elucidation of the termination chemistry. The lability of the endgroups under the conditions of preparation, storage, and analysis may cause the end product to differ from the material resulting from the polymerization chemistry. Howell and Rajaram showed that polymer dehydrohalogenation can be catalyzed by cupric chloride along the backbone of polyvinylidine chloride.[8] However, they also showed that dehydrohalogenation can occur in the presence of moderately acidic species similar to MALDI matrices.[9] Post source

decay due to a strong laser pulse [10] or the MALDI ionization event[11] can also be responsible for this phenomenon at the endgroup. NMR end group analysis for the presence of chlorine prior to MALDI-MS can help determine if differences between predicted and measured masses are due to decomposition during ionization or some other event.[12]

Previously, block length distributions have been determined by GPC analysis of intermediate polymerizations; immediately prior to addition of a subsequent monomer, an aliquot of the previous block polymerization product would be characterized for molecular weight distribution and the current block distribution calculated by difference from the one immediately preceding. GPC coupled with MALDI-TOF analysis and, later, statistical modeling of stand alone MALDI-TOF data allowed direct determination of the individual block lengths of A-B-A and A-B type block copolymers of styrene and methyl styrene.[13-15] These estimates were based on the statistical probabilities of the abundances of different ion species making up any given isobaric peak. Van Rooij and coworkers have shown that analysis by an external source MALDI-FTICR-MS greatly improves the characterization of of these isobaric species but, due to time-of-flight effects in ion transfer from source to analyzer cell, the polymer is sampled in several mass-to-charge windows and the distribution reconstructed afterwards.[16] Here we examine the molecular weight distributions and individual block-length distributions of three A-B diblock copolymers of styrene and methylstyrene by Fourier transform ion cyclotron resonance mass spectrometry with an internal MALDI source.[17] This instrument allows the full distribution to be sampled in each mass spectrum. These mass spectra allow calculation of average molecular weights for the distribution and

assignment of most of the individual oligomeric species. Subsequent ultrahigh resolution spectra provide unambiguous assignment of isotopic abundances of overlapping species, from which block length distributions can be extracted.

EXPERIMENTAL

Materials: Para-methylstyrene and styrene were dried over calcium hydride, distilled under reduced pressure, and stored at -15E C. Cuprous chloride (98%), 2,2'-bipyridine (bipy) (99+%), and 2-chloropropionitrile (97%): used as received from Aldrich Chemical Company (P. O. Box 355, Milwaukee, WI 53201). The matrix material, 2, 5-dihydroxybenzoic acid (DHB), came from Lancaster Synthesis (1 Industrial Drive, Pelham, NH 03076), the cation sources, silver trifluoroacetate (AgTFA) and cupric chloride, were obtained from Aldrich, and acetone (ACS grade) from J. T. Baker (Phillipsburg, NJ 08865); all were used without further purification.

The polymers were synthesized by atom transfer radical polymerization (ATRP) from bulk materials. The initiator was 2-chloropropionitrile, the catalyst was CuCl and the ligand was 2,2'-bipyridine (bipy). The ligand is required to solubilize the copper catalyst in the styrene. There is no formal termination step in this synthesis and it was predicted that the polymer should be capped by a chlorine atom. CuCl and bipy were charged into a round bottom flask that had been flame dried. A three-way stopcock equipped with a septum was used to seal the flask. The stopcock was connected to a Schlenk line. The 2-chloropropionitrile was then added by syringe, followed by the styrene monomer. The mixture was then degassed by two freeze-pump-thaw cycles (freeze with liquid nitrogen, open Schlenk line to vacuum, to remove air, purge with

nitrogen through the Schlenk line, remove liquid nitrogen, let the sample thaw). Once the sample was thawed, it was placed in an oil bath at 130E C. The homopolymer sample was heated for 45 minutes minutes respectively. The first block of the copolymer samples were synthesized similarly for three hours at which time para-methylstyrene was added. The three block copolymers were then heated an additional 30, 60, and 120 minutes respectively. At the end of the heating cycles, the samples were removed from the oil bath and allowed to cool to room temperature. Each sample was then dissolved in THF and precipitated into methanol three times to remove catalyst and ligand. The final polymer was then dried under vacuum. The polymer molecular weights were measured by gel permeation chromatography at McGill University; these will be referred to as Poly 1, Poly 2, and Poly 3 in order of increasing reaction time for the second block.

A 4.7 Tesla MALDI FTICR-MS constructed in-house has been used for all experiments described herein.[17] The analyzer cell is of open-ended cylindrical design with the detection region of the cell 8.5 cm (3-3/8") long and 5.6 cm (2-1/4") diameter.[18] Samples were applied to a 2.5 cm (1") diameter titanium puck that is positioned in the vacuum chamber by a magnetically coupled manipulator. The sample target is located perpendicular to the principle axis and within 1 cm of the ICR cell, thus reducing time-of-flight mass discrimination effects. Working pressure for the mass spectrometer is 10^{-9} to 10^{-10} torr. The spectrometer is controlled by a commercial data station (Ionspec Corporation, Irvine, California).

Samples were prepared by electrospray deposition.[19, 20] Matrix (2, 5-dihydroxybenzoic acid, or DHB), analyte, and cation solutions were mixed at a molar ratio of 400:1:1 in an electrospray needle and deposited on the MALDI puck at 4.5 kV.

Silver trifluoroacetate was used as the cation source in the earliest experiments. However, initial attempts to use AgTFA as the cation source for the analysis were hampered by interference from silver clusters, precipitation of AgCl, and competitive cationization by copper. Since cupric chloride was already present and since typical methods of cleanup such as GPC, ultrafiltration, and ion exchange might skew the distribution or introduce other chemistry, cupric chloride was used as the cation source. A 0.1 M cupric chloride suspension in acetone was prepared as an alternate. The samples were subsequently desorbed by a pulse from a frequency tripled Nd:YAG laser (θ = 355 nm).

The ions thus formed are captured in the analyzer cell by using gated trapping.[18] The rear trapping electrodes of the cell are held at an initial trapping potential of 8 volts while the trapping electrodes near the probe are held at ground potential. Nitrogen is pulsed into the vacuum system to a peak pressure of 10^{-6} torr to more efficiently trap a wider mass distribution, and to reduce the kinetic energy of the trapped ions by collisional thermalization.[21, 22] The front plate is then raised to the same potential as the rear plate 400-600 μsec after the laser ionization pulse. A delay of 8 seconds prior to ion detection allows the analyzer pressure to return to ~10^{-9} torr following the pulsed introduction of gas.

Broadband excitation over the range m/z 300-5000 was used to measure the entire polymer distribution. Representative mass resolving power (inversely proportional to the mass-to-charge ratio) for the broadband measurements was 8100 at m/z 2155.2902. High resolution was achieved on narrow bands (~200-250 m/z units wide) via rF burst quadrupolar excitation. A two-plate quadrupolar field of 10-20 V at the unperturbed

cyclotron frequency of a target ion is applied in the presence of a neutral collision gas introduced in a pulse at 10^{-4} torr; this results in axialization of the 250 m/z units wide band of ions and ejection (via magnetron expansion) of the other ions.[23] In this way, the ions of a given mass-to-charge were found to maintain coherence for a longer detection period (ca. 9 s), increasing typical resolving power at m/z 2000 to 160,000.

RESULTS AND DISCUSSION

The internal source MALDI FTICR-MS is ideal for capturing and measuring wide distributions of ions.[20] Figures 6.1 and 6.2 are single shot MALDI-FTICR mass spectra that show distributions of a polystyrene homopolymer and a polystyrene-block-polymethylstyrene copolymer with peaks from approximately m/z 300-4000, each. From these, M_n, M_w, and polydispersity were calculated as shown in Table 6.1. For the homopolymer, the agreement between GPC and MALDI-FTICR data is very good. The M_n value obtained by mass spectrometry is low by 1%, and the M_w is low by 2.5% compared to GPC. The polydispersity is low by 1%. For the block copolymer, the mass spectrometry values for M_n and M_w are both low by 9%, but the polydispersity is the same for both the mass spectrometry and GPC data. It should be noted that the larger errors were obtained for the polymer with polydispersity index of 1.22; MALDI mass spectrometry is known to have difficulty analyzing polymers with polydispersity indices higher than 1.10.[16, 24-30]

Close examination of the mass spectrum in Figure 6.2 shows that, due to the isotopic distributions of the various oligomers, there is at least one peak at each nominal

Figure 6.1. MALDI-FTICR mass spectrum of polystyrene homopolymer. Inset shows two series of peaks differing in mass by 14 amu, corresponding to unsaturated PS_n (m/z 1409) and unsaturated $_{Psn-1}$-b-MS_1 (m/z 1423).

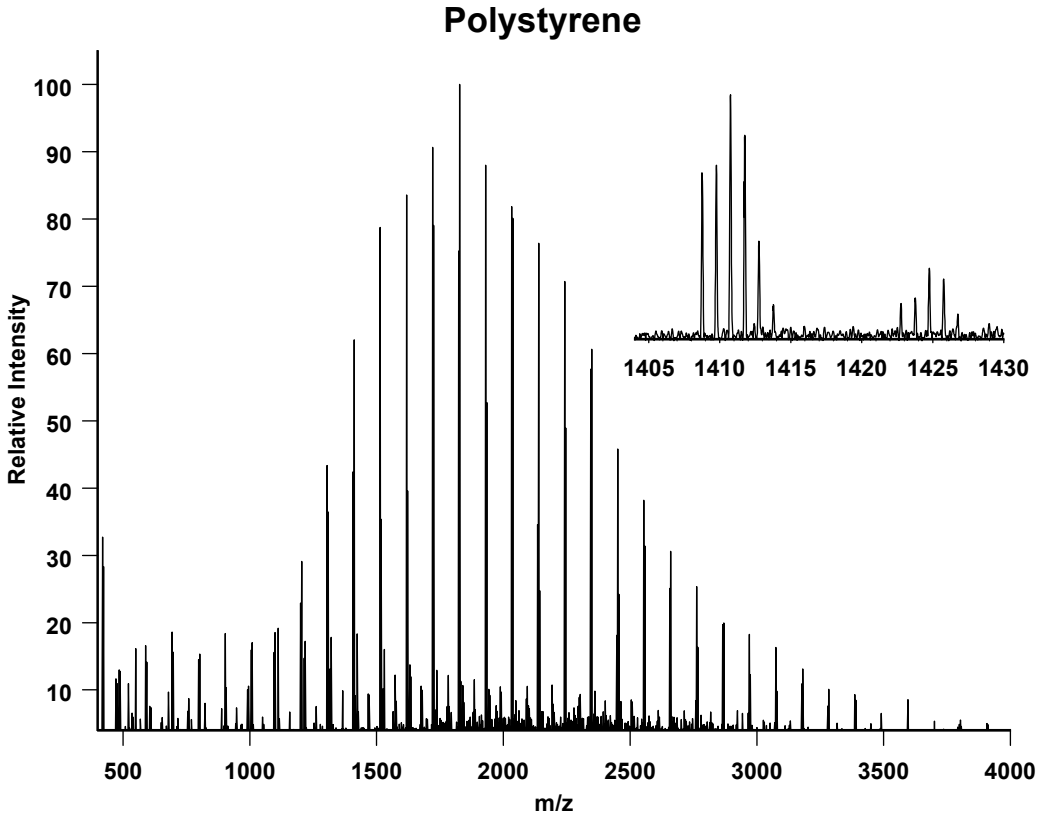
Polystyrene
Relative Intensity
100
90
80
70
60
50
40
30
20
10
500
1000
1500
2000
2500
3000
3500
4000
m/z
1405
1410
1415
1420
1425
1430

Figure 6.2. MALDI-FTICR mass spectrum of Poly 3 acquired with a single laser shot Low population density was maintained to achieve isotopic resolution at the expense of signal-to-noise and representative isotope statistics (inset).

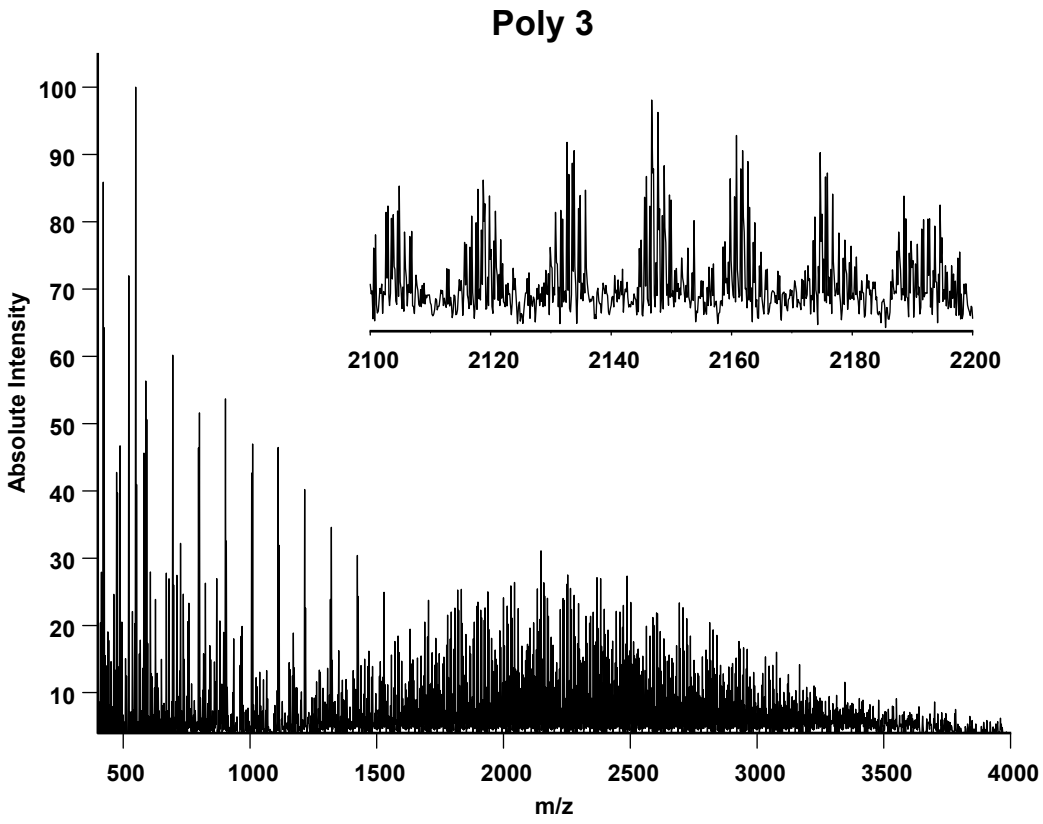
Poly 3
Absolute Intensity
100
90
80
70
60
50
40
30
20
10
500
1000
1500
2000
2500
3000
3500
4000
m/z
2100
2120
2140
2160
2180
2200

Table 6.1. Comparison of molecular weight averages and polydispersity obtained for entire distributions by FTICR-MS versus GPC.

$PS_{9.2}$	M_n	M_w	M_w/M_n
GPC	**1860**	**2090**	**1.12**
FTICR-MS	**1840**	**2040**	**1.11**
$PS_{9.1}$-*b*-$PmS_{6.9}$	M_n	M_w	M_w/M_n
GPC	**1920**	**2340**	**1.22**
FTICR-MS	**1750**	**2140**	**1.22**

mass-to-charge under normal conditions. In fact, peaks are often composed of two or more components of differing exact mass but different nominal mass. Such mass spectra have been analyzed previously by use of statistical modeling of the distributions.[14, 15] An alternative approach available with FTICR is manipulation of the trapped ions to produce a longer transient and, thereby, resolution of the isobaric species.[31, 32] To achieve this high resolution, a number of experimental procedures were employed. Quadrupolar excitation (QE) axializes the ions in the cell allowing the ion cloud to remain coherent longer during measurement.[23] The amplitude of rF excitation prior to measurement was optimized to maximize ion coherence at a given radius. Minimization of the trapping potential (from 0.5 V in the broad distribution to 0.2 V in the axialized spectra) reduced the magnetron drift of the ions, and reduced space charge by allowing ions to occupy a larger volume of the cell without significant ion-ion interaction. Most important to achieving isobaric resolution (that is, resolution of two or more peaks of nominally the same mass) is abatement of the problem of phase locking which occurs when two ions of very similar cyclotron frequency are forced together by a relatively large ion population in the cell.[31] Figure 6.3 demonstrates resolution of isobaric species in the mass spectrum of poly(styrene-b-methylstyrene). The spectrum of Figure 6.3a exhibits peak coalescence for some of the more closely spaced isobars at m/z 3072-3074, resulting in ambiguous assignment of peaks and incorrect assignment of peak intensities; the spectrum in Figure 6.3b, obtained by reducing the ion population, achieves baseline resolution of species as close as 0.050 Da from each other at a resolving power of 123,000.

Attempts to achieve isobaric resolution for the entire polymer distribution over a mass-to-charge range of 3000 proved unsuccessful. Recording a measurable population

Figure 6.3. A comparison of block copolymer mass spectra at high (m/) m =26,000) and ultrahigh (m/) m = 120,000) resolving power. (A) The upper spectrum shows isobaric separation of relatively distant peaks (0.126 Da peak separation through the middle of the mass range) at 0.75 V_{trap} . (B) More closely spaced peaks (0.050 Da differences nominally at 3071.8 m/z) are resolved by using a lower abundance of ions and V_{trap} = 0.25. The signal-to-noise improvement in the lower mass spectrum results from longer signal duration.

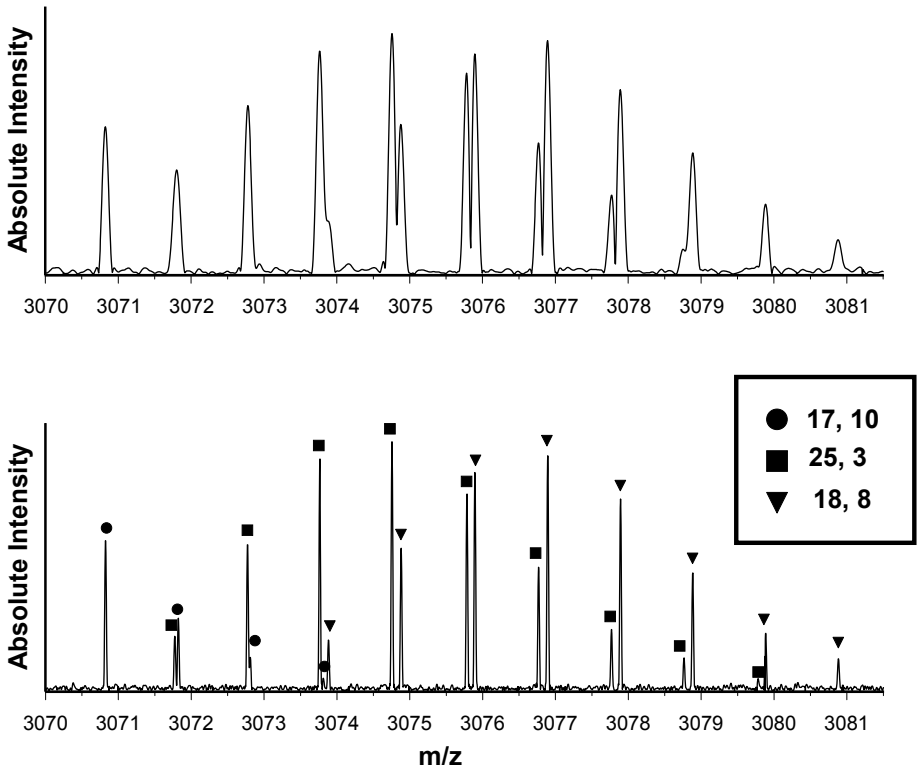
Absolute Intensity
3070
3071
3072
3073
3074
3075
3076
3077
3078
3079
3080
3081
Absolute Intensity
17, 10
25, 3
18, 8
m/z

of each of the 2000+ ion components of the mixture within a single mass spectrum results in relatively high ion space charge, leading to peak coalescence. Instead, we analyzed the distribution by isolating groups of ions in m/z 250-wide windows by using 20 - 25 V single frequency burst QE.[33] The resulting fractions produced transients that persisted up to 10 seconds. Each group of ions thus measured was normalized for intensity using overlapping species,[34] and the total ion intensities for the isotopes of each oligomer was calculated. Figure 6.4 shows the mass spectrum reconstructed from the narrow windows for the polymer Poly 3. Figures 6.5a and 6.5b show areas of detail demonstrating isobaric resolution and the assignment of the contribution of each oligomer to the overall signal.

Tables of measured mass-to-charge ratio and signal intensity are derived from the mass spectra within the data acquisition software, with each table typically containing 150-250 assignable entries (and as many as 2165 unique isotope peaks for the reconstructed spectra). Data reduction was achieved by first normalizing the signal intensities of the spectra by matching peaks from adjacent 250 mass-to-charge units wide windows and scaling the intensities of all peaks by the factor necessary for these overlaps to agree. A computer program was written to calculate molecular weights and isotope distributions for all possible poly("-methylstyrene-co-styrene) species and these were used to assign the composition of each peak in the mass spectra. The intensities for all peaks found within a given isotopic envelope were summed to produce a single intensity value for each oligomer. From these data, the number- and weight-average block lengths, N_n and N_w, can be obtained. Table 6.2 compares GPC and MALDI-FTICR-MS derived number- and weight-average block lengths for the three block

Figure 6.4. Full mass spectrum of a block copolymer of styrene and paramethylstyrene reconstructed from isobarically resolved data each covering a mass window of about m/z 250 and overlapping by a few oligomers, each. The overlap allows normalization of the spectral ion intensities prior to combining the data.

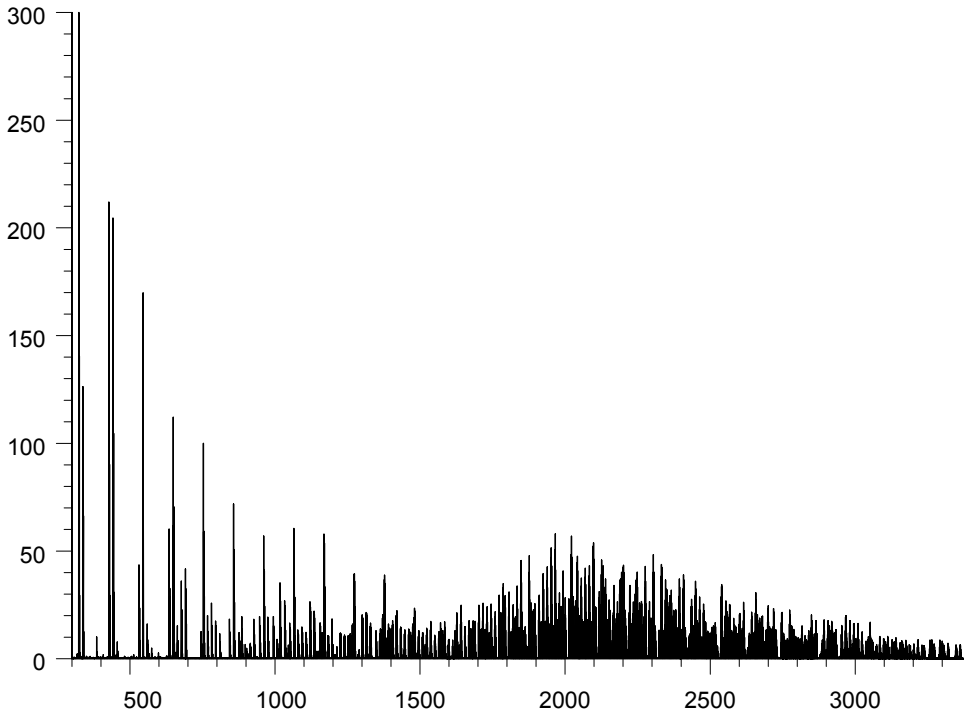
300
250
200
150
100
50
0
500
1000
1500
2000
2500
3000

Figure 6.5. (A) Expansion of ultrahigh resolution mass spectrum of Figure 6.4 showing as many as three oligomeric species in 0.101 Da mass range (¯ = isotopic species of styrene 18 + methylstyrene 8, · = styrene 1 + methylstyrene 23, ± = styrene 9 + methylstyrene 16). (B) Expansion of ultrahigh resolution mass spectrum of Figure 6.4 showing as many as three oligomeric species in 0.134 Da mass range (¯ = isotopic species of styrene 21 + methylstyrene 6, · = styrene 4 + methylstyrene 21, ± = styrene 12 + methylstyrene 14).

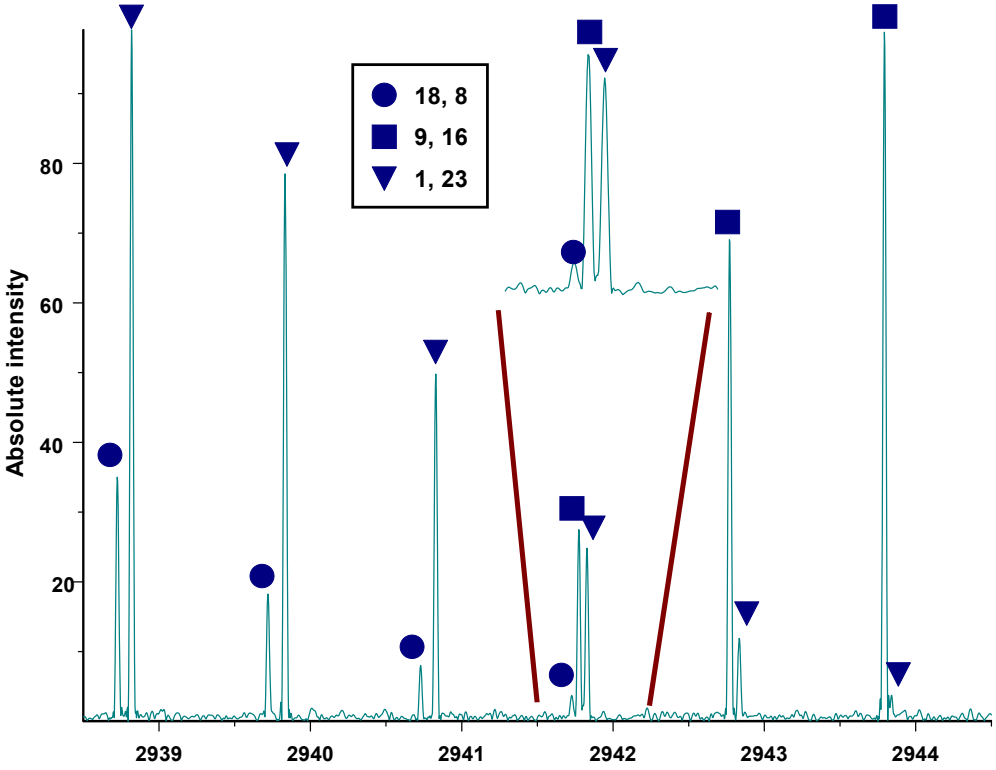
18, 8
9, 16
1, 23
Absolute intensity
80
60
40
20
2939
2940
2941
2942
2943
2944

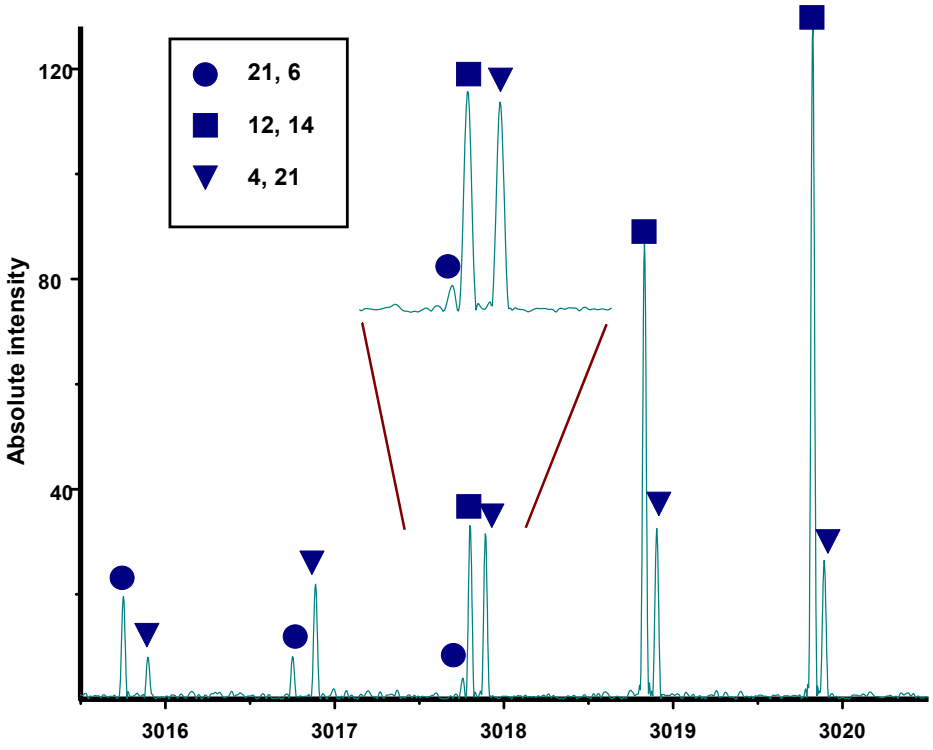
21, 6
12, 14
4, 21
Absolute intensity
120
80
40
3016
3017
3018
3019
3020

copolymers. The MALDI-FTICR-MS data is further broken down to demonstrate the utility of isobarically resolved mass spectra (RP = 157,000 at m/z 2155) versus isotopically resolved mass spectra (RP = 17,000), versus use of only the monoisotopic peaks to assign the oligomeric intensity, as proposed by van Rooij et al.[16] The isobarically resolved data is found to provide the best agreement with the GPC data for obtaining the average block lengths.

The assignment of the various peaks to the correct oligomeric species was achieved by best fit to the calculated mass. While the abundance of heavy isotopes becomes more significant at higher mass due to the statistical distribution of the isotope species as the number of atoms increases, it is interesting to note that the inability to assign peaks within the mass spectra in which isobaric peaks are not resolved produces a mass error that is as significant as ignoring the secondary isotopes when calculating the block distributions from the monoisotopic peaks. Three factors should be noted in examining this phenomenon; first, the isotopically resolved mass spectra have broader peaks than the isobarically resolved peaks so that the precision of the measurement is reduced in the former case; second, peak coalescence exacerbates this problem by presenting peaks that are the convolution of two different mass-to-charge values and signal intensities; and, third, the monoisotopic calculations are from the fully resolved spectra which eliminates one of the previous two problems.

Endgroup analysis of the polystyrene and block copolymers demonstrated unexpected termination chemistry. The data indicates that each chain is terminated in a site of unsaturation, and not by the expected chlorine substituted end group. Further, there is little evidence of any saturated termini. There was concern that the absence of

Table 6.2: Number- and weight-average block lengths determined by GPC and MALDI-FTICR-MS, further separated by level of resolution (isobaric and isotopic) and use of the monoisotopic peak for assignment of oligomer abundance by calculation of the expected isotopic distribution. Note: [1] Value not obtained by GPC.

		n_n^{sty}	n_n^{msty}	n_w^{sty}	n_w^{msty}
Poly 1	**GPC**	**9.1**	**3.2**	**–[1]**	**–[1]**
	Isobaric	**9.2**	**3.2**	**12.5**	**6.2**
	Isotopic	**9.2**	**3.0**	**12.1**	**6.0**
	Monoisotopic	**8.9**	**3.2**	**12.0**	**5.5**
Poly 2	**GPC**	**9.1**	**4.3**	**–[1]**	**–[1]**
	Isobaric	**8.9**	**4.1**	**11.9**	**7.5**
	Isotopic	**9.5**	**3.4**	**12.5**	**6.2**
	Monoisotopic	**7.2**	**2.7**	**10.6**	**5.9**
Poly 3	**GPC**	**9.1**	**6.9**	**–[1]**	**–[1]**
	Isobaric	**9.2**	**6.9**	**12.5**	**11.2**
	Isotopic	**10.1**	**6.8**	**13.2**	**10.2**
	Monoisotopic	**9.7**	**6.7**	**12.7**	**10.9**

chlorine was an artifact of the sample preparation protocol or of the MALDI ionization, which can cause dehydrohalogenation of the chlorine terminus.[9-11] Proton NMR spectra of these samples, however, exhibit peaks consistent with unsaturated end groups, and show no evidence of chlorine termination. The data suggest that the unsaturated termini are a result of dehydrohalogenation during the polymerization reaction due to copper catalysis, and are not an artifact of MALDI analysis.[8, 35]

CONCLUSIONS

The use of an internal source MALDI FTICR-MS is demonstrated to be especially useful in the analysis of the di-block copolymer poly(styrene-block-polymethylstyrene). Wide mass distributions can be captured and measured simultaneously to determine overall molecular weight distributions with reasonable agreement with GPC data. Subsequently, ultrahigh resolution spectra may be obtained to unequivocally assign the relative composition of the various species that are present in these complex mixtures. This data can then be used to determine the block length distributions of the polymer in good agreement with standard chromatographic methods. These methods should be extended to other types of copolymers to include graft and random copolymers and, with the inclusion of MS^n sequencing studies, to tri- and higher order block copolymers.

ACKNOWLEDGEMENTS

The authors gratefully acknowledge the financial support of the National Science Foundation (NSF #CHE-9974579) and E. I DuPont and Nemours. Advice on

interpretation of NMR data from Dr. Quincy Teng of the University of Georgia Chemistry Department is also gratefully acknowledged.

REFERENCES

(1) Flosenzier, L. S.; Rohlfing, J. H.; Schwark, A. M.; Torkelson, J. M. *Polym. Eng. Sci.* **1990,** *30*, 1180-1181.

(2) Flosenzier, L. S.; Torkelson, J. M. *Macromolecules* **1992,** *25*, 735-742.

(3) Deline, V. R.; Brown, H. R.; Char, K. *J. Vac. Sci. Technol. A-Vac. Surf. Films* **1991,** *9*, 1283-1286.

(4) Stokke, B. T.; Draget, K. I.; Smidsrod, O.; Yuguchi, Y.; Urakawa, H.; Kajiwara, K. *Macromolecules* **2000,** *33*, 1853-1863.

(5) Barclay, G. G.; King, M.; Orellana, A.; Malenfant, P. R. L.; Sinta, R.; Malmstrom, E.; Ito, H.; Hawker, C. J. *Org. Thin Films* **1998,** *695*, 360-370.

(6) Baixia, L.; Yimin, C.; Booth, C.; Yunzhu, L. *Polym. Comm.* **1991,** *32*, 348-352.

(7) Zhu, J.; Eisenberg, A.; Lennox, R. B. *Macromolecules* **1992,** *25*, 6547-6555.

(8) Howell, B. A.; Debney, M. F.; Rajaram, C. V. *Thermochim. Acta* **1992,** *212*, 115-122.

(9) Howell, B. A.; Rajaram, C. V. *J. Therm. Anal.* **1993,** *40*, 575-585.

(10) Fountain, S. T.; Lee, H.; Lubman, D. M. *Rapid Commun. Mass Spectrom.* **1994,** *8*, 407-416.

(11) Przybilla, L.; Francke, V.; Rader, H. J.; Mullen, K. *Macromolecules* **2001,** *34*, 4401-4405.

(12) Ronda, J. C.; Serra, A.; Mantecon, A.; Cadiz, V. *Macromol. Chem. Phys.* **1995,** *196*, 599-609.

(13) Wilczek-Vera, G.; Yu, Y. S.; Waddell, K.; Danis, P. O.; Eisenberg, A. *Rapid Commun. Mass Spectrom.* **1999,** *13*, 764-777.

(14) Wilczek-Vera, G.; Yu, Y. S.; Waddell, K.; Danis, P. O.; Eisenberg, A. *Macromolecules* **1999,** *32*, 2180-2187.

(15) Wilczek-Vera, G.; Danis, P. O.; Eisenberg, A. *Macromolecules* **1996,** *29*, 4036-4044.

(16) van Rooij, G. J.; Duursma, M. C.; de Koster, C. G.; Heeren, R. M. A.; Boon, J. J.; Schuyl, P. J. W.; van der Hage, E. R. E. *Anal. Chem.* **1998,** *70*, 843-850.

(17) Easterling, M. L.; Pitsenberger, C. C.; Kulkarni, S. S.; Taylor, P. K.; Amster, I. J. *Int. J. Mass Spectrom. and Ion Proc.* **1996,** *158*, 97-113.

(18) Beu, S. C.; Laude, D. A. *Int. J. Mass Spectrom. and Ion Proc.* **1992,** *112*, 215-230.

(19) Hensel, R. R.; King, R. C.; Owens, K. G. *Rapid Commun. Mass Spectrom.* **1997,** *11*, 1785-1793.

(20) Easterling, M. L.; Mize, T. H.; Amster, I. J. *Int. J. Mass Spectrom.* **1997,** *169*, 387-400.

(21) Guan, Z. Q.; Campbell, V. L.; Drader, J. J.; Hendrickson, C. L.; Laude, D. A. *Rev. Sci. Instrum.* **1995,** *66*, 4507-4515.

(22) Li, Y. Z.; Little, D. P.; Koster, H.; Hunter, R. L.; McIver, R. T. *Anal. Chem.* **1996,** *68*, 2090-2096.

(23) Hendrickson, C. L.; Drader, J. J.; Laude, D. A. *J. Am. Soc. Mass Spectrom.* **1995,** *6*, 448-452.

(24) Montaudo, G.; Montaudo, M. S.; Puglisi, C.; Samperi, F. *Rapid Commun. Mass Spectrom.* **1995,** *9*, 453-460.

(25) Whittal, R. M.; Schriemer, D. C.; Li, L. *Anal. Chem.* **1997,** *69*, 2734-2741.

(26) Kassis, C. E.; DeSimone, J. M.; Linton, R. W.; Remsen, E. E.; Lange, G. W.; Friedman, R. M. *Rapid Commun. Mass Spectrom.* **1997,** *11*, 1134-1138.

(27) Dey, M.; Castoro, J. A.; Wilkins, C. L. *Anal. Chem.* **1995,** *67*, 1575-1579.

(28) Larsen, B. S.; Simonsick, W. J.; McEwen, C. N. *J. Am. Soc. Mass Spectrom.* **1996,** *7*, 287-292.

(29) Schriemer, D. C.; Li, L. A. *Anal. Chem.* **1997,** *69*, 4176-4183.

(30) Nielen, M. W. F. *Mass Spectrom. Rev.* **1999,** *18*, 309-344.

(31) Stults, J. T. *Anal. Chem.* **1997,** *69*, 1815-1819.

(32) Shi, S. D. H.; Hendrickson, C. L.; Marshall, A. G.; Simonsick, W. J.; Aaserud, D. J. *Anal. Chem.* **1998,** *70*, 3220-3226.

(33) Pitsenberger, C. C.; Easterling, M. L.; Amster, I. J. *Anal. Chem.* **1996,** *68*, 3732-3739.

(34) Oconnor, P. B.; Duursma, M. C.; vanRooij, G. J.; Heeren, R. M. A.; Boon, J. J. *Anal. Chem.* **1997,** *69*, 2751-2755.

(35) Mork, P. C.; Heldal, J. A. *J. Catal.* **1982,** *75*, 49-55.

CHAPTER 7

COMPARISON OF RELATIVE TEMPERATURES OF INDIVIDUAL NYLON-6 OLIGOMER IONS: INTERNAL MALDI-FTICR-MS VS. EXTERNAL ESI-FTICR-MS [†]

[†] Mize, T. H., de Koster, C. G., Koster, S., Heeren, R. M. A., Jonathan Amster, I. J. To be submitted to *International Journal of Mass Spectrometry and Ion Processes*.

ABSTRACT

Individual protonated linear Nylon-6 oligomers with 4 to 8 repeat units were subjected to collision induced dissociation (CID) in two Fourier transform ion cyclotron resonance (FTICR) mass spectrometers to determine the relative internal energy delivered by the ionization sources, one an internal matrix assisted laser desorption/ionization (MALDI) source and the other an atmospheric pressure electrospray ionization (ESI) source. Precursor ions were mass selected for CID by means of correlated harmonic excitation fields (CHEF) in each source; additionally, the experiments were repeated in the MALDI instrument with precursor isolation occurring by quadrupolar excitation axialization (QEA) to provide a comparison using thermal ions. The kinetic energies (laboratory frame) required to fragment 50% of the precursor ions ranged from 49-132 eV for the MALDI-CHEF experiments versus 131-316 eV for the ESI-CHEF experiments, suggesting that the MALDI source deposits significantly more energy to the analyte ions than does ESI. MALDI formed ions that were thermalized by QEA prior to activation required 151-355 eV of kinetic energy to achieve 50% dissociation of the precursor The energy required for fragmentation was found to increase linearly with degree of polymerization. The contribution of the method for ion isolation to the total energy of the precursor ion was examined. These experiments suggest that ion isolation by CHEF adds to the internal energy of the ions, shifting the breakdown curves by approximately 63 eV in the laboratory frame of reference (3.4 eV in center-of-mass frame).

INTRODUCTION

It is generally accepted that matrix assisted laser desorption/ionization (MALDI) deposits a higher level of internal energy into analyte ions than does electrospray ionization (ESI).[1-7] This difference can be exploited to yield fragment ions from post-source decay (PSD) in MALDI time-of-flight mass spectrometry (TOF-MS).[2, 3, 5, 8] In contrast, further addition of energy from nozzle-skimmer or cone voltage acceleration is required to cause in-source fragmentation with ESI mass spectrometry.[4, 7, 9] Although the ions delivered to the mass analyzer from each of these two ionization sources have different internal energies, quantification of this difference in the literature has been limited to a study of gangliosides.[7]

Measurement of the internal energy of neutral molecules desorbed by MALDI has been attempted by first desorbing the molecule followed by wavelength dependent photodissociation.[10] This study showed that MALDI desorbed molecules had internal energies proportional to their initial kinetic energies by varying the delay between desorption and application of the vacuum UV dissociation pulse; this conclusion is in opposition to the measurements that show many "hot" matrices, such as á-cyano-hydroxy cinnamic acid, produce ions with lower initial translational energies than "cool" matrices, such as 2,5-dihydroxybenzoic acid.[11, 12] Other researchers have examined the effects of ESI source temperature, skimmer voltage, and transfer region background pressure on the final internal energy of ESI ions.[9, 13] These studies focused primarily on the various regions of ion generation and transfer as sources of ion activation and dissociation, rather than examining the level of internal energy deposited in the surviving intact ions.

By measuring collisionally-induced dissociation (CID) mass spectra at various levels of added energy, a relative measure of the preactivation internal energy, the excess internal energy from desorption/ionization of the ions can be obtained. The preactivation energy is found to vary greatly with ionization technique or other treatment of the ions.[7, 14-17] For instance, Harrison et al. showed that varying the cone voltages during ESI produces energy-resolved mass spectra in single quadrupole mass spectrometers that are similar to those obtained by varying the collision energy in a quadrupole collision cell.[17] Ion breakdown curves have been used to characterize energy deposition in ions desorbed from different MALDI matrices.[8] Internal energy deposition into polymer and polymer additive samples have been successfully examined with respect to electron ionization, chemical ionization, liquid secondary ion mass spectrometry and field desorption ion sources.[18] Nylon-6 oligomer dissociation has been studied previously to determine fragmentation differences using electrospray ionization (ESI) and matrix assisted laser desorption/ionization (MALDI) in time of flight (TOF) mass analyzers.[19] In that study, similarities in ion activation energies were noted anecdotally for the two sources; more important to the present work, cationized species were not observed to fragment at all perhaps due to the stability of the gas phase conformation of the oligomer when coordinated with a cation.[19]

FTICR-MS has been used by the Lebrilla group to compare the qualitative differences between MALDI and ESI ion sources on a single mass analyzer.[7] They attributed the differences not only to the internal energy acquired at ionization but also during the transfer of ions to the analyzer since the higher kinetic energy of ions from a MALDI source requires different trapping conditions than ESI.[7] Other parameters that

can effect the ion internal energy between the source and the FTICR analyzer include laser power and choice of cation in MALDI,[2, 7, 20, 21] skimmer voltage in ESI,[4, 7, 9, 13] and use of a collision gas to reduce an ion's translational kinetic energy.[22] Collision gases at the source, in particular, are effective at minimizing the initial internal energy of ions produced by either source.[22] Recent work with atmospheric MALDI,[23-25] and intermediate pressure MALDI[26] support this later conclusion.

The CID experiment provides comprehensible results only when the precursor species are well-defined. Several methods of ion isolation with high mass resolution are available for FTICR-MS, including stored waveform inverse Fourier transform excitation (SWIFT),[27, 28] correlated harmonic excitation fields (CHEF),[29, 30] and quadrupolar excitation/axialization (QEA),[31-33] Ion isolation by SWIFT results in no net addition of kinetic energy to the selected ions and efficiently removes the remainder of the ion population by calculation of the waveform that corresponds to a preferred, predetermined power spectrum.[27, 28] CHEF achieves the same net effect by adjusting the width and duration of successive single frequency radio frequency (RF) bursts around an ion of interest such that the off-resonance excitation and de-excitation cycles, ideally, return the ion to its starting radius.[29] QEA uses multiple collisions in the presence of a resonant RF quadrupolar field to collapse a mass selected ion to the center of the cell while other ions are lost to collisionally-induced magnetron expansion.[34] Ions axialized by QEAareexpected to have the lowest net translational and internal energy as a result of multiple thermalizing collisions.[31, 32, 35]

The algorithm for CHEF is straightforward to apply to most FTICR mass spectrometers. Off-resonance excitation results in expansion and contraction of ions by the applied rF irradiation, as described by equation 1:

$$r_{ion} = \frac{\beta\, V_{p-p}}{d\, B}\left[\frac{\sin\left\{\left(\omega_{ion} - \omega_{excite}\right)\frac{T_{excite}}{2}\right\}}{\left(\omega_{ion} - \omega_{excite}\right)}\right]^2 \qquad (1)$$

where $, $V_{p\text{-}p}$, d, and B describe the cell, applied off resonance field amplitude, and the magnetic field, T_{ion} and T_{excite} describe the ion's resonant and the applied off-resonance frequencies, respectively, in radians/second, and T_{excite} is the duration of the applied frequencies. The ion returns to the starting radius if, for all integer number, n, of single frequency pulses necessary to eject a mass-to-charge range around the targeted m/z, the applied frequencies are

$$\omega_{excite} = \omega_{ion} - \frac{2\pi n}{T_{excite}} \quad ; \quad for \quad n \neq 0 \qquad (2)$$

CHEF exploits this phenomenon to deliver the targeted ions back to their starting radius at the end of the n excitation steps. The implementation of this simple version of CHEF requires the proper selection of $V_{p\text{-}p}$ and T_{excite} such that the maximum orbit of the ion during the isolation step never exceeds the radius of the trap.

For ESI experiments, CHEF works well as an isolation method. With ESI, shot-to-shot variations in ion populations are neglible,[36] and the observed frequency, T_{ion}, remains constant. However, MALDI is well known to produce ion populations that vary considerably shot-to-shot and spot-to-spot, resulting in space-charge induced ion

frequency shifts up to several Hertz.[20, 37-40] While ions can be isolated by CHEF for MALDI FTICR-MS, the frequency shift can cause a residual amount of cyclotron excitation in the isolated ion with an amplitude that varies shot-to-shot. One of the goals of this study is to characterize the impact of this residual energy on the measurement of breakdown curves.

Nylon-6 is a polyamide of great industrial importance and yet only a few structural studies have been made by MALDI- or ESI-MS^n.[41] Murgasova et al. have studied single oligomer CID of Nylon-6 using ions produced by ESI and MALDI and proposed breakdown pathways comparable to those of proteins, although the pathways depend in a complex way on the end groups that are present.[19, 21] Ignoring the end group effects, Nylon-6 fragments along the amide backbone to an increasing degree of completeness with increasing collision energy.[21]

In this study, we present a comparison between the internal energies imparted to Nylon-6 oligomers by an external ESI source and an internal MALDI source. This ESI source makes use of collision gas to facilitate trapping while the internal MALDI source is operated with no gas assistance; this configuration examines the extremes of internal energy deposition in these two, most popular of soft ionization sources. CHEF isolation, used for ions from both sources, is compared to QEA isolation with respect to pre-CID internal energy to measure the differences in the radial excitation of the isolated oligomers, and the effect that these isolation methods have on measured breakdown curves.

EXPERIMENTAL

Nylon-6 was provided by DSM Research (Geleen, Netherlands) and samples prepared for both ESI and MALDI by dissolving approximately 1 mg/mL in pure formic acid. Ions were produced by ESI at ~1500 V, atmospheric pressure, and a flow rate of ~1 ìL/min. The ions were introduced to a 7 Tesla FTICR-MS (Bruker Daltoniks, Switzerland) fitted with an open cylindrical cell and trapped by assymetric trapping potentials (4 V and 2 V) combined with pulsed argon as collision gas (peak pressure ~10^{-6} torr) to remove the residual kinetic energy of the ions from the ion transfer step.

The MALDI matrix was 2,5-dihydroxybenzoic acid (DHB, obtained from Lancaster Synthesis, Pelham, NH, USA) and recrystallized from 2 M acetone solution by adding an equal volume of formic acid then drying the precipitate in vacuo. The recrystallized DHB was dissolved in acetone at 1 M and 1ìL of this was mixed on a titanium sample stage with 1ìL of the Nylon-6 solution and allowed to air dry at room temperature. The sample stage was transferred into the internal source of a home built MALDI-FTICR mass spectrometer.[42] The sample was irradiated with a frequency tripled Nd:YAG laser (355 nm) and a distribution of the ions from m/z 300-4000 trapped by gated trapping.[40, 43] A mass spectrum of an equimolar mixture of polyethylene glycols with average masses of 1000, 2000, and 3400 Da respectively showed no mass discrimination over the mass range m/z 300-4200.

Ion selection was achieved by application of correlated harmonic excitation field (CHEF) ejection, resulting in the singly protonated monoisotopic and A + 1 ions of, in turn, the linear tetramer, pentamer, hexamer, heptamer, and octomer. For the ESI experiments, CHEF was available as an integrated tool in the data acquisition software;

for MALDI, the CHEF sequence was written to a Stanford 345 programmable waveform generator (Stanford Research Systems, location) which was activated by a TTL pulse from the mass spectrometer data acquisition software. In a parallel series of experiments, oligomer ions were also isolated in the MALDI instrument using low-voltage azimuthal quadrupolar excitation/axialization to compare the initial energy of the CHEF isolated ions to the fully thermalized ions thus separated.

Collisionally induced dissociation (CID) was achieved via resonant excitation. Collision gas was argon pulsed to approximately 10^{-5} torr and the isolated ions excited at 10 V (MALDI) to ~20 V (ESI) for varying durations (85-230 μs for ESI and 50-500 μs for MALDI). A reaction delay of 5-10 s also allowed the collision gas to be pumped away and the analyzer pressure to return to 10^{-9} torr. The transient signal was collected for 131 ms (256 k points at 2 MHz in MALDI and 128 k points at 1 MHz in ESI). ESI mass spectra were the sum of five consecutive shots while the MALDI mass spectra are single shots. Fragment peaks were assigned, and each peak abundance normalized against the sum of all fragment and precursor peaks in a given experiment. The ion survival yields reported are the sum of the precursor ions in the CID mass spectrum divided by the sum of all ions.

RESULTS AND DISCUSSION

The ESI- and MALDI-FTICR mass spectra of the entire Nylon-6 distribution correlate well. All species were protonated, and a deconvolution of the multiple charge states in the ESI mass spectrum revealed a molecular weight distribution of Mn = 1350, Mw = 1640, and polydispersity of D = 1.2, while the MALDI mass resulted in a

molecular weight distribution one repeat unit less than that obtained by ESI with Mn = 1200, Mw = 1470, and D = 1.2. The five most abundant linear oligomers were selected for the CID experiments based on these analyses.

The number of degrees of freedom of the oligomer molecule increases linearly with the degree of polymerization. The amount of internal energy needed for dissociation is related to the degrees of freedom, as shown in the breakdown curves for the ions produced by ESI, Figure 7.1a, and the ions produced by internal MALDI, Figures 7.1b and 1c, although at lower degrees of polymerization the experimental scatter makes this effect less pronounced. The shift in the breakdown curves results from differences in internal energy prior to CID. The ions fragment in a reproducible, predictable manner with losses of one monomer unit at a time and the accumulation of an ion corresponding to monomer (less water) as the precursor fully dissociates. The progression is shown for the QE isolated octomer in Figure 7.2.

In the case of the ESI experiments, the pre-CID energy includes all excitation and relaxation pathways involved in the atmospheric pressure ionization, desolvation during ion storage and transport across the magnet field lines, the adiabatic and collisional cooling involved in the trapping arrangement, and any heating involved in the CHEF pulses from off-resonance excitation and de-excitation. For the MALDI experiments, excess pre-CID energy is a function of heating by the ionization event, any radiative cooling prior to the isolation event, heating or net radial expansion due to imperfectly executed CHEF pulses, or collisional thermalization during the QE isolation event.

These data provide a direct measure of the relative internal energy depositions due to the ion sources. The 5% survival yield (SY) energy, that amount of energy

required to convert 50% of the precursor into fragments, is presented in Figure 7.3 for MALDI (CHEF and QEA) and ESI (CHEF). It is clear that the MALDI source produces much hotter ions which require 4.5-7.7 eV less center-of-mass CID energy than similar ESI produced ions to achieve 50% fragmentation. However, MALDI ions cooled by QEA during isolation require an additional 1.6-5.3 eV collison energy than the ESI produced ions for 50% dissociation. Thus QEA is shown to reduce the internal energy of the ions.

The difference in center-of-mass energy required for 50% fragmentation between MALDI (CHEF) and MALDI (QE) ranges from 8.0 to 9.8 eV, greater than the dissociation energy of a C-N single bond. It appears that the CHEF pulses as applied in the MALDI experiment were pre-heating the ions, either by collisional excitation or by imparting excess cyclotron excitation in the isolated ions. Tuning the system on the homemade CHEF apparatus was found to be difficult for ions of higher mass-to-charge; the most likely explanation is that the difference in frequencies between isotopes decreases with increasing mass-to-charge, making it necessary to isolate two peaks to achieve reproducible results. The monoisotopic or the A+1 peak must have some residual cyclotron radius greater than the thermal radius due to off- resonance excitation. To determine the amount of energy that results from CHEF isolation alone, MALDI formed ions that were first isolated by QEA were subsequently exposed to a CHEF pulse. The breakdown curve for the hexamer ion isolated in this manner is shown in Figure 7.4 superimposed on the hexamer breakdown curves for the previous ESI and MALDI experiments. The MALDI-QEA-CHEF isolated ions require 3.4 eV less kinetic energy than the ions prepared by MALDI-QEA. This demonstrates that the CHEF isolation

Figure 7.1. CID breakdown curves for Nylon-6 linear, protonated oligomers from a) external ESI produced ions isolated by CHEF, and MALDI produced ions isolated by CHEF (b) and QEA (c).

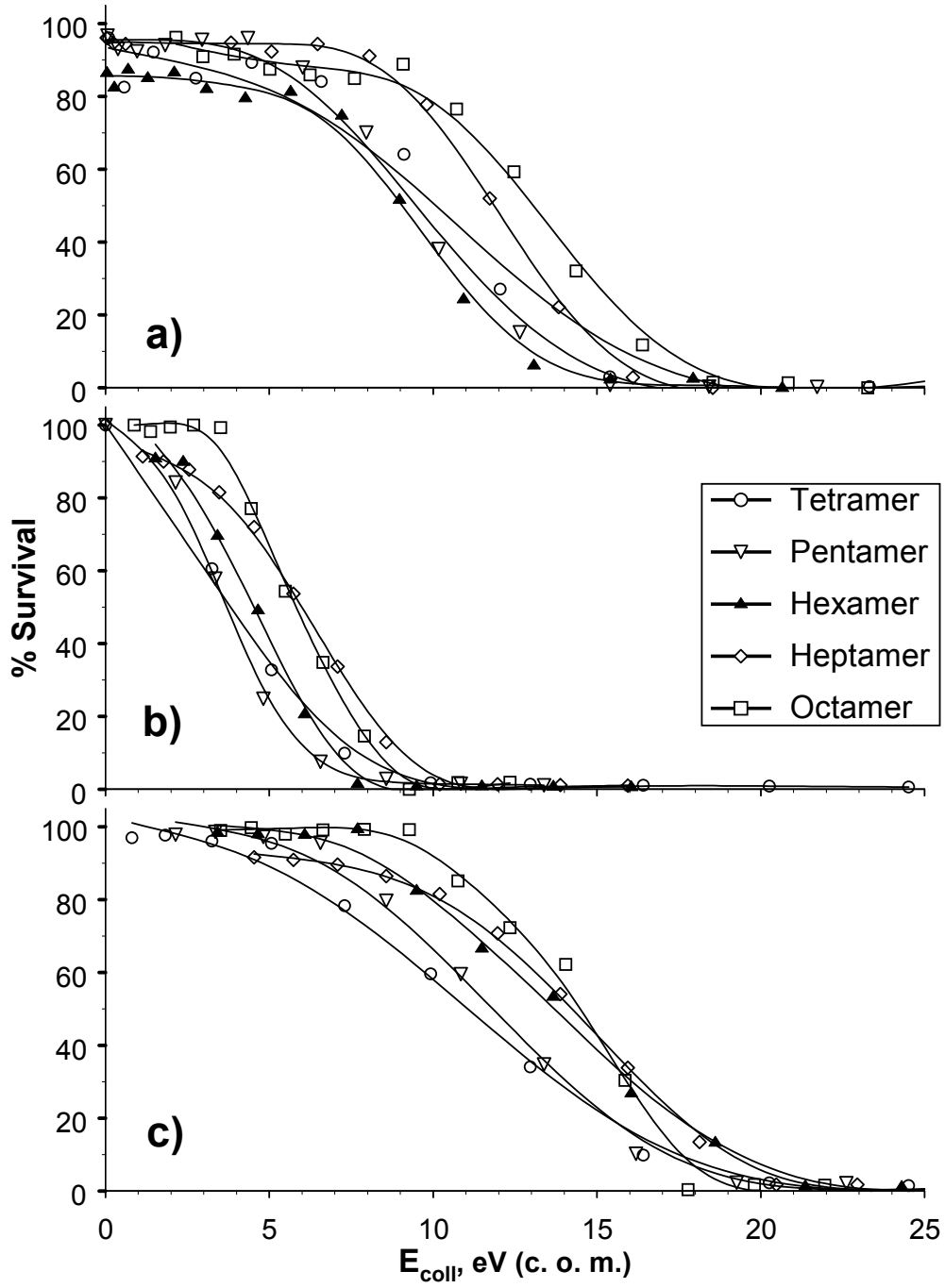
a)
b)
c)
% Survival
E_{coll}, eV (c. o. m.)
Tetramer
Pentamer
Hexamer
Heptamer
Octamer

Figure 7.2. Typical breakdown behavior of the Nylon-6 oligomers as represented by the linear octomer ions produced in the internal MALDI source and isolated using QE. Mostly intact oligomer ions are produced with some water losses and the products accumulating in the monomer (without water, at m/z = 114). In the breakdown graph, the breakdown of the precursor ion (m/z = 923) leads, at increasing energy, to the breakdown of the product ions.

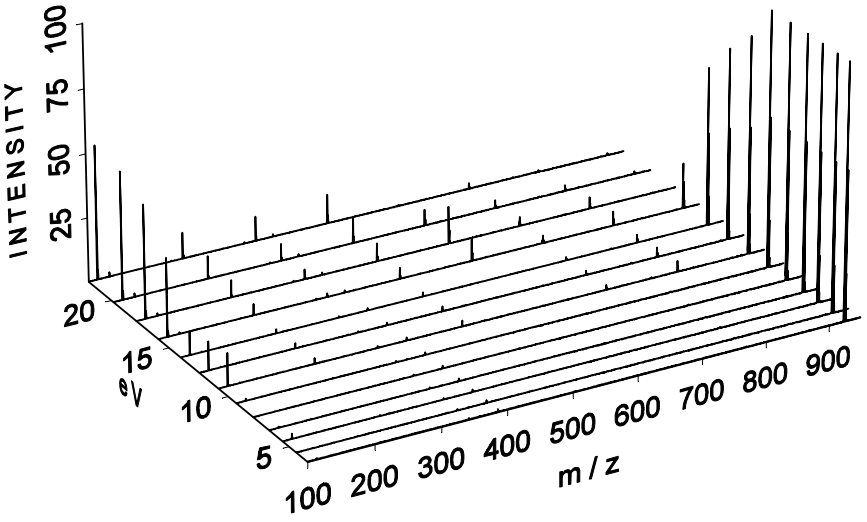
INTENSITY
25
50
75
100
20
15
eV
10
5
100
200
300
400
500
600
700
800
900
m / z

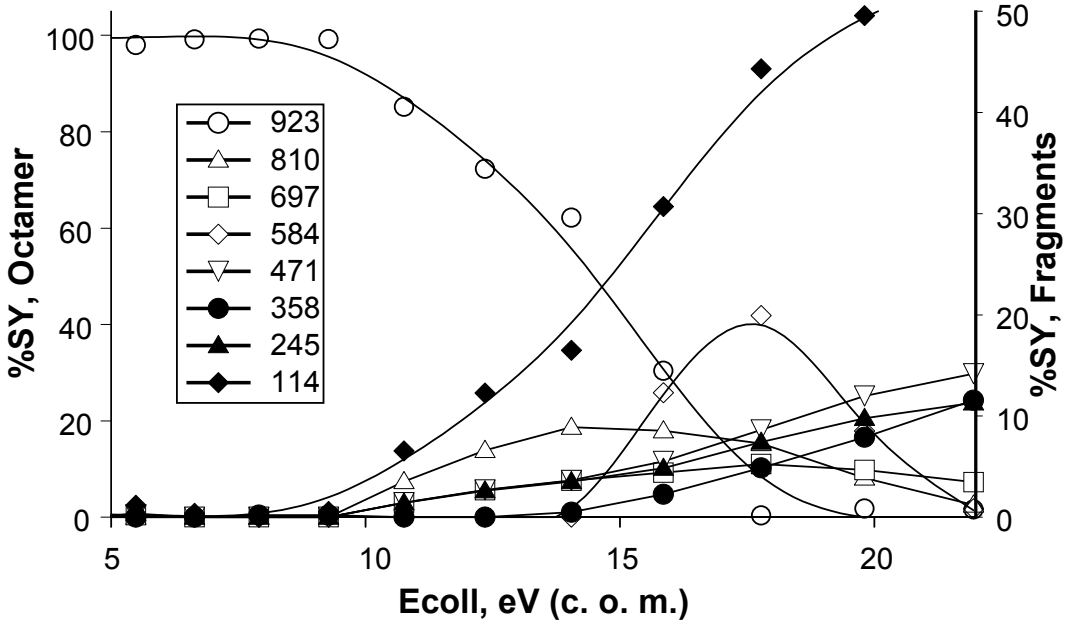
%SY, Octamer
%SY, Fragments
Ecoll, eV (c. o. m.)
923
810
697
584
471
358
245
114
0
20
40
60
80
100
10
30
50
5
15

Figure 7.3. 50% survival yield for each Nylon-6 oligomer with respect to methods of ionization and isolation. The slopes of the regression lines show that energy increases with the number of degrees of freedom in a regular manner.

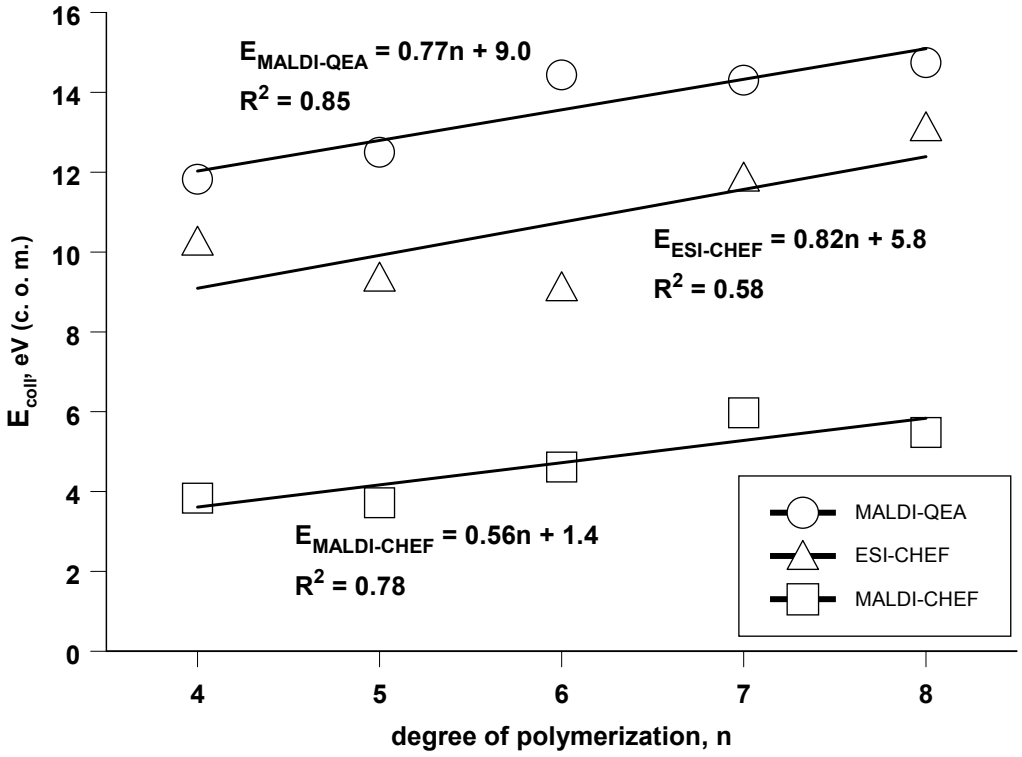
$E_{MALDI-QEA}$ = 0.77n + 9.0
R^2 = 0.85
$E_{ESI-CHEF}$ = 0.82n + 5.8
R^2 = 0.58
$E_{MALDI-CHEF}$ = 0.56n + 1.4
R^2 = 0.78
MALDI-QEA
ESI-CHEF
MALDI-CHEF
E_{coll}, eV (c. o. m.)
degree of polymerization, n
0
2
4
6
8
10
12
14
16
4
5
6
7
8

procedure adds energy to the precursor ion, probably in the form of kinetic energy. The difference between the MALDI-CHEF and the MALDI-QEA-CHEF curves indicates the energy due to the MALDI process itself, corresponding to a 5.4 eV shift in the breakdown curve. Furthermore, the MALDI-QEA-CHEF isolated ions required 1.9 eV more energy to achieve 50% dissociation than the ESI-CHEF isolated ions. This small difference can be ascribed to the ESI process or, more likely, to energy acquired during the transfer and capture of ESI-formed ions.

CONCLUSIONS

Nylon-6 shows a marked tendency to dissociate in a stepwise fashion, fragmenting along the amide backbone one repeat unit at a time with occasional water losses. The applied collision energy required for 50% conversion of the individual oligomers was shown to decrease in the order MALDI with QE isolation, ESI with CHEF isolation, and MALDI with CHEF isolation.

However, applying CHEF to ions precooled by QE isolation resulted in ions of similar internal energy to the ESI/CHEF ions. This is a significant point to note in studies of this sort. The method of isolation used in preparation for CID experiments in FTICR-MS has been shown to be a potentially significant source of internal energy, even under ultrahigh vacuum and, therefore, virtually collision free conditions. In the experiments detailed in this paper, this is probably a result of some residual excitation of cyclotron motion due to imperfect application of the CHEF pulse. For the purposes of comparing two ion sources, at least one of the instruments should be capable of complete thermalization by a technique such as QEA.

Figure 7.4. Breakdown graph for the Nylon-6 hexamer ions comparing the isolation methods used. E_{CHEF} (3.4 eV), the difference in center-of-mass energy for 50% dissociation from that of the presumed thermal ions from MALDI-QEA, and E_{MALDI} (5.4 eV), the residual internal energy contribution from the MALDI process, are also noted.

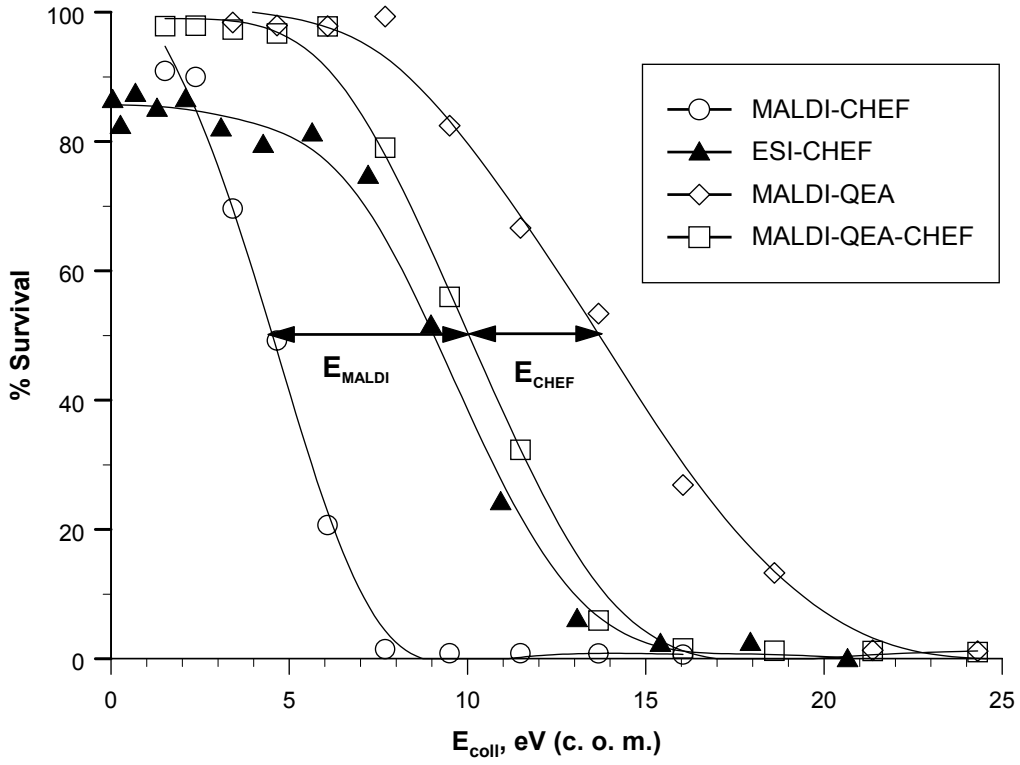
100
80
60
40
20
0
% Survival
0
5
10
15
20
25
E_coll, eV (c. o. m.)
MALDI-CHEF
ESI-CHEF
MALDI-QEA
MALDI-QEA-CHEF
E_MALDI
E_CHEF

REFERENCES

(1) Carroll, J. A.; Penn, S. G.; Fannin, S. T.; Wu, J. Y.; Cancilla, M. T.; Green, M. K.; Lebrilla, C. B. *Anal. Chem.* **1996,** *68*, 1798-1804.

(2) Zhang, X.; Jai-Nhuknan, J.; Cassady, C. J. *Int. J. Mass Spectrom.* **1997,** *171*, 135-145.

(3) Alving, K.; Korner, R.; Paulsen, H.; Peter-Katalinic, J. *J. Mass Spectrom.* **1998,** *33*, 1124-1133.

(4) Maziarz, E. P.; Baker, G. A.; Lorenz, S. A.; Wood, T. D. *J. Am. Soc. Mass Spectrom.* **1999,** *10*, 1298-1304.

(5) Cramer, R.; Corless, S. *Rapid Commun. Mass Spectrom.* **2001,** *15*, 2058-2066.

(6) Laskin, J.; Lifshitz, C. *J. Mass Spectrom.* **2001,** *36*, 459-478.

(7) Penn, S. G.; Cancilla, M. T.; Green, M. K.; Lebrilla, C. B. *Eur. Mass Spectrom.* **1997,** *3*, 67-79.

(8) Stimson, E.; Truong, O.; Richter, W. J.; Waterfield, M. D.; Burlingame, A. L. *Int. J. Mass Spectrom.* **1997,** *169*, 231-240.

(9) Kilby, G. W.; Sheil, M. M. *Org. Mass Spectrom.* **1993,** *28*, 1417-1423.

(10) Mowry, C. D.; Johnston, M. V. *J. Phys. Chem.* **1994,** *98*, 1904-1909.

(11) Beavis, R. C.; Chait, B. T. *Chemical Physics Letters* **1991,** *181*, 479.

(12) Juhasz, P.; Vestal, M. L.; Martin, S. A. *J. Am. Soc. Mass Spectrom.* **1997,** *8*, 209-217.

(13) Schmidt, A.; Bahr, U.; Karas, M. *Anal. Chem.* **2001,** *73*, 6040-6046.

(14) Heeren, R. M. A.; Vekey, K. *Rapid Commun. Mass Spectrom.* **1998,** *12*, 1175-1181.

(15) Smith, R. D.; Barinaga, C. J. *Rapid Commun. Mass Spectrom.* **1990,** *4*, 54-57.

(16) Martinez, R. I.; Ganguli, B. *J. Am. Soc. Mass Spectrom.* **1992,** *3*, 427-444.

(17) Harrison, A. G. *Rapid Commun. Mass Spectrom.* **1999,** *13*, 1663-1670.

(18) Jackson, A. T.; Jennings, K. R.; Scrivens, J. H. *Rapid Commun. Mass Spectrom.* **1996,** *10*, 1459-1462.

(19) Shan, L.; Murgasova, R.; Hercules, D. M.; Houalla, M. *J. Mass Spectrom.* **2001,** *36*, 140-144.

(20) Gusev, A. I.; Wilkinson, W. R.; Proctor, A.; Hercules, D. M. *Anal. Chem.* **1995,** *67*, 1034-1041.

(21) Murgasova, R.; Hercules, D. M. *J. Mass Spectrom.* **2001,** *36*, 1098-1107.

(22) Guan, S. H.; Li, G. Z.; Marshall, A. G. *Int. J. Mass Spectrom.* **1997,** *167*, 185-193.

(23) Erickson, B. *Anal. Chem.* **2000,** *72*, 186A-186A.

(24) Laiko, V. V.; Moyer, S. C.; Cotter, R. J. *Anal. Chem.* **2000,** *72*, 5239-5243.

(25) Laiko, V. V.; Baldwin, M. A.; Burlingame, A. L. *Anal. Chem.* **2000,** *72*, 652-657.

(26) O'Connor, P. B.; Costello, C. E. *Rapid Commun. Mass Spectrom.* **2001,** *15*, 1862-1868.

(27) Guan, S. H.; Marshall, A. G. *Anal. Chem.* **1993,** *65*, 1288-1294.

(28) Guan, S. H.; Marshall, A. G. *International Journal Of Mass Spectrometry And Ion Processes,* **1996,** *158*, 5-37.

(29) de Koning, L. J.; Nibbering, N. M. M.; van Orden, S. L.; Laukien, F. H. *Int. J. Mass Spectrom.* **1997,** *165*, 209-219.

(30) Heck, A. J. R.; Derrick, P. J. *Anal. Chem.* **1997,** *69*, 3603-3607.

(31) Guan, S. H.; Wahl, M. C.; Wood, T. D.; Marshall, A. G. *Anal. Chem.* **1993,** *65*, 1753-1757.

(32) Wood, T. D.; Ross, C. W.; Marshall, A. G. *J. Am. Soc. Mass Spectrom.* **1994,** *5*, 900-907.

(33) Hendrickson, C. L.; Drader, J. J.; Laude, D. A. *J. Am. Soc. Mass Spectrom.* **1995,** *6*, 448-452.

(34) Marshall, A. G.; Hendrickson, C. L.; Jackson, G. S. *Mass Spectrom. Rev.* **1998,** *17*, 1-35.

(35) Hendrickson, C. L.; Laude, D. A. *Anal. Chem.* **1995,** *67*, 1717-1721.

(36) Bruce, J. E.; Anderson, G. A.; Wen, J.; Harkewicz, R.; Smith, R. D. *Anal. Chem.* **1999,** *71*, 2595-2599.

(37) Solouki, T.; Gillig, K. J.; Russell, D. H. *Rapid Commun. Mass Spectrom.* **1994,** *8*, 26-31.

(38) Giannakopulos, A. E.; Bashir, S.; Derrick, P. J. *Eur. Mass Spectrom.* **1998,** *4*, 127-131.

(39) Haddleton, D. M.; Waterson, C.; Derrick, P. J. *Eur. Mass Spectrom.* **1998,** *4*, 203-207.

(40) Easterling, M. L.; Mize, T. H.; Amster, I. J. *Int. J. Mass Spectrom.* **1997,** *169*, 387-400.

(41) Nielen, M. W. F. *Mass Spectrom. Rev.* **1999,** *18*, 309-344.

(42) Easterling, M. L.; Pitsenberger, C. C.; Kulkarni, S. S.; Taylor, P. K.; Amster, I. J. *Int. J. Mass Spectrom. Ion Process.* **1996,** *158*, 97-113.

(43) Beu, S. C.; Laude, D. A. *Int. J. Mass Spectrom. Ion Process.* **1992,** *112*, 215-230.

CHAPTER 8

CONCLUSIONS

A general series of conclusions can be drawn from the preceding research. Broadly, it can be noted that MALDI-FTICR-MS is useful for the analysis of low molecular weight polymers of a wide variety of chemical compositions; that there are structural details that require the high resolution analytical capabilities of the FTICR-MS; and, that the continued development of this mass spectrometric technique will at once make it more attractive to the synthetic polymer industry as well as making the mass spectrometry of increasingly complex mixtures possible. This is an especially exciting prospect to the proteomics community.

Broadband accumulated trapping extends the utility of the internal MALDI source FTICR-MS by improving the signal to noise ratio and population statistics for low abundance samples. Signal-to-noise increases in direct proportion to the number of accumulation steps. Ions originally lost in the noise can be observed after only ten laser shots, a vast improvement over conventional signal averaging.

Insertion of external calibrants as internal standards provide the highest degree of mass accuracy by eliminating space charge differences between the calibrant and analyte spectra. This will be useful for the identification of the components of complex mixtures of proteins digested together without further separation of the resultant peptides. It is also useful in the case of true unknowns where the mass range to be calibrated can only be determined after initial mass analysis.[1, 2] This method will be useful for the analysis of complex proteomic mixtures where both high mass resolution and mass accuracy will be required in addition to high sensitivity.

High mass resolution and high mass accuracy facilitate the assignment of peaks in copolymer mass spectra. The determination of repeat unit and endgroup elemental

compositions and various calibration corrections were explored to improve the analysis. Isobaric resolution was shown to further enhance the assignment of overlapping species. Molecular weight and component distributions were calculated from single shot spectra and the component distributions found to be consistent with the expected composition. The preparatory application of capillary GPC for providing low polydispersity fractions of a high polydispersity sample proved crucial to its mass spectral characterization; the technique is simple to implement and could find use in the preparation for analysis of other complex mixtures by MALDI.

These features of MALDI-FTMS polymer analysis serve as a general first step toward full exploitation of the capabilities of trapped ion analysis. Future work will build on the MS/MS experiments for determining the sequence of terpolyesters, dendrimers, and, most challenging of all, random copolymers.[3-6]

The use of an internal source MALDI FTICR-MS is demonstrated to be especially useful in the analysis of the di-block copolymer poly(styrene-block-polymethylstyrene). Wide mass distributions can be captured and measured simultaneously to determine overall molecular weight distributions with reasonable agreement with GPC data. Subsequently, ultrahigh resolution spectra may be obtained to unequivocally assign the relative composition of the various species that are present in these complex mixtures. This data can then be used to determine the block length distributions of the polymer in good agreement with standard chromatographic methods. These methods should be extended to other types of copolymers to include graft and random copolymers and, with the inclusion of MS^n sequencing studies, to tri- and higher order block copolymers.

Nylon-6 shows a marked tendency to dissociate in a stepwise fashion, fragmenting along the amide backbone one repeat unit at a time with occasional water losses. The applied collision energy required for 50% conversion of the individual oligomers was shown to decrease in the order MALDI with QE isolation, ESI with CHEF isolation, and MALDI with CHEF isolation.

However, applying CHEF to ions precooled by QE isolation resulted in ions of similar internal energy to the ESI/CHEF ions. This is a significant point to note in studies of this sort. The method of isolation used in preparation for CID experiments in FTICR-MS has been shown to be a potentially significant source of internal energy, even under ultrahigh vacuum and, therefore, virtually collision free conditions. In the experiments detailed in this paper, this is probably a result of some residual excitation of cyclotron motion due to imperfect application of the CHEF pulse. For the purposes of comparing two ion sources, at least one of the instruments should be capable of complete thermalization by a technique such as QEA.

The comparison of MALDI and ESI produced ions, shows that the MALDI process produces ions with more energy than ions from an ESI source. The study does not resolve whether this energy is present as internal energy or kinetic energy.

REFERENCES

(1) Gygi, S. P.; Rist, B.; Gerber, S. A.; Turecek, F.; Gelb, M. H.; Aebersold, R. *Nat. Biotechnol.* **1999,** *17*, 994-999.

(2) Goodlett, D. R.; Bruce, J. E.; Anderson, G. A.; Rist, B.; Pasa-Tolic, L.; Fiehn, O.; Smith, R. D.; Aebersold, R. *Anal. Chem.* **2000,** *72*, 1112-1118.

(3) Walker, K. L.; Kahr, M. S.; Wilkins, C. L.; Xu, Z. F.; Moore, J. S. *Journal Of The American Society For Mass Spectrometry* **1994,** *5*, 731-739.

(4) Leon, J. W.; Frechet, J. M. J. *Polymer Bulletin* **1995,** *35*, 449-455.

(5) Koster, S.; de Koster, C. G.; van Benthem, R.; Duursma, M. C.; Boon, J. J.; Heeren, R. M. A. *Int. J. Mass Spectrom.* **2001,** *210*, 591-602.

(6) Montaudo, M. S. *Polymer* **2002,** *43*, 1587-1597.